DECEMBER '25

International Compilation, Research and Studies in the Field of

ELECTRICAL-ELECTRONICS AND COMMUNICATIONS ENGINEERING

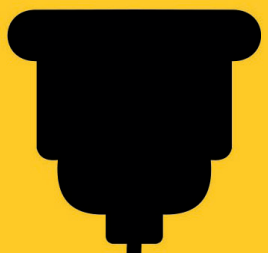

EDITOR
ASSOC. PROF. DR. HİLMİ ZENK

SERÜVEN YAYINEVİ

Genel Yayın Yönetmeni / Editor in Chief • C. Cansın Selin Temana

Kapak & İç Tasarım / Cover & Interior Design • Serüven Yayınevi

Birinci Basım / First Edition • © Aralık 2025

ISBN • 978-625-8682-58-8

Serüven Yayınevi / Serüven Publishing
Türkiye Adres / Turkey Address: Kızılay Mah. Fevzi Çakmak 1. Sokak
Ümit Apt No: 22/A Çankaya/ANKARA
Telefon / Phone: 05437675765
web: www.seruvenyayinevi.com
e-mail: seruvenyayinevi@gmail.com

Baskı & Cilt / Printing & Volume
Sertifika / Certificate No: 47083

INTERNATIONAL COMPILATION, RESEARCH AND STUDIES IN THE FIELD OF ELECTRICAL-ELECTRONICS AND COMMUNICATIONS ENGINEERING

EDITOR

ASSOC. PROF. DR. HİLMİ ZENK

Contents

Chapter 1

STRUCTURAL HEALTH MONITORING OF WIND TURBINES BASED ON IMAGE PROCESSING AND ARTIFICIAL INTELLIGENCE: NEXT-GENERATION APPROACHES

Umut Saray[1]

1 Department of Electronic Automation, Turhal Vocational School, Tokat Gaziosmanpaşa University, Tokat, Türkiye,(umutsaray@gmail.com) (ORCID: 0000-0003-3339-6876)

1. Introduction

Wind energy has gained strategic importance worldwide due to the increasing demand for sustainable and environmentally friendly energy sources. In recent years, rising energy consumption and the depletion of fossil fuel reserves have accelerated the transition toward renewable energy resources, with wind turbines playing a crucial role in power generation. Ensuring the efficient, safe, and sustainable operation of wind turbines has therefore become critical not only for maintaining energy production capacity but also for extending the service life of system components (Lüy & Saray, 2012; Şenkal & Emeksiz, 2023; Lüy & Metin, 2022).

Maintaining the structural integrity of wind turbines is critically important, particularly for key components such as blades, towers, and generators. Early detection of structural damage in these components is essential for both system safety and the continuity of energy production. Conventional inspection approaches are largely based on manual examinations and visual assessments, which are often time-consuming, costly, and prone to subjective errors (Yang, Tavner, Crabtree, Feng & Qiu, 2014; Akbulut & Onur, 2025). Consequently, the demand for automated, rapid, and reliable structural health monitoring systems continues to increase.

In this context, image processing techniques and artificial intelligence–based algorithms offer innovative and effective solutions for structural health monitoring of wind turbines. The analysis of data acquired through unmanned aerial vehicles (UAVs) and high-resolution imaging systems using deep learning models enables the early detection of cracks, erosion, and surface degradation (Xiao, Liu, Zhang, & Zhang, 2021). This approach not only contributes to reducing maintenance and repair costs but also helps prevent unforeseen failures that may lead to production losses (Zou, Wang, Bi, & Sun, 2022).

This chapter comprehensively examines the role of image processing and deep learning–based systems in wind turbine structural health monitoring, focusing on the technologies employed, representative applications in the literature, and emerging research trends shaping future work in this field.

2. Image Processing Technologies

Structural degradations in wind turbine components commonly manifest as surface cracks, blade erosion, coating degradation, geometric deformations, and material fatigue. Reliable detection of such defects requires detailed analysis of high-resolution visual data. Image processing technologies enable the automated inspection of visual information acquired from turbine surfaces, allowing potential damage regions to be identified without direct human intervention and significantly improving inspection efficiency (Deng, Guo, & Chai, 2021; Dorafshan, Thomas & Maguire, 2018).

2.1 Image Sources and Types

In image processing–based structural health monitoring applications, the selection of data sources varies depending on the type of damage and the specific monitoring objective. One of the most commonly used data types is RGB (color) imagery, which is typically acquired using unmanned aerial vehicles (UAVs) or fixed camera systems. RGB images are widely employed for detecting surface cracks, erosion, coating degradation, and geometric deformations under visible light conditions (Ye, Chen & Li, 2019).

Thermal imaging plays a crucial role in identifying abnormal temperature distributions within wind turbine components. This technique is particularly effective for early fault detection in generators, gearboxes, and bearing systems, where heat-related anomalies often indicate underlying mechanical or electrical issues before visible damage occurs (Yang, Court & Jiang, 2013).

Multispectral and hyperspectral imaging systems are considered advanced monitoring tools that provide additional spectral information beyond the visible range. By analyzing material responses across multiple wavelength bands, these systems enable the detection of subsurface defects, coating irregularities, and early-stage structural degradations, offering significant advantages over conventional RGB imaging in complex inspection scenarios (Fırat & Hanbay, 2021).

2.2 Image Preprocessing Techniques

Raw image data are often unsuitable for direct analysis due to noise, low contrast, and environmental disturbances. Therefore, various preprocessing steps are applied prior to analysis in image processing–based structural health monitoring systems. These steps enhance image quality and significantly improve the accuracy of damage detection algorithms (Umbaugh, 2023).

During the denoising stage, sensor-induced noise and unwanted distortions are reduced using filters such as Gaussian, median, and bilateral filters. These techniques aim to suppress random noise while preserving essential structural details within the image (Buades, Coll & Morel, 2005).

Contrast enhancement techniques are employed to improve the visibility of damaged regions relative to the background. Methods such as histogram equalization and adaptive contrast enhancement are particularly effective in highlighting surface defects in images captured under poor lighting conditions (Pizer et al., 1987).

Edge detection algorithms play a critical role in identifying the boundaries of damaged areas. Techniques including Sobel, Canny, and Laplacian operators analyze intensity variations to extract structural features such as cracks and deformations (Canny, 1986). In the final stage of preprocessing, segmentation methods are applied to isolate regions of interest using techniques such as thresholding, region growing, and k-means clustering, thereby preparing the image for further analysis (Pham, Xu & Prince, 2000).

2.3 Data Annotation and Labeling Process

In order to effectively train machine learning and deep learning–based models, defect types present in image data must be clearly and consistently labeled. This process, known as data annotation, plays a crucial role in enabling models to learn and distinguish between different types of structural damage. During annotation, common defect categories observed in wind turbines—such as cracks, wear, corrosion, material separation, and surface deformation—are first defined (Ren, He, Girshick & Sun, 2015).

Based on the defined damage classes, various labeling techniques are applied to the images. While bounding boxes are widely used for object-based damage detection tasks, pixel-level segmentation masks are preferred in applications requiring more detailed analysis. These labeling approaches allow

models to learn both the location and shape characteristics of damaged regions (Ronneberger, Fischer & Brox, 2015).

Annotation tasks are typically performed using manual or semi-automatic tools. Software such as LabelImg and the VGG Image Annotator (VIA) enable efficient labeling of images and storage of annotations in formats compatible with machine learning workflows (Dutta & Zisserman, 2019). The resulting labeled datasets serve as the foundational knowledge used to train deep learning algorithms.

3. Deep Learning-Based Damage Detection in Wind Turbines

With the advancement of image processing–based structural health monitoring approaches, deep learning algorithms have increasingly assumed a central role in damage detection for wind turbines. Although traditional image processing methods can produce satisfactory results under certain conditions, they often struggle with complex damage patterns, varying environmental conditions, and large-scale datasets. In this context, deep learning–based models offer significant advantages through automatic feature extraction, high detection accuracy, and strong generalization capabilities across different damage types (LeCun, Bengio & Hinton, 2015).

Among deep learning approaches, Convolutional Neural Networks (CNNs) are widely used for extracting meaningful features from wind turbine images. CNN-based models can hierarchically learn surface cracks, erosion patterns, and coating degradation through their multi-layer architectures, achieving superior detection performance compared to conventional methods (Krizhevsky, Sutskever & Hinton, 2012).

Recent advances in object detection and segmentation using deep learning have further expanded the application scope of automated wind turbine inspection. Architectures such as YOLO, Faster R-CNN, and U-Net are frequently employed in the literature for localizing damaged regions and extracting their geometric characteristics. When combined with UAV-based imaging systems, these models significantly enhance inspection efficiency and support the optimization of maintenance strategies (Redmon & Farhadi, 2018; Ronneberger, Fischer & Brox, 2015).

This section provides a comprehensive overview of the main deep learning architectures employed for damage detection in wind turbines, highlighting their operational principles, advantages, and limitations through a comparative perspective.

3.1 Convolutional Neural Networks (CNNs)

Convolutional Neural Networks (CNNs) are among the most widely used deep learning architectures for image-based damage detection applications. Owing to their multi-layered structures that enable automatic feature extraction, CNNs have demonstrated high performance in detecting surface-level and geometric degradations in wind turbine structural components. CNN-based approaches offer significant advantages over traditional methods, particularly in learning complex patterns such as cracks, erosion marks, and coating defects (LeCun, Bengio & Hinton, 2015).

CNN architectures are primarily composed of convolutional, activation, and pooling layers. While convolutional layers learn local features such as edges, corners, and textures, deeper layers extract more abstract and damage-specific representations. This hierarchical learning capability allows CNNs

to detect various damage types ranging from small-scale cracks on wind turbine blades to large-area surface deformations (Krizhevsky, Sutskever & Hinton, 2012).

The literature reports the successful application of several CNN architectures—including AlexNet, VGGNet, ResNet, and EfficientNet—to wind turbine image analysis. In particular, ResNet architectures incorporating residual connections mitigate the vanishing gradient problem and enable stable training of deeper networks, leading to improved detection accuracy (He, Zhang, Ren & Sun, 2016). Scalable architectures such as EfficientNet provide high performance with reduced computational cost, making them attractive for real-time and field-deployed inspection systems (Tan & Le, 2019).

CNN-based damage detection systems are typically formulated as image-level classification or regional localization problems. While classification-based approaches focus on identifying whether a turbine component is damaged, more advanced methods integrate CNNs with object detection and segmentation models to determine the precise location and extent of damage. Consequently, CNNs serve as a fundamental building block in automated wind turbine inspection frameworks.

3.2 Object Detection Models for Damage Localization

While image-level classification approaches are effective in determining whether wind turbine components are damaged, they are limited in identifying the exact location and spatial extent of defects. Consequently, object detection–based deep learning models have gained increasing attention for both detecting and localizing damaged regions. These models identify defect areas using bounding boxes, providing actionable information for maintenance and repair operations (Girshick et al., 2014).

Among object detection architectures, Faster R-CNN achieves high detection accuracy through the use of Region Proposal Networks (RPNs). Faster R-CNN–based approaches are particularly effective in localizing cracks and localized surface defects; however, their relatively high computational cost limits their applicability in real-time inspection scenarios (Ren, He, Girshick & Sun, 2015).

For real-time applications, the You Only Look Once (YOLO) family offers a single-stage detection framework that enables faster inference speeds. When integrated with UAV-based imaging systems, YOLO architectures facilitate rapid inspection of large wind farm areas. Versions such as YOLOv3 and YOLOv5 have been widely adopted in the literature due to their balanced trade-off between detection accuracy and computational efficiency (Redmon & Farhadi, 2018; Karaca & Yaşar, 2024).

One of the primary challenges in applying object detection models to wind turbine inspection lies in the small-scale and irregular geometry of many damage types. This issue directly affects the model's ability to detect small objects. To address this challenge, techniques such as multi-scale feature extraction, data augmentation, and customized loss functions are commonly employed. As a result, object detection models represent a powerful tool for automated damage localization in wind turbine structural health monitoring.

3.3 Segmentation-Based Approaches for Damage Delineation

While object detection–based approaches are effective in identifying approximate locations of damaged regions, they are limited in precisely delineating the boundaries and geometric structure of defects. Consequently, segmentation-based deep learning approaches that enable pixel-level analysis of damage have attracted increasing attention in wind turbine structural health monitoring. Segmentation models provide detailed separation of damaged and healthy regions, offering more precise information for maintenance and repair decisions (Ronneberger, Fischer & Brox, 2015).

Among deep learning–based segmentation models, the U-Net architecture is widely adopted in wind turbine inspection applications due to its ability to achieve high performance with relatively limited training data. The encoder–decoder structure and skip connections of U-Net preserve low-level spatial information, enabling accurate segmentation of fine details such as cracks, delamination, and surface degradation (Ronneberger, Fischer & Brox, 2015).

In addition to U-Net, advanced segmentation models such as SegNet, DeepLab, and Mask R-CNN have been employed for damage detection in wind turbine imagery. In particular, Mask R-CNN integrates object detection and segmentation within a unified framework, allowing simultaneous localization and shape extraction of damaged regions (He, Gkioxari, Dollár & Girshick, 2017). These approaches contribute to more informed maintenance decision-making.

Despite their advantages, segmentation-based methods require pixel-level annotations, which involve substantial labeling effort and high preparation costs. As a result, weakly supervised and semi-supervised segmentation approaches have emerged as promising research directions for reducing annotation requirements while maintaining acceptable performance levels in wind turbine structural health monitoring applications (Zhou et al., 2018).

3.4 Performance Metrics and Evaluation Criteria

Objective evaluation of deep learning–based damage detection and segmentation models requires the use of appropriate performance metrics. In wind turbine structural health monitoring applications, evaluation metrics vary depending on whether the task involves classification, object detection, or segmentation. These metrics enable quantitative comparison of model accuracy, robustness, and generalization capability (Powers, 2011).

For classification-based approaches, commonly used metrics include accuracy, precision, recall, and F1-score. These measures provide a balanced assessment of model performance in distinguishing between damaged and healthy classes. However, in the presence of class imbalance, accuracy alone may be misleading, and metrics such as recall and F1-score should be prioritized (Sokolova & Lapalme, 2009).

Object detection models are typically evaluated using mean Average Precision (mAP), which summarizes detection performance across different confidence thresholds. In wind turbine inspection scenarios involving small-scale defects, reporting mAP values at lower Intersection over Union (IoU) thresholds is particularly important for capturing detection sensitivity (Everingham et al., 2010).

For segmentation-based approaches, pixel-level evaluation metrics such as Intersection over Union (IoU), Dice coefficient, and pixel accuracy are widely adopted. These metrics assess how

accurately damaged regions are delineated and provide insight into the spatial precision of segmentation models (Milletari, Navab & Ahmadi, 2016). In addition to accuracy-related measures, inference time and computational cost should also be considered when assessing model suitability for real-world deployment.

4. Case Studies and Real-World Applications

The effectiveness of image processing and deep learning–based structural health monitoring systems can be more clearly evaluated through real-world applications and case studies. In recent years, case studies conducted in countries with rapidly expanding wind energy capacity have demonstrated how these technologies transform maintenance strategies and reduce operational costs. In particular, UAV-based imaging systems combined with artificial intelligence–driven analysis enable faster and safer inspection of large-scale wind farms (Shihavuddin et al., 2019).

This section examines representative case studies from different countries to assess the practical performance, benefits, and challenges of image processing and AI-based structural health monitoring systems in wind turbine applications.

4.1 China – UAV-Based Inspection Systems

China, as one of the countries with the largest installed wind energy capacity worldwide, has been at the forefront of adopting advanced technologies for wind turbine inspection and maintenance. Due to the extensive geographical distribution of wind farms, manual inspection methods are often time-consuming and costly. As a result, UAV-based imaging systems have been widely deployed to capture high-resolution images of wind turbine blades, which are subsequently analyzed using deep learning models (Liao et al., 2024; Altice et al., 2024).

Field studies have reported that object detection models such as YOLO and Faster R-CNN can accurately identify cracks, erosion, and surface degradation. In wind farms located in mountainous or hard-to-access areas, drone-assisted automated inspection systems significantly enhance personnel safety and support more efficient maintenance planning (Shihavuddin et al., 2019).

These applications demonstrate substantial reductions in inspection time and maintenance costs compared to conventional methods, highlighting the feasibility and effectiveness of AI-driven inspection systems in large-scale wind energy infrastructures.

4.2 Germany – Thermal-Based Condition Monitoring

Germany is among the leading countries in wind energy technologies due to its strong engineering infrastructure and well-established industrial standards. Thermal imaging–based systems are widely employed in maintenance and predictive monitoring strategies for wind turbines. Thermal cameras enable the detection of abnormal temperature distributions in turbine components, facilitating early identification of mechanical and electrical faults (Yang, Court & Jiang, 2013).

Field applications in Germany have reported the use of machine learning and deep learning algorithms to analyze thermal data obtained from generators, gearboxes, and bearing systems. These approaches allow early detection of fault indicators such as overheating, increased friction, and insulation degradation before visible damage occurs (Stetco et al., 2019).

When combined with time-series thermal data, deep learning–based thermal analysis systems support trend monitoring and optimization of maintenance schedules. Implementations in German wind farms have demonstrated reductions in unplanned downtime and significant operational cost savings, highlighting the industrial feasibility of integrating thermal imaging with artificial intelligence.

4.3 Turkey – Onshore Camera-Based Monitoring Systems

With the rapid growth of installed wind energy capacity in recent years, Turkey has emerged as a country where the need for practical and locally applicable wind turbine monitoring solutions has become increasingly evident. In many onshore wind farms, monitoring practices increasingly rely on visual inspection workflows supported by camera-based systems due to their accessibility and cost-effectiveness. These systems enable periodic acquisition of visual data from turbine blades and tower surfaces, which can be further analyzed using artificial intelligence–based models (Akbulut & Onur, 2025).

Recent developments in Turkey indicate that artificial intelligence is being actively integrated into wind power plant monitoring and maintenance processes at the industrial level. In particular, industry-driven initiatives demonstrate the use of AI-supported data analytics, image-based inspection, and predictive maintenance solutions to enhance operational efficiency and reduce maintenance costs. A notable example is the deployment of AI-powered solutions by GÜRİŞ Technology, which focuses on condition monitoring, predictive maintenance, and intelligent analysis of operational and visual data in wind power plants (Kul, 2025).

Camera-based monitoring systems offer the advantage of providing continuous or periodic data streams at relatively low operational cost. However, factors such as camera viewing angle, lighting conditions, and environmental variability may affect system performance. Consequently, hybrid monitoring strategies that integrate camera-based inspection with UAV-assisted surveys and multi-source data fusion are increasingly recognized as a promising direction for improving the reliability and robustness of wind turbine structural health monitoring in Turkey.

4.4 Open Datasets and Benchmarking

Ensuring the comparability and reproducibility of image processing and deep learning–based structural health monitoring studies requires the use of open-access and standardized datasets. In this context, open datasets and benchmarking studies play a critical role in objectively evaluating damage detection models for wind turbines. Open datasets enable multiple research groups to address the same problem, thereby facilitating clearer identification of strengths and limitations of proposed methods (Everingham et al., 2010).

Open image datasets for wind turbine inspection typically include defects such as cracks, erosion, coating degradation, and corrosion on blade surfaces. These datasets, acquired using UAVs or fixed camera systems, provide annotated images for classification, object detection, and segmentation tasks. Commonly used datasets include wind turbine image collections provided by the National Renewable Energy Laboratory (NREL) and UAV-based inspection datasets shared by academic institutions (Altice et al., 2024).

Benchmarking studies aim to evaluate model performance using standardized metrics such as accuracy, mAP, IoU, and F1-score. Reporting comparative results of CNN-, YOLO-, and U-Net–based models on the same dataset helps identify the most suitable approaches for specific damage types and inspection scenarios (Shihavuddin et al., 2019).

Nevertheless, limitations such as limited dataset diversity, insufficient representation of environmental variability, and class imbalance can restrict the generalizability of benchmark results. Therefore, future research efforts should prioritize the development of large-scale, multi-source, and geographically diverse open datasets to enhance the robustness and applicability of benchmarking studies.

4.5 Application-Oriented Comparison

The effectiveness of image processing and artificial intelligence–based structural health monitoring systems for wind turbines varies depending on the imaging technology employed, monitoring objectives, and site conditions. Therefore, an application-oriented comparison of UAV-based, thermal imaging–based, and fixed camera–based systems is essential for selecting the most appropriate approach. Such comparisons require simultaneous evaluation of technical performance, operational cost, safety, and sustainability considerations (Stetco et al., 2019).

UAV-based imaging systems offer significant advantages in large-scale wind farms by enabling rapid inspection of extensive areas with high-resolution imagery. These systems provide high accuracy in detecting visible defects such as blade cracks and erosion but are constrained by weather dependency and regulatory requirements. In contrast, thermal imaging–based systems excel in predictive maintenance by identifying abnormal temperature patterns in components before visible damage occurs (Yang, Court & Jiang, 2013).

Fixed camera–based monitoring systems provide continuous and long-term observation with relatively low installation and operational costs. While particularly suitable for onshore wind farms, these systems are affected by limited viewing angles and environmental variability. As a result, hybrid monitoring strategies that integrate multiple imaging technologies have gained increasing attention in recent studies (Heo & Na, 2025).

Application-oriented evaluations clearly indicate that no single monitoring method is universally optimal for all scenarios. Instead, selecting an appropriate monitoring strategy should consider wind farm scale, geographical conditions, maintenance philosophy, and budget constraints. In this context, AI-enabled hybrid systems represent one of the most promising future directions for wind turbine structural health monitoring.

5. Discussion and Future Perspectives

The studies discussed in this chapter clearly demonstrate that image processing and artificial intelligence–based methods have brought a significant transformation to structural health monitoring of wind turbines. Compared to traditional manual inspection approaches, deep learning–driven systems offer faster, safer, and more cost-effective solutions, particularly contributing to the optimization of maintenance strategies in large-scale wind farms.

The reviewed CNN-, object detection–, and segmentation-based approaches exhibit complementary characteristics for different damage types and monitoring scenarios. While CNN-based classification models are effective for general damage identification, object detection architectures such as YOLO and Faster R-CNN enable precise localization of defects. Segmentation models, including U-Net, further enhance maintenance decision-making by accurately delineating damage boundaries and geometric extent.

Despite these advancements, several challenges remain. Limited dataset diversity, high annotation costs, environmental variability affecting image quality, and class imbalance issues continue to impact model performance. Additionally, the computational demands of deep learning models pose challenges for real-time deployment and edge-based implementations

Looking ahead, emerging paradigms such as federated learning, transfer learning, and self-supervised learning present promising opportunities for wind turbine structural health monitoring. These approaches enable collaborative model training across multiple sites while preserving data privacy and reducing reliance on large labeled datasets. Furthermore, hybrid monitoring systems that integrate multiple data sources—including visual, thermal, vibration, and SCADA data—are expected to deliver more robust and comprehensive damage assessment capabilities.

In conclusion, image processing and artificial intelligence–based structural health monitoring systems play a pivotal role in achieving sustainable, safe, and efficient operation of wind energy infrastructures. Continued interdisciplinary research efforts and strong industry–academia collaborations will be essential for accelerating the deployment of these technologies in real-world wind turbine applications.

References

Akbulut, K., & Onur, T. Ö. (2025). Rüzgar Türbini Kanat Hasarlarının Görüntü İşleme Yöntemleri ile Belirlenmesi ve Hasar Alanının Hesaplanması. Black Sea Journal of Engineering and Science, 8(6), 1715-1722. https://doi.org/10.34248/bsengineering.1664405

Altice, B., Nazario, E., Davis, M., Shekaramiz, M., Moon, T. K., & Masoum, M. A. S. (2024). Anomaly Detection on Small Wind Turbine Blades Using Deep Learning Algorithms. Energies, 17(5), 982. https://doi.org/10.3390/en17050982

Buades, A., Coll, B., & Morel, J. (2005). A non-local algorithm for image denoising. 2005 IEEE Computer Society Conference on Computer Vision and Pattern Recognition (CVPR'05), 2, 60-65 vol. 2. https://doi.org/10.1109/CVPR.2005.38

Canny, J.F. (1986). A Computational Approach to Edge Detection. IEEE Transactions on Pattern Analysis and Machine Intelligence, PAMI-8, 679-698.

Deng, L., Guo, Y., & Chai, B. (2021). Defect detection on a wind turbine blade based on digital image processing. Processes, 9(8), 1452. https://doi.org/10.3390/pr9081452

Dutta, A., & Zisserman, A. (2019). The VGG image annotator (VIA). arXiv preprint arXiv:1904.10699. https://doi.org/10.1145/3343031.3350535

Everingham, M., Van Gool, L., Williams, C. K. I., Winn, J., & Zisserman, A. (2010). The Pascal Visual Object Classes (VOC) challenge. International Journal of Computer Vision, 88(2), 303–338. https://doi.org/10.1007/s11263-009-0275-4

Fırat, H., & Hanbay, D. (2021). 4CF-Net: Hiperspektral uzaktan algılama görüntülerinin spektral uzamsal sınıflandırılması için yeni 3B evrişimli sinir ağı. Gazi Üniversitesi Mühendislik Mimarlık Fakültesi Dergisi, 37(1), 439–454. https://doi.org/10.17341/gazimmfd.901291

Girshick, R.B., Donahue, J., Darrell, T., & Malik, J. (2014). Rich Feature Hierarchies for Accurate Object Detection and Semantic Segmentation. 2014 IEEE Conference on Computer Vision and Pattern Recognition, 580-587.

He, K., Gkioxari, G., Dollár, P., & Girshick, R. (2017). Mask R-CNN. In Proceedings of the IEEE International Conference on Computer Vision (ICCV) (pp. 2980–2988). IEEE. https://doi.org/10.1109/ICCV.2017.322

He, K., Zhang, X., Ren, S., & Sun, J. (2016). Deep residual learning for image recognition. In Proceedings of the IEEE Conference on Computer Vision and Pattern Recognition (CVPR) (pp. 770–778). IEEE. https://doi.org/10.1109/CVPR.2016.90

Heo, S.-J., & Na, W. S. (2025). Review of Drone-Based Technologies for Wind Turbine Blade Inspection. Electronics, 14(2), 227. https://doi.org/10.3390/electronics14020227

Karaca, V., & Yaşar, E. (2024). Performing distance measurements of fixed objects detected with YOLO using web camera. International Scientific and Vocational Studies Journal, 8(1), 87–93. https://doi.org/10.47897/bilmes.1502873

Krizhevsky, A., Sutskever, I., & Hinton, G. E. (2012). ImageNet classification with deep convolutional neural networks. Advances in Neural Information Processing Systems, 1097–1105.

Kul, M. (2025). GÜRİŞ Technology drives the future of wind power plants with AI-powered solutions. Wind Energy Turkey. https://www.ruzgarenerjisi.com.tr/en/guris-technology-drives-the-future-of-wind-power-plants-with-ai-powered-solutions/

LeCun, Y., Bengio, Y., & Hinton, G. (2015). Deep learning. Nature, 521(7553), 436–444. https://doi.org/10.1038/nature14539

Liao, Y., Lv, M., Huang, M., Qu, M., Zou, K., Chen, L., & Feng, L. (2024). An improved YOLOv7 model for surface damage detection on wind turbine blades based on low-quality UAV images. Drones, 8(9), 436. https://doi.org/10.3390/drones8090436

Lüy, M., & Metin, N. A. (2022). PID Control Medium Size Wind Turbine Control with Integrated Blade Pitch Angle. International Scientific and Vocational Studies Journal, 6(1), 22-31. https://doi.org/10.47897/bilmes.1091968

Lüy, M., & Saray, U. (2012). Wind speed estimation for missing wind data with three different backpropagation algorithms. Energy Education Science and Technology Part A: Energy Science and Research, 30(1), 45–54.

Pham, D. L., Xu, C., & Prince, J. L. (2000). Current methods in medical image segmentation. Annual Review of Biomedical Engineering, 2, 315–337.

Pizer, S. M., Amburn, E. P., Austin, J. D., Cromartie, R., Geselowitz, A., Greer, T., … Zimmerman, J. B. (1987). Adaptive histogram equalization and its variations. Computer Vision, Graphics, and Image Processing, 39(3), 355–368.

Powers, D. M. W. (2011). Evaluation: From precision, recall and F-measure to ROC, informedness, markedness and correlation. Journal of Machine Learning Technologies, 2(1), 37–63.

Redmon, J., & Farhadi, A. (2018). YOLOv3: An incremental improvement. arXiv preprint arXiv:1804.02767.

Ren, S., He, K., Girshick, R., & Sun, J. (2015). Faster R-CNN: Towards real-time object detection with region proposal networks. Advances in Neural Information Processing Systems, 91–99.

Ronneberger, O., Fischer, P., & Brox, T. (2015). U-Net: Convolutional Networks for Biomedical Image Segmentation. ArXiv, abs/1505.04597.

Shihavuddin, A., Chen, X., Fedorov, V., Nymark Christensen, A., Andre Brogaard Riis, N., Branner, K., Bjorholm Dahl, A., & Reinhold Paulsen, R. (2019). Wind Turbine Surface Damage Detection by Deep Learning Aided Drone Inspection Analysis. Energies, 12(4), 676. https://doi.org/10.3390/en12040676

Sokolova, M., & Lapalme, G. (2009). A systematic analysis of performance measures for classification tasks. Information Processing & Management, 45(4), 427–437. https://doi.org/10.1016/j.ipm.2009.03.002

Stetco, A., Dinmohammadi, F., Zhao, X., Robu, V., Flynn, D., Barnes, M., … Nenadic, G. (2019). Machine learning methods for wind turbine condition monitoring: A review. Renewable Energy, 133, 620–635. https://doi.org/10.1016/j.renene.2018.10.047

Şenkal, S., & Emeksiz, C. (2023). The Effect of Data Decomposition on Prediction Performance in Wind Speed Prediction with Artificial Neural Network. International Scientific and Vocational Studies Journal, 7(2), 213-223. https://doi.org/10.47897/bilmes.1406384

Tan, M., & Le, Q.V. (2019). EfficientNet: Rethinking Model Scaling for Convolutional Neural Networks. ArXiv, abs/1905.11946.

Umbaugh, S. E. (2023). Digital image processing and analysis: Computer vision and image analysis (4th ed.). CRC Press. https://doi.org/10.1201/9781003221135

Xiao, C., Liu, Z., Zhang, T., & Zhang, X. (2021). Deep Learning Method for Fault Detection of Wind Turbine Converter. Applied Sciences, 11(3), 1280. https://doi.org/10.3390/app11031280

Yang, W., Court, R., & Jiang, J. (2013). Wind turbine condition monitoring by the approach of SCADA data analysis. Renewable Energy, 53, 365–376.

Yang, W., Tavner, P. J., Crabtree, C. J., Feng, Y., & Qiu, Y. (2014). Wind turbine condition monitoring: Technical and commercial challenges. Wind Energy, 17(5), 673–693. https://doi.org/10.1002/we.1508

Zhou, Z., Siddiquee, M. M. R., Tajbakhsh, N., & Liang, J. (2018). UNet++: A nested U-Net architecture for medical image segmentation. Deep Learning in Medical Image Analysis and Multimodal Learning for Clinical Decision Support, 3–11. https://doi.org/10.1007/978-3-030-00889-5_1

Zou, L., Wang, Y., Bi, J., & Sun, Y. (2022). Damage Detection in Wind Turbine Blades Based on an Improved Broad Learning System Model. Applied Sciences, 12(10), 5164. https://doi.org/10.3390/app12105164

Chapter 2

PHOTONIC INTEGRATED CIRCUITS

İremnur DURU[1], Timuçin Emre TABARU[2]

1 Research Assistant, Department of Electrical and Electronics Engineering, Sivas University of Science and Technology, Sivas, Türkiye, ORCID: 0000-0001-5492-803X
2 Associate Professor, Department of Electrical and Electronics Engineering, Sivas University of Science and Technology, Sivas, Türkiye, ORCID: 0000-0002-1373-3620

1. Introduction

Modern high-performance computing infrastructures, including routers and large-scale data centers, are experiencing a rapidly g rowing demand for data transmission driven by cloud computing, artificial intelligence, and data-intensive applications. The electrical interconnects that constitute the fundamental communication backbone of these systems are increasingly constrained by intrinsic physical limitations, primarily arising from frequency-dependent attenuation and distance-related signal degradation. As a consequence, the bandwidth–distance product of conventional electrical interconnects is limited imposing a critical bottleneck on system scalability. (Lukashchuk et al., n.d.-a, n.d.-b)Further attempts to increase data throughput under these constraints result in a disproportionate degradation of energy efficiency, leading to power density increases (Augendre et al., n.d.)**.** This trend significantly exacerbates thermal management challenges in routers and data centers, where efficient heat dissipation has become a primary design concern. These limitations highlight the urgent need for alternative interconnection technologies capable of sustaining continued performance scaling while maintaining acceptable power and thermal budgets (Doylend et al., n.d.). In this context, silicon photonics has emerged as a compelling technological solution by enabling the co-integration of optical and electronic functionalities on a single chip-scale platform (Marchetti et al., n.d.). Leveraging its compatibility with established very-large-scale integration (VLSI) manufacturing processes, silicon photonics offers a unique combination of high bandwidth density, enhanced energy efficiency, reduced cost, and compact footprint**.** By utilizing photons rather than electrons as information carriers, silicon photonic interconnects fundamentally overcome the bandwidth and loss limitations inherent to electrical wiring, thereby providing a scalable and robust platform for next-generation communication and signal processing architectures (Koch et al., n.d.).

This chapter provides a systematic overview of the material platforms that form the foundation of Photonic Integrated Circuits (PICs)**,** followed by a detailed discussion of the key photonic components realized on these platforms. Finally, the chapter explores the system-level applications enabled by integrated photonic technologies, with particular emphasis on their role in advanced communication, computing, and emerging sensing systems.

2. Basic Platforms and Materials

Material selection plays a critical role in the design and analysis of photonic integrated circuits (PICs), as the chosen platform fundamentally determines key performance metrics such as propagation loss, component footprint, and the level of compatibility with electronic integrated circuits (Buzaverov et al., 2024; Falconi et al., n.d.; N. M. Park et al., 2001; technology & 1995, 1995). Since no single material system can simultaneously satisfy all the requirements imposed by diverse photonic applications, a variety of material platforms and integration strategies have been developed, each optimized for specific functional objectives and system-level constraints(Marshall et al., n.d.).

The silicon-on-insulator (SOI) platform constitutes the foundational technology for silicon photonics (Taghavi et al., 2022). The operating principle of this platform relies on the high refractive index contrast between the silicon core and the surrounding silicon dioxide cladding(Augendre et al., n.d.). This strong index contrast enables efficient optical confinement within waveguides featuring sub-micron cross-sectional dimensions. As a result, extremely

compact photonic components can be realized, allowing for high-density and large-scale photonic integration (Doylend et al., n.d.).

A defining advantage of silicon photonics is its inherent compatibility with complementary metal–oxide–semiconductor (CMOS) fabrication processes (Kimerling et al., n.d.). This compatibility enables the monolithic integration of photonic components alongside electronic circuits within standard CMOS manufacturing lines (Kimerling et al., n.d.). Consequently, silicon photonic systems benefit from enhanced performance, improved scalability, and significantly reduced fabrication costs, making the SOI platform a leading candidate for high-volume photonic integration.

The silicon nitride Si_3N_4 platform has emerged as a prominent alternative for applications that require exceptionally long optical propagation distances. Second-generation Si_3N_4 waveguides exhibit ultra-low propagation losses on the order of 0.007 dB/cm**,** distinguishing this material system from conventional silicon waveguides. This loss level is approximately 50 times lower than that typically observed in silicon-based waveguides (Buzaverov et al., 2024; N. M. Park et al., 2001). Owing to this remarkably low propagation loss, silicon nitride is widely preferred for the realization of high-quality-factor (Q) resonators**,** optical delay lines, and precision photonic components, where low noise, long coherence length, and high stability are critical performance requirements .

Polymer-based platforms are a method developed to overcome the fundamental limitations of traditional crystalline material systems, such as $LiNbO_3$ and III-V semiconductors, including lattice coherence constraints and fabrication challenges (Technology & 1993, n.d.-a). The unique advantages of polymers include the flexibility to fabricate them on a wide variety of substrates, such as semiconductors, insulators, and ceramics. (Technology & 1993, n.d.-b) Furthermore, the ability to control the refractive index profile during fabrication allows for the production of specialized optical devices. Polymer waveguides routinely achieve propagation losses as low as 0.1 dB/cm, making them a viable option for high-performance passive devices.

To overcome the inherent limitations of a single material system, hybrid (Elshaari et al., n.d.; Fang et al., n.d.; H. Park et al., 2008) and heterogeneous integration approaches (Conference & 2015, n.d.; Komljenovic et al., n.d.; Marshall et al., n.d.; Xiang et al., n.d.) have been adopted.

Group-IV elements—carbon (C), silicon (Si), germanium (Ge), and tin (Sn)—occupy a central role in semiconductor technology due to their four valence electrons, which enable strong covalent bonding and well-defined crystalline structures (Koch et al., n.d.). Among these materials, silicon forms the foundation of modern microelectronics and is fully compatible with mature CMOS (Complementary Metal-Oxide-Semiconductor) fabrication processes. This intrinsic compatibility makes Group-IV materials particularly attractive for large-scale electronic–photonic co-integration(technology & 1995, 1995).

A fundamental limitation of Group-IV semiconductors is their indirect bandgap nature, where the conduction band minimum and valence band maximum occur at different crystal momenta. Consequently, radiative recombination requires phonon assistance to satisfy momentum conservation, significantly reducing light-emission efficiency and making electrically pumped silicon lasers inherently challenging. Despite this limitation, Group-IV materials remain highly attractive for integrated photonics owing to their high thermal stability, abundance, low cost, and compatibility with industrial manufacturing processes.

To address the inefficiency of light emission in silicon, extensive research efforts have focused on band-structure engineering and material modification strategies. Alloying approaches such as SiGe and GeSn have been shown to modify the band structure and enable quasi-direct or direct bandgap behaviour, thereby enhancing optical gain and enabling laser action. These developments indicate that Group-IV-based materials can serve as viable alternatives to III–V semiconductors, opening new pathways toward monolithic integration in silicon photonics.

In parallel, several alternative approaches have been investigated to tailor silicon's optical properties, including porous silicon (Feng & Tsu, 1994; technology & 1995, 1995), hexagonal silicon phases (Kon et al., 2017) and silicon quantum dots (QDs) (Alice Francis et al., 2014; N. M. Park et al., 2001). Moreover, owing to silicon's relatively high Raman gain coefficient, silicon-based Raman lasers have demonstrated the ability to achieve sufficiently large optical gain under appropriate pumping conditions. Together, these strategies highlight the growing potential of IV-based heterogeneous integration for scalable and CMOS-compatible on-chip light sources.

III–V / Silicon Heterogeneous Integration

Despite significant progress in Group-IV light-emitting materials, III–V compound semiconductors remain the benchmark for efficient light generation due to their direct bandgap nature. As a result, heterogeneous integration of III–V materials with silicon photonic platforms have become a key enabling technology for high-performance photonic integrated circuits (PICs). This hybrid approach combines the superior optical gain and emission efficiency of III–V semiconductors with the low-loss waveguiding, scalability, and CMOS compatibility of silicon.

The integration of III–V materials such as InP, InGaAsP, and GaAs onto silicon enables the realization of high-performance optoelectronic devices spanning high-speed optical communications, sensing, and LiDAR systems (Liang et al., 2009; Marshall et al., n.d.; Roelkens et al., 2010a) .The primary objective of III–V/silicon heterogeneous integration is to overcome the intrinsic limitation of silicon's indirect bandgap, which fundamentally restricts the efficiency of silicon-based lasers. By incorporating III–V gain media, high optical gain and low threshold laser operation can be achieved on silicon platforms, significantly advancing the development of integrated laser sources (Nelson et al., n.d.; Yang et al., n.d.; Zander et al., 2020) In addition, wide-bandwidth, low-noise optical amplifiers can be realized through this approach (Fang et al., n.d.; H. Park et al., 2008).

From a system-level perspective, the integration of light sources directly on silicon chips is particularly transformative for on-chip LiDAR architectures, as it reduces packaging complexity, footprint, and cost while improving robustness and scalability. Recent studies consistently identify heterogeneous integration as a key enabling technology for next-generation photonic LiDAR and sensing systems (Roelkens et al., 2010b)

Among the various heterogeneous integration techniques, wafer bonding has emerged as the most widely adopted and industrially mature approach (Jo et al., n.d.; Luo et al., n.d.; Roelkens et al., n.d.) In this method, III–V epitaxial layers are bonded onto processed silicon substrates, after which the original III–V substrate is removed. Active devices such as lasers or photodetectors are then fabricated within the bonded III–V layers. Several technical variants of this approach have been reported, including direct bonding (Augendre et al., n.d.) plasma-

activated bonding (Marchetti et al., n.d.) and polymer-based bonding techniques (Taghavi et al., 2022; Technology & 1993, n.d.-a). These methods offer high optical efficiency, CMOS compatibility, and favorable thermal stability. Consequently, a large number of heterogeneous silicon laser demonstrations reported in the literature rely on wafer-bonding-based integration schemes (Augendre et al., n.d.) (Marchetti et al., n.d.) (Taghavi et al., 2022; Technology & 1993, n.d.-a).

3. Fundamental Building Blocks of PICS

The essential functional components of photonic integrated circuits (PICs) are the basic building blocks that allow light generation, manipulation, and detection on a chip-scale platform (Errando-Herranz et al., n.d.; Xiang et al., n.d.). Each of these components—optical waveguides, directional couplers, splitters, modulators, phase shifters, resonators, and photodetectors—has a specific function in managing optical signals (He et al., n.d.; Nanophotonics & 2017, 2017). The underlying material platform, waveguide geometry, and fabrication tolerances all have a significant impact on these components' performance. Together, these factors determine important metrics like insertion loss, modulation efficiency, bandwidth, and footprint. For photonic systems to be scalable and high-performing, careful co-design of individual parts and circuit architectures is therefore essential (Circuits & 2025, 2026; Doylend et al., n.d.; Lukashchuk et al., n.d.-a).

4. Integration Strategies

Integration strategies are key in determining the functionality, scalability and manufacturability of photonic integrated circuits. Different approaches - namely monolithic (Mekis et al., n.d.), heterogeneous (Conference & 2015, n.d.; Marshall et al., n.d.) and hybrid integration (Elshaari et al., n.d.; Fang et al., n.d.; H. Park et al., 2008; Peyrou, 2023) have been developed to combine photonic and electronic components in a single system, depending on the requirements of the application. Monolithic integration allows for high density integration and fabrication simplicity, but is constrained by material constraints, while heterogeneous integration allows for integration of different materials, such as silicon III-V semiconductors, to increase performance. Hybrid integration offers design flexibility by combining separately optimised components, but at the cost of increasing the complexity of packaging. The choice of the appropriate integration strategy involves trade-offs between performance, yield, costs and complexity at the level of the system.

5. Conclusion

Photonic integrated circuits are a transformative technology which address the fundamental limitations of conventional electronic systems by exploiting the unique advantages of signal processing based on light. Thanks to advances in material platforms, component design and integration strategies, PICs are becoming compact, energy-efficient and scalable solutions for a wide range of applications, including high-speed communications, signal processing and the emerging sensing systems. As fabrication technologies mature and integration with electronics continues to advance, photonic integrated circuits are expected to play an increasingly important role in architectures for next generation information processing and sensing.

REFERENCES

Alice Francis, A., Mohan, S., Koech, P. K., -, al, Kong, L., Wang, J., & Zhang, Y. (2014). Silicon quantum dots: surface matters. *Iopscience.Iop.Org*, *26*, 173201. https://doi.org/10.1088/0953-8984/26/17/173201/META

Augendre, E., Fedeli, J., … D. B.-2010 P., & 2010, undefined. (n.d.). Direct bonding for silicon photonics. *Ieeexplore.Ieee.OrgE Augendre, JM Fedeli, D Bordel, BB Bakir, C Kopp, L Grenouillet, JM Hartmann, J Harduin2010 Photonics Global Conference, 2010•ieeexplore.Ieee.Org*. Retrieved November 21, 2025, from https://ieeexplore.ieee.org/abstract/document/5705965/

Buzaverov, K. A., Baburin, A. S., Sergeev, E. V., Avdeev, S. S., Lotkov, E. S., Bukatin, S. V., Stepanov, I. A., Kramarenko, A. B., Amiraslanov, A. S., Kushnev, D. V., Ryzhikov, I. A., & Rodionov, I. A. (2024). Silicon nitride integrated photonics from visible to mid-infrared spectra. *Wiley Online Library*, *18*(12). https://doi.org/10.1002/LPOR.202400508

Circuits, Y. Y.-F. 2D to 3D P. I., & 2025, undefined. (2026). Fundamentals of Photonic Integrated Circuits. *Springer*, 17–31. https://doi.org/10.1007/978-3-031-91508-6_2

Conference, J. B.-2015 O. F. C., & 2015, undefined. (n.d.). Heterogeneous silicon III–V Photonic Integrated Circuits. *Ieeexplore.Ieee.Org*. Retrieved November 14, 2025, from https://ieeexplore.ieee.org/abstract/document/7121893/

Doylend, J., XV, S. G.-S. P., & 2020, undefined. (n.d.). An overview of silicon photonics for LIDAR. *Spiedigitallibrary.Org*. https://doi.org/10.1117/12.2544962.SHORT

Elshaari, A., Pernice, W., Srinivasan, K., photonics, O. B.-…, & 2020, undefined. (n.d.). Hybrid integrated quantum photonic circuits. *Nature.Com*. Retrieved December 24, 2025, from https://idp.nature.com/authorize/casa?redirect_uri=https://www.nature.com/articles/s41566-020-0609-x&casa_token=WbHE6aULp-UAAAAA:1YP39WlQu0f-5oit90c8rvUvyHz0e1XhiLp_ggILNksaBjpmcYFFAGPMFW88z55aZTB0ihAM4gw2Rg

Errando-Herranz, C., … A. T.-I. J. of, & 2019, undefined. (n.d.). MEMS for photonic integrated circuits. *Ieeexplore.Ieee.Org*. Retrieved December 24, 2025, from https://ieeexplore.ieee.org/abstract/document/8847362/

Falconi, F., Melo, S., Scotti, F., … M. M.-J. of L., & 2020, undefined. (n.d.). A combined radar & lidar system based on integrated photonics in silicon-on-insulator. *Ieeexplore.Ieee.Org*. Retrieved December 24, 2025, from https://ieeexplore.ieee.org/abstract/document/9195117/?casa_token=5aKYWInAnHsAAAAA:COydVK7uruYM_s-wArDrI2kEf8p9_3YCCoOxbXol_P2OcjfOrYFwmCgnRWiGckg5C6yWX2zc0Q

Fang, A., Park, H., Kuo, Y., Jones, R., Cohen, O., today, D. L.-M., & 2007, undefined. (n.d.). Hybrid silicon evanescent devices. *Elsevier*. Retrieved November 21, 2025, from https://www.sciencedirect.com/science/article/pii/S1369702107701773

Feng, Z., & Tsu, R. (1994). *Porous silicon*. https://books.google.com/books?hl=tr&lr=&id=h0TYnv63Qb0C&oi=fnd&pg=PA3&dq=porous+silicon&ots=VhwWeUXm_u&sig=2Ftj9zF3uODqOAqFQ4F0LwC8lhg

He, J., Dong, T., Access, Y. X.-I., & 2020, undefined. (n.d.). Review of photonic integrated optical phased arrays for space optical communication. *Ieeexplore.Ieee.Org*. Retrieved November 14, 2025, from https://ieeexplore.ieee.org/abstract/document/9222022/

Isaac, B., Song, B., Pinna, S., … L. C.-I. J. of, & 2019, undefined. (n.d.). Indium phosphide photonic integrated circuit transceiver for FMCW LiDAR. *Ieeexplore.Ieee.Org*. Retrieved November 14, 2025, from https://ieeexplore.ieee.org/abstract/document/8693564/

Jo, G., Edinger, P., Bleiker, S., … X. W.-P., & 2022, undefined. (n.d.). Wafer-level hermetically sealed silicon photonic MEMS. *Opg.Optica.Org*. Retrieved November 21, 2025, from https://opg.optica.org/abstract.cfm?uri=prj-10-2-a14

Kimerling, L., Ahn, D., Apsel, A., photonics, M. B.-…, & 2006, undefined. (n.d.). Electronic-photonic integrated circuits on the CMOS platform. *Spiedigitallibrary.Org*. https://doi.org/10.1117/12.654455.SHORT

Koch, T., Electronics, U. K.-I. J. of Q., & 2002, undefined. (n.d.). Semiconductor photonic integrated circuits. *Ieeexplore.Ieee.Org*. Retrieved December 24, 2025, from https://ieeexplore.ieee.org/abstract/document/81373/?casa_token=Xv5thxYeA7IAAAAA:QIKJfpJI6Z7PNVciS7sRdVu-0IuUT-IdLndRMGlkl2J2MM28JORbq-FMd_nVy138jv6AIpAVoQ

Komljenovic, T., Huang, D., … P. P.-P. of the, & 2018, undefined. (n.d.). Photonic integrated circuits using heterogeneous integration on silicon. *Ieeexplore.Ieee.Org*. Retrieved December 24, 2025, from https://ieeexplore.ieee.org/abstract/document/8451879/?casa_token=kM5DoXBWeAIAAAAA:zXTjlYqPhHCLPNKSDPFAD7dQgFUwpgi9fjYkRRXxFPB5BdscP4vL3BvuBNDDfUxYUo0ntSF1uQ

Kon, H., Hauge, I. T., Verheijen, M. A., Conesa-Boj, S., Etzelstorfer, T., Watzinger, M., Kriegner, D., Zardo, I., Fasolato, C., Capitani, F., Postorino, P., Kö, S., Li, A., Assali, S., Stangl, J., & Bakkers, E. P. A. M. (2017). Single-crystalline hexagonal silicon–germanium. *ACS Publications*, *17*(1), 85–90. https://doi.org/10.1021/ACS.NANOLETT.6B03488

Liang, D., Letters, J. B.-E., & 2009, undefined. (2009). Photonic integration: Si or InP substrates? *IETD Liang, JE BowersElectronics Letters, 2009•IET*, *45*(12), 578–581. https://doi.org/10.1049/EL.2009.1279

Liang, D., Manufacturing, J. B.-L. A., & 2021, undefined. (2021). Recent progress in heterogeneous III-V-on-silicon photonic integration. *Light-Am.Com*, *2*(1). https://doi.org/10.37188/LAM.2021.005

Lukashchuk, A., Yildirim, H., … A. B.-N., & 2024, undefined. (n.d.-a). Photonic-electronic integrated circuit-based coherent LiDAR engine. *Nature.Com*. Retrieved December 24, 2025, from https://www.nature.com/articles/s41467-024-47478-z

Lukashchuk, A., Yildirim, H., … A. B.-N., & 2024, undefined. (n.d.-b). Photonic-electronic integrated circuit-based coherent LiDAR engine. *Nature.Com*. Retrieved December 24, 2025, from https://www.nature.com/articles/s41467-024-47478-z

Luo, X., Cheng, Y., Song, J., … T. L.-I. J. of, & 2016, undefined. (n.d.). Wafer-scale die-to-wafer transfer bonding technology for hybrid III/V-on-silicon photonic integrated circuit application. *Ieeexplore.Ieee.Org*. Retrieved November 21, 2025, from https://ieeexplore.ieee.org/abstract/document/7452540/

Marchetti, R., Lacava, C., Carroll, L., … K. G.-P., & 2019, undefined. (n.d.). Coupling strategies for silicon photonics integrated chips. *Opg.Optica.Org*. Retrieved November 21, 2025, from https://opg.optica.org/abstract.cfm?uri=prj-7-2-201

Marshall, O., Hsu, M., Wang, Z., … B. K.-P. of the, & 2018, undefined. (n.d.). Heterogeneous integration on silicon photonics. *Ieeexplore.Ieee.OrgO Marshall, M Hsu, Z Wang, B Kunert, C Koos, D Van ThourhoutProceedings of the IEEE, 2018•ieeexplore.Ieee.Org*. Retrieved November 21, 2025, from https://ieeexplore.ieee.org/abstract/document/8453029/

Mekis, A., Abdalla, S., … B. A.-… I. C., & 2008, undefined. (n.d.). Monolithic integration of photonic and electronic circuits in a CMOS process. *Spiedigitallibrary.Org*. https://doi.org/10.1117/12.766815.SHORT

Nanophotonics, M. H.-, & 2017, undefined. (2017). Highly integrated optical phased arrays: photonic integrated circuits for optical beam shaping and beam steering. *Degruyterbrill.Com*, *6*(1), 93–107. https://doi.org/10.1515/NANOPH-2015-0152/HTML

Nelson, R., Semimetals, N. D.-S. and, & 1985, undefined. (n.d.). Review of InGaAsP/InP laser structures and comparison of their performance. *Elsevier*. Retrieved November 21, 2025, from https://www.sciencedirect.com/science/article/pii/S0080878408630409

Park, H., Fang, A. W., Liang, D., Kuo, Y. H., Chang, H. H., Koch, B. R., Chen, H. W., Sysak, M. N., Jones, R., & Bowers, J. E. (2008). Photonic integration on the hybrid silicon evanescent device platform. *Wiley Online Library*, 17. https://doi.org/10.1155/2008/682978

Park, N. M., Choi, C. J., Seong, T. Y., & Park, S. J. (2001). Quantum confinement in amorphous silicon quantum dots embedded in silicon nitride. *APS*, *86*(7), 1355–1357. https://doi.org/10.1103/PHYSREVLETT.86.1355

Peyrou, M. (2023). *Design and testing of hybrid InP/Si photonic integrated components/circuits for LIDAR applications*. https://theses.hal.science/tel-04145296/

Roelkens, G., Campenhout, J. Van, Today, J. B.-M., & 2007, undefined. (n.d.). III-V/Si photonics by die-to-wafer bonding. *Elsevier*. Retrieved November 21, 2025, from https://www.sciencedirect.com/science/article/pii/S1369702107701785

Roelkens, G., Liu, L., Liang, D., Jones, R., Fang, A., Koch, B., & Bowers, J. (2010a). III-V/silicon photonics for on-chip and intra-chip optical interconnects. *Wiley Online LibraryG Roelkens, L Liu, D Liang, R Jones, A Fang, B Koch, J BowersLaser & Photonics Reviews, 2010•Wiley Online Library*, *4*(6), 751–779. https://doi.org/10.1002/LPOR.200900033

Roelkens, G., Liu, L., Liang, D., Jones, R., Fang, A., Koch, B., & Bowers, J. (2010b). III-V/silicon photonics for on-chip and intra-chip optical interconnects. *Wiley Online LibraryG Roelkens, L Liu, D Liang, R Jones, A Fang, B Koch, J BowersLaser & Photonics Reviews, 2010•Wiley Online Library*, *4*(6), 751–779. https://doi.org/10.1002/LPOR.200900033

Taghavi, I., Moridsadat, M., Tofini, A., Raza, S., Jaeger, N. A. F., Chrostowski, L., Shastri, B. J., & Shekhar, S. (2022). Polymer modulators in silicon photonics: review and projections. *Degruyterbrill.Com*, *11*(17), 3855–3871. https://doi.org/10.1515/NANOPH-2022-0141/HTML

technology, B. H.-S. science and, & 1995, undefined. (1995). Porous silicon. *Iopscience.Iop.Org*, *10*, 1187–1207. https://doi.org/10.1088/0268-1242/10/9/001/META

Technology, R. C.-O. & L., & 1993, undefined. (n.d.-a). Polymer-based photonic integrated circuits. *Elsevier*. Retrieved November 21, 2025, from https://www.sciencedirect.com/science/article/pii/003039929390001V

Technology, R. C.-O. & L., & 1993, undefined. (n.d.-b). Polymer-based photonic integrated circuits. *Elsevier*. Retrieved December 24, 2025, from https://www.sciencedirect.com/science/article/pii/003039929390001V

Xiang, C., Jin, W., Huang, D., … M. T.-I. J. of, & 2021, undefined. (n.d.). High-performance silicon photonics using heterogeneous integration. *Ieeexplore.Ieee.Org*. Retrieved November 14, 2025, from https://ieeexplore.ieee.org/abstract/document/9609553/

Yang, G., Liu, T., Li, J., Chen, B., Sensors, C. T.-, & 2025, undefined. (n.d.). High-Speed and Broadband InGaAs/InP Photodiode with InGaAsP Graded Bandgap Layers. *Mdpi.Com*. Retrieved November 21, 2025, from https://www.mdpi.com/1424-8220/25/9/2841

Zander, M., Rehbein, W., Moehrle, M., Breuer, S., Franke, D., Schell, M., Kolpatzeck, K., & Balzer, J. C. (2020). High performance BH InAs/InP QD and InGaAsP/InP QW mode-locked lasers as comb and pulse sources. *Opg.Optica.Org*. https://opg.optica.org/abstract.cfm?uri=ofc-2020-T3C.4

Chapter 3

PHASE-ONLY NULLING OF LINEAR ANTENNA ARRAYS FOR 6G WIRELESS COMMUNICATION USING HONEY FORMATION OPTIMIZATION

Ali Akdagli[1] , Ali Yildiz[2], Filiz Karaomerlioglu[3]

1 Prof. Dr. Ali AKDAGLI, ORCID: [0000-0003-3312-992X].
2 Assoc. Prof. Ali YILDIZ, ORCID: [0000-0003-3904-6017].
3 Assist. Prof. Filiz KARAOMERLIOGLU, ORCID: [0000-0002-4677-4365].
Department of Electrical and Electronics Engineering, Mersin University, Ciftlikkoy Mersin/Turkey.

1. Introduction

The rapid evolution toward sixth-generation (6G) wireless networks is driving stringent requirements on capacity, coverage, latency, and robustness. These goals necessitate advanced antenna architectures, such as phased arrays and digital arrays, operating with intelligent beamforming and adaptive spatial processing. In particular, base station antenna arrays play a central role in increasing network capacity, improving link throughput, and reducing inter-user interference by controlling the radiation pattern in space.

Linear antenna arrays, due to their structural simplicity and accurate beam steering capability, are widely used as fundamental building blocks in 5G and emerging 6G infrastructures. However, in dense deployment scenarios, these arrays must support adaptive main beams while simultaneously forming deep and accurately placed nulls in the directions of interference sources. This dual requirement is critical for maintaining Quality of Service (QoS), suppressing co-channel interference and jamming, and ensuring acceptable signal-to-noise ratios in practical systems.

A large body of research has been devoted to antenna pattern synthesis with interference suppression through deep null generation in prescribed directions (Abdulqader et al., 2020; Aljaf & Mohammed, 2023; Bhattacharyya, 2025). These techniques are applicable not only to wireless communication but also to radar and sonar systems. In many modern applications, wide null regions are required rather than narrow, single-angle nulls, especially when interferers have uncertain or time-varying directions of arrival (Bhattacharyya, 2025; Jin et al., 2025). In such cases, narrow nulls would require continuous real-time adjustment, which complicates system design and increases computational burden.

Conventional null steering techniques can be categorized according to the array parameter being controlled: complex weights (both amplitude and phase), amplitude-only, phase-only, or element positions. The main objective is to preserve the main beam gain towards the intended user or target while producing deep nulls towards interferers. Amplitude-only control, realized through networks of attenuators, is straightforward but less flexible and may lead to non-uniform power distribution (Aljaf & Mohammed, 2023; Dib et al., 2010). Phase-only and position-only controls generally lead to nonlinear optimization problems that lack closed-form solutions. Linearization approaches can be applied under small phase-perturbation assumptions, but these usually restrict the ability to place symmetric nulls around the main beam. On the other hand, position-only control can achieve symmetric nulling but requires mechanical actuators such as servomotors for real-time adjustment, which increases implementation complexity (Dib et al., 2010).

Phase-only control is particularly attractive for phased arrays because phase shifters are already integral components in the beamforming network. No additional RF hardware is required, and existing control mechanisms can be exploited (Guney et al., 2008; He et al., 2022). However, the resulting optimization problem remains highly nonlinear and multimodal. Traditional gradient-based optimization algorithms are extremely sensitive to the choice of initial solution and may easily converge to local minima, especially in high-dimensional design spaces.

To address these difficulties, artificial intelligence (AI)-based metaheuristic algorithms have been widely adopted for antenna array synthesis, including null steering and sidelobe suppression. Popular

methods include Genetic Algorithms (GA), Particle Swarm Optimization (PSO), Differential Search (DS), Grey Wolf Optimization (GWO), Moth–Flame Optimization (MFO), Whale Optimization Algorithm (WOA), and various hybrid or improved versions (Chakraborty et al., 2024; Durmus et al., 2021; Kumar & Singh, 2023; Poddar et al., 2022; Sharma, 2023). Although these algorithms have demonstrated good performance, there remains a need for robust optimizers offering high solution accuracy and fast convergence without excessive parameter tuning.

Honey Formation Optimization (HFO) is a more recent nature-inspired metaheuristic that emulates the biological process of honey formation in bee colonies (Yetgin & Abaci, 2021; Yetgin & Şamdan, 2021). The original HFO framework adopts a multi-component structure, while a later variant termed HFO-1 (Honey Formation Optimization with Single Component, HFOSC) simplifies the algorithm by allowing each candidate solution to evolve independently (Yetgin & Ercan, 2023). Benchmark studies on 60 standard test functions have shown that HFOSC can outperform PSO, DS, MFO, WOA, and Improved Grey Wolf Optimizer (IGWO) in terms of both accuracy and convergence speed (Yetgin & Şamdan, 2021).

In this chapter, the HFOSC algorithm is employed for the synthesis of linear antenna arrays under phase-only control. The amplitudes and element positions are kept fixed, and only the excitation phases are optimized. The cost function is designed to account for multiple pattern requirements, including sidelobe level and null depth, with appropriate weighting to enforce design priorities. The proposed methodology is applied to a 25-element, half-wavelength spaced linear array at 28 GHz, synthesized to follow a 25 dB Chebyshev pattern. Additional constraints are imposed to realize various configurations: single narrow null, deeper single null, dual nulls, triple nulls, and a broad null sector. A final example investigates the sensitivity of null depth to phase-quantization errors.

The numerical results demonstrate that the HFOSC algorithm can obtain robust solutions that simultaneously satisfy stringent interference suppression criteria, maintain the main beam characteristics, and preserve the general Chebyshev sidelobe profile. Owing to its phase-only control and high effectiveness, the proposed approach is well suited for interference cancellation and anti-jamming functions in emerging 6G communication systems and other advanced wireless applications.

2. Problem Formulation

This section summarizes the mathematical model of the linear antenna array and introduces the optimization-based pattern synthesis framework used for phase-only nulling.

2.1 Array Factor of a Linear Array

Consider a linear antenna array consisting of $(2N+1)$ isotropic radiating elements placed symmetrically about the array center. The far-field array factor in the azimuth plane, for angles $\theta \in [-90°, 90°]$ measured from the broadside direction, can be written as

$$AF(\theta) = \sum_{n=-N}^{N} a_n e^{jnkd_n sin(\theta)} \qquad -90^o \leq \theta \leq 90^o \qquad (1)$$

where a_n is the excitation amplitude of n-th element; d_n is the position of the n-th element measured from the array center; $k=2\pi/\lambda$ is the wavenumber, with λ denoting the wavelength; θ is the observation angle with respect to broadside.

In this work, the geometry is fixed as a 25-element linear array with half-wavelength spacing. The amplitude distribution is fixed to generate an initial 25 dB Chebyshev pattern. Thus, the only design variables are the excitation phases of the elements.

2.2 Cost Function for Pattern Nulling

The synthesis of the desired array radiation pattern is formulated as a numerical optimization problem. The objective is to minimize the discrepancy between the obtained array factor and a desired pattern, subject to constraints on null depths in specific directions.

Let $AF_o(\theta)$ be the array factor of the current solution, and $AF_d(\theta)$ be the desired array factor. A scalar cost function is defined as

$$C = |AF_o(\theta) - AF_d(\theta)| + ENDL \qquad (2)$$

where *ENDL* represents an additional term enforcing the required null depth at selected angular positions. The desired pattern $AF_d(\theta)$ is typically chosen as the initial Chebyshev pattern, except at specific nulling angles where strong suppression is required. For a single nulling angle θ_{na}, the desired array factor is defined piecewise as

$$AF_d(\theta) = \begin{cases} 0, & \text{if } \theta = \theta_{na} \\ \text{Initial Chebyshev pattern}, & \text{otherwise} \end{cases}$$

This piecewise definition localizes the required suppression to the chosen sidelobe peak, enabling the rest of the pattern to remain close to the original Chebyshev response. To avoid unnecessary penalization once a sufficient null depth is achieved, a threshold-based error term is introduced:

$$ENDL = \begin{cases} 0, & if\ AF_o(\theta_{na}) \leq NDL \\ 100, & otherwise \end{cases}$$

where *NDL* is the null depth level, specified in dB (e.g., −130 dB, −180 dB). When multiple nulls are required, *ENDL* is extended to include every nulling direction, or to integrate over a target angular sector in the case of broad nulls.

By minimizing this cost function, the HFOSC algorithm searches for the set of excitation phases that generate the desired nulls while preserving the main beam and sidelobe characteristics of the reference Chebyshev pattern as closely as possible.

3. Honey Formation Optimization with Single Component (HFOSC)

This section describes the HFOSC algorithm used to solve the phase-only nulling problem. HFOSC is a single-component variant of the Honey Formation Optimization framework and is designed to provide efficient exploration and exploitation of the search space.

3.1 Overview of Honey Formation Optimization

Honey Formation Optimization (HFO) is a metaheuristic algorithm inspired by the biological process by which bees produce honey from nectar (Yetgin & Abaci, 2021; Yetgin & Şamdan, 2021). In natural colonies, nectar collected from flowers undergoes multi-stage processing and refinement involving enzymatic reactions, mixing, and repeated transfer among worker bees. Over time, the nectar's chemical composition and water content are adjusted until mature honey is produced.

The original HFO algorithm models this process using multiple components that interact and exchange information. Each component corresponds to a group or phase in the honey formation process. While this multi-component structure can be powerful, it also introduces additional algorithmic complexity and computational overhead.

To address these issues, Yetgin and Ercan (2023) proposed a single-component variant, referred to as HFO-1 or Honey Formation Optimization with Single Component (HFOSC). In HFOSC, each candidate solution (or "source") evolves independently, which simplifies implementation and reduces computational cost while preserving the key mechanisms of HFO.

3.2 Single-Component Framework and Solution States

In HFOSC, the search is performed by a population of sources (candidate solutions). Each source encodes a possible set of design variables—in this case, the excitation phases of the antenna elements. The algorithm progresses through several conceptual stages:

1. **Initialization**
   - A population of sources is randomly generated within the allowed phase range.
   - The global best solution (Gbest) and personal best solutions (Pbest) are initialized from the initial population.
2. **Quality States**

   Each source passes through three quality states:
   - **Raw**: Initial or low-quality solutions.
   - **Semi-mature**: Solutions that have improved but not converged.
   - **Mature**: Solutions that have stabilized in terms of fitness.

   Transitions between these states are controlled by monitoring fitness improvements across iterations.

3. **Mixing Phases**

   HFOSC employs a multi-stage mixing process, consisting of Mixing-0, Mixing-1, and Mixing-2.

   - **Mixing-0** mimics the initial ingestion and basic processing of nectar and corresponds to a local search around the current source.
   - **Mixing-1** and
   - **Mixing-2** model more advanced mixing and refinement phases, where solutions exchange information and combine promising characteristics.

4. **Maturation and Saturation**

   - When the fitness of a source does not significantly improve over a predefined number of iterations, it is classified as mature.
   - A saturation mechanism is then activated. During saturation, the Best Global Solution (BGS) is injected into the population to act as a catalyst and accelerate convergence.

3.3 Algorithmic Skeleton

The general operation of HFOSC can be summarized as follows (Ercan et. al., 2025):

1. **Initialize sources**

   - Generate initial sources and evaluate their fitness.
   - Set Gbest← to the best among the initial sources.
   - Set *Pbest*← to the best solution for each source.

2. **Iterative Optimization**

   - For each worker (source), perform local exploitation using Mixing-0-like operations.
   - For each onlooker, select a source based on its fitness and further exploit it.
   - If the algorithm is in a mixing phase, apply Mixing-1 and Mixing-2 operations to combine honey forms (solutions), ensuring that the current Pbest is not degraded.
   - If a maturation phase is reached, reinitialize sources and mark a new exploration site.
   - If in saturation, inject Gbest into a randomly selected source to spread high-quality information without collapsing diversity.

3. **Adaptive Mechanisms**

   - If Gbest is not improved for an entire maturation period, adjust the mixing sizes and parameters to enhance exploration and escape potential local minima.

4. **Termination**

   - The algorithm repeats the above steps until the maximum number of iterations is reached or a convergence criterion based on the cost function is satisfied.

Due to its adaptive mixing, maturation, and saturation mechanisms, HFOSC effectively balances exploration and exploitation. Benchmark results have shown that HFOSC can achieve rapid convergence and high solution quality, making it a suitable candidate for complex optimization tasks such as antenna array pattern synthesis (Yetgin & Ercan, 2023).

4. Numerical Results and Discussion

To examine the performance of HFOSC for phase-only null steering, six numerical examples are presented. All examples consider a 25-element linear array with half-wavelength spacing operating at 28 GHz. The initial pattern is a 25 dB Chebyshev pattern, and the goal is to impose various nulling constraints while preserving the main beam and sidelobe characteristics, as shown in Figure 1.

The pattern synthesis and optimization are implemented in Python. The radiation pattern is sampled at an angular resolution of 0.25° over the interval [−90°, 90°]. All simulations are performed on a computer with a 10th-generation Intel Core i5 processor and 16 GB of RAM. Convergence is typically achieved within 3–6 minutes.

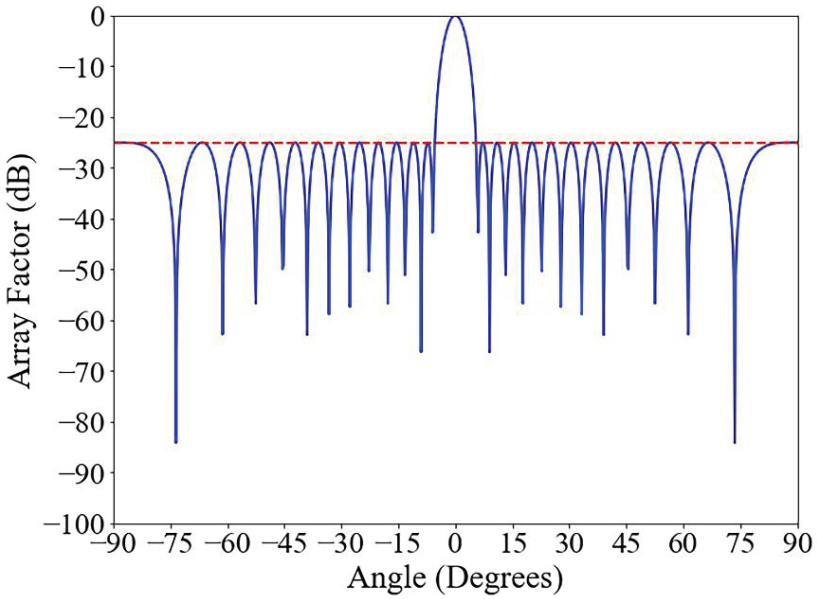

Figure 1 The initial 25-dB Chebyshev pattern

4.1 Example 1: Single Null at a Sidelobe Peak

In the first example, a single narrow null is required in the array radiation pattern. The nulling direction θ_{na}=20.25° corresponds to the fourth sidelobe peak on the right side of the initial Chebyshev pattern.

The desired pattern is specified by setting $AF_d(\theta_{na})=0$, while the remaining angles follow the Chebyshev response. The null depth threshold *NDL* is set to −130 dB. The HFOSC algorithm optimizes the excitation phases while keeping the amplitudes and positions fixed.

The resulting pattern achieves a null depth of −131.6 dB at $\theta_{na}=20.25°$. As depicted in Figure 2, the main lobe width and half-power beamwidth (HPBW) remain almost identical to those of the original Chebyshev pattern, indicating that the phase-only adjustment has minimal impact on the primary beam. Owing to the constant amplitude constraint, some increase in the sidelobe level is observed at the angle symmetric to the nulling direction, reflecting energy redistribution in the pattern.

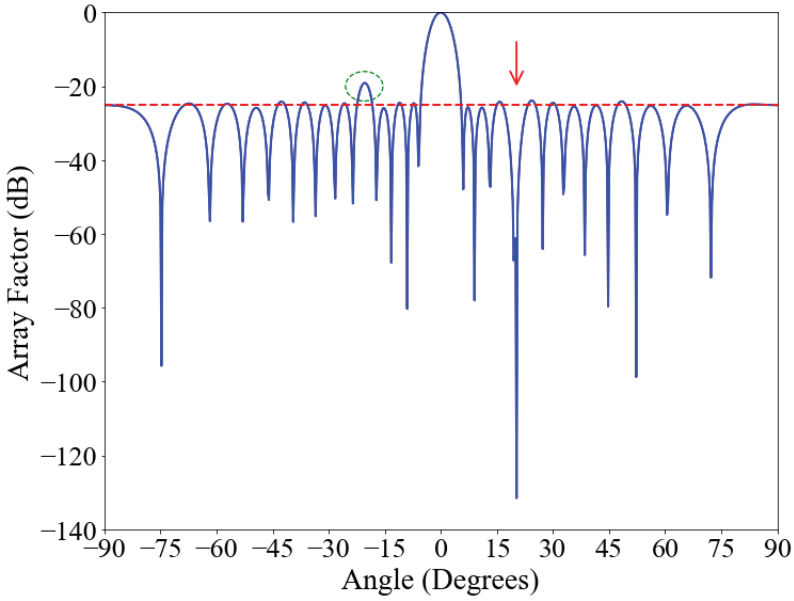

Figure 2 The array factor obtained having a single null at 20.25°

4.2 Example 2: Deeper Single Null

The second example illustrates the capability of HFOSC to realize deeper nulls by tightening the null depth requirement. The scenario is identical to Example 1, except that *NDL* is reduced from −130 dB to −180 dB. The optimization procedure is repeated, using the same array and pattern specifications.

The new pattern exhibits a significantly deeper null at $\theta_{na}=20.25°$, with a null depth reaching approximately −181.8 dB (within numerical and computational limits). The main beam width and HPBW remain close to the initial Chebyshev values, demonstrating that the algorithm can enhance null depth without compromising the main lobe. The resulting radiation pattern is illustrated in Figure 3. This example confirms the flexibility of the proposed approach: by adjusting the null depth threshold in the cost function, the designer can tradeoff between null depth and secondary pattern attributes as needed.

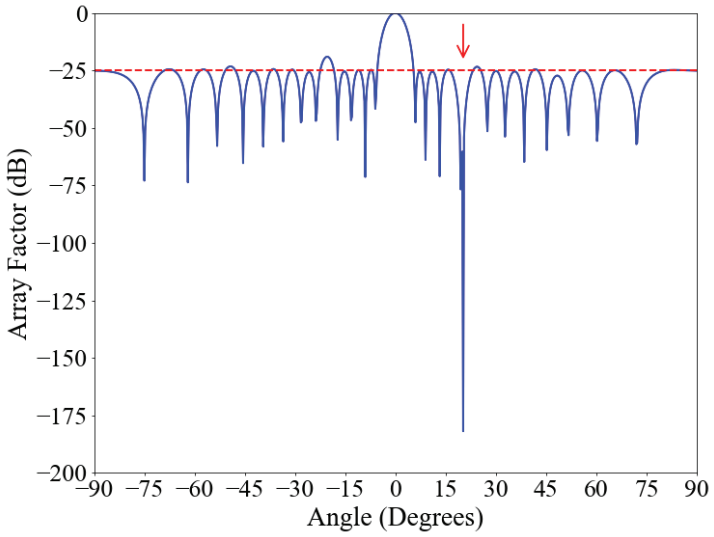

Figure 3 The array factor obtained having a single null at 20.25° with deeper null

4.3 Example 3: Dual Nulls

In the third example, dual nulls are imposed at two sidelobe peaks: −30.5° and 20.25°. These angles correspond to the sixth sidelobe peak on the left side and the fourth sidelobe peak on the right side of the Chebyshev pattern, respectively. The desired pattern is defined to set the array factor to zero at these two angles and to follow the Chebyshev pattern elsewhere. The HFOSC algorithm optimizes the excitation phases to satisfy both nulling constraints simultaneously.

The resulting radiation pattern successfully exhibits deep nulls at both −30.5° and 20.25°. The null depths are approximately −134.8 dB and −130.5 dB, respectively. The main beam width and HPBW remain close to the original pattern, demonstrating that multi-null steering is feasible with phase-only control under constant amplitude constraints. The resulting radiation pattern with nulls at these specified angles is shown in Figures 4.

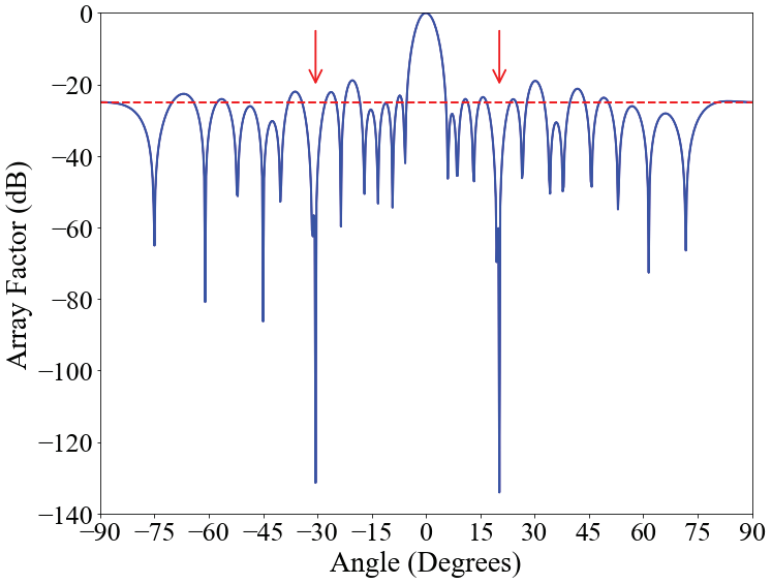

Figure 4 The array factor obtained with double nulls at -30.5° and 20.25°

4.4 Example 4: Triple Nulls

The fourth example further extends the null steering capability to triple nulls. In this case, nulls are required at −30.5°, 20.25°, and 42.0°, which coincide with the sixth sidelobe peak on the left and the fourth and eighth sidelobe peaks on the right. The HFOSC-based synthesis yields a pattern with deep nulls at all three designated angles. The achieved null depths are approximately -132.2 dB at −30.5 °, -132.8 dB at 20.25 °, and -132.9 dB at 42.0 ° in Figure 5. The main beam characteristics remain very close to those of the initial Chebyshev pattern, and the HPBW is largely preserved. These results highlight the ability of the proposed phase-only HFOSC method to handle multiple nulls without destabilizing the main beam.

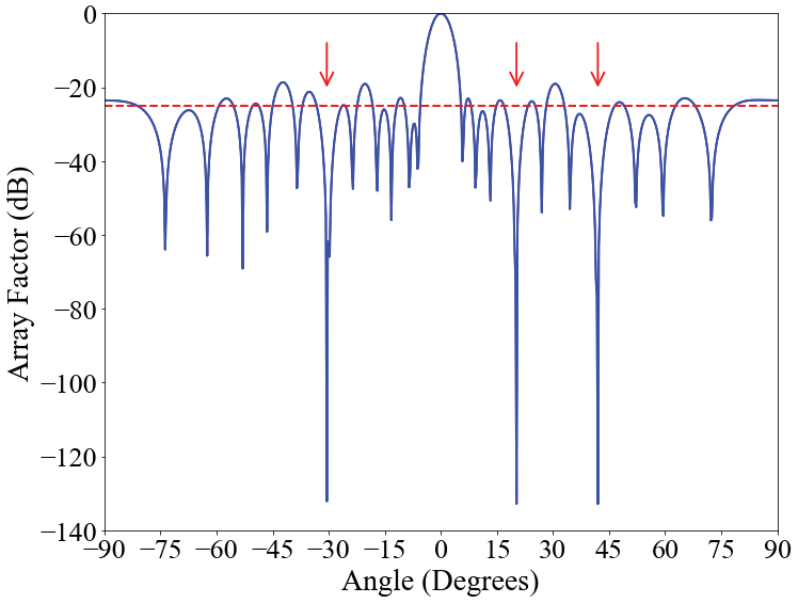

Figure 5 The array factor obtained with triple nulls at -30.5°, 20.25°, and 42.0°

4.5 Example 5: Broad Null Sector

In many practical scenarios, interferers may not be confined to a single direction but instead occupy a spatial region with uncertain or slowly varying angular positions. To handle such cases, the fifth example aims to generate a broad null over a predefined angular sector. A null sector centered at 20.25° with Δθ=5° is considered, leading to the angular interval [17.75° - 22.75°]. The null depth threshold *NDL* is set to −65 dB throughout this sector.

The HFOSC-optimized pattern achieves a null depth of approximately −65 dB or lower across the entire specified region. The sampled null depths at various points within the sector include:

- −66.8 dB at 17.75°
- −66.9 dB at 18.25°
- −67.5 dB at 18.75°
- −99.7 dB at 19.25°

- −65.6 dB at 20.25°
- −66.6 dB at 22.75°

which confirms that the desired broad null is maintained with robust suppression within the target sector, as shown in Figure 6. The main beam remains centered at broadside, and the HPBW stays close to the original Chebyshev design.

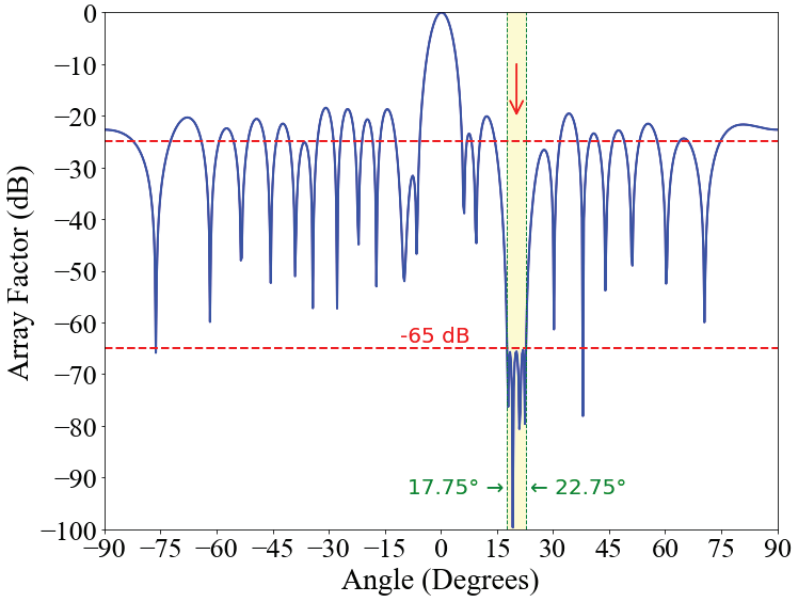

Figure 6 The array factor obtained with a broad null at 17.75° - 22.75°

4.6 Example 6: Sensitivity to Phase Quantization

The final example investigates the sensitivity of null depth to phase quantization or rounding errors, which are unavoidable in practical phase shifter implementations. Starting from the optimized phases obtained in Example 1, each phase value is rounded to two decimal places (in degrees). The radiation pattern corresponding to these quantized phases is then evaluated in Figure 7.

The resulting pattern preserves the overall shape of the original design and maintains the main beam and sidelobe distribution with minimal visual differences. However, the null depth at θ_{na}=20.25° is degraded from −131.6 dB to approximately −117.7 dB.

This example highlights a key practical consideration: the high null depths achievable by HFOSC and phase-only control are sensitive to fine phase variations. In real implementations, the resolution and accuracy of phase shifters must be accounted for during the design stage, particularly when very deep nulls are required. Nevertheless, the residual null depth of around −118 dB is still more than sufficient for most wireless communication and interference mitigation applications.

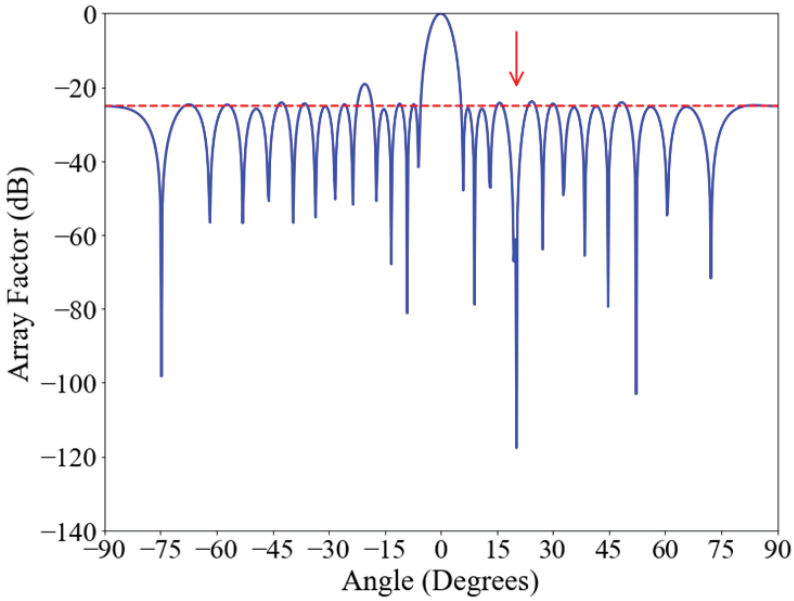

Figure 7 Effect of rounding phase weights to two decimal places on the radiation pattern of the first example.

4.7 Element Amplitudes, Phases, and Performance Metrics

Table 1 lists the element amplitudes of the initial 25 dB Chebyshev pattern and the optimized excitation phases obtained by HFOSC for the patterns corresponding to Examples 1–6. Each row corresponds to a pair of symmetric elements with odd phase symmetry about the array center.

Table 1 Element amplitudes of the initial Chebyshev pattern and HFOSC-computed phases (in degrees) for the patterns in Examples 1–6.

Index	Amplitudes of Initial Chebyshev Pattern	Computed Phases with HFOSC Algorithm					
n	Figure 1	Figure 2	Figure 3	Figure 4	Figure 5	Figure 6	Figure 7
0	1.00000	0.00000	0.00000	0.00000	0.00000	0.00000	0.00
± 1	0.99235	4.84287	3.87219	-3.88683	4.40151	-2.39680	4.84
± 2	0.96966	4.03679	5.87914	7.85459	1.48229	-7.48671	4.04
± 3	0.93274	0.78237	-1.57907	3.84355	10.24075	-11.03434	0.78
± 4	0.88288	-4.81264	-5.79238	-9.68588	-2.98663	3.94914	-4.81
± 5	0.82180	-5.50508	-2.87112	-10.66799	-13.12204	2.24415	-5.51
± 6	0.75159	2.37352	1.01153	8.10296	3.99307	-0.74992	2.37
± 7	0.67457	5.81701	6.79739	8.65644	17.99999	3.61251	5.82
± 8	0.59321	5.01000	4.77992	4.49334	-7.28011	15.50674	5.01
±9	0.51003	-1.59495	-4.00751	-10.67637	-10.58994	0.09786	-1.59
± 10	0.42748	-8.28011	-5.77622	-4.92879	3.04716	-28.88807	-8.28
± 11	0.34782	-5.76337	-8.88265	4.93480	-16.13380	-65.75855	-5.76
± 12	0.66446	9.12091	8.70539	1.48863	3.32161	8.40278	9.12

Table 2 summarizes several pattern performance metrics, including main lobe width, HPBW, and null depth level (NDL) for each example.

Table 2 Design parameters for the radiation patterns corresponding to Figures 1–7.

Figures	Main Lobe Width (°)	HPBW (°)	NDLL (dB)
1	6.00	4.65	
2	6.00	4.75	-131.564 @20.25°
3	6.00	4.75	-182.508 @20.25°
4	6.00	4.75	-134.760 @-30.5o -130.505 @20.25o
5	6.25	4.75	-132.162 @-30.5° -132.839 @20.25° -132.888 @42.0°
6	6.50	4.75	-66.791 @17.75° -66.879 @18.25° -67.548 @18.75° -99.672 @19.25° -67.762 @19.75° -65.611 @20.25° -70.485 @20.75° -77.353 @21.25° -66.011 @21.75° -67.388 @22.25° -66.555 @22.75°
7	6.00	4.75	-117.708 @20.25°

The HPBW of the synthesized nulling patterns closely matches that of the initial Chebyshev pattern in all cases. The achieved null depths indicate strong interference suppression capability, even under multiple nulls and broad null constraints. The patterns exhibit anti-symmetry with respect to the main beam, a direct consequence of the odd-symmetric phase distribution around the array center.

5. Conclusion

The primary objective in radiation pattern synthesis with nulling constraints is to suppress interference and jamming by forming deep nulls in the directions of undesired signals, without compromising the main beam directed towards the desired user or target. Achieving this objective under phase-only control with fixed amplitudes and element positions is a challenging nonlinear optimization problem, especially when multiple or broad nulls are required.

In this chapter, Honey Formation Optimization with Single Component (HFOSC) has been employed for the phase-only synthesis of linear antenna arrays. The proposed method formulates a composite cost function that incorporates both sidelobe control and null depth requirements. HFOSC is used to

optimize the excitation phases of a 25-element, half-wavelength spaced linear array operating at 28 GHz, initially configured to generate a 25 dB Chebyshev pattern.

Several numerical examples have been presented, including single-narrow nulls, very deep single nulls, dual and triple nulls at prescribed sidelobe peaks, a broad null sector, and an analysis of the impact of phase rounding. In all cases, HFOSC successfully generated patterns that satisfy the requested nulling constraints while maintaining the main beam width, HPBW, and general sidelobe characteristics of the Chebyshev reference. The results also indicate that extremely deep null depths are sensitive to phase quantization, which should be considered in hardware implementation.

Overall, the HFOSC-based phase-only synthesis approach offers a robust, flexible, and computationally efficient solution for array pattern control in advanced interference mitigation scenarios. Its ability to achieve precise and deep null placement with minimal distortion of the desired pattern makes it particularly attractive for next-generation wireless systems, including 6G networks, where robust jamming resistance and interference cancellation are essential requirements.

References

Abdulqader, A. J., Mohammed, J. R., & Thaher, R. H. (2020). Phase-only nulling with limited number of controllable side elements. *Progress in Electromagnetics Research C, 99*, 167–178. https://doi.org/10.2528/PIERC20010203

Adriansyah, M. A., Wahdiyat, A. I., Fitri, I. R., Murad, N. A., & Apriono, C. (2025). Sidelobe level suppression in linear and planar phased arrays using Grey Wolf optimization with local search refinements. *IEEE Access, 13*, 27818–27832. https://doi.org/10.1109/ACCESS.2025.3540456

Aljaf, D. A., & Mohammed, J. R. (2023). Multiple antenna array patterns reconfiguration with common excitation amplitudes and optimized phases. *Journal of Engineering Science and Technology, 18*(2), 1199–1208.

Babayigit, B., Guney, K., & Akdagli, A. (2008). A clonal selection algorithm for array pattern nulling by controlling the positions of selected elements. *Progress in Electromagnetics Research B, 6*, 257–266. https://doi.org/10.2528/PIERB08031218

Bhattacharyya, A. K. (2025). Wide-band pattern nulling in phased array and phased array-fed reflector antennas. *Progress in Electromagnetics Research C, 153*, 149–157. https://doi.org/10.2528/PIERC25012001

Chakraborty, A., Mishra, A., Singh, I., Ahmad, S., Khan, M. J., Sharma, D., Alkhayyat, A., & Gupta, S. (2024). Optimal design of smart antenna arrays for beamforming, direction finding, and null placement using the soft computing method. *International Journal of Numerical Modelling: Electronic Networks, Devices and Fields, 37*(6), 1–13. https://doi.org/10.1002/jnm.3302

Dib, N., Goudos, S. K., & Muhsen, H. (2010). Application of Taguchi's optimization method and self-adaptive differential evolution to the synthesis of linear antenna arrays. *Progress in Electromagnetics Research, 102*, 159–180.

Durmus, A., Kurban, R., & Karakose, E. (2021). A comparison of swarm-based optimization algorithms in linear antenna array synthesis. *Journal of Computational Electronics, 20*(4), 1520–1531. https://doi.org/10.1007/s10825-021-01711-w

Dutta, K. P., Misra, B., & Mahanti, G. K. (2022). Meta-heuristic optimization algorithms for placement of multiple nulls and minimization of side lobe level in quadrant symmetric sparse array antenna. *International Journal of Communication Systems, 35*(10), 1–15. https://doi.org/10.1002/dac.5149

Ercan, U., Boyar, I., Kilic, T. O., Yetgin, Z., & Ertekin, C. (2025). Parameter optimization of drying models using Honey Formation Optimization-1 (HFO-1). *Food and Bioproducts Processing, 154*, 392–401. https://doi.org/10.1016/j.fbp.2025.09.016

Guney, K., Babayigit, B., & Akdagli, A. (2007). Position-only pattern nulling of linear antenna array by using a clonal selection algorithm (CLONALG). *Electrical Engineering, 90*(2), 147–153. https://doi.org/10.1007/s00202-006-0056-9

Guney, K., Babayigit, B., & Akdagli, A. (2008). Interference suppression of linear antenna arrays by phase-only control using a clonal selection algorithm. *Journal of the Franklin Institute, 345*(3), 254–266. https://doi.org/10.1016/j.jfranklin.2007.09.002

He, J., Cheng, Z., He, Z., & Yuan, K. (2022). Phase-only transmit beampattern design for large phased array antennas with multi-point nulling. *Multidimensional Systems and Signal Processing, 33*(2), 597–619. https://doi.org/10.1007/s11045-021-00815-7

Hesari, M., & Ebrahimzadeh, A. (2017). Introducing deeper nulls and reduction of side-lobe level in linear and non-uniform planar antenna arrays using gravitational search algorithm. *Progress in Electromagnetics Research B, 73*, 131–145. https://doi.org/10.2528/PIERB16091101

Jin, X. R., Zhang, Q., Kong, L. B., Ding, G. W., & Wang, S. Y. (2025). Wide null steering of realistic antenna array. *Results in Engineering, 26*, 105038. https://doi.org/10.1016/j.rineng.2025.105038

Kadhim, M. A. (2018). Null steering using phase shifters. *ARPN Journal of Engineering and Applied Sciences, 13*(9), 3045–3051.

Kaur, B., Marwaha, A., & Rani, S. (2017). Characterization of 4 element compact microstrip patch antenna array for efficient null steering. *Applied Computational Electromagnetics Society Journal, 32*(12), 1105–1112.

Kumar, S., & Singh, H. (2023). Antenna array pattern synthesis using nature-inspired computational techniques: A review. *Archives of Computational Methods in Engineering, 30*(5), 4041–4072. https://doi.org/10.1007/s11831-023-09900-5

Lee, Y. (2020). Adaptive interference suppression of phase-only thinned arrays via convex optimization. *IEEE Transactions on Antennas and Propagation, 68*(6), 4583–4592. https://doi.org/10.1109/TAP.2020.2977732

Liang, J., Fan, X., Fan, W., Zhou, D., & Li, J. (2017). Phase-only pattern synthesis for linear antenna arrays. *IEEE Antennas and Wireless Propagation Letters, 16*, 3232–3235. https://doi.org/10.1109/LAWP.2017.2771380

Lin, Y. D., Chang, J. H., & Lai, Y. C. (2025). Deep reinforcement learning-based adaptive nulling in phased array under dynamic environments. *IEEE Access, 13*, 130988–131002. https://doi.org/10.1109/ACCESS.2025.3591643

Luyen, T. V., Cuong, N. V., & Hung, P. D. (2024). Convex optimization-based linear and planar array pattern nulling. *Progress in Electromagnetics Research M, 128*, 21–30. https://doi.org/10.2528/PIERM24042403

Mohammed, J. R. (2024). Array pattern synthesis using a new adaptive trapezoid window function for sidelobe suppression and nulls control. *Progress in Electromagnetics Research M, 129*, 83–90. https://doi.org/10.2528/PIERM24083102

Mohammed, J. R., & Abdulqader, A. J. (2024). Accurate control of the antenna array feeding networks using programmable microcontroller. *International Journal of Microwave and Optical Technology, 19*(5), 481–486.

Mohammed, J. R., Thaher, R. H., & Abdulqader, A. J. (2021). Linear and planar array pattern nulling via compressed sensing. *Journal of Telecommunications and Information Technology, 3*, 50–55. https://doi.org/10.26636/jtit.2021.152921

Otsapa, E. A., Tekanyi, A. M. S., Kabir, M. T., Abdulkareem, H. A., Abba, A. M., Bello, M., Dalhatu A., & Oyeleke O. D. (2023). An efficient broadband null-steering beamformer for interference mitigation in wireless communication. In 2023 2nd International Conference on Multidisciplinary Engineering and Applied Science (ICMEAS) (pp. 1–6). https://doi.org/10.1109/ICMEAS58693.2023.10429910

Poddar, S., Paul, P., Chakraborty, A., Ram, G., & Mandal, D. (2022). Design optimization of linear arrays and time-modulated antenna arrays using meta-heuristics approach. *International Journal of Numerical Modelling: Electronic Networks, Devices and Fields, 35*(5), 1–18. https://doi.org/10.1002/jnm.3010

Qassim, N. M., & Mohammed, J. R. (2024). Non-uniformly spaced antenna arrays with overlapped elements constraint. *Journal of Telecommunications and Information Technology, 4*, 23–30. https://doi.org/10.26636/jtit.2024.4.1740

Raghuvanshi, A., Sharma, A., & Awasthi, A. K. (2025). Pattern synthesis of linear antenna array using chaos game optimization algorithm. *COMPEL – The International Journal for Computation and Mathematics in Electrical and Electronic Engineering*. Advance online publication. https://doi.org/10.1108/COMPEL-12-2024-0549

Rosic, Z., Mihic, O., Aleksic, D., & Drajic, D. (2017). Novel method for optimal synthesis of 5G millimeter wave linear antenna array. *International Journal of Antennas and Propagation, 2017*, Article 6848234. https://doi.org/10.1155/2017/6848234

Sharma, A. (2023). Antenna array pattern synthesis using metaheuristic algorithms: A review. *IETE Technical Review, 40*(1), 90–115. https://doi.org/10.1080/02564602.2022.2051616

Tong, L. V., Kha, K. M., Nguyen, C. V., Nguyen, T. L., & Truong, G. B. V. (2022). Null-steering beamformers for suppressing unknown direction interferences in sidelobes. *Journal of Communications, 17*(8), 600–607. https://doi.org/10.12720/jcm.17.8.600-607

Wang, S. T., & Zhu, L. (2023). Proposal and design of a null reconfigurable patch antenna on the basis of multimode method. *IEEE Transactions on Antennas and Propagation, 71*(8), 6286–6296. https://doi.org/10.1109/TAP.2023.3276512

Ye, X., Li, L., Wang, H., & Tao, S. (2023). An effective array beamforming scheme based on branch-and-bound algorithm. *Journal of Systems Engineering and Electronics, 34*(6), 1483–1489. https://doi.org/10.23919/JSEE.2022.000123

Yetgin, Z., & Abaci, H. (2021). Honey formation optimization framework for design problems. *Applied Mathematics and Computation, 394*, 125815. https://doi.org/10.1016/j.amc.2020.125815

Yetgin, Z., & Ercan, U. (2023). Honey formation optimization with single component for numerical function optimization: HFO-1. *Neural Computing and Applications, 35*(35), 24897–24923. https://doi.org/10.1007/s00521-023-08984-1

Yetgin, Z., & Şamdan, M. (2021). Honey formation optimization: HFO. *Turkish Journal of Engineering, 5*(2), 81–88.

Zhang, Y., Hu, H., Li, T., Chen, B., Tian, J., & Lei, S. (2024). Array nulling synthesis based on hyper-parameter optimized self-paced learning convolutional neural networks. *IEEE Transactions on Antennas and Propagation, 72*(6), 5325–5330. https://doi.org/10.1109/TAP.2024.3378385

Zhao, Z., Zhao, H., Wang, Z., Zheng, M., & Xun, Q. (2021). Radial basis function neural network optimal modeling for phase-only array pattern nulling. *IEEE Transactions on Antennas and Propagation, 69*(11), 7971–7975. https://doi.org/10.1109/TAP.2021.3083787

Zhao, Z., Zhao, H., Zheng, M., & Tang, J. (2019). Real-time phase-only nulling based on deep neural network with robustness. *IEEE Access, 7*, 142287–142294. https://doi.org/10.1109/ACCESS.2019.2943420

Chapter 4

A REVIEW FOR BLDC MOTOR DRIVER AND PWM SIGNALS CONTROL WITH DEEP LEARNING MODELS

M. Murat TEZCAN[1], Elif Sinem AKTAŞ[2]

1 Kütahya Dumlupınar University Faculty of Engineering, Dept. of Electrical Electronics Engineering
ORCID ID: 0000-0002-5390-4527, murat.tezcan@dpu.edu.tr
2 Kütahya Dumlupınar University Faculty of Engineering, Dept. of Electrical Electronics Engineering
ORCID ID: 0009-0001-8619-3282, elif.aktas3@dpu.edu.tr

1) MOTIVATION

The study addresses the integration of deep learning and artificial intelligence in motor driver control and PWM (Pulse Width Modulation) signal generation, combining machine learning with power electronics principles for advanced research and analysis. This approach aims to optimize motor driver performance. Motor drivers regulate the speed and torque of motors by adjusting operating parameters (such as current, voltage, etc.) over time. PWM signals, a technique used in speed and torque control, serve to regulate the power delivered to devices by managing motor energy through switching pulses. This, in turn, ensures effective speed and torque control, preventing potential damage to devices and improving motor performance.The key focus of this study is to advance PWM signal output control through artificial intelligence, moving beyond traditional methods. By examining the limitations of conventional control methods in motor drivers, the research explores how deep learning-based approaches can introduce flexibility, adaptability, and significant advantages to such systems. The use of deep learning-based control in power converters and motor drivers offers numerous benefits, particularly in reducing control errors, enhancing energy efficiency, and optimizing performance.

The importance of electric motor drivers in today's industrial sector is significant due to their role in optimizing production processes, improving energy efficiency, and enhancing the precision of machinery. To begin by detailing the importance and types of electric motors in industrial applications today: Electric motors are devices that use electrical energy to produce mechanical energy and are widely used across various industries. Adjustable Speed Drives

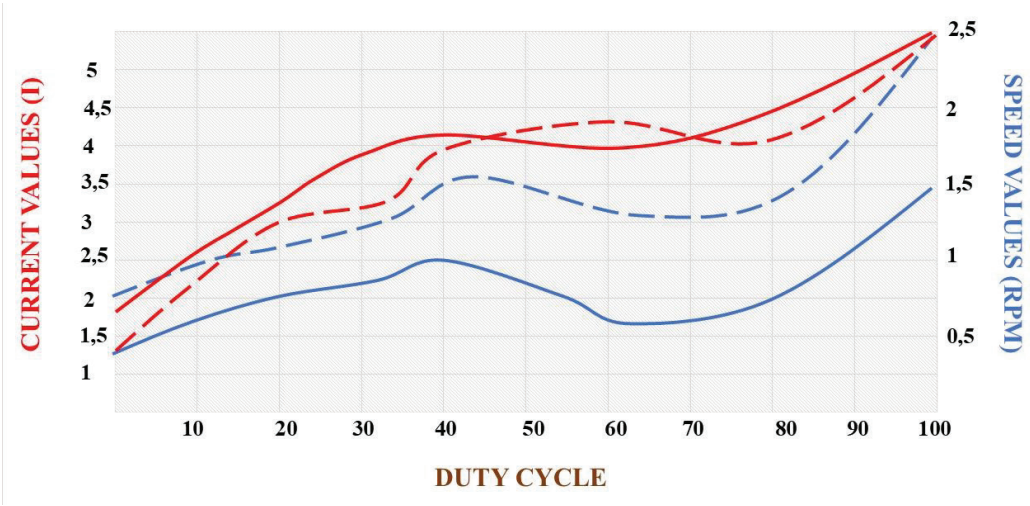

Figure 1. Variation of Current and Speed of a BLDC Motor According to PWM Duty Cycle

(ASDs) adapt to various production processes by controlling the speed and torque of the motor. These systems not only improve motor performance but also optimize energy consumption. Modern motor drivers have significantly enhanced the performance of electric motors through precise control mechanisms. In this context, Pulse Width Modulation (PWM) is a critical technique that increases the effectiveness of motor driver systems. PWM optimizes motor speed, torque, and energy consumption by controlling the voltage and current levels in motor drivers. When examining PWM's contributions to motor performance, it allows for energy efficiency by enabling the motor to conserve energy at variable speeds, providing precise control over speed and torque, and ensuring an efficient optimization environment.

According to the values presented in Figure 1, the PWM duty cycle is represented along the X-axis, while the motor speed (—) and current (—) parameters are shown along the Y-axis. Observing the blue line, we can see that as the PWM duty cycle increases, the motor speed increases linearly. In contrast, the red line illustrates that the current drawn by the motor is directly proportional to the PWM duty cycle. This graph clearly demonstrates how PWM signals are utilized in motor speed and torque control and the effects of the duty cycle on motor performance. It can be observed that at higher duty cycles, the motor consumes more power and accelerates, whereas at lower duty cycles, it consumes less energy and experiences a decrease in speed.[1].

2. MOTOR OPERATING SYSTEMS AND DATA CONTROL

The plan analysis conducted using the sensors shown in Figure 2 provides a technical review of sensorless methods for controlling Brushless Direct Current (BLDC) motor drivers, including limitations and developments. Figure 2 specifically illustrates graphs displaying various measurements such as temperature, voltage, and current, or a diagram explaining how sensors' feedback is utilized in motor control systems. It also briefly analyzes the most relevant techniques based on predictions and models, such as Artificial Neural Networks. The control of BLDC motors can be performed in either sensor-based or sensorless mode. However, to reduce the overall cost of drive devices, sensorless control techniques are typically used. The advantage of sensorless BLDC motor control is that it eliminates the sensing part, significantly reducing

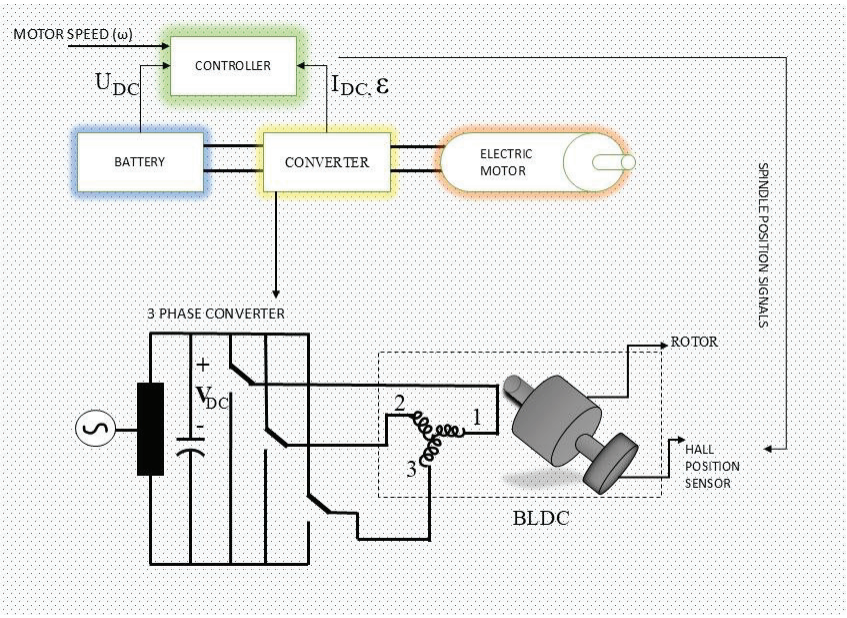

Figure 2. Motor Operating System and PWM Relationship

overall costs. [2]. The disadvantages of sensorless control include increased requirements for control algorithms and more complex electronics. In contrast, sensor-based control facilitates real-time data acquisition with greater accuracy and speed. An example illustrating the operation of a BLDC motor using a Hall sensor is provided. [3]. BLDC motors are typically powered by a series of currents that have a trapezoidal waveform for operation. To rotate these motors, the stator windings must be energized in a specific sequence. Knowing the rotor position is crucial for determining this energization sequence. The rotor position is detected by

Hall effect sensors located within the motor. These sensors detect changes in the magnetic field to determine the rotor's position. Hall sensors are used to control the motor's speed, direction,

and torque, producing output signals based on magnetic field intensity. These signals are sent to the motor driver control system, allowing for continuous monitoring of the rotor position. PWM signals are generated using this information to precisely adjust the motor's speed and torque. Furthermore, the data collected from the data acquisition systems are processed in a digital environment, and this information is analyzed through microcontrollers to provide feedback to the control system. This process helps optimize motor performance, ensuring that the rotor position is continuously monitored and that PWM signals can accurately adjust the motor's speed and torque. Hall sensors are commonly used, especially in brushless DC motors. [4]. The data collected from the example data acquisition systems (DAQ) processes the information in a digital environment. The processed data is analyzed using microcontrollers, providing feedback within the control system.

PWM Analysis Stages with Microcontroller:

1. **Data Acquisition:** Microcontrollers receive data obtained from PWM through sensors. Data is transmitted to the microcontroller using speed, torque, and current sensors, thus enabling data flow.
2. **Signal Processing:** The collected data is analyzed in real-time and accurately to generate PWM signals aimed at enhancing motor performance. The motor's performance is measured through the pulse width of the signals based on speed and torque information. The processing of the measured data directly affects the voltage and current of the motor.
3. **Control Algorithms:** The microcontroller optimizes the motor speed and torque by continuously updating the PWM signals. Especially under varying load conditions, the pulse width of the signals keeps the motor's performance under control.

2.1. Data Analysis and Control Algorithms Using Microcontrollers

PWM controls the motor speed and torque by regulating the voltage and current through changes in the pulse width of the signal. Microcontrollers generate these PWM signals and play a role in data flow for analysis. Sensors facilitate the collection of data on speed, torque, current, and voltage, enabling the transmission of this information to the microcontrollers. By processing the transmitted information and data, appropriate PWM signals for motor operation are generated.

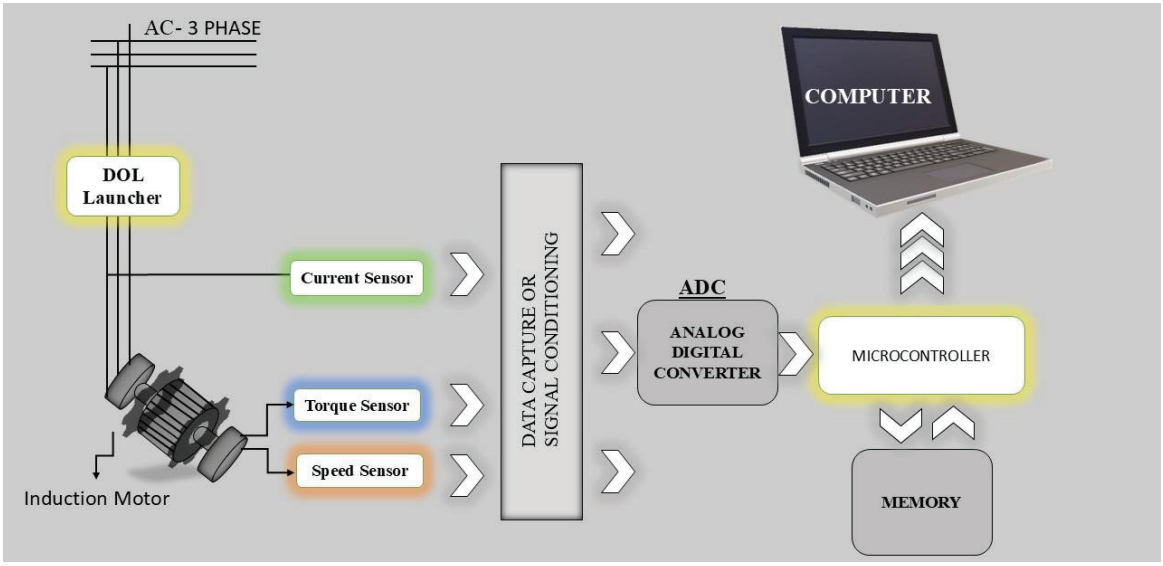

Figure 3. Relationship Diagram of Motor Driver Data with Sensors and Microcontrollers

The diagram depicted in Figure 3 illustrates how critical data, including speed, torque, current, and voltage, is collected through sensors from electric motor drivers and transmitted to the microcontroller. The microcontroller processes this data to facilitate real-time control of the motor driver. Furthermore, the analysis of this data is employed for various applications, including optimizing motor performance, enhancing energy efficiency, enabling fault diagnostics, and controlling PWM signals in real time via motor drivers, thus ensuring effective data management through microcontrollers.[5].

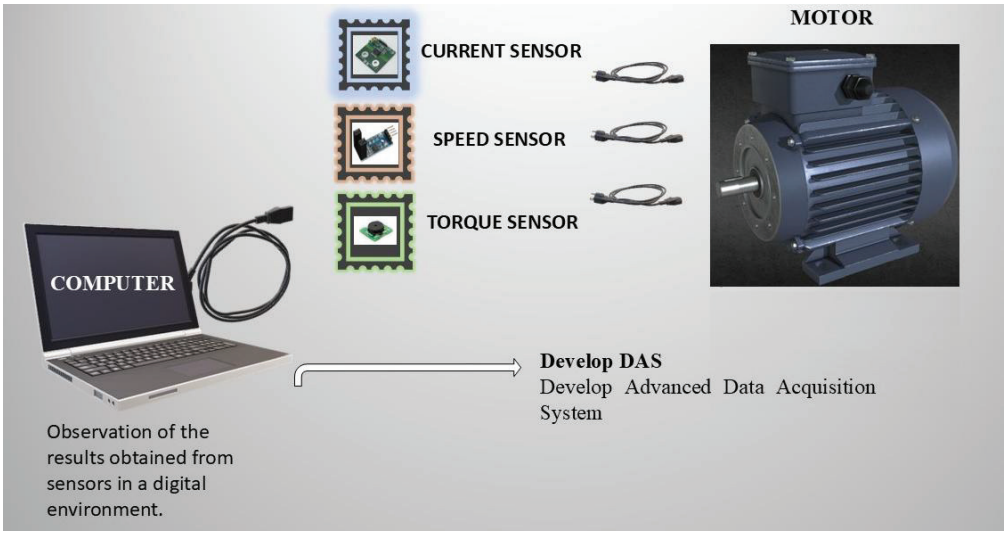

Figure 4. The Data Acquisition System and the Collaboration of Microcontrollers with Sensors

In **Figure 4**, a system is presented where torque, speed, and current sensors are controlled through an advanced data acquisition system and microcontrollers. In this system, microcontrollers are seen to work together with the Develop Data Acquisition System (DAS). The advanced data acquisition system (Develop DAS) enables the collection, processing, and analysis of data obtained from various sensors. The analyzed data can be used, for example, to monitor the performance of electric motors. These systems enable the continuous monitoring of critical parameters such as the motor's speed, torque, and current by obtaining real-time data.

2.2. Real-Time Model Training and Artificial Neural Networks

2.2.1 Artifical Neurals Networks (ANN)

Machine learning, particularly artificial neural networks (ANN), is widely used to solve complex problems that are difficult to approach or cannot be solved by traditional computational methods. Artificial neural networks are commonly employed in image processing and engineering applications due to their ability to model complex and nonlinear relationships, as well as their low error tolerance. Various libraries and tools for artificial neural networks have been developed in numerous programming languages. Some of the most commonly used and widely accepted ones are listed below.: **[6].**

- The Stuttgart Neural Network Simulator (SNNS) is a simulator developed by the Institute of Parallel and Distributed Systems (IPVR) at the University of Stuttgart specifically for artificial neural networks. It is designed to provide an efficient and flexible simulation environment for neural network applications and research.
- FANN (Fast Artificial Neural Network Library) is a library written in the C programming language that facilitates the implementation of multilayer perceptrons in artificial neural networks.
- JOONE (Java Object-Oriented Neural Engine) is a library for artificial neural networks developed in a Java environment.
- The MATLAB Neural Network Toolbox is a MATLAB-based tool that enables the design, implementation, visualization, and simulation of artificial neural networks.

Artifical Neurals Networks (ANN) Models

Single-Layer Perceptrons: This is a simple artificial neural network model that consists of an input layer and a single output layer. Each input is multiplied by a weight, summed, and then passed through an activation function. It is capable of performing only linear classification.	**Perceptron Model**: This is an algorithm that multiplies input values by weights, sums them up, and classifies the resulting value based on a threshold. It is capable of distinguishing only between two classes. Doesn't exis to complex layer.
Adaline Model (Adaptive Linear Neuron): This model utilizes error feedback to adjust the weights of the inputs. The output is determined through a linear combination based on the weighted sum of the inputs. The least squares method is employed for error minimization.	**Multi-Layer Perceptrons (MLP):** This architecture includes one or more hidden layers. Each layer receives outputs from the previous layer. MLPs can model complex relationships using non-linear functions and are trained using the backpropagation algorithm.

Among the artificial neural network models mentioned above, Multi-Layer Perceptrons (MLP) are the most suitable for controlling PWM signals due to their ability to learn complex relationships [6].

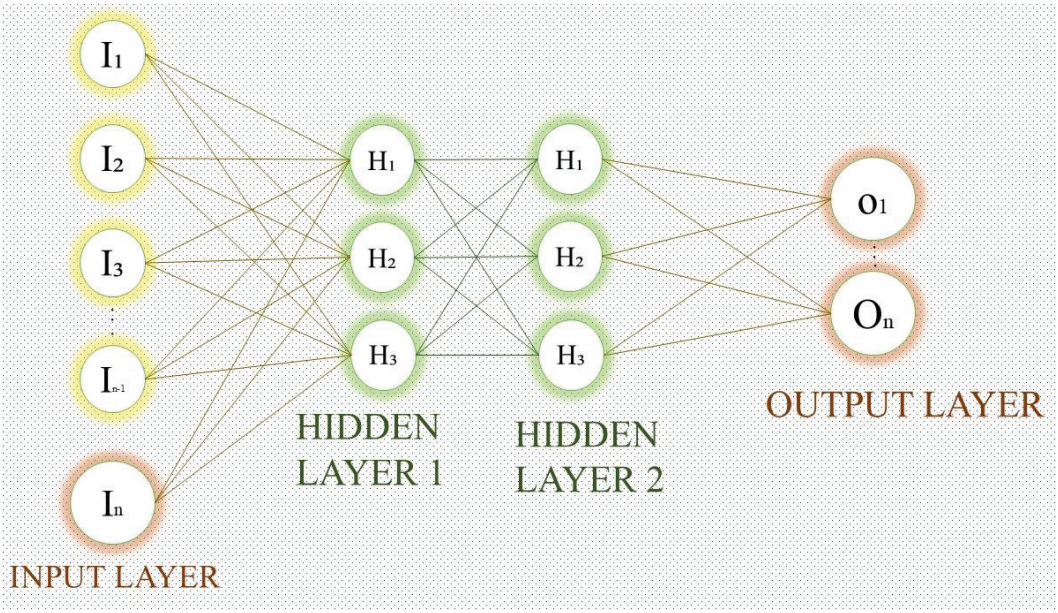

Figure 5. Basic Logical Structure of Multi-Layer Perceptrons with Neural Network Architecture

As illustrated in the logical structure of multilayer perceptrons in Figure 5, multilayer perceptrons (MLPs) comprise an input layer for data entry, one or more hidden layers, and an output layer. Within MLPs, there exist forward and backward transitions, commonly referred to as feedforward and backpropagation. In the feedforward phase, the network's output and the error value are computed. Subsequently, in the backpropagation phase, the connection weights between the layers are adjusted to minimize the computed error value. This architecture effectively provides a solution for optimizing PWM signals by accepting sensor data such as speed, torque, and current as input, thereby facilitating a multi-layered information system. Examples of such complex structures include the Stuttgart Neural Network Simulator (SNNS), FANN, MATLAB, and JOONE.

[8]. YOLOv8 offers significant advancements over its predecessors, exhibiting enhanced speed and reduced latency, making it particularly suitable for real-time applications. This model achieves a higher accuracy rate, resulting in superior performance in object detection tasks. Consequently, YOLOv8 is frequently employed in image processing and model training endeavors, demonstrating its effectiveness and reliability in various computational vision applications.

Considering real-time trained models and libraries, YOLO versions can be utilized during the model training phase. YOLOv8 is a robust computer vision algorithm capable of quickly and efficiently detecting various objects, as it is trained on a large dataset. [7]. In addition, deep learning models such as **YOLOv5 and YOLOv8** are commonly integrated with popular libraries like **PyTorch and TensorFlow**. Consequently, establishing direct integration with artificial neural network libraries such as the Stuttgart Neural Network Simulator (SNNS), FANN, or JOONE may pose certain challenges. However, the **MATLAB Neural Network Toolbox** serves as an effective platform for training and deploying these models. MATLAB offers a comprehensive suite of tools tailored for the development of deep learning architectures and facilitates seamless integration with YOLO. Throughout this research, both the integration process and practical applications will be conducted using **MATLAB**, ensuring a robust framework for model implementation and evaluation.

2.2.2. Integration of PWM Signal and Deep Learning Model with MATLAB

The steps for integrating the PWM signal into a deep learning model using MATLAB are outlined below:

a) Model Training

- **Data Collection**: Microcontrollers receive data obtained from PWM through sensors. Data is transmitted to the microcontroller using speed, torque, and current sensors, thereby facilitating a data flow in conjunction with PWM. [page. 7]
- **Feature Selection**: Input and output data are determined; for example, speed and torque can be used as inputs, while PWM can be utilized as outputs. The feedback of the identified data is facilitated through microcontrollers. In summary, it can be observed that the collected data is related to PWM in conjunction with microcontrollers. [page. 8]
- **Network Design**: The appropriate network architecture is determined based on the model to be trained. If the model includes complex structures, multilayer perceptrons are selected; otherwise, single-layer or less complex perceptrons are chosen. An artificial neural network model algorithm is developed that aligns with the selected network structure. The chosen structures consist of a multilayer neural network implemented using the Neural Network Toolbox in MATLAB, and a system is created that is compatible with this network architecture. [page. 10]

b) Training Process and FNN Structure

- **Model Training**: The necessary input and output data for the PWM signal are collected. The input data typically includes information such as the motor's speed, torque, current, and voltage conditions, which are provided through sensors. The input data contains sensor data. The output data consists of the values of the PWM signal over a specific time interval. Using the collected data, the artificial neural network is defined, and an appropriate algorithm for its fundamental logic structure is created and trained. The trained neural network is constructed using the MLP model in MATLAB. Software functions, such as (train), are utilized to enable the network to learn and recognize the data. The model is integrated to produce PWM signal output. Data is extracted through the integrated model, and the network structure is established. PWM (Pulse Width Modulation) signals are frequently used in motor driver control systems. In this study, to provide PWM signal output, we will examine the design and implementation phases of a Fuzzy Neural Network (FNN) in conjunction with the MATLAB Neural Network Toolbox; FNN is a type of artificial neural network that combines the ability to process uncertain information with learning capability. These structures are used, particularly to achieve better control performance in complex systems.

  Utilization of FNN in PWM Control:

  - Input Data: Parameters such as speed and torque required for generating the PWM signal serve as input data.

Design of a Fuzzy Neural Network (FNN) with MATLAB Neural Network Toolbox:

- The implementation process involves defining the network architecture and training the FNN to accurately predict PWM signals based on the provided input parameters..

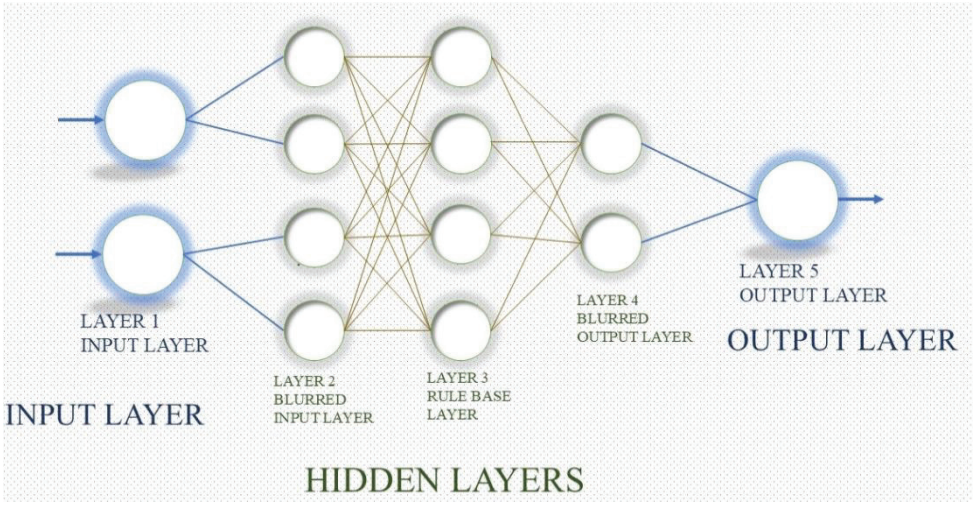

Figure 6. Basic Logic Diagram of the FNN Structure

The layers of the diagram shown in **Figure 6** are listed as follows:

Input Layer: In this layer, the error (e) and delta error (Δe) are processed.

Membership-Fuzzy Input Layer: This layer is responsible for processing fuzzy (if-then) logic rules. Membership functions corresponding to each input are defined at this stage.

Rule Layer: Fuzzy (if-then) rules based on the input parameters are executed within this layer. For example, straightforward rules such as "if the error is significant, then the PWM output signal should also be substantial" are applied.

Output Layer: The PWM signal generated in this layer is subsequently transmitted to the motor driver.

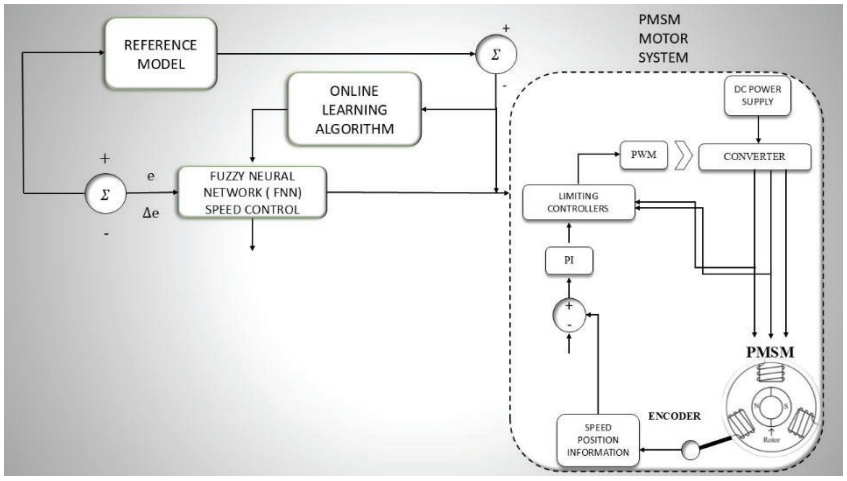

Figure 7. Signal Diagram Controlling the PWM Signal Output of the PMSM Motor in Conjunction with a Neural Network

[9]. **Figure 7** depicts a diagram illustrating the generation of control signals for the PWM signal output of a Permanent Magnet Synchronous Motor (PMSM) utilizing a Fuzzy Neural Network (FNN) structure. In this FNN control system, the input layer consists of critical parameters, namely the error signal (e) and the change in error (Δe). These parameters are calculated based on the difference between the motor's target speed and its actual speed. The primary objective of the system is to accurately adjust the PWM signals to minimize these errors, thereby maintaining the motor's speed and torque at a constant level. The neural network provides the necessary inputs to generate the PWM signal. The PWM output is represented as a control signal denoted by qi, which can be expressed through the following formulas:[9].

Error signal: $\mathbf{e(t)=\omega r(t)-\omega m(t)}$ (ωr(t): actual rotor speed , ωm(t): Desired rotor speed)

Delta Error: $\mathbf{\Delta e(t)=e(t)-e(t-1)}$

These data are fed into the neural network, and the Fuzzy Neural Network (FNN) generates an output PWM signal based on these errors.

FNN Training Process

The training of the FNN is conducted using supervised and continuous learning. The neural network is trained on datasets and the arguments derived from these datasets, and the system performs the learning process in a way that minimizes errors. In particular, the digital learning capability provides continuous adaptation against parameter uncertainties and changes in motor control. The training of the FNN is typically achieved using a supervised backpropagation algorithm.

Advantages of FNN- Based Contol [10].

- **Adaptability**: The Fuzzy Neural Network (FNN) can adapt to changing system conditions and uncertainties.
- **Accuracy**: It controls the PWM signal precisely based on error and delta error information. Continuous monitoring ensures data accuracy
- **Rapid Response**: Thanks to its precise and continuous control structure, the FNN can quickly adjust the PWM signal in response to external influences, providing a high level of accuracy.

Briefly, generating PWM signals in a PMSM motor driver using an FNN-based control system enhances both the accuracy and speed of the system while improving its stability. This approach not only reduces errors arising from external influences and enables rapid adaptation to changing conditions but also optimizes motor performance. The learning capability of the FNN continuously optimizes PWM signals based on errors, thereby ensuring effective control of the motor's speed and torque, which ultimately leads to an improvement in motor performance.

3. INTEGRATION OF MOTOR DRIVERS AND DEEP LEARNING ALGORITHMS

In recent years, the utilization of artificial intelligence and deep learning algorithms in industrial automation and robotic systems has been increasing. Deep learning-based image processing algorithms, such as YOLOv8, not only excel in object detection but also provide valuable inputs in areas like motor driver control. Parameters such as speed and torque control in motor drivers can be optimized through accurate signal processing, leading to enhanced performance. Artificial intelligence positively influences the accuracy and speed metrics of the system through autonomous intervention.

Motor Drivers and PWM Signals:

PWM (Pulse Width Modulation) signals in motor drivers are fundamental parameters that control the speed and torque of the motor. [1]. In traditional control systems, PWM signals are optimized using information obtained from sensor data, whereas deep learning algorithms enhance this process, making it more precise and predictive.

Advanced Control with Deep Learning and YOLOv8:

YOLOv8 is a model that provides fast and accurate object detection.[8]. Object data obtained through image processing can be critical in motor control. For instance, the distance of a robotic arm from an object can influence the PWM signals. These signals are processed by a Fuzzy Neural Network (FNN) based on the analysis of data received from YOLOv8, thereby optimizing driver control.[10].

3.1. Real-Time Control Integration with Artificial Intelligence

The motor control is achieved by utilizing a model trained to detect and recognize objects using the YOLOv8 model. The model processes input images to identify the location and class of specific objects. For real-time data streaming in MATLAB, the YOLOv8 model is executed through Python, utilizing the integration features between Python and MATLAB. Invocations are made through Python.In example, By invoking the Python detect() function, operations are performed on the detected objects and their positions. To facilitate data sharing between MATLAB and Python, the matlab.engine is used. This tool allows you to execute MATLAB commands within Python code, enabling data transfer between Python-based projects and MATLAB, and allowing direct invocation of MATLAB functions from Python.

3.2 Integration of YOLOv8 in MATLAB and PWM Signal Generation

The position or status of the detected objects can provide parameters (error, delta error) that will be used in PWM signal generation. For instance, deviations in an object's position or instantaneous parameter changes, such as excessive current values, can be utilized to adjust the PWM signal accordingly.

3.3. Integration with FNN

Model Integration: The trained model is integrated into the PWM control circuit. Outputs from the model that generates the PWM signal are utilized to connect to the motor driver. In summary, an integrated system is established through the FNN neural network by calculating error and feedback parameters for controlling the PWM signal based on image data processed by the YOLOv8 model. This integration is achieved through MATLAB-Python integration and data sharing.

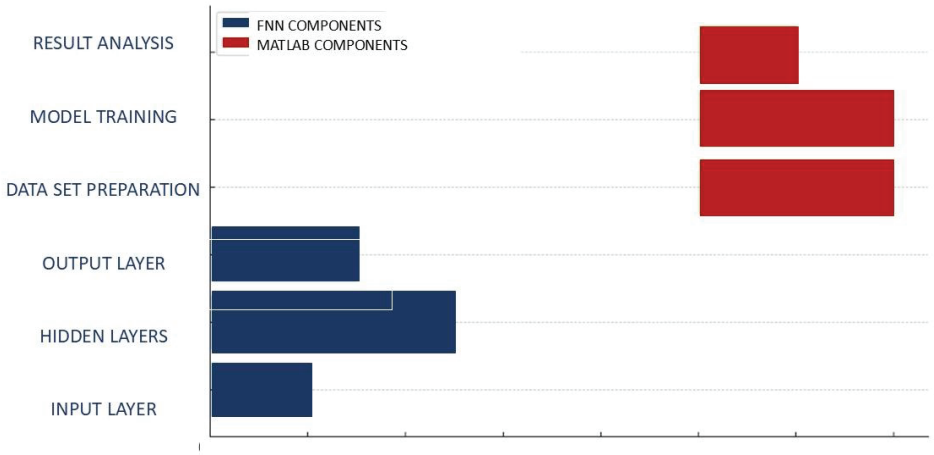

Figure 8. Components of Fuzzy Neural Network (FNN) and MATLAB Integration

In **Figure 8**, a diagram illustrating the integration of the Fuzzy Neural Network (FNN) and MATLAB is presented. The details are outlined as follows:

Input Data: At the top of the diagram, there is a block labeled "Input Data," representing the raw data necessary for the system's operation. This data includes PWM control data from sensors or other sources, as well as motor speed, position information, or object recognition results obtained from a model such as YOLOv8.

FNN Structure: Following the preprocessing of the input data, there is a block representing the FNN structure. This section contains a network model created by combining fuzzy (if-then)logic and artificial neural networks. This model is designed to control the PWM signal output using predefined fuzzy rules and neural network learning algorithms. The output of the FNN block is a signal that represents the PWM signal, which will function as the PWM signal used to control the motor drivers. The PWM signal is a critical component for controlling the motor's speed and torque, and the FNN can enhance the motor's performance by optimizing this signal.

Output Signal: The output of the FNN block produces a signal that represents the PWM output. This signal will serve as the PWM signal utilized for controlling the motor drivers.

Feedback Loop: Following the output signal, a feedback loop is illustrated. This loop is utilized to assess the system's performance and make necessary adjustments. Feedback is crucial for the stabilization and accuracy of the system.

MATLAB Integration: All these components are integrated within the MATLAB environment to form a control system. MATLAB serves as the platform for the training,

simulation, and integration of the FNN. Utilizing the tools available in MATLAB, data analysis and system optimization can be effectively performed. [11].

4. CONCLUSIONS

The study addresses the integration of deep learning and artificial intelligence in motor driver control and PWM (Pulse Width Modulation) signal generation, combining machine learning with power electronics principles for advanced research and analysis. This approach aims to optimize motor driver performance. Motor drivers regulate the speed and torque of motors by adjusting operating parameters (such as current, voltage, etc.) over time. PWM signals, a technique used in speed and torque control, serve to regulate the power delivered to devices by managing motor energy through switching pulses. This, in turn, ensures effective speed and torque control, preventing potential damage to devices and improving motor performance.The key focus of this study is to advance PWM signal output control through artificial intelligence, moving beyond traditional methods. By examining the limitations of conventional control methods in motor drivers, the research explores how deep learning-based approaches can introduce flexibility, adaptability, and significant advantages to such systems. The use of deep learning-based control in power converters and motor drivers offers numerous benefits, particularly in reducing control errors, enhancing energy efficiency, and optimizing performance.

A brief summary of the stages of the study is as follows:

1. **Data Acquisition During Motor Operation:** Speed, torque, current, and voltage feedbacks are collected using sensors (speed sensors, torque sensors, current sensors). These data from the sensors are typically transmitted in digital form to microcontrollers or data acquisition systems, allowing the initial states and effects of PWM signals to be observed.

2. **Real-Time Model Training:** Based on the collected data, the deep learning model is trained to understand how the motor responds under various operating conditions. The model can be trained using several deep learning applications such as Python, OpenCV, Keras, YOLOv5, and YOLOv8. Thus, the feedback data can be analyzed in real-time by the deep learning model or stored for later processing. This approach provides flexibility and control in terms of PWM signal adaptation. The model determines the PWM signals to ensure the motor operates at its optimal performance, dynamically adjusting the signal based on varying speed and load conditions.

3. **Collaboration Between Motor Driver and Deep Learning Algorithm:** The motor driver uses PWM signals generated by the deep learning algorithm to power the motor. These PWM signals regulate the motor's current and voltage, thereby controlling its speed and torque. Since the pulse width of the PWM signals determines the motor's supply voltage, the quality of these signals directly impacts motor performance. Through deep learning, these signals are optimized in real-time and continuously, enhancing the motor's efficiency.

5. REFERENCES

[1]. Heggo, M. et al., 2019. “Operation of aerial inspections vehicles in HVDC environments Part B: Evaluation and mitigation of magnetic field impact.” , Journal of physics. https://doi.org/10.1088/1742-6596/1356/1/012010.

[2]. Becerra, RC; Ehsani, “M. Fırçasız Kalıcı Mıknatıs Motorlarının Yüksek Hızlı Tork Kontrolü.” IEEE Trans. Ind. Electronics 1988 , 35 , 402–406.

[3]. AN10661 Brushless DC motor control using the LPC2141 - NXP Semiconductors ; AN10661, NXP Semiconductors: Eindhoven, Hollanda; Ekim; 2007.

[4]. Fault tolerant BLDC motor control for hall sensors failure . 2015 21st International Conference on Automation and Computing (ICAC)

[5]. T.Ugale, R. et al., 2012. “A low cost fast data acquisition system for capturing electric motor starting and dynamic load transients.” 2012 IEEE International Conference on Power Electronics, Drives and Energy Systems (PEDES)

[6]. A. C. Kınacı, “Görsel yazilim geliştirme ortami ile beraber bir yapay sinir ağı kütüphanesi tasarimi ve gerçekleştirimi,” Ege Üniversitesi, 2006.

[7]. NurOrtataş, F. & Kaya, M., 2023. “Performance Evaluation of YOLOv5 YOLOv7 and YOLOv8 Models in Traffic Sign Detection.” 2023 8th International Conference on Computer Science and Engineering (UBMK). http://dx.doi.org/10.1109/ubmk59864.2023.10286611.

[8]. https://docs.ultralytics.com/tr/models/

[9]. Lin, C.-H. & Lin, C.-P., 2009. “Fuzzy neural network control for a permanent magnet synchronous motor drive system” 2009 4th IEEE Conference on Industrial Electronics and Applications. Available at: http://dx.doi.org/10.1109/iciea.2009.5138697

[10]. Feedforward neural network - Wikipedia İleri beslemeli sinir ağı (FNN)

[11]. Arafat, Yunus Bakhtiar, and H. U. Weiwei. "The Development of a Matlab-Based Fuzzy PID Controller and The Simulation." *International Journal of Engineering Continuity* 2.1 (2023): 14-26.

Chapter 5

THE ROLE OF SMART METERS IN SMART GRIDS: ARCHITECTURAL, COMMUNICATION, ANALYTICAL, AND SOCIAL IMPACTS

Mesut Akkoyun[1], Ercan Köse[2]

1 Mesut Akkoyun, Tarsus Universitesi / Mühendislik Fakültesi/ Elektrik Elektronik Müh.
E-mail: mesut.gym@gmail.com, ORCID: 0009-0007-4163-7787
2 Doç. Dr. Ercan Köse, Tarsus Universitesi / Mühendislik Fakültesi/ Elektrik Elektronik Müh.
E-mail: ekose@tarsus.edu.tr ORCID: 0000-0001-9814-6339

In today's energy sector, combating climate change, integrating renewable energy sources, and increasing energy demand are pushing the limits of traditional electricity grids. In this context, Smart Grids have the potential to transform the reliability, efficiency, and sustainability of grids by enabling the integration of information and communication technologies (ICT) with energy systems (Komninos et al., 2014). Smart meters, one of the cornerstones of smart grids, not only measure energy consumption but also redefine grid operations with advanced features such as real-time data flow, remote management, and demand-side interaction (Barai et al., 2015). Moving away from the passive nature of traditional electromechanical meters, these devices have become active systems equipped with two-way communication and advanced analytical capabilities; thus, they play a critical role in increasing energy efficiency, combating losses and theft, and achieving economic optimization (Aouini & Azzouz, 2015).

The importance of smart meters is particularly evident in developing countries. In Turkey, technical and non-technical losses (NTL) in electricity distribution systems raise the total loss rate to 17-20 percent; this increases the financial burden on distribution companies and deepens energy poverty (Depuru et al., 2011; Eke & Ayrancı, 2018). Smart meters offer solutions to these problems by providing high-resolution data through Advanced Metering Infrastructure (AMI). for example, enabling individual consumption separation through anomaly detection based on Kirchhoff's law and NILM (Nonintrusive Load Monitoring) techniques (Cavdar, 2004; Bin-Halabi et al., 2019). However, the widespread adoption of these technologies also brings challenges such as cybersecurity threats (e.g., side-channel attacks - SCA) and data privacy; therefore, cryptographic measures and compliance with standards become mandatory (Shakiba et al., 2024; Fan & Gong, 2013).

This book chapter aims to comprehensively examine the role, functions, technological architecture, and security challenges of smart meters within smart grids. The first chapter will address the smart grid vision and the historical development of meters; the second chapter will discuss hardware architecture, measurement methods, and accuracy analysis. The third chapter will focus on communication infrastructure and protocols; the fourth chapter will cover applications such as network management, demand-side integration (DSI), and loss detection. The fifth section will examine data analysis, anomaly detection (Isolation Forest, LOF, FbProphet), and consumption forecasting methods; the sixth section will be devoted to cybersecurity principles and energy poverty. Finally, the findings will be synthesized to identify future trends.

This review aims to synthesize current studies in the literature (e.g., Barai et al., 2015; Depuru et al., 2011) and bring together the theoretical and practical dimensions of smart meters, with a particular focus on providing policy and implementation recommendations in the Turkish context. Smart meters, as an indispensable element in the digital transformation of energy systems, open the door to a carbon-free and equitable future.

1. Smart Grid Vision and the Critical Role of Smart Meters

1.1. Historical Development and the Concept of Smart Grids

Electricity energy systems worldwide are facing a fundamental transformation triggered by the necessity to decarbonize energy supply, renew aging assets, and effectively utilize rapidly developing information and communication technologies (ICT) (Barai et al., 2015). Smart meters are not just simple devices that measure energy consumption; they are embedded systems that keep time-stamped data records, have advanced communication capabilities, and can be read and managed remotely. The high-resolution data obtained through these meters can be used both for classic functions such as billing and loss tracking, as well as for demand-side management, load analysis, and energy efficiency applications (Aouini & Azzouz, 2015).

These objectives converge in the concept of the Smart Grid (Komninos et al., 2014). The smart grid utilizes advanced information and communication systems to control this new energy system in a reliable, flexible, and efficient manner (Fan & Gong, 2013). Smart meters are the real components of smart grids in the field, enabling not only the measurement of electrical energy, but also the tracking of consumption habits, the analysis of grid behavior, and information-based energy management (Barai et al., 2015). Thanks to their two-way communication and advanced measurement capabilities, smart meters have a special place in supporting monitoring, control, and demand-side management processes in distribution networks. By making energy consumption visible, smart meters offer both distribution companies and users the opportunity for conscious energy management (Aouini & Azzouz, 2015).

Electricity measurement systems began before 1970 with electromechanical cumulative meters that recorded energy consumption and manual reading. Before 2000, Automatic Meter Reading (AMR) systems were developed, which typically involved the monthly transmission of energy consumption information via one-way communication networks. However, after 2000, the performance of the measurement infrastructure ( ) significantly improved; AMR transitioned to two-way communication supporting applications such as variable tariffs, demand-side bidding, and remote connection/disconnection. The Smart Grid vision envisions expanding these capabilities to support a wide range of applications, including distribution automation, control, and power quality monitoring (Advanced Metering Infrastructure - AMI).

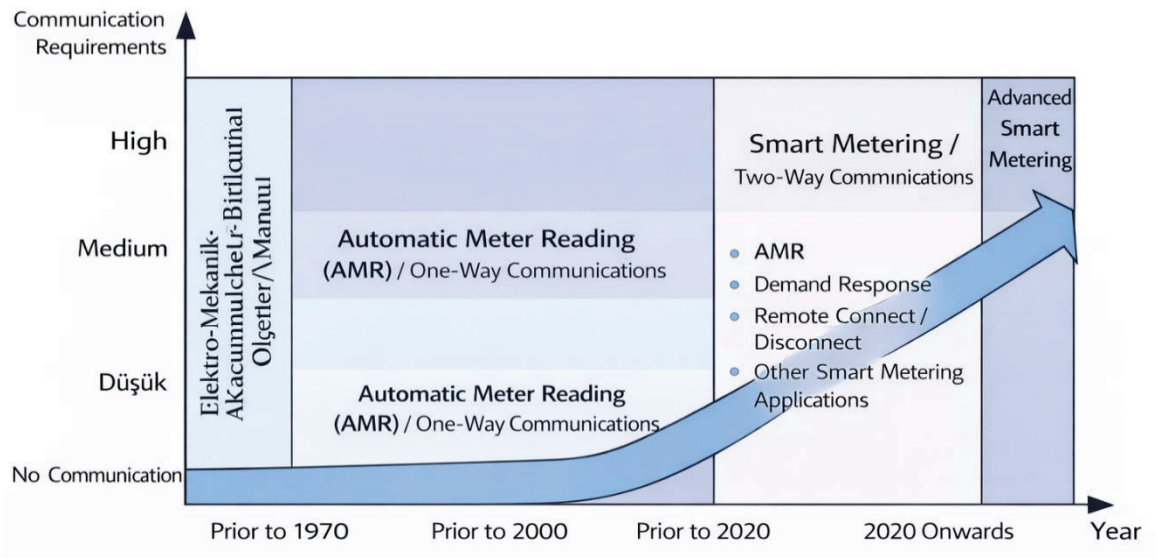

Figure 1: Visualization of the Evolution of Electricity Measurement proposed by John Wiley & Sons

1.2. Definition and Basic Functions of Smart Meters

Smart electricity meters are intelligent metering devices that measure electrical values in the power grid, generate billing calculations based on measurement evaluations, and enable remote monitoring and control (switching on/off) of energy through communication technologies (Barai et al., 2015; Aouini & Azzouz, 2015). These devices play a central role in ensuring sustainability for the efficient use of energy (Komninos et al., 2014).

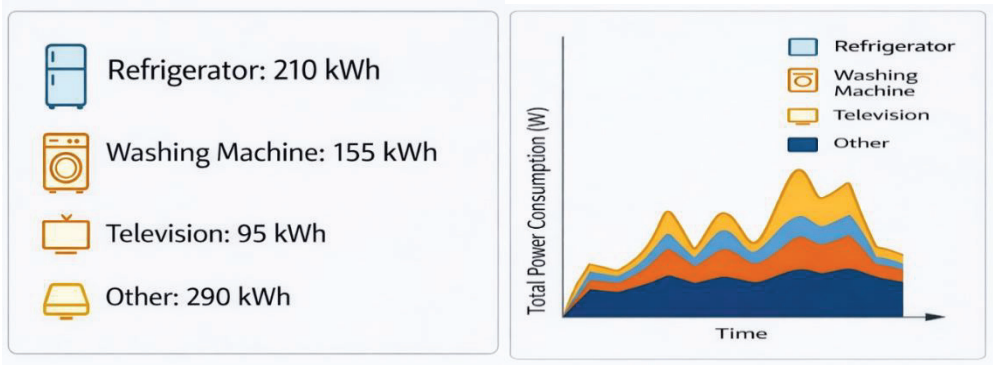

Figure 2: Energy disaggregation (Images generated using artificial intelligence)

Smart meters enable consumers to understand their consumption habits, identify inefficiencies, and make informed decisions by allowing real-time, individual assessment of each device's energy consumption in the home through a single measurement point.

The basic function of smart meters, unlike traditional meters, is to provide two-way information flow. This allows energy suppliers to manage load, protect the distribution network, and increase operational efficiency. From the consumer's perspective, smart meters support energy

efficiency and cost savings by offering adaptive pricing and automatic data collection functions (Fan & Gong, 2013).

While traditional meters are passive measurement tools that only record energy consumption at specific intervals, smart meters are active system components that continuously generate data, transmit this data via a communication infrastructure, and enable interaction between the grid and the consumer. In other words, while traditional meters show consumption retrospectively, smart meters allow consumption to be monitored in real time. With their two-way and advanced data processing capabilities, they transform the operational structure of distribution systems. While traditional meters are the end point of measurement, smart meters form the starting point of a communication chain that extends from measurement to decision-making processes (Barai et al., 2015).

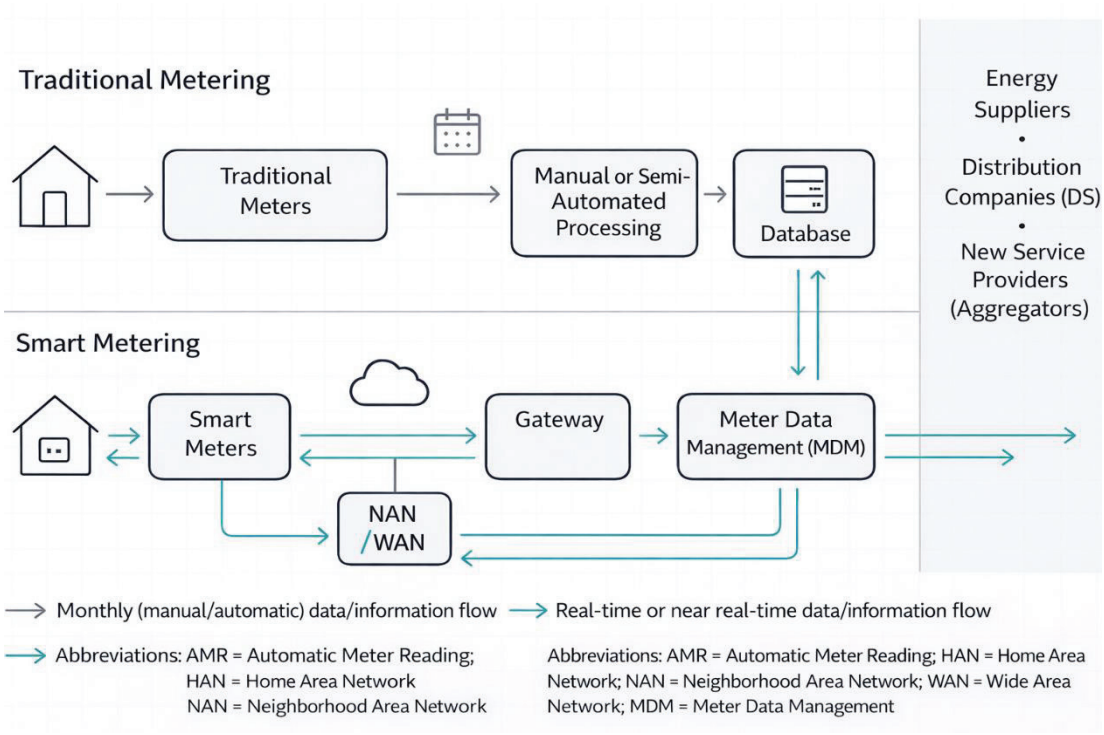

Figure 3: Comparison of smart meters and traditional meters as proposed by John Wiley & Sons

The hardware architecture of a typical smart meter consists of a measurement unit, an analog processing and ADC layer, a microcontroller/DSP unit, a power supply and auxiliary circuits, communication modules, and security and protection elements. These components are typically logically separated on the printed circuit board into measurement and processing/communication layers (Shakiba et al., 2024).

The most commonly used methods for current measurement are current transformers and shunt resistors. Current transformers offer advantages in terms of galvanic isolation and safety, while shunt resistors offer high accuracy and compact design, especially at low currents. For voltage measurement, high-accuracy resistive dividers are mostly used, supported by isolation booster circuits when necessary.

Signals from measurement transducers pass through input protection circuits, anti-aliasing filters, and gain/offset adjustment layers before reaching the ADC. High-resolution sigma-delta ADC architectures or integrated energy measurement chips are commonly used for energy measurement in smart meters.

The processor core in the meter is typically a 32-bit microcontroller or DSP-based component. This processor handles tasks such as reading and processing measurement data, performing energy and power calculations, applying tariffs, maintaining event logs, executing communication protocols, and managing the local user interface. The program memory, data memory, and working memory are configured to support these functions. The Real-Time Clock (RTC) is critical for time-of-use tariffs and matching records with the correct time stamp.

In power supply design, structures that can operate over a wide input voltage range, withstand short-term voltage fluctuations, and comply with insulation/safety standards are preferred. In addition to the main DC lines, battery or supercapacitor-backed backup power lines are used for the RTC and some critical memory areas. Electromagnetic compatibility (EMC), grounding arrangement, and ESD protection are fundamental elements that determine long-term reliability in field conditions.

On the communication module side, power line communication (PLC), radio frequency (RF)

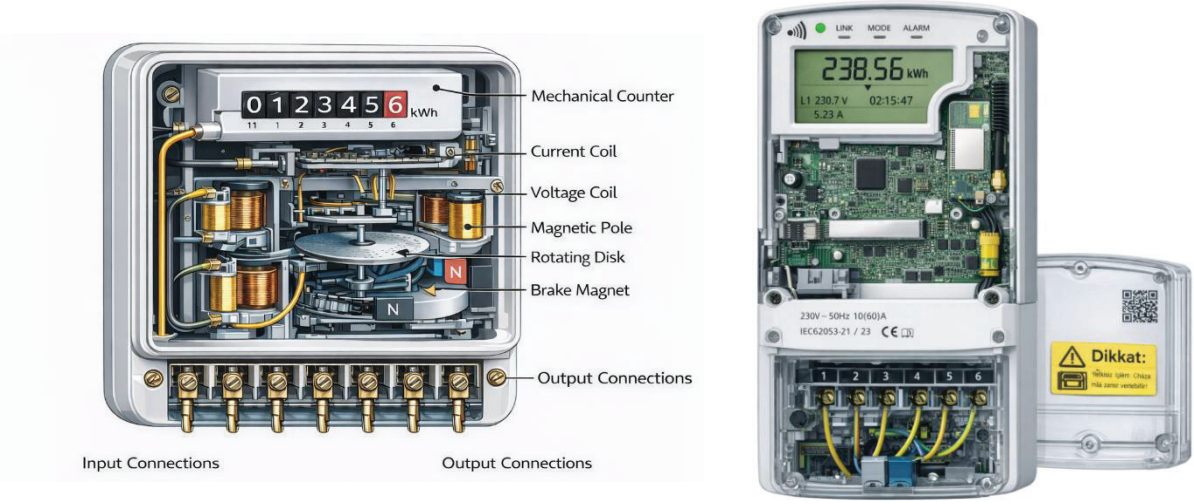

Figure-4: Visuals of traditional meters and smart meters (generated using artificial intelligence)

modules, GSM/GPRS/4G, and various wired interfaces (RS-485, Ethernet, optical port, etc.) are commonly used. Card placement, shielding, and grounding design are crucial to prevent the electromagnetic emissions of these modules from affecting the measurement circuits.

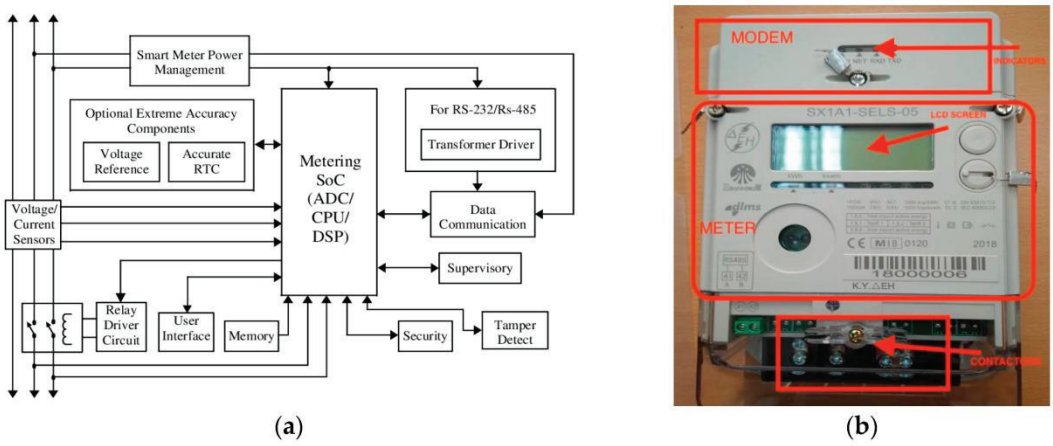

Figure 5: Smart digital meter: **(a)** Schematic diagram showing the processing and communication layers; (b) Layout showing the meter's connection points and modem (Konstantinos G. Koukouvinos, 2025)

In terms of security and protection hardware, cover opening switches, magnetic field sensors, circuits that detect reverse current and connection errors, and physical sealing solutions are prominent. Hardware-based crypto modules and secure memory structures, used in conjunction with software security mechanisms, increase the meters' resistance to counterfeiting and side-channel attacks.

1.3. Energy Quality and Its Importance

The quality of electrical energy is a critical factor that encompasses all issues related to the amplitude, phase, and frequency of the voltage and current waveforms in a power circuit. Quality electrical energy means that the voltage amplitude and frequency at a defined point in the network maintain their nominal values and that the voltage waveform is sinusoidal (Barai et al., 2015).

Smart meters have the ability to measure the power quality of the entire grid. The main factors that degrade energy quality are: sudden interruptions, changes in voltage amplitude and frequency, harmonics, and load imbalance. For example, changes in voltage amplitude, interruptions, voltage surges, flicker (fluctuations in light brightness in lighting devices due to voltage fluctuations), and three-phase imbalances are defined as poor energy quality (Aouini & Azzouz, 2015). Preventing or eliminating these disturbances (e.g., limiting harmonics, performing shunt compensation) is an important part of the monitoring task of smart grids and, consequently, smart meters (Komninos et al., 2014).

2. Technical Architecture and Measurement Methods

2.1. Smart Meter Hardware Architecture

Smart meters are advanced devices used to measure and manage electricity consumption. Their technical architecture and measurement features ensure that these devices perform their basic functions properly.

HARDWARE	DESCRIPTION
Microcontroller (MCU)	Manages meter operations
Digital Signal Processor (DSP)	Signal processing and analysis
Memory (RAM, ROM, EEPROM)	Data storage and processing
Communication Modules (GPRS, ZigBee, LoRa)	Remote communication and data transfer
Power Management Circuits	Power supply and management
Measurement Circuits (Current, Voltage, Power)	Energy measurement and analysis
LCD Display Driver	Display and User Interface
Buttons and Keys	User Input and Control
Alarm and Warning Circuits	Abnormal condition detection and warning

Smart meters measure and manage electricity consumption by performing signal acquisition, signal conditioning, meter calculation, and communication functions, thereby increasing energy efficiency and enabling remote monitoring.

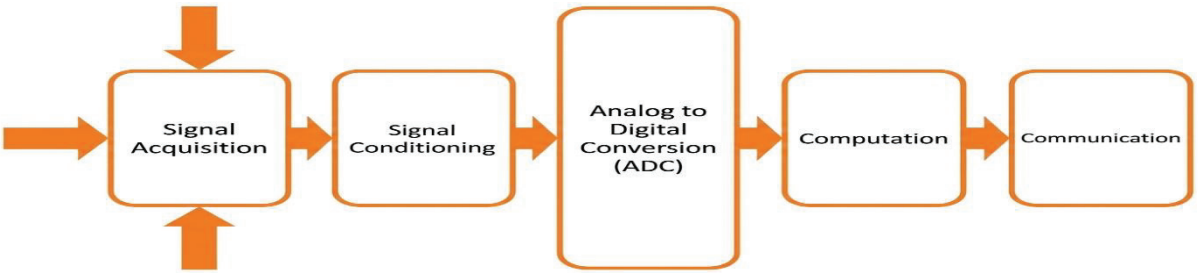

Figure 6: Functional block diagram of smart meters

The hardware architecture of a smart meter is essentially divided into five main sections: signal acquisition, signal conditioning, Analog-to-Digital Conversion (ADC), calculation, and communication.

The ADC architecture of smart meters works accurately and reliably by converting analog signals into digital data to measure energy consumption; this process involves signal

acquisition, filtering, sampling, and conversion stages and contributes to increasing energy efficiency.

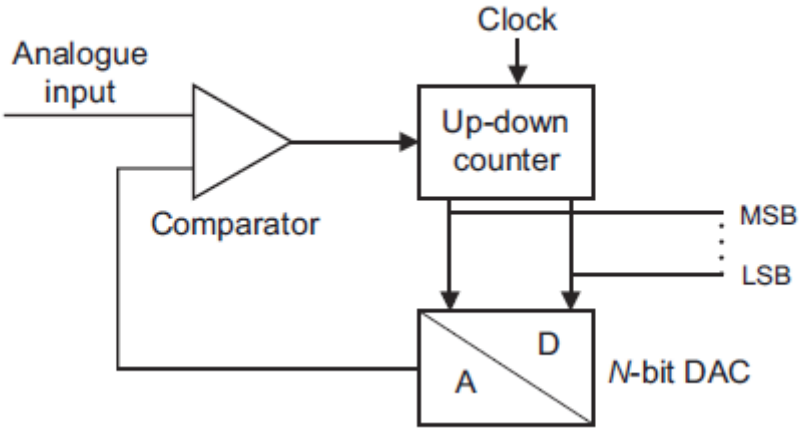

Figure 7: Simplified successive approximation ADC architecture proposed by John Wiley & Sons

1. Signal Acquisition (Sensors): Current and voltage sensors measure the magnitude and phase shift of the current and voltage at the supply point. Low-cost meters use shunt resistors for current and resistive voltage dividers for voltage. For applications requiring high accuracy, more sophisticated methods can be preferred, such as Rogowski coils, which calculate current by measuring magnetic field changes and offer high accuracy and measurement range, or Hall Effect sensors, which measure current using the magnetic field effect while providing galvanic isolation and operating with high accuracy.

2. Signal Conditioning: This section prepares the signals for the next step (ADC) and may include processes such as attenuation/amplification, addition/subtraction, and filtering to bring the signal amplitude within the ADC's input limits. Low-pass filters (LPF) are used to eliminate noise and interference, operational amplifiers (Op-Amp) are used to increase the signal level, isolation amplifiers are used to ensure signal integrity, and analog or digital correction techniques are applied for signal linearization and calibration.

3. Analog-to-Digital Conversion (ADC): Responsible for converting analog signals from sensors into digital form. Methods such as successive approximation (power-efficient and compact, for medium-level energy measurement applications) and sigma-delta (noise reduction and compact, high-precision energy measurement and applications) are used for measurement.

4. Calculation and Control Unit: This is the main processing unit that coordinates all arithmetic operations in the meter, data stamping, data preparation for communication, and routines such as payment/tamper detection. Microcontrollers such as STM32F407VGT6 or STM32F103 are used in designs.

5. Input/Output and Indicators: These include user interfaces, LCD/LED displays, and keypads. Some meters use colored lights or analog indicators to visualize energy consumption and encourage consumers.

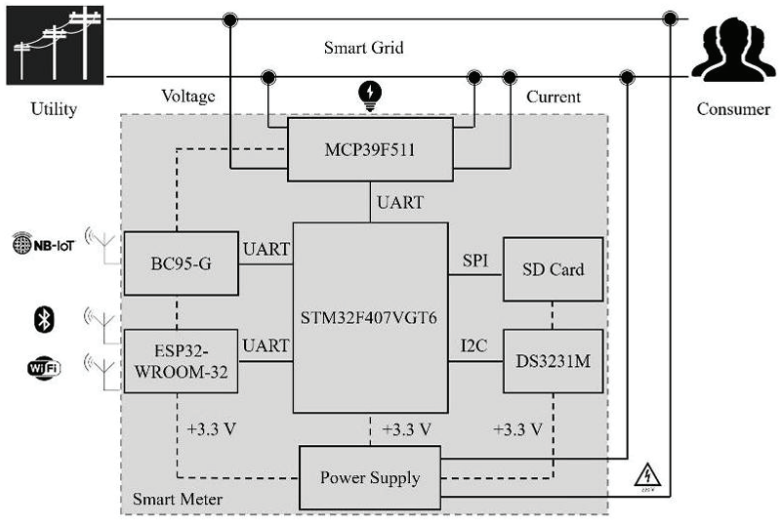

Figure 8: Hardware building blocks of a smart meter design (Akkaya, O. – 2021)

2.2. Measured Parameters and Calculations

Smart meters measure or calculate a series of electrical parameters that are critical for billing and network monitoring:

• Voltage (V) and Current (A): RMS values are measured.

• Active Power (*Pact*): This is the real power value. In three-phase systems, it is calculated using the formula $P=3IV\cos\theta$.

• Reactive Power (*Qreact*): Measures reactive power. It can be calculated using the formula $Q=3IV\sin\theta$.

• Apparent Power (S): The vector sum of active and reactive power.

• Power Factor (PF): It is the cosine of the phase angle between voltage and current waveforms ($\cos\theta$).

• Line Frequency (LF): Measures the grid frequency (e.g., 50 Hz).

• Energy Consumption (E): The integral of active power over a specific time interval (kWh).

• Phase Difference: The phase angle between current and voltage.

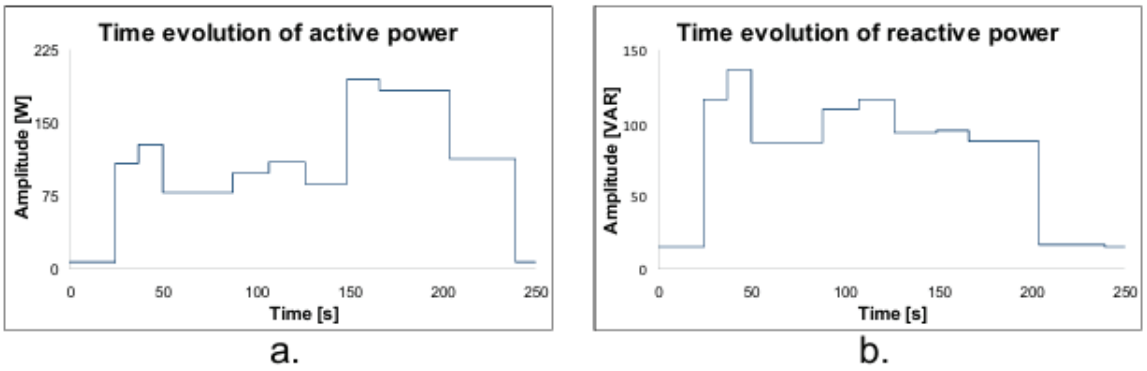

Figure 9: Evolution of power generated by switching four consumers on and off: **a.** active power evolution; **b.** reactive power evolution (Temneanu, M. – 2013)

2.3. Measurement Accuracy

Experimental studies have shown that the measurement accuracy of smart meter devices is greater than 99% (Barai et al., 2015). High accuracy ensures that meters are reliable for billing and energy tracking (Aouini & Azzouz, 2015). For example, in one design, voltage (VRMS) accuracy was determined to be approximately 99.65%, with values ranging from 99.78% to 99.86%, while current (IRMS) accuracy ranged from 99.10% to 99.85%. Although the theoretical error rate for some integrated circuits (such as CS5490) is stated as 0.1%, deviations of up to 4% can be observed in practical measurements for current (Shakiba et al., 2024).

2.4. Disaggregating Energy Consumption to Individual Consumers

Smart meters greatly assist consumers in understanding and optimizing their energy usage habits by allocating energy consumption to individual consumers. This increases energy efficiency, reduces costs, and minimizes environmental impacts.

Smart meters have the ability to disaggregate total consumption by individual devices in the home (SigMET) to help users better understand their energy consumption. This is done by analyzing voltage and current changes obtained from a single main meter using Nonintrusive Load Monitoring (NILM) techniques.

Devices are identified based on electrical signatures that analyze voltage and current fluctuations when they are turned on and off. The parameters that characterize this signature are active and reactive power changes, transient signal profiles, harmonic components of the current, instantaneous power, and admittance. For example, while the phase shift is 0 degrees for a resistive consumer, inductive or capacitive components can cause different phase shifts.

Figure 10: Electrical Signature Identification (ESI) Algorithm (Images Generated by Artificial Intelligence)

The algorithm's primary task is to continuously monitor events on the grid, extract their unique signatures, and match them with known device profiles to decompose total consumption.

3. Communication Infrastructure and Protocols

3.1. Advanced Metering Infrastructure (AMI)

Smart meters use Advanced Metering Infrastructure (AMI) to transmit data to energy suppliers and control centers. AMI is a system that includes smart meters (hardware), a communication network, and a data management system (software). One of the most important achievements of smart grids, AMI collects, measures, and analyzes the power quality and energy consumption data of each user. AMI's communication structure includes communication interfaces at different levels: Wide Area Network (WAN), Neighborhood Area Network (NAN), and Home Area Network (HAN).

3.2. Wireless Communication Technologies

Wireless technologies used in smart grids offer advantages such as flexibility, ease of scalability, and relatively low cost.

Technology	**Description and Application Area**	**Key Features**
NB-IoT	Ideal for long-range communication over wide geographic areas. Utilizes existing LTE cellular infrastructure.	Low Power Consumption (LPWAN), high capacity, reliable data transmission, long range.
Wi-Fi	Provides WLAN for residential, commercial office, and industrial facilities with internet access.	Wide bandwidth, theoretically high speed (up to 10 Gbps for Wi-Fi 6), easy setup.

LoRa RF	An alternative long-range solution for geographic areas without internet access.	Low power consumption, long range, electricity meters can be used as modems.
ZigBee	WPAN standard for HAN and small-scale applications.	Low cost, easy to program, low power consumption.
Bluetooth	Short-range device-to-device communication (e.g., transmitting meter readings to mobile devices).	Low cost, low power (BLE), WPAN.
GSM/GPRS/LTE	Widely used for remote reading of meters, especially those in dispersed locations.	Wide coverage area, utilizes existing network infrastructure.

3.3. Wired Communication Technologies

• Fiber Optic: The preferred choice for WAN backbones due to its immunity to electromagnetic interference and ability to provide high-bandwidth communication over long distances.

• Power Line Communication (PLC): Uses existing electrical cables as a communication channel. Its advantage is that it does not require additional cable costs; its disadvantage is exposure to signal interference and changes in communication impedance.

• Ethernet: Used in local area networks (LAN) and home area networks (HAN) in SCADA systems.

3.4. Protocols and Data Transfer

• MQTT (Message Queuing Telemetry Transport): A telemetry messaging protocol that offers low bandwidth and operates on a publish/subscribe principle. It is widely used for IoT devices.

• IEC 61850: An international, function-based industrial communication protocol that enables interoperability in substations and network systems.

• MODBUS: An application layer messaging protocol used for device-to-device communication in industrial applications.

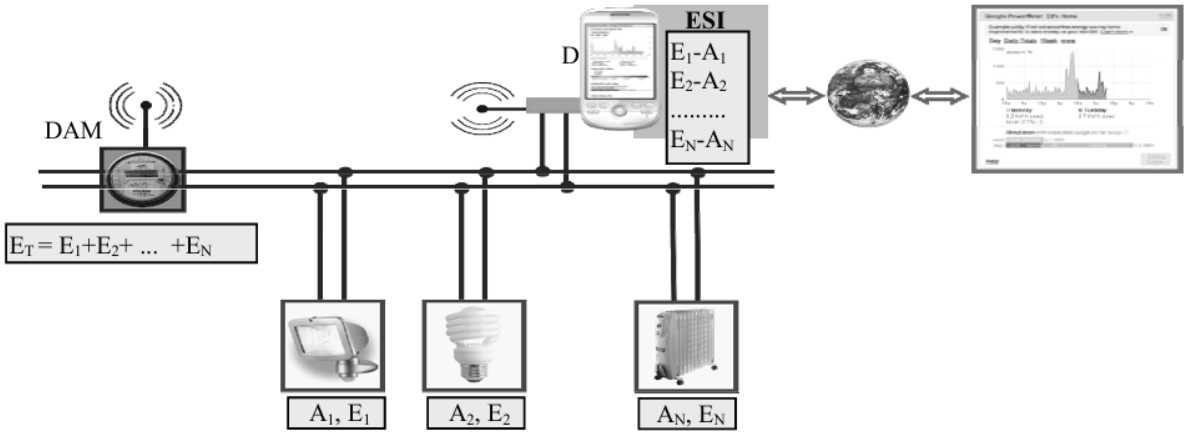

Figure 11: General architecture of SigMET: DAM – Data Acquisition Module, D – display, Ai – i device, Ei – energy consumption for Ai, ESI – Electrical Signature Identification (Temneanu, M. – 2013)

4. Smart Meters and Network Management

4.1. Demand-Side Integration (DSI) and Economic Impacts

Smart meters provide consumers with real-time consumption data, enabling them to reduce unnecessary expenses and lower their bills. This ensures the security of supply and demand balance through the efficient use of electrical energy. DSI is a set of measures that supports grid operation by utilizing consumers' loads and local production.

DSI is implemented either price-based or incentive-based. Price-based DSI applications include:

1. Time-of-Use (ToU) Pricing: Different unit prices are applied at different times of the day (e.g., daytime, peak hours (5:00 p.m. to 10:00 p.m.), and nighttime). The high prices applied during peak hours encourage consumers to shift their demand to off-peak hours.

2. Real-Time Pricing (RTP): Typically offers hourly fluctuating prices that reflect changes in wholesale electricity prices.

3. Critical Peak Pricing (CPP): This is essentially a ToU tariff, but a much higher price is applied when the system experiences operational problems or when the supply price is very high.

DSI services include load shifting (moving energy usage from peak to off-peak hours), valley filling (increasing off-peak demand, e.g., with electric vehicle charging), and peak shaving (reducing peak load demand). Through smart meters, consumers (or collectively, prosumers) provide flexibility to the grid by changing their consumption patterns.

4.2. Remote Control of Energy and Detection of Losses/Theft

Smart meters can enable remote on/off control of energy through communication technologies. This control allows electricity service providers to manage load.

Remote monitoring and control of energy enables real-time analysis of consumption data, allowing for the rapid detection and effective prevention of losses and theft.

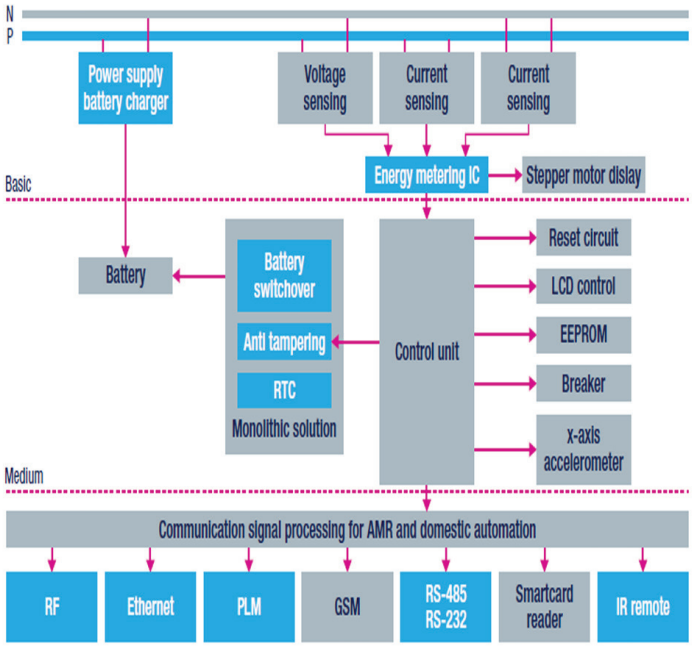

Figure 12: E-Smart meter block diagram (Mustafa, I. – 2019)

Combating Losses and Unauthorized Consumption: In Turkey, the total loss rate in electricity distribution systems, including technical losses and unauthorized (illegal) energy use, has remained high for many years. Electricity theft and other non-technical losses (NTL) cause serious economic problems for distribution companies, especially in developing countries, and negatively affect grid reliability (Depuru et al., 2011; Smith, 2004). These losses limit the investment and maintenance capacity of distribution companies, while also creating an additional burden on consumers through the reflection of increased costs in electricity tariffs.

Smart meters and Advanced Metering Infrastructure (AMI) offer significant advantages over traditional methods in detecting non-technical losses. AMI-based systems enable remote monitoring of the distribution network through two-way communication and high-time-resolution measurements (Depuru et al., 2013). This makes it possible to compare the total power measured at the distribution transformer level with the consumption reported by the meters of subscribers connected to the same transformer. This approach enables the detection of energy imbalances in the system based on Kirchhoff's current law (Cavdar, 2004).

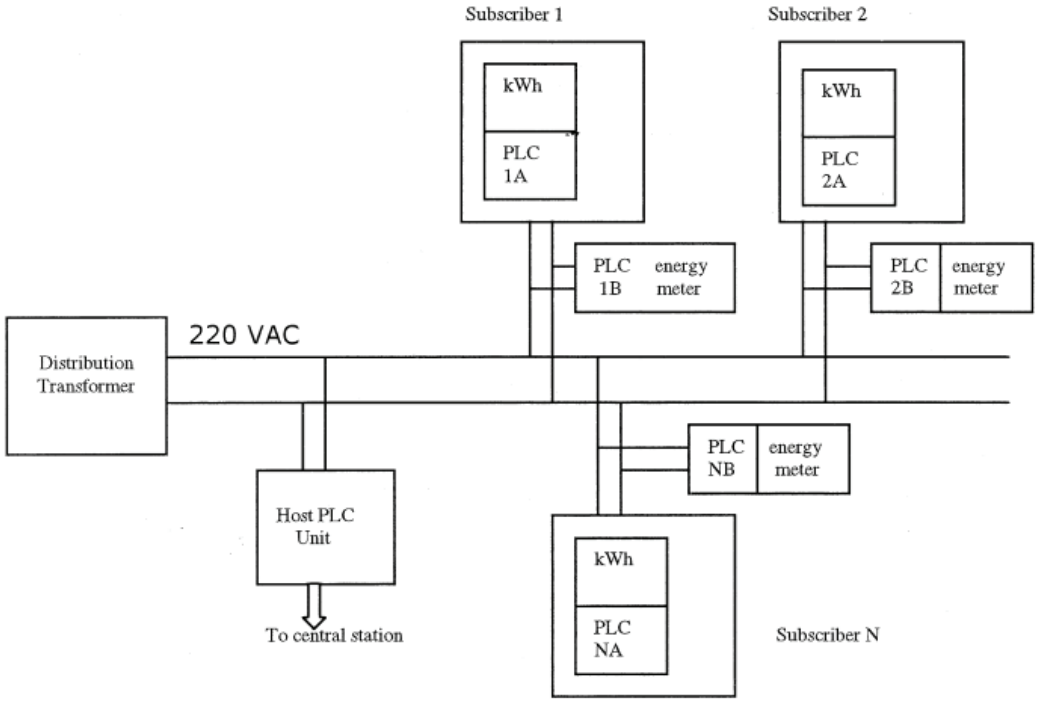

Figure 13: Illegal electricity detection scheme proposed by Cavdar (2004)

In the literature, one of the commonly used methods for detecting unauthorized energy use is to analyze the difference between the total power at the transformer output and the total consumption of the subscriber meters. A significant increase in this difference indicates either tampering with the meters or energy being drawn directly from the line before the meters (Depuru et al., 2011). However, most methods such as historical data analysis, fuzzy logic, support vector machines, or artificial neural networks are limited in practice due to high computational costs and real-time application difficulties (Nagi et al., 2010; Glauner et al., 2017).

In this context, the real-time detection approach proposed by Bin-Halabi et al. (2019) offers a low-cost and fast solution based on the time-dependent change (running difference) in the instantaneous power difference between the transformer and subscriber meters. In the proposed method, deviations between the power measured at the transformer level and the instantaneous consumption of subscribers are monitored; sudden increases in these deviations are defined as suspicious consumption behavior. This approach differs from many methods in the literature in that it does not require extensive historical data storage or complex statistical preprocessing.

Additionally, measuring phase and neutral currents in meters and examining imbalances between these currents can serve as a complementary tool for detecting irregularities such as meter bypassing. Particularly when a parallel connection is made to meters, sudden drops in consumption measured at subscriber meters are observed, while no significant decrease occurs in the total power measured at the transformer level (Bat-Erdene et al., 2011; Bat-Erdene et al.,

2013). Real-time detection of such anomalies allows for the differentiation of the type of irregular use (meter tampering or unauthorized use via the line).

The effective detection and reduction of non-technical losses is critical for controlling costs in electricity distribution systems. As emphasized by Depuru et al. (2011), preventing unauthorized usage increases the financial sustainability of distribution companies and prevents unnecessary increases in unit electricity costs. This plays an important indirect role in alleviating energy poverty by contributing to the reduction of electricity access costs, especially for low-income households. In fact, when considering this critical situation in terms of ethical values and social benefit, it is perhaps more valuable than anything else.

5. Data Analysis, Anomaly Detection, and Forecasting

Smart meters generate large amounts of time series data that exhibit seasonality (annual, monthly), which is vital for energy management.

Population and economic growth are placing increasing pressure on existing electricity grids. Since electrical energy cannot be stored efficiently, production and consumption must be balanced in real time. This means that even the smallest error can have major consequences. Smart meters play a pivotal role in monitoring the grid in real time and enabling more efficient energy management by making data-driven decisions.

The fundamental goal in anomaly detection is to ensure that abnormal points are not labeled as normal; in this process, some normal points being labeled as anomalies does not pose a problem. It is important to closely monitor and control energy consumption. When considering energy distribution, smart meters play a milestone role in controlling this energy. Any power outage, error, or incorrect measurement that may occur in meters that measure energy consumption affects many parties, from distribution companies to end users. Data analytics studies and big data technologies conducted to detect such anomalies in the energy sector play a significant role in producing clear and actionable outputs that aim to increase efficiency and savings by analyzing time series data collected from sensors and meters in real-time or in batches.

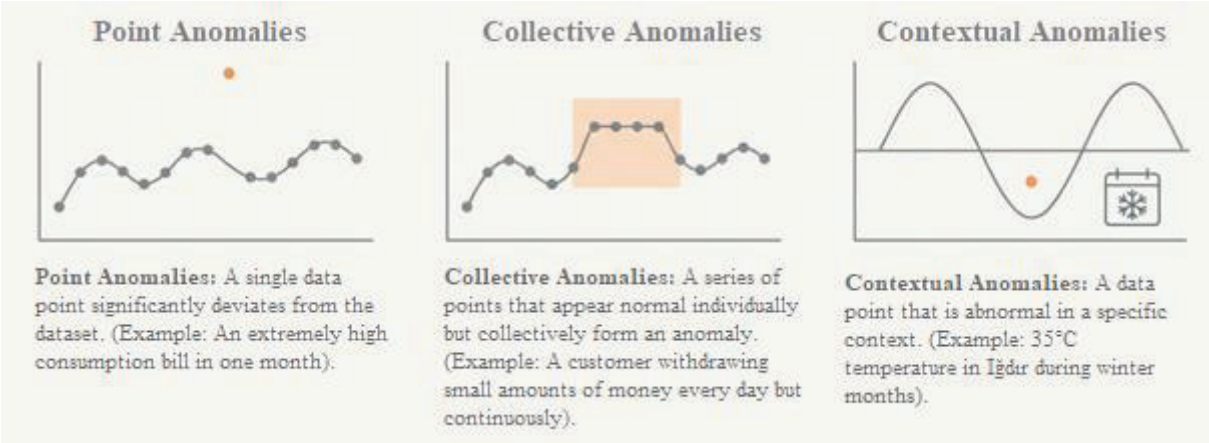

Figure 14: Outliers that do not conform to normal behavior patterns in the data set (Yarat, S. & Orman, Z. (2023))

5.1. Anomaly Detection Methods

Anomalies are defined as outlier observations that deviate significantly from the general behavior patterns observed in a dataset. In the literature, anomalies are classified as individual observations (point anomalies), groups of observations that exhibit abnormal behavior when evaluated together (collective anomalies), and observations that deviate from the norm in a context-specific manner (contextual anomalies) (Chandola, Banerjee, & Kumar, 2009). Detecting anomalies in energy consumption data is critical for energy distribution companies, particularly in terms of reducing financial losses arising from technical losses, unauthorized use, and measurement errors.

To this end, unsupervised machine learning algorithms, which eliminate the need for labeled data, are widely used. One such algorithm, Isolation Forest (IF), is based on the assumption that anomaly observations can be isolated with fewer splits compared to normal data. In isolation trees created using randomly selected features and splitting points, data points isolated at levels closer to the root of the tree are considered anomalies. The IF algorithm performs particularly well in detecting global outliers (Liu, Ting, & Zhou, 2008).

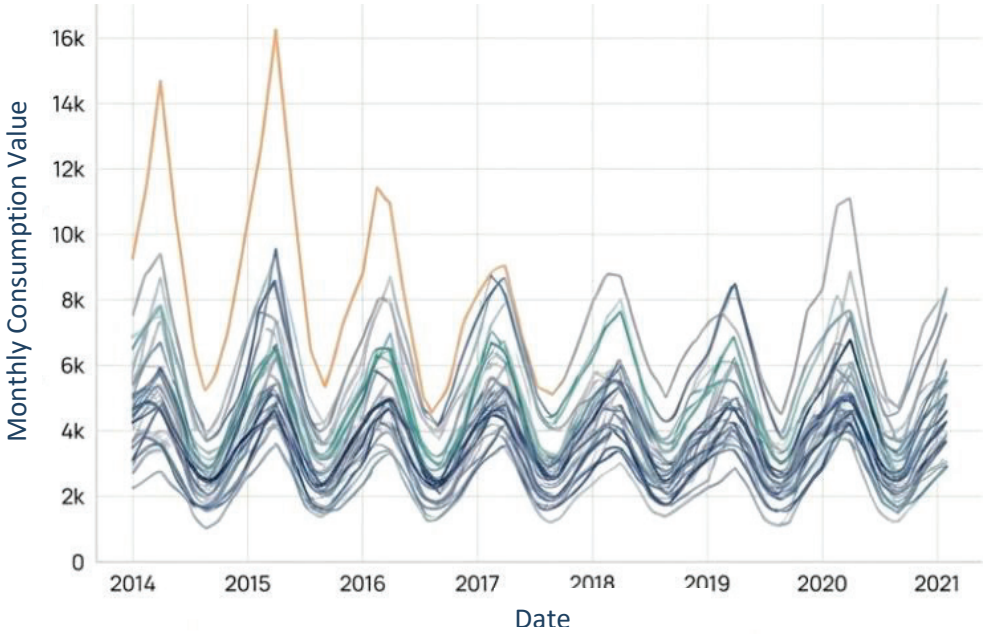

Figure 15: 8-year general lighting consumption records (Yarat, S. & Orman, Z. (2023))

monthly consumption value

Another common method, the Local Outlier Factor (LOF), adopts a density-based approach and measures the degree of anomaly of a data point by comparing it to the density of its neighboring points. This method focuses on local neighborhood relationships rather than the overall structure of the dataset, producing effective results, especially in identifying local anomalies (Breunig, Kriegel, Ng, & Sander, 2000).

FbProphet (Prophet), a time series-based approach, produces future predictions by separating trends, seasonality, and holiday effects. Observations that fall outside the confidence intervals of the predictions generated by the model can be labeled as anomalies. This feature enables FbProphet to be used for anomaly detection in time-dependent and seasonal data such as energy consumption (Taylor & Letham, 2018).

Empirical studies in the literature report that the Isolation Forest, Local Outlier Factor, and FbProphet algorithms can successfully detect potential extreme and abnormal observation points in energy consumption data. Using these methods together or comparatively allows for a more comprehensive identification of different types of anomalies.

5.2. Consumption Forecasting

Time series forecasting aims to predict future energy demand using historical data. Forecasts are classified as short-term (a few hours to a week), medium-term (a week to a year), and long-term (more than a year) based on their duration.

In a comparison of forecasting studies conducted on smart meter data, the FbProphet algorithm was found to yield better results than the XGBoost algorithm on time series data containing seasonality. The mean absolute percentage error (MAPE) for FbProphet was 8.37%, while for XGBoost it was calculated as 11.10%.

6. Cybersecurity, Energy Poverty

6.1. Cybersecurity Principles and Threats

The operation of smart grids is largely dependent on ICT, which makes them vulnerable to cyber attacks. The fundamental elements of cybersecurity are as follows:

1. Availability: Ensuring that services are continuously and uninterruptedly provided to authorized users. It is considered the highest priority security principle in smart grids.

2. Integrity: This refers to preventing unauthorized individuals from altering information (particularly consumption data used for billing). Integrity attacks target the alteration of important data such as billing information or network operation information.

3. Confidentiality: This refers to protecting sensitive information, such as energy usage data, from unauthorized access, as this data allows inferences to be made about personal lifestyles.

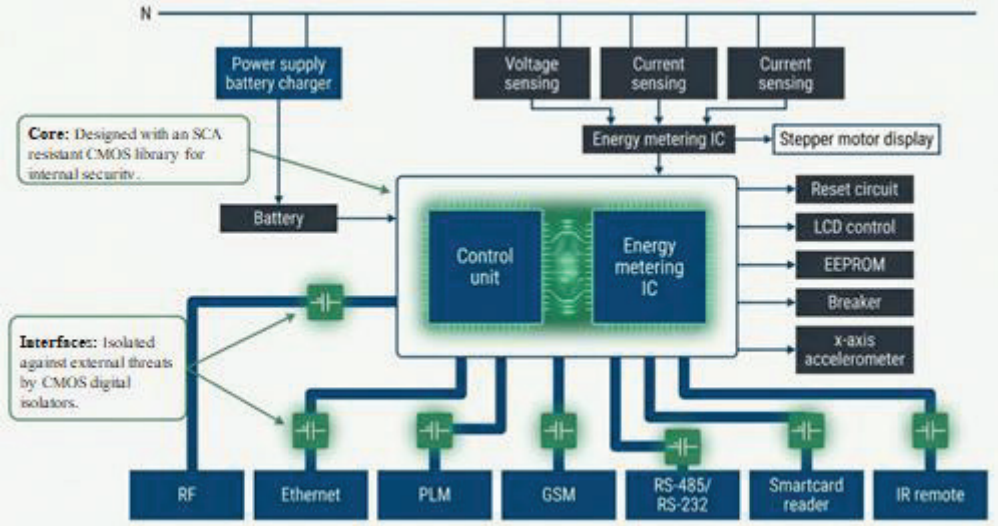

Figure 16: Anatomy of the New Secure Architecture (Created with visual artificial intelligence.)

Types of Cyber Attacks: Attacks can be passive (data theft) or active (data modification). The most dangerous active attacks are Denial of Service (DoS) attacks, which overload the system's resources, rendering it unusable, or modify data to cause the system to make incorrect decisions.

Side-Channel Attacks (SCA): A critical security vulnerability in smart meter hardware is Side-Channel Attacks. These attacks attempt to obtain secret keys by observing variations in power consumption or electromagnetic radiation while the device is operating normally. To counter these threats, it is necessary to develop SCA-resistant digital CMOS (Complementary Metal-Oxide-Semiconductor) infrastructure that reduces power consumption variations.

Strong cryptographic protocols alone cannot protect against physical vulnerabilities at the hardware level. Security at the hardware level directly impacts the integrity and security of the entire Advanced Metering Infrastructure (AMI).(directly affects its integrity and security. SCA-resistant hardware forms a foundation for the industry. It is a secure platform for future cryptographic chips. A more resilient energy infrastructure against cyber threats and the adoption of secure data protocols for the benefit of society are of paramount importance.

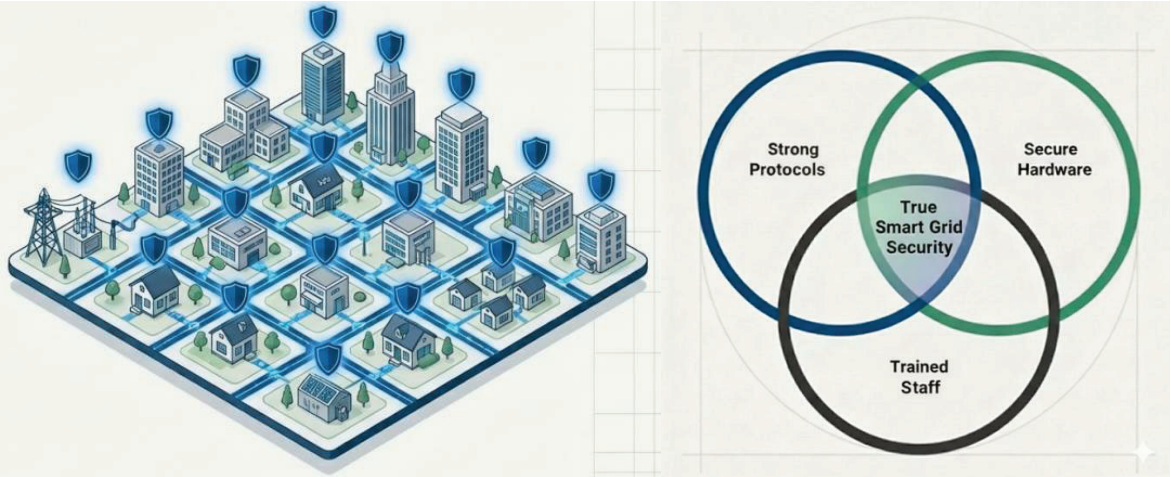

Figure 17: Holistic Security to Protect the Entire Smart Grid by Strengthening a Single Meter (Created with visual AI.)

Strengthening the security of a single meter will contribute to protecting the entire smart grid with a comprehensive security approach that addresses not only that device but also hardware, software, and the human factor in an integrated manner.

True resistance against SCA attacks must begin at the CMOS cell level, the fundamental building block of security.

CMOS libraries and digital isolators provide a double layer of defense against both intentional attacks and environmental threats. No matter how advanced the technology is, it is imperative that employees are adequately trained to avoid attacks such as social engineering.

6.2. Energy Poverty and the Role of Smart Meters

Energy poverty is defined as the inability of an individual or household to access sufficient energy to meet basic goods and services within defined living standards. In Turkey, two basic approaches are used to identify energy poverty in line with the literature: the quantity method and the income ratio approach. In the quantity method, the minimum amount of electricity that a household should consume is set as a threshold, and consumption below this threshold is considered an indicator of energy poverty. Studies conducted for Turkey indicate that households consuming less than approximately 100–120 kWh of electricity per month can be considered energy poor (Eke & Ayrancı, 2018).

In the income ratio approach, the share of household energy expenditures in disposable income is taken as the basis, and allocating more than 10% of income to electricity is considered an indicator of energy poverty. This approach is widely preferred because it reveals the economic burden of energy access more objectively, despite differences in income levels and regional conditions (Eke & Ayrancı, 2018).

Regional analyses conducted specifically for Turkey show that energy poverty is concentrated in the Southeast and Eastern Anatolia regions, where loss/theft rates are particularly high. In provinces within the Dicle and Van Lake electricity distribution regions, it was found that household electricity consumption levels often fell below thresholds determined by the quantity method; conversely, electricity expenditures exceeded 10% of income in low-income groups. These findings indicate that energy poverty in these regions has deepened in terms of both consumption volume and income burden (Eke & Ayrancı, 2018).

High loss/theft rates increase electricity distribution costs, causing these costs to be passed on to all consumers through tariffs and indirectly deepening energy poverty. In this context, smart meters and advanced metering infrastructures reduce network operators' costs by detecting and reducing losses/theft ; they contribute indirectly but significantly to combating energy poverty by contributing to the reduction of unit electricity costs in the long term (Eke & Ayrancı, 2018).

On the other hand, the legal responsibilities of electricity network operators arising from power outages are assessed within the framework of connection and system usage agreements made with consumers. The continuity of electricity supply is critical for both economic prosperity and the prevention of energy poverty, and uninterrupted access to energy is particularly important in the context of social policy for low-income and vulnerable households (Eke & Ayrancı, 2018).

Conclusion

Smart grids, as a transformative paradigm shaping the future of modern energy systems, are designed to overcome the limitations of traditional electricity infrastructure. In this context, smart meters stand out as the most critical components of the grid in the field; they serve as a bridge that not only measures energy but also supports data-driven management, demand-side integration, and sustainability goals (Barai et al., 2015; Komninos et al., 2014). As examined in this study, the historical evolution of smart meters—from electromechanical manual readings in the 1970s to post-2000 AMI-based two-way communication systems—has laid the foundation for increasing energy efficiency and enhancing grid reliability (Fan & Gong, 2013).

From a technical architecture perspective, smart meters are integrated systems equipped with high-accuracy sensors (shunt resistors, sigma-delta ADCs), advanced processing units (STM32 series microcontrollers), and multiple communication modules (PLC, NB-IoT, ZigBee) These components enable individual device separation using NILM techniques by calculating parameters such as active/reactive power, power factor, and energy consumption with over 99% accuracy, thereby providing consumers with real-time insights (Aouini & Azzouz, 2015). The communication infrastructure is supported by protocols such as MQTT, IEC 61850, and MODBUS at the WAN/NAN/HAN layers, ensuring secure and efficient data transmission.

In the context of network management, smart meters enhance demand-side integration (DSI), encouraging load balancing with pricing models such as ToU, RTP, and CPP; thus reducing peak demand and providing economic savings. Particularly in Turkey, where loss/theft rates (NTL) are high at around 17-20%, methods such as transformer-subscriber comparisons based

on Kirchhoff's law and phase-neutral current imbalance analyses offer real-time detection capabilities, reducing costs and alleviating energy poverty (Depuru et al., 2011; Cavdar, 2004; Bin-Halabi et al., 2019). In terms of data analysis, unsupervised algorithms such as Isolation Forest, LOF, and FbProphet play a critical role in anomaly detection and consumption forecasting (with an accuracy of up to 8.37% MAPE) and effectively model seasonal time series (Liu et al., 2008; Taylor & Letham, 2018).

However, the proliferation of these technologies also brings cyber security challenges. Violations of accessibility, integrity, and confidentiality principles can lead to network instability through DoS attacks or side-channel attacks (SCA); therefore, SCA-resistant CMOS designs and cryptographic measures are becoming mandatory (Shakiba et al., 2024; Fan & Gong, 2013). The problem of energy poverty in Turkey – consumption below the 100-120 kWh threshold and expenditures exceeding 10% of income – is intertwined with loss/theft in regions such as Southeast and Eastern Anatolia and can be alleviated indirectly (through cost reduction) with the contribution of smart meters (Eke & Ayrancı, 2018).

In conclusion, smart meters, as the cornerstone of smart grids, have the potential to make energy systems more efficient, flexible, and equitable. However, for this potential to be fully realized, increased security investments, deeper integration of data analytics, and overcoming socio-economic barriers (energy poverty, legal liabilities) in developing countries are necessary. Future work addressing these challenges through AI-based prediction models and blockchain-enabled secure communication will accelerate a more environmentally friendly and accessible energy future. Smart meters are positioned as an indispensable element of sustainable development, beyond being merely a measurement tool.

References

Acar, F., Altınok, Y., Görgülü Balcı, S., Lüy, M., & Metin, N. A. (2024). Sustainable grids: Smart meter solutions for efficient energy measurement. *International Scientific and Vocational Studies Journal, 8*(1), 49–64. https://dergipark.org.tr/en/pub/bilmes/issue/85878/1485662

Akkaya, O. S., & Soy, H. (2021). Hardware design of single-phase smart electricity meter based on multiple wireless connectivity technologies. *European Journal of Science and Technology, (27)*, Article 1040829. https://doi.org/10.31590/ejosat.1040829

Alev, N., & Erdemli, M. (2019). The relationship between electricity consumption and economic growth: An analysis for European Union countries and Turkey. *ASSAM International Journal of Social Sciences, 4*(12), Article 623546. https://dergipark.org.tr/tr/pub/assam/issue/50607/623546

Amal, E., Yılmaz, K., & Özdemir, E. (2022). Examining the effects of wind power plants on the electricity grid. *Kocaeli University Journal of Science*. https://www.acarindex.com/kocaeli-universitesi-fen-bilimleri-dergisi/ruzgar-enerji-santrallerinin-elektrik-sebekesine-etkilerinin-incelenmesi-1204778

Ateş, M. A. (2024). The legal basis for the responsibility of electricity grid operators arising from power outages. *Çukurova University Journal of Law Research, (5)*, Article 1424599. https://dergipark.org.tr/tr/pub/cuhad/article/1424599

Bat-Erdene, B., Lee, B., Kim, M.-Y., Ahn, T. H., & Kim, D. (2013). Extended smart meters-based remote detection method for illegal electricity usage. *IET Generation, Transmission & Distribution, 7*(11), 1332–1343. https://doi.org/10.1049/iet-gtd.2013.0066

Bat-Erdene, B., Nam, S.-Y., & Kim, D.-H. (2011). A novel remote detection method of illegal electricity usage based on smart resistance. In *Future information technology* (pp. 214–223). Springer.

Bayındır, R., & Demirtaş, K. (2014). Smart grids: Electronic meter applications. *Politeknik Dergisi, 17*(2), Article 368010. https://dergipark.org.tr/tr/pub/politeknik/issue/33070/368010

Breunig, M. M., Kriegel, H.-P., Ng, R. T., & Sander, J. (2000). LOF: Identifying density-based local outliers. *ACM SIGMOD Record, 29*(2), 93–104. https://doi.org/10.1145/342009.335388

Cavdar, I. H. (2004). A solution to remote detection of illegal electricity usage via power line communications. In *Proceedings of the IEEE Power Engineering Society General Meeting* (pp. 896–900).

Chandola, V., Banerjee, A., & Kumar, V. (2009). Anomaly detection: A survey. *ACM Computing Surveys, 41*(3), Article 15. https://doi.org/10.1145/1541880.1541882

Dereli, İ., & Temiz, İ. (2019). Wireless power measurement system enabling the monitoring of electrical power consumption data over the internet for smart grids. *Erzincan University Journal of Science and Technology, 7*(2), Article 534876. https://dergipark.org.tr/tr/pub/erzifbed/issue/51325/534876

Depuru, S. S. S. R., Wang, L., & Devabhaktuni, V. (2011). Electricity theft: Overview, issues, prevention and a smart meter based approach to control theft. *Energy Policy, 39*(2), 1007–1015. https://doi.org/10.1016/j.enpol.2010.11.037

Depuru, S. S. S. R., Wang, L., Devabhaktuni, V., & Green, R. C. (2013). High performance computing for detection of electricity theft. *International Journal of Electrical Power & Energy Systems, 47*, 21–30. https://doi.org/10.1016/j.ijepes.2012.10.037

Doğru, C. (2010). A look at the restructuring process of the electricity market in Turkey. *Sakarya University Journal of Economics, (2)*, Article 610194. https://dergipark.org.tr/tr/pub/sbm/issue/48003/610194

Ekanayake, J. B., Jenkins, N., Liyanage, K., Wu, J., & Yokoyama, A. (2012). *Smart grid: Technology and applications*. John Wiley & Sons.

Eke, E. U., & Ayrancı, E. (2018). Evaluation of the electricity sector in Turkey in terms of energy poverty. *Political Economic Theory, 2*(2), 109–129. https://doi.org/10.30586/pek.456009

Glauner, P., Meira, J. A., Valtchev, P., State, R., & Bettinger, F. (2017). The challenge of non-technical loss detection using artificial intelligence: A survey. *International Journal of Computational Intelligence Systems, 10*(1), 760–775. https://doi.org/10.2991/ijcis.2017.10.1.51

Güçlü, B., Bayrakçı, H. C., & Süzen, A. A. (2018). Remote reading of electricity meters and energy analysis. *International Journal of Technological Sciences, 10*(3), Article 517963. https://dergipark.org.tr/tr/pub/utbd/issue/42841/517963

Gündüz, M. Z., & Daş, R. (2021). *Smart grids: Data transmission with cybersecurity elements.*

Jenipher, R. N. (2017). Software and hardware implementation of a smart meter with demand response using Proteus. *Journal of Scientific Instruments*.

Kabalcı, E., & Kabalcı, Y. (2017). Design and implementation of a wireless energy monitoring system for smart grids. *Gazi University Journal of Science Part C: Design and Technology, 5*(2), Article 638529. https://dergipark.org.tr/tr/pub/gujsc/issue/49772/638529

Kocaman, B. (2016). *Providing cost savings by using electronic meters in residential areas*.

Liu, F. T., Ting, K. M., & Zhou, Z.-H. (2008). Isolation forest. In *Proceedings of the 2008 IEEE International Conference on Data Mining* (pp. 413–422). IEEE. https://doi.org/10.1109/ICDM.2008.17

Mustafa, I., Anjum, A., & Kouahla, Z. (n.d.). (2019) *Security of smart-meters against side-channel-attacks (SCA)*. https://www.researchgate.net/publication/339593548_Security_of_Smart-Meters_against_Side-Channel-Attacks_SCA

Nagi, J., Yap, K. S., Tiong, S. K., Ahmed, S. K., & Mohamad, M. (2010). Non-technical loss detection for metered customers in power utility using support vector machines. *IEEE Transactions on Power Delivery, 25*(2), 1162–1171. https://doi.org/10.1109/TPWRD.2009.2030890

Nane, M., Gök, H., Akyazı, Ö., & Aksoy, C. (2023). Monitoring and control of energy with smart electricity meters. *Gümüşhane University Journal of Science and Technology, 13*(4), Article 1227095. https://dergipark.org.tr/tr/pub/gumusfenbil/issue/80368/1227095

Smith, T. B. (2004). Electricity theft: A comparative analysis. *Energy Policy, 32*(18), 2067–2076. https://doi.org/10.1016/S0301-4215(03)00182-4

Tabak, B., & Yalçın, M. A. (n.d.). *Energy quality in electrical power systems*.

Taylor, S. J., & Letham, B. (2018). Forecasting at scale. *The American Statistician, 72*(1), 37–45. https://doi.org/10.1080/00031305.2017.1380080

Temneanu, M., & Ardeleanu, A. S. (2013). Hardware and software architecture of a smart meter based on electrical signature analysis. In *2013 IEEE International Conference on Automation, Quality and Testing, Robotics* (pp. 1–6). IEEE. https://doi.org/10.1109/AQTR.2013.6563499

Utma, A., Özçelik, M. A., & Yılmaz, A. S. (2017). The design of a smart energy management system for microgrids. *International Journal of Energy and Smart Grid, 2*(2), 34–42.

Uzun, P., & Temiz, İ. (2021). *The use of communication technology in smart grids*.

Yarat, S., & Orman, Z. (2023). Anomaly detection and prediction for smart meter data in electric power distribution. *Journal of Computer Science and Technologies, 3*(2), 72–85. https://doi.org/10.54047/bibted.1224628

Koukouvinos, K. G. & Koukouvinos, G. K. & Chalkiadakis, P. & Kaminaris, S. D. & Orfanos, V. A. & Rimpas, D. (2025). Evaluating the Performance of Smart Meters: Insights into Energy Management, Dynamic Pricing and Consumer Behavior.

https://doi.org/10.3390/app15020960

Chapter 6

MICROGRID ENERGY MANAGEMENT: ARCHITECTURAL STRUCTURES, CONTROL LAYERS, AND ARTIFICIAL INTELLIGENCE SOLUTIONS

Ahmet TOP [1]

1 Dr. Öğr. Üyesi Ahmet TOP

Department of Electrical and Electronics Engineering, Faculty of Technology, Fırat University, Turkey, ORCID ID: http://orcid.org/0000-0001-6672-2119

1. INTRODUCTION

Numerous power outages on global power grids have been observed in recent years. Millions of dollars have been lost economically as a result of these disruptions. These interruptions affect millions of individuals annually in the United States alone, costing billions of dollars in lost revenue [1]. Transmission line failure, power plant faults, extreme weather, and natural disasters are all examples of power system failures. The long-term effects on vital loads, such as hospitals, airports, and continuous process industries, are a major worry with these occurrences. Furthermore, it may take a long time to rebuild the grid following severe power outages. In order to guarantee grid restoration, it is occasionally necessary to disconnect even healthy transmission cables [2]. Therefore, concerns about the future of global power grids must be addressed [3].

The International Energy Agency draws attention to the notable increase in power demand, which heralds the start of a new "Electric Age" propelled by the expanding need for air conditioning, data centers, buildings, transportation, and industry [4]. Demand rose by 4.3% in 2024 and is expected to expand at a rate of about 4% annually, increasing to 3500 TWh in three years, which is comparable to Japan's total power consumption. Energy consumption in Canada is predicted to rise from 624 TWh in 2020 to more than 819 TWh in 2050 [5]. Concerns are developing as the need for energy rises [4]. First, if this growth is not properly controlled, it may result in increased emissions, especially from fossil fuel sources. Second, even while renewable energy sources (RESs) like solar and wind help cut emissions, their unpredictability can lead to power supply instability and make emission reduction efforts more difficult if they are not well balanced [6].

It is appropriate to think about reorganizing the electrical grid in light of the issues mentioned. Microgrids (MGs), which are installed in comparatively tiny geographic areas and are usually connected at the distribution side, are one such restructure. MGs can function in both islanded and grid-connected modes. This eliminates the need for costly transmission lines and enables application in remote locations like rural areas [7–9]. Additionally, in the event of adjacent grid failures or cascading power outages, a microgrid can disconnect itself from the grid. This improves local systems' resilience and dependability, which is essential for important loads, particularly during natural disasters. However, because of its smaller size, if backup alternatives like Energy Storage Systems (ESS) are poorly designed, a distributed energy resource (DER) failure could affect the entire system.

Microgrids require complex energy management systems (EMS) because they must consider the optimal operation and real-time control of DERs to meet the microgrid's stability and other requirements. EM optimization for microgrids has gained significant attention over the past decade, with several proposed methods ranging from mathematical methodologies to advanced learning algorithms. Furthermore, metaheuristic methods have also been frequently used to the optimal deployment of DERs to lower total operational expenses.

By addressing dependability concerns brought on by the expanding demand in contemporary electrical grids, the erratic nature of renewable energy sources, and the requirement for continuous power for important loads, this chapter emphasizes the significance of microgrid (MG) technology. A thorough explanation of microgrids is provided, along with information on their architectural structures (AC, DC, and hybrid MGs), operating modes, and the functions of mechanical, electrochemical, and electrical energy storage systems in MG performance.

The basic goals of MG control systems are explained, along with centralized, decentralized, and distributed control strategies as well as hierarchical control structures (primary, secondary, and tertiary control). The improvement of distributed control systems using deep learning, machine learning, and artificial intelligence techniques is then covered as a contemporary trend. These techniques' benefits for load forecasting, fault detection, energy management, integration of renewable energy, demand-side management, and autonomous decision-making are examined.

The chapter emphasizes the crucial role of MG control strategies in the sustainable energy vision and provides significant considerations for researchers, practitioners, and policymakers. It also highlights the opportunities presented by hybrid MG structures, multi-MG networks (MMGs), and advanced communication infrastructures in future smart energy systems.

2. MICROGRID

An interconnected collection of distributed generators, energy storage devices, and loads that can exchange power with the main grid via a single common connection point (PCC) is called a microgrid [10]. Microgrids can function as independent units (i.e., islands) or in tandem with the main grid. As a result, MGs can be used to generate, distribute, and control the flow of power to nearby customers in remote locations. MGs are regarded as one of the key ideas that will make it possible to integrate a significant amount of renewable energy sources into our electrical systems [11]. Photovoltaic (PV) modules, small-capacity hydropower facilities, ocean energy, and wind turbines are examples of current and emerging RESs that are commonly integrated into MGs, as illustrated in Figure 1. By integrating complementing distributed renewable resources, MGs can enhance the local power grid's energy security and dependability. Future smart grids, which have the ability to convert current centralized power grids into fully distributed infrastructures, depend heavily on MGs. Alternating current microgrids (ACMG), direct current microgrids (DCMG), and hybrid microgrids (HMG) are the three types of MG architectures [12].

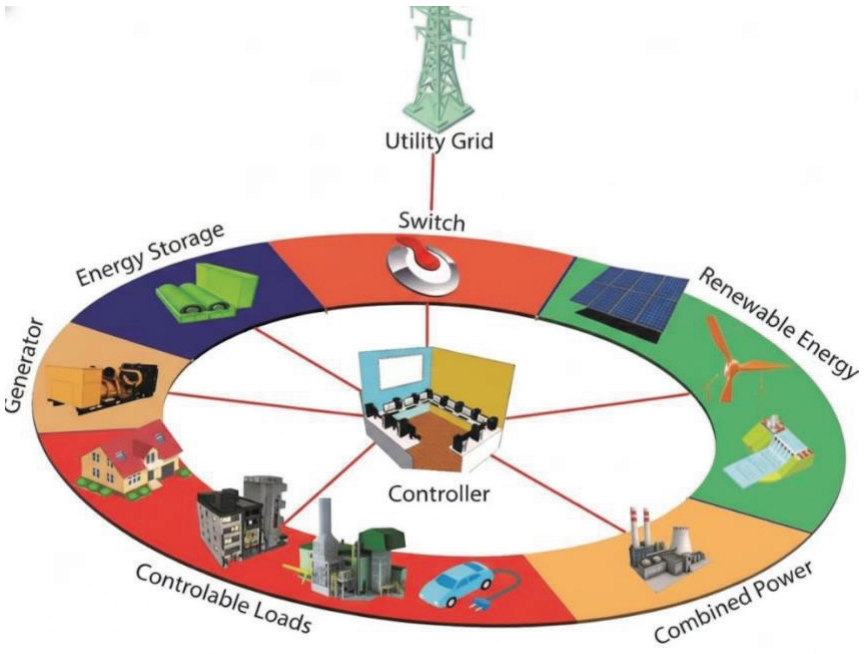

Figure 1. Schematic view of a generalized microgrid

2.1. Microgrid Structures

2.1.1 AC Microgrids (ACMG)

Local wind turbines, power plants, and loads are all linked to a single AC busbar in ACMGs. Dedicated DC-AC inverters are required to connect all DC generating units (such as PV panels) and power plants (such as batteries) to the common AC busbar [13]. The existence of critical and non-critical loads that necessitate harmonic currents makes ACMG control and management difficult [14]. Resynchronizing an ACMG with the main grid is difficult, while integrating AC microgrids into the main grid is simple. In order to synchronize an ACMG, the voltage amplitude, frequency, and phase at the PCC must match those of the main grid. The literature identifies three primary AC distribution topologies for microgrids: single-phase, three-phase with neutral, and three-phase without neutral. An AC microgrid's connectivity design is depicted in Figure 2 [15].

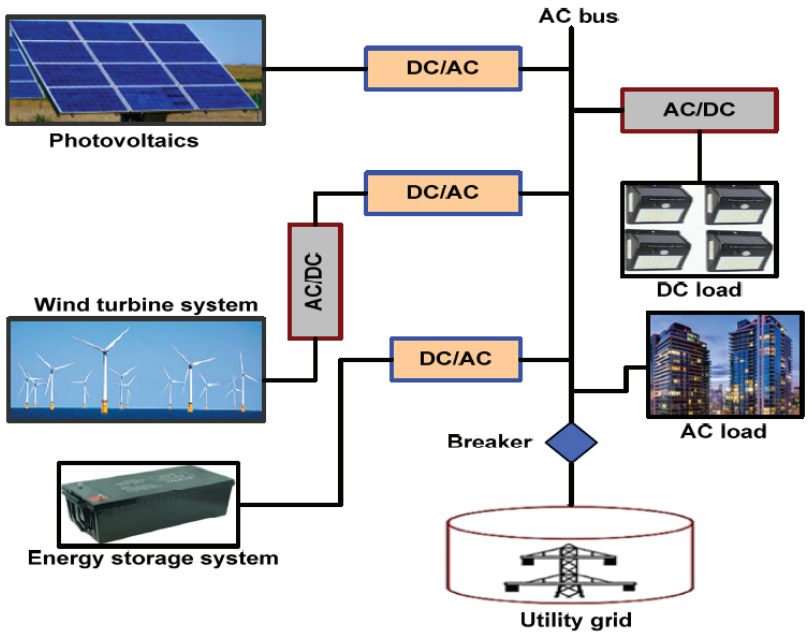

Figure 2. Architecture of AC microgrid [16].

2.1.2. DC Microgrids (DCMG)

Local wind power generating, power plants, and loads are all connected to a single DC busbar in these MGs. Dedicated AC-DC passive/active rectifiers are required to link all AC sources and loads to the common busbar. In the literature, monopolar, bipolar, and homopolar distribution systems are the three primary forms of DC microgrids. A two-wire distribution system with a fixed DC bus voltage makes up a monopolar DC grid. In contrast, three-wire DC distribution systems are used in bipolar and homopolar DC grids. A homopolar DC grid has two low-voltage conductors of the same voltage polarity, whereas a bipolar DC grid includes two low-voltage conductors of different polarities in addition to the ground return conductor. Compared to their AC equivalents, DCMGs have a number of advantages, including as increased stability, efficiency (fewer power electronic converters), and dependability. Recently, DC microgrids have been employed in specific applications

such as telecommunication networks, electric vehicles, and shipboard microgrids. However, compared to AC microgrids, the primary drawback of DC microgrids is their more complicated and expensive protection system [17]. A DC microgrid's connectivity design is seen in Figure 3 [15].

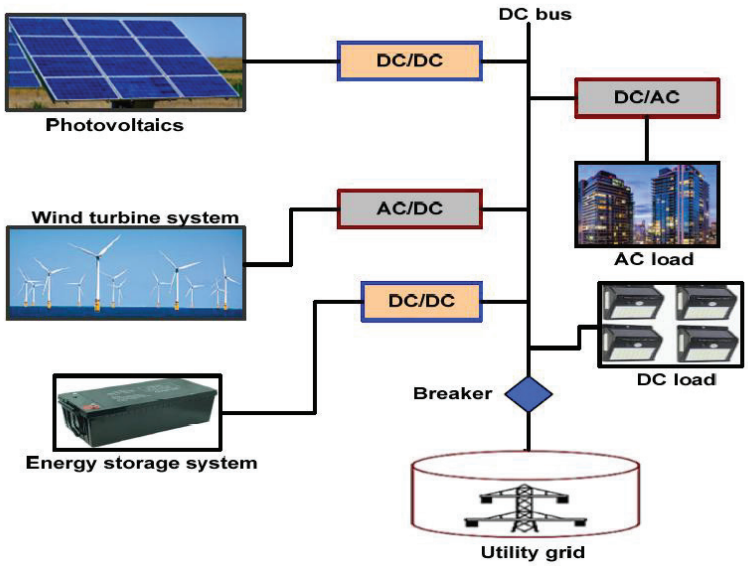

Figure 3. Architecture of DC microgrid [16].

2.1.3. Hybrid microgrids (HMGs)

The AC busbar in HMGs is connected to AC sources and loads, while the DC busbar is connected to DC sources and DC loads. Because they can accommodate both AC and DC sources/loads concurrently, HMGs have the benefits of both ACMGs and DCMGs and require fewer power conversion stages. A bidirectional link converter connects the DC and AC subgrids. Managing and controlling the power flow both within and across the subgrids, this converter is the most crucial component of the HMG. The HMG converts voltage on the DC side using a DC-DC converter and on the AC side using a transformer [17, 18]. The hybrid microgrid's link architecture is depicted in Figure 4.

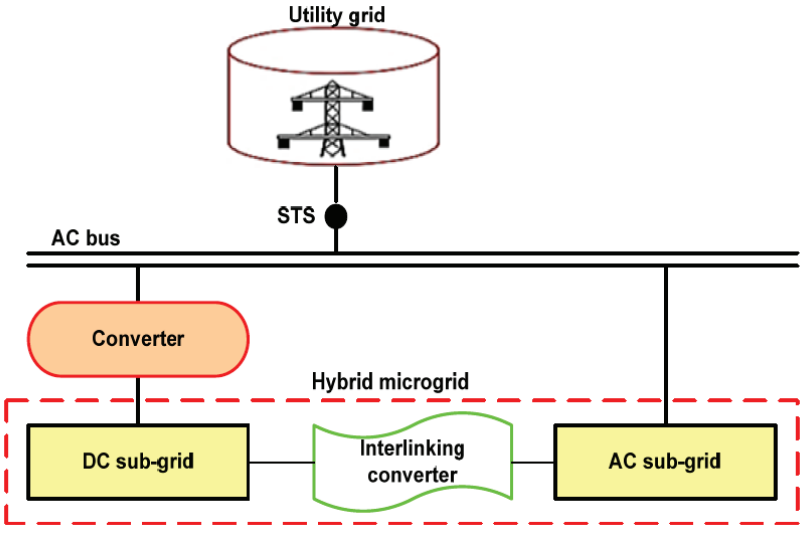

Figure 4. Architecture of a hybrid (AC/DC) microgrid [16].

2.2. Modes of Microgrid Operation

2.2.1. Operation Linked to the Grid

In this configuration, a single PCC connects the MG to the main grid. Depending on the discrepancy between the power produced by the RESs and the load power, the MG swaps power with the main grid. When load demand is low and generation is high, the RESs' excess electricity can be used to charge the RES. The extra electricity produced inside the microgrid can be transmitted to the main grid once the RES is fully charged. However, depending on the current State of Charge (SoC), the load can be provided by the RES in partially shaded or cloudy situations (i.e., when generation is lower than load demand). The necessary power can be taken straight from the main grid after the ESS reaches its lower SoC limit. Therefore, the RES, ESS, and main grid must work together to preserve the microgrid's stability and dependability. As a result, a PCC may have bidirectional power flow [12].

2.2.2. Operation in an Islanded Mode

The PCC of the microgrid may experience aberrant conditions as a result of main grid faults. In this case, the microgrid can function as an islanded microgrid while being cut off from the main grid. In this mode, distributed RESs (such as solar and wind photovoltaics) and ESSs control local frequency and voltage [19]. ESSs are essential components of MGs in this mode because they can reduce power fluctuations, preserve energy balance, and boost system efficiency and dependability [20]. When RES generation surpasses demand, ESSs absorb the excess. When demand outpaces local generation, ESSs can be deployed to supply power to the MG. This reduces the requirement for load shedding and/or RES power disruptions. Additionally, the islanded microgrid's voltage and frequency regulation can be enhanced by ESSs.

3. ENERGY STORAGE SYSTEMS OVERVIEW

Large-scale electrical energy storage is not possible within the technological constraints of thermodynamics. Other forms of energy storage, like chemical, mechanical, and thermal, are more widely available and far more sustainable. Energy storage systems can be categorized based on their power and energy density, component life cycle, and charge/discharge rates to help choose the best technology for a particular application. The round-trip energy efficiency of the storage bank from DC to storage and back, or the percentage of energy stored that can be retrieved, can be used to characterize the efficiency of an ESS. ESSs are essential for enhancing an MG's operating capability. Although not all ESSs can be successfully used in MGs, there are many different types [21].

3.1. Mechanical Storage Systems (MSS)

Based on how they work, mechanical storage devices can be divided into two categories: kinetic energy (such as flywheels) and potential energy (such as compressed gas, pressure springs, and pumped storage) [22]. Energy from tidal sources, waves, and water currents can be converted and stored using MSS techniques. The primary benefit of MSS techniques is their ease of energy conversion and transmission [23]. They come in a variety of forms, including pumped hydro storage systems (PHSS), compressed air energy storage (CAES), and flywheel energy storage systems (FESS).

3.2. Systems for Electrochemical Storage (ECS)

Chemical energy in the reaction partners—the cathode and anode—is transformed into electrical energy in electrochemical storage devices [24]. In this case, the energy is accessible as an electric

current at a fixed voltage. Conventional batteries and flow batteries are the two main types of ECSs. The primary benefit of this technology is that, based on the availability of voltage and current, storage devices can be built and produced in any size [25]. Lead-acid battery storage systems, lithium-ion (Li-ion) battery storage systems, sodium-sulfur battery storage systems, redox flow battery storage systems, and fuel cells—hydrogen energy storage are the different types.

3.3. Systems for Storing Electrical Energy

Systems that produce, store, and deliver electrical energy on demand are known as electrical energy storage systems (EESs) [26]. EESs that are frequently utilized in microgrids include supercapacitors and supermagnetic energy storage systems.

4. ANALYSIS OF MICROGRID LOADS

Because MGs include a variety of load types, precise load management in MG systems has become crucial. To guarantee MG power management efficiency, a fail-safe load management solution is necessary [27]. For every power system operator, achieving generation and load balance is a crucial concern. In a similar vein, to attain this balance, the MG control system must constantly assess and rank loads. As illustrated in Figure 5 [28], MG loads can generally be separated into critical and non-critical loads. Critical loads are essential to a facility and must be maintained under all conditions. Hospitals, care facilities, data centers, etc. are a few examples. Conversely, a non-critical load can be separated into emergency load reduction and discretionary loads. During peak hours, discretionary loads can be lowered to temporarily lessen the load. This includes water heaters, dryers, washing machines, and HVAC (heating, ventilation, and air conditioning) equipment. For MG protection to avoid power disruptions, emergency load shedding in residential and commercial buildings is essential. Ref. [29] suggested the use of a smart load shedding module coupled in series with non-critical loads to identify circumstances in which non-essential loads must be islanded. A hybrid approach based on demand-side management and multi-agent systems was presented by Abdelazeem et al. [30] for managing energy in residential, commercial, and industrial microgrids.

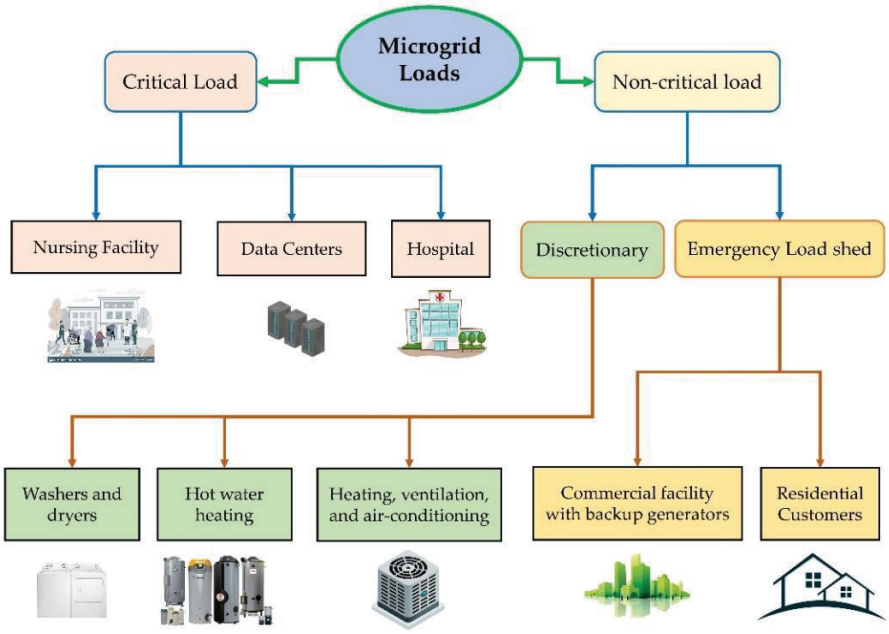

Figure 5. Microgrid load classification.

5. MICROGRID CONTROL ARCHITECTURE

The categorization and constraints of MG control architectures, including centralized and decentralized control systems, are examined in this section [31]. The following standards should be satisfied by the MG control strategy's goals:

• Independent management of active and reactive power,

• Correction of voltage sags and system imbalances,

• Smooth transition between MG operating modes,

• Increased energy efficiency,

• Monitoring of energy flow and critical equipment, and grid fault management,

• Meeting grid load dynamics requirements [32].

5.1 Strategies for Hierarchical Control

Hierarchical control solutions in MGs entail splitting the control structure into layers, each of which addresses issues at a single level. The operational components of MGs are successfully controlled and regulated thanks to this hierarchical method [33]. Primary Control, Secondary Control, and Tertiary Control are some of these control layers. For every function of a particular DER or element inside an MG, primary control is carried out locally [34]. In order to maintain system stability and solve local issues, it entails reflexive acts that are independent of central authority [35, 36]. Primary control provides basic functions, including voltage control and frequency regulation [33]. Aiming for decentralized inter-DER coordination, the second control layer functions at a higher level than the primary control layer [37]. In order to guarantee optimal energy transfer and calm chaotic behavior, it transmits information between subsystems [38]. In order to achieve GO goals like load balance and the best use of RESs, secondary control assists individual input resources in contributing to an integrative spatial and functional coordination [33]. Lastly, a centralized EMS or GO controller is necessary for the tertiary control level [36], [39]. Adaptive management, which employs long-term planning and global knowledge growth to create strategies based on predetermined goals, is the foundation of tertiary control [37]. Additionally, it manages the GO, carries out tasks like energy planning, and works with other organizations like the main grid or other organizations where government incentives are important [35]. Additionally, control layers for various GO controls can be implemented using three distinct implementation methodologies, as seen in Figure 6.

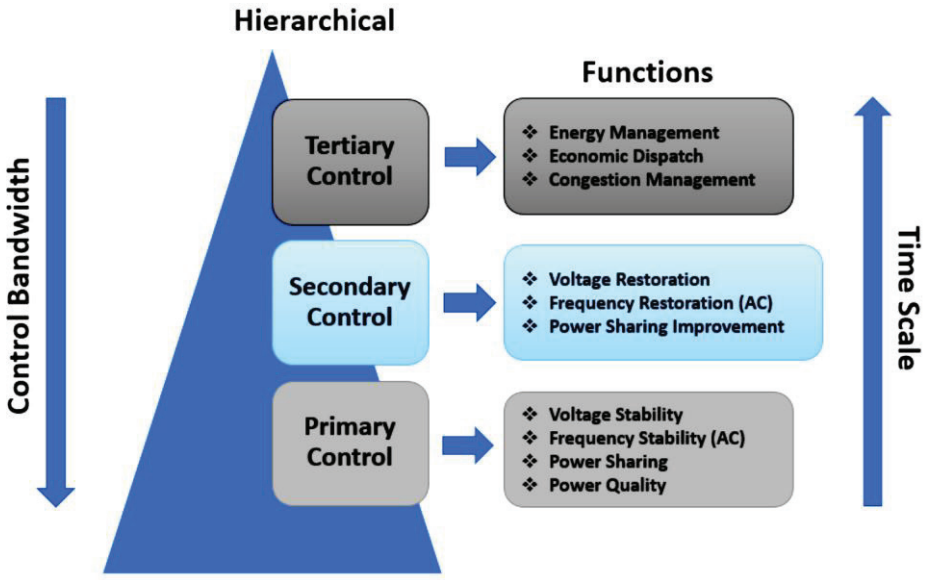

Figure 6 Hierarchical control strategies of microgrid.

5.2. Centralized Control

The MG's DERs and loads are managed and coordinated by a single controller. In this scenario, as seen in Figure 7(a), a centralized controller is necessary for the MG to interact with every DER in the system and process data received from the MG's other DERs. Although centralized decision-making and coordination are made possible by their implementation, it should be highlighted that centralized controllers are less reliable and may result in communication issues and a single point of failure [40].

5.3. Decentralized Control

Several local controllers (LCs) are dispersed among MGs in this method, as seen in Figure 7(b), and each LC is in charge of overseeing a DER or a portion of the loads. These LCs have the ability to function independently and make control choices depending on local targets and measurements [41]. Because each LC can function independently of central coordination, decentralized management offers more flexibility and scalability. The control system receives entirely locally measured data from each DER unit (agent). Control approaches frequently concentrate on voltage-reactive power (V-Q) and frequency-active power (f-P) droops [42]. A physical link with droop controllers has been used to study load sharing among DG units based on their power capacity [41]. However, because it excludes communication channels, this method makes secondary and tertiary control system development more difficult. To get around this problem, some techniques have been suggested in the literature, such as high-pass filters [43].

5.4. Distributed Control

Decision-making and dispersed intelligence are integrated into the DCT approach. As seen in Figure 7(c), every device, DER, or load has its own controller and can make local control decisions based on measurements and communication with nearby devices. A centralized controller is not necessary for this approach [44]. In particular, control activities are dispersed throughout the MG, where independent agents work together to accomplish global goals during the inspection [43,45]. By increasing MG scalability, DCT systems strengthen the system's overall resistance to single-fault topologies [40].

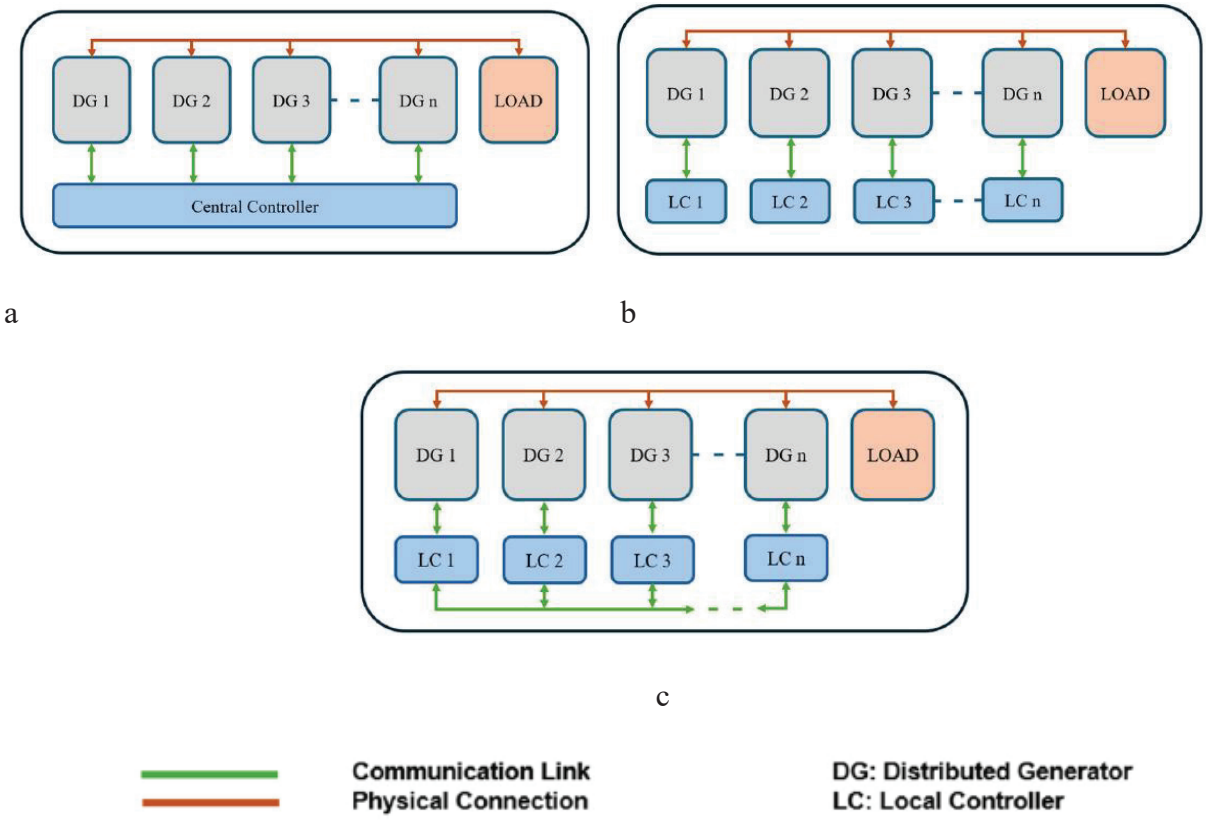

Figure 7. Control strategies for microgrid. a) merkezi kontrol sistemi, b) merkezi olmayan kontrol sistemi ve c) dağitilmiş kontrol sistemi

6. USE OF ARTIFICIAL INTELLIGENCE IN DISTRIBUTED CONTROL

Artificial intelligence is one of the most recent advances in computer science. Because AI can efficiently use current data and support decision-making processes for safer and more dependable MG management and operation in difficult real-world settings, it has important applications in the MG environment [46]. The control environment for both single and multiple machine learning networks can be efficiently utilized thanks to developments in AI-based algorithms and computational capacity with big data processing capabilities [47]. ML and DL are two significant subfields in AI [48]. ML and DL models can often be supervised or unsupervised, depending on the input training data [46]. System control and analysis in the MG setting necessitates a sophisticated approach that blends data-driven and physical model-based modeling in order to successfully address the issues of observability and controllability. MAS, a crucial AI tool, assigns intelligent agents that represent various MG components to optimize the system [49]. These agents can control networks and react independently to disordered situations in an MG by encouraging self-organizing activity [50].

Because the system is decentralized, DCT for MGs poses a number of difficulties [51]. The main issues that make it difficult and complex are coordination and communication across distributed controllers [52]. However, it can be difficult to provide efficient information flow and decision-making across dispersed controllers while preserving system stability and performance, particularly in large-scale MGs. It is difficult to reach consensus between many DERs with varying behaviors and control discrepancies. Additionally, the design and implementation of DCT are made much more difficult by the need to strike a balance between the system's local control and global goals, such as

guaranteeing grid stability, maximizing power efficiency, and enabling RES integration [51]. The intricacy of coordinating several DERs, the dynamic nature of RES, communication needs, cybersecurity issues, scalability concerns, and regulatory compliance are the root causes of all of this, while maintaining performance and dependability are crucial factors. AI techniques like machine learning (ML) and deep learning (DL) can be used to solve many of the problems that DCT presents. These techniques can be used to develop robust mechanisms like distributed consensus algorithms and dependable communication networks to help ensure system stability and reliability in the event of communication outages in the distributed system, as well as to derive adaptive control methods to incorporate higher levels of renewable energy into the grid [53]. Furthermore, AI is essential in the demand-side management and optimization on the MG side. DCT strategies use AI algorithms that allow DERs to manage energy demands and supply by responding independently to real-time data [54].

6.1. Machine Learning

A subfield of artificial intelligence called machine learning (ML) has the potential to enhance machine learning performance and management. Based on the learning technique, four broad types of machine learning may be identified: semi-supervised, supervised, unsupervised, and reinforcement learning (RL). Machine learning is also used in machine learning systems for anomaly prediction and error detection. Neural technologies and clustering are examples of instrumental machine learning models in DCT frameworks that can identify skills that anticipate a system breakdown or inefficient operation. This enables DCTs to react quickly without interfering with machine learning processes. By accurately estimating energy output and consumption, it enhances load forecasting and renewable energy integration [55].

6.1.1 Supervised Learning

The "supervised learning" approach trains computers to categorize or forecast target attributes with continuous values using labeled datasets. Regression and classification are two key categories in this learning process [56]. MGcontrol can use the categorization problem to find outages brought on by variations in load and temporary circumstances. Assessments of voltage stability and power quality can be made using fault detection and classification. Prediction issues include PV generation forecasting, power demand forecasting, energy market pricing forecasting, etc. [57].

6.1.2 Unsupervised Learning

This method can be used to efficiently analyze and cluster unlabeled datasets. It is described as an algorithm that, without human oversight, can recognize patterns and trends in an unlabeled dataset and forecast any values that have not yet been found [58]. It makes learning simpler and quicker. The clustering class automatically detects distinct patterns in data and entity segmentation. From an MG perspective, this includes load profile clustering, consumer/producer-consumer segmentation, and network topology identification [59].

6.1.3 Semi-Supervised Learning

Both labeled and unlabeled data have recently been used to train machine learning algorithms. Using both labeled and unlabeled input, semi-supervised learning teaches the model to forecast future data at any given time. Generative adversarial networks are the most popular algorithm for this method [56]. Similar to the generative adversarial network architecture, semi-supervised learning may synthesis trained data from noise and minimize gaps between learned and real data in the MG to create time-series power generation profiles of DERs and build solar power plants. For real-time control in MGs, generative adversarial networks can also be combined with deep neural networks and reinforcement learning.

6.1.4. Reinforcement Learning

An agent, an environment, a reward, and an action make up a reinforcement learning algorithm. In reinforcement learning (RL), an agent actively engages with the environment in order to gain information; in certain situations, this entails altering the environment and receiving a reward for each action [60]. The agent seeks to maximize the total payoff by going through a cycle of rewards and penalties for different actions. RL can optimize energy allocation and enhance the MG's decision-driven control and operation [61].

6.2. Deep Learning

By creating patterns on its own, deep learning is a machine learning function that simulates how the human brain interprets data and makes judgments. This is also known as a multilayer neural network. More layers are added to this neural network [60]. In order to accomplish learning, it also employs supervised, unsupervised, and semi-supervised methods. Deep learning architectures include deep neural networks, feedforward deep networks, convolutional neural networks, deep belief networks, and recurrent neural networks. Convolutional neural networks and recurrent neural networks are the most crucial deep learning designs because they are most effective at managing massive volumes of dispersed data. Recurrent neural networks, on the other hand, perform exceptionally well when processing time series data [50].

CONCLUSIONS

Due to rising electricity consumption, the quick adoption of renewable energy sources, and the growing importance of power grid dependability, energy systems are changing dramatically today. At the core of this change are microgrids, which are now an essential part of contemporary power systems for both improving the security of the energy supply and optimizing local production and consumption. In response to rising energy consumption, the unpredictability of renewable resources, and the requirement to maintain power system stability, the microgrids covered in this section stand out as essential elements of contemporary electrical infrastructures**.** Microgrids not only improve supply security but also present strategic potential for flexible and sustainable energy management when various architectural elements, energy storage technologies, and control systems are taken into account collectively. Specifically, integrating data-driven techniques like artificial intelligence, machine learning, and deep learning with distributed control approaches greatly enhances decision-making in intricate and dynamic microgrid environments and permits scalable management of numerous microgrid structures. The resilience and efficiency of energy systems are anticipated to be substantially improved in the future by AI-based control techniques combined with hybrid microgrid configurations, sophisticated communication infrastructures, and autonomous energy management systems. In this regard, research on microgrid control is essential for both applied energy policy and scholarly study.

REFERENCES

[1] Haes Alhelou, H., Hamedani-Golshan, M. E., Njenda, T. C., & Siano, P. (2019). A survey on power system blackout and cascading events: Research motivations and challenges. *Energies*, *12*(4), 682.

[2] Che, L., Khodayar, M., & Shahidehpour, M. (2013). Only connect: Microgrids for distribution system restoration. *IEEE power and energy magazine*, *12*(1), 70-81.

[3] Ahmad, S., Shafiullah, M., Ahmed, C. B., & Alowaifeer, M. (2023). A review of microgrid energy management and control strategies. *IEEe Access*, *11*, 21729-21757.

[4] International Energy Agency. Electricity 2025. Available online: https://www.iea.org/reports/electricity-2025 (accessed on 14 Oct. 2025).

[5] Esparza, A., Blondin, M., & Trovão, J. P. F. (2025). A review of optimization strategies for energy management in microgrids. *Energies*, *18*(13), 3245.

[6] Rahman, S. M., Al-Ismail, F. S. M., Haque, M. E., Shafiullah, M., Islam, M. R., Chowdhury, M. T., ... & Khan, Z. A. (2021). Electricity generation in Saudi Arabia: Tracing opportunities and challenges to reducing greenhouse gas emissions. *Ieee Access*, *9*, 116163-116182.

[7] Al-Ismail, F. S. (2021). DC microgrid planning, operation, and control: A comprehensive review. *IEEe Access*, *9*, 36154-36172.

[8] Alam, M. S., Al-Ismail, F. S., & Abido, M. A. (2021). Power management and state of charge restoration of direct current microgrid with improved voltage-shifting controller. *Journal of Energy Storage*, *44*, 103253.

[9] Shafiullah, M., Haque, M. E., Hossain, S., Hossain, M. S., & Rana, M. J. (2022). 3 community microgrid energy scheduling based on the grey wolf optimization algorithm. *strategies*, *14*, 16.

[10] Rajesh, K. S., Dash, S. S., Rajagopal, R., & Sridhar, R. (2017). A review on control of ac microgrid. *Renewable and sustainable energy reviews*, *71*, 814-819.

[11] Mohammed, A., Refaat, S. S., Bayhan, S., & Abu-Rub, H. (2019). AC microgrid control and management strategies: Evaluation and review. *IEEE Power Electronics Magazine*, *6*(2), 18-31.

[12] Kandari, R., Neeraj, N., & Micallef, A. (2022). Review on recent strategies for integrating energy storage systems in microgrids. *Energies*, *16*(1), 317.

[13] Lotfi, H., & Khodaei, A. (2015). AC versus DC microgrid planning. *IEEE transactions on smart grid*, *8*(1), 296-304.

[14] Planas, E., Andreu, J., Gárate, J. I., De Alegría, I. M., & Ibarra, E. (2015). AC and DC technology in microgrids: A review. *Renewable and Sustainable Energy Reviews*, *43*, 726-749.

[15] Ojo, K. E., Saha, A. K., & Srivastava, V. M. (2025). Microgrids' control strategies and real-time monitoring systems: A comprehensive review. *Energies*, *18*(13), 3576.

[16] Patrao, I., Torán, E., González-Medina, R., Liberos, M., Figueres, E., & Garcerá, G. (2023). Dc-bus signaling control laws for the operation of dc-microgrids with renewable power sources. *IEEE Journal of Emerging and Selected Topics in Industrial Electronics*, *5*(3), 1120-1131.

[17] Justo, J. J., Mwasilu, F., Lee, J., & Jung, J. W. (2013). AC-microgrids versus DC-microgrids with distributed energy resources: A review. *Renewable and sustainable energy reviews*, *24*, 387-405.

[18] Unamuno, E., & Barrena, J. A. (2015). Hybrid ac/dc microgrids—Part I: Review and classification of topologies. *Renewable and Sustainable Energy Reviews*, *52*, 1251-1259.

[19] Mogaka, L. O., Nyakoe, G. N., & Saulo, M. J. (2020). Islanded and grid-connected control in a microgrid with wind-PV hybrid. *International Journal of Applied Engineering Research*, *15*(4), 352-357.

[20] Talapur, G. G., Suryawanshi, H. M., Xu, L., & Shitole, A. B. (2018). A reliable microgrid with seamless transition between grid connected and islanded mode for residential community with enhanced power quality. *IEEE Transactions on Industry Applications*, *54*(5), 5246-5255.

[21] Chaudhary, G., Lamb, J. J., Burheim, O. S., & Austbø, B. (2021). Review of energy storage and energy management system control strategies in microgrids. *Energies*, *14*(16), 4929.

[22] Liu, Z., Ustolin, F., Spitthoff, L., Lamb, J. J., Gundersen, T., Pollet, B. G., & Burheim, O. S. (2020). Liquid air energy storage: analysis and prospects. In *Micro-Optics and Energy: Sensors for Energy Devices* (pp. 115-130). Cham: Springer International Publishing.

[23] Singh, V., Kuthe, S., & Skorodumova, N. V. (2023). Electrode fabrication techniques for Li ion based energy storage system: a review. *Batteries*, *9*(3), 184.

[24] Divya, K. C., & Østergaard, J. (2009). Battery energy storage technology for power systems—An overview. *Electric power systems research*, *79*(4), 511-520.

[25] Xu, X., Bishop, M., Oikarinen, D. G., & Hao, C. (2016). Application and modeling of battery energy storage in power systems. *CSEE journal of power and energy systems*, *2*(3), 82-90.

[26] Kousksou, T., Bruel, P., Jamil, A., El Rhafiki, T., & Zeraouli, Y. (2014). Energy storage: Applications and challenges. *Solar Energy Materials and Solar Cells*, *120*, 59-80.

[27] Shafiullah, M., Refat, A. M., Haque, M. E., Chowdhury, D. M. H., Hossain, M. S., Alharbi, A. G., ... & Hossain, S. (2022). Review of recent developments in microgrid energy management strategies. *Sustainability*, *14*(22), 14794.

[28] Moran, B. (2016, May). Microgrid load management and control strategies. In *2016 IEEE/PES Transmission and Distribution Conference and Exposition (T&D)* (pp. 1-4). IEEE.

[29] Kennedy, J., Ciufo, P., & Agalgaonkar, A. (2012, July). Intelligent load management in microgrids. In *2012 IEEE Power and Energy Society General Meeting* (pp. 1-8). IEEE.

[30] Abdelsalam, A. A., Zedan, H. A., & ElDesouky, A. A. (2020). Energy management of microgrids using load shifting and multi-agent system. *Journal of Control, Automation and Electrical Systems*, *31*(4), 1015-1036.

[31] Bellido, M. H., Rosa, L. P., Pereira, A. O., Falcao, D. M., & Ribeiro, S. K. (2018). Barriers, challenges and opportunities for microgrid implementation: The case of Federal University of Rio de Janeiro. *Journal of cleaner production*, *188*, 203-216.

[32] Jamil, N., Qassim, Q. S., Bohani, F. A., Mansor, M., & Ramachandaramurthy, V. K. (2021). Cybersecurity of microgrid: state-of-the-art review and possible directions of future research. *Applied Sciences*, *11*(21), 9812.

[33] Espina, E., Llanos, J., Burgos-Mellado, C., Cardenas-Dobson, R., Martinez-Gomez, M., & Saez, D. (2020). Distributed control strategies for microgrids: An overview. *IEEe Access*, *8*, 193412-193448.

[34] Serban, I., Cespedes, S., Marinescu, C., Azurdia-Meza, C. A., Gomez, J. S., & Hueichapan, D. S. (2020). Communication requirements in microgrids: A practical survey. *IEEe Access*, *8*, 47694-47712.

[35] Sabri, Y., El Kamoun, N., & Lakrami, F. (2019, October). A survey: Centralized, decentralized, and distributed control scheme in smart grid systems. In *2019 7th mediterranean congress of telecommunications (CMT)* (pp. 1-11). IEEE.

[36] Nawaz, F., Pashajavid, E., Fan, Y., & Batool, M. (2023). A comprehensive review of the state-of-the-art of secondary control strategies for microgrids. *IEEE Access*, *11*, 102444-102459.

[37] Khayat, Y., Shafiee, Q., Heydari, R., Naderi, M., Dragičević, T., Simpson-Porco, J. W., ... & Bevrani, H. (2019). On the secondary control architectures of AC microgrids: An overview. *IEEE Transactions on Power Electronics*, *35*(6), 6482-6500.

[38] Chen, M., & Xiao, X. (2018). Secondary voltage control in islanded microgrids using event-triggered control. *IET Generation, Transmission & Distribution*, *12*(8), 1872-1878.

[39] Machele, I. L., Onumanyi, A. J., Abu-Mahfouz, A. M., & Kurien, A. M. (2024). Interconnected smart transactive microgrids—A survey on trading, energy management systems, and optimisation approaches. *Journal of Sensor and Actuator Networks*, *13*(2), 20.

[40] Mohammadi, F., Mohammadi-Ivatloo, B., Gharehpetian, G. B., Ali, M. H., Wei, W., Erdinç, O., & Shirkhani, M. (2022). Robust control strategies for microgrids: A review. *IEEE Systems Journal*, *16*(2), 2401-2412.

[41] Ahmed, A. A. S. (2021). Digital Twin-Based Cooperative Control Techniques for Secure and Intelligent Operation of Distributed Microgrids.

[42] Ahmed, K., Hussain, I., Seyedmahmoudian, M., Stojcevski, A., & Mekhilef, S. (2023). Voltage stability and power sharing control of distributed generation units in DC microgrids. *Energies*, *16*(20), 7038.

[43] Ahsan, M., Rodriguez, J., & Abdelrahem, M. (2023). Distributed control algorithm for dc microgrid using higher-order multi-agent system. *Sustainability*, *15*(10), 8336.

[44] Singh, S., & Singh, S. (2024). Advancements and challenges in integrating renewable energy sources into distribution grid systems: A comprehensive review. *Journal of Energy Resources Technology*, *146*(9), 090801.

[45] Shi, S., Wang, Y., & Jin, J. (2023). Multi-agent-based control strategy for centerless energy management in microgrid clusters. *Frontiers in Energy Research*, *11*, 1119461.

[46] Trivedi, R., & Khadem, S. (2022). Implementation of artificial intelligence techniques in microgrid control environment: Current progress and future scopes. *Energy and AI*, *8*, 100147.

[47] Lopez-Garcia, T. B., Coronado-Mendoza, A., & Domínguez-Navarro, J. A. (2020). Artificial neural networks in microgrids: A review. *Engineering Applications of Artificial Intelligence*, *95*, 103894.

[48] Wu, T., & Wang, J. (2021). Artificial intelligence for operation and control: The case of microgrids. *The Electricity Journal*, *34*(1), 106890.

[49] O'Dwyer, E., Pan, I., Acha, S., & Shah, N. (2019). Smart energy systems for sustainable smart cities: Current developments, trends and future directions. *Applied energy*, *237*, 581-597.

[50] Tabassum, T., Lim, S., & Khalghani, M. R. (2024). Artificial intelligence-based detection and mitigation of cyber disruptions in microgrid control. *Electric Power Systems Research*, *226*, 109925.

[51] Saeed, M. H., Fangzong, W., Kalwar, B. A., & Iqbal, S. (2021). A review on microgrids' challenges & perspectives. *IEEe Access*, *9*, 166502-166517.

[52] Shafiullah, M., Ahmed, S. D., & Al-Sulaiman, F. A. (2022). Grid integration challenges and solution strategies for solar PV systems: A review. *IEEE Access*, *10*, 52233-52257.

[53] Liu, M., Cheng, Z., Zhang, Z., Sun, M., Deng, R., Cheng, P., & Chow, M. Y. (2021, July). A multi-agent system based hierarchical control framework for microgrids. In *2021 IEEE Power & Energy Society General Meeting (PESGM)* (pp. 01-05). IEEE.

[54] Uddin, M., Mo, H., Dong, D., Elsawah, S., Zhu, J., & Guerrero, J. M. (2023). Microgrids: A review, outstanding issues and future trends. *Energy Strategy Reviews*, *49*, 101127.

[55] Yan, R., Wang, Y., Xu, Y., & Dai, J. (2022). A multiagent quantum deep reinforcement learning method for distributed frequency control of islanded microgrids. *IEEE Transactions on Control of Network Systems*, *9*(4), 1622-1632.

[56] Seyedi, Y., Karimi, H., Grijalva, S., Mahseredjian, J., & Sanso, B. (2021). A supervised learning approach for centralized fault localization in smart microgrids. *IEEE Systems Journal*, *16*(3), 4060-4070.

[57] Ma, M., Lahmadi, A., & Chrisment, I. (2020, June). Detecting a stealthy attack in distributed control for microgrids using machine learning algorithms. In *2020 IEEE Conference on Industrial Cyberphysical Systems (ICPS)* (Vol. 1, pp. 143-148). IEEE.

[58] Salehi, N., Martínez-García, H., & Velasco-Quesada, G. (2022). Networked microgrid energy management based on supervised and unsupervised learning clustering. *Energies*, *15*(13), 4915.

[59] Saldarriaga-Zuluaga, S. D., López-Lezama, J. M., & Muñoz-Galeano, N. (2021). Optimal coordination of over-current relays in microgrids using unsupervised learning techniques. *Applied Sciences*, *11*(3), 1241.

[60] Chandrasekaran, K., Kandasamy, P., & Ramanathan, S. (2020). Deep learning and reinforcement learning approach on microgrid. *International transactions on electrical energy systems*, *30*(10), e12531.

Chapter 7

COMPARATIVE EVALUATION OF DEEP LEARNING TIME SERIES MODELS FOR SHORT-TERM WIND ENERGY FORECASTING

Hüseyin Aydilek[1], Mustafa Yasin Erten[2]

1 Dr. Öğr. Üyesi, Kırıkkale Üniversitesi, Elektrik-Elektronik Müh. Bölümü, ORCID: 0000-0003-3051-4259
2 Dr. Öğr. Üyesi, Kırıkkale Üniversitesi, Elektrik-Elektronik Müh. Bölümü, ORCID: 0000-0002-5140-1213

Introduction

Energy production and consumption constitute one of the primary indicators of economic development and technological capacity in modern societies. For many decades, global energy demand has been largely met through fossil fuel–based resources; however, this approach has resulted in outcomes that are neither environmentally nor economically sustainable. Carbon-intensive emissions arising from fossil fuel combustion have become a major driver of global warming and climate change, leading to increasingly visible impacts such as extreme weather events, disruptions in precipitation patterns, and large-scale ecosystem degradation. In addition to environmental concerns, the finite nature of fossil fuel reserves and their high sensitivity to price volatility have amplified macroeconomic vulnerability, particularly in countries that are heavily dependent on energy imports. Against this backdrop, renewable energy sources have emerged as a strategic necessity, not only to enhance energy supply security but also to support global efforts to mitigate climate change. Resources such as solar, wind, biomass, and geothermal energy rely on natural cycles and therefore offer a long-term, non-depleting energy base, while enabling low-carbon operation during power generation. Among these alternatives, wind energy has become one of the cornerstone technologies of the global energy transition. Its relatively mature technological infrastructure, broad geographical applicability, and near-zero marginal emissions during operation make wind power especially attractive. Nevertheless, the inherently variable and partially unpredictable nature of wind introduces significant challenges for power system engineering, particularly in the context of short-term generation forecasting. Uncertainty in wind power prediction increases balancing requirements in electrical grids, necessitates additional reserve capacity, and may lead to planning inaccuracies in both day-ahead and intraday electricity markets. For this reason, achieving accurate and reliable forecasts of wind power production at hourly and sub-hourly horizons is of critical importance for system operators as well as market participants on the generation side. Although traditional physical and statistical models have long served as fundamental tools in wind power forecasting, the nonlinear and multi-scale characteristics of wind-related time series impose inherent limitations on these methodologies. In recent years, advances in machine learning, and deep learning in particular, have significantly reshaped this research domain. Recurrent neural networks and long short-term memory structures are increasingly employed to model wind speed dynamics and wind-driven power generation due to their ability to capture complex temporal dependencies. Within this context, this book chapter investigates short-term wind power forecasting using deep learning–based approaches, focusing on the Turkish electricity market. Hourly production data obtained from a wind power plant located in the Selçuk region of İzmir are utilized, and the comparative performance of different deep learning architectures is systematically examined.

1.1. Variability Characteristics of Wind Energy

Wind energy is based on the conversion of the kinetic energy of air movements, which arise from atmospheric pressure differences and temperature gradients, into electrical energy. In theoretical terms, the power that can be extracted from a wind turbine is modeled by Equation (1).

$P = \frac{1}{2}\rho A v^3$	(1)

Here, P denotes the generated power, ρ represents air density, A is the swept area of the turbine rotor, and v indicates wind speed. The cubic dependence of power on wind speed implies that even small variations in velocity can lead to disproportionately large changes in power output. This characteristic makes wind energy simultaneously an attractive high-potential resource and a challenging one in terms

of power system integration. The temporal behavior of wind speed is inherently non-stationary, multi-scale, and highly variable. Turbulent components occurring on the order of seconds, transient meteorological phenomena evolving over minutes and hours, and seasonal synoptic patterns collectively form distinct frequency bands within the same time series. While classical statistical methods are capable of representing linear relationships at specific temporal scales, they often struggle to fully capture the strong nonlinearities and pronounced seasonal structures that characterize wind-related time series. In short-term forecasting applications in particular, there is a clear need for more flexible modeling approaches that can simultaneously represent abrupt production fluctuations and regular diurnal cycles. In the Turkish context, wind power plants concentrated in the Aegean and Marmara regions contribute to significant variability in regional generation profiles. This variability directly affects both transmission system operation and electricity market activities, rendering forecast accuracy a critical factor. Consequently, a systematic investigation of deep learning–based methods capable of internalizing the multi-scale and nonlinear nature of wind resources is of substantial importance when applied to Turkish wind power data.

1.2. Related Works

Research in the field of wind power forecasting has experienced a notable methodological evolution, shifting from physical and statistical approaches toward data-driven paradigms. Classical statistical models, which dominated the literature for an extended period, have proven effective in datasets characterized by strong linear correlations. Nevertheless, their performance remains limited when confronted with the nonlinear and multi-scale nature of wind dynamics. Owing to their representational flexibility, deep learning methods have gained considerable attention in recent years as a promising alternative.

Wu, Luo, and Yang conducted a systematic investigation of deep learning techniques employed in wind forecasting applications and demonstrated that recurrent neural networks are particularly effective for short-term prediction tasks. Wang et al. assessed the role of deep neural networks in wind speed and power forecasting, reporting that models built upon LSTM and GRU architectures yield lower error levels compared with conventional statistical approaches. In a similar vein, the comprehensive survey by Liu et al. compared machine learning– and deep learning–based wind power forecasting methods, emphasizing the superior capability of deep architectures in capturing nonlinear patterns embedded in wind data.

In practice-oriented studies, LSTM-based architectures have emerged as a dominant modeling framework. Galphade et al. proposed a stacked LSTM model for multivariate short-term wind power forecasting and demonstrated its improved performance relative to traditional machine learning techniques. Ma and Mei achieved high forecasting accuracy using a hybrid convolutional and LSTM-based model augmented with attention mechanisms, highlighting the benefit of explicitly accounting for temporal importance weights. In another study, Ibrahim compared different LSTM variants and showed that these architectures exhibit strong predictive performance, particularly at hourly and sub-hourly time horizons.

Taken together, these studies indicate a growing adoption of deep learning–based models in wind power forecasting research, with the LSTM family occupying a central position in the literature. However, most existing contributions remain constrained by specific geographical regions, turbine characteristics, or data resolutions. Consequently, there is still a need for detailed case studies based on country- and region-specific datasets. The present study seeks to partially address this gap by conducting a comparative analysis using data from the Turkish electricity market.

2. Material and Methods

Short-term wind power forecasting is of critical importance for grid balancing, reserve allocation, and market commitments due to the relatively short forecasting horizon, which typically ranges from fifteen minutes to several hours. Models developed in this domain aim to infer future power generation from historical observations by accounting for the physical and statistical characteristics of wind resources. In the literature, the main methodological approaches are commonly categorized into three groups: physical-based, statistical, and data-driven methods.

Physical-based models attempt to estimate wind speed over a spatial grid by utilizing numerical weather prediction outputs and atmospheric flow equations. However, their high computational requirements and limited capability to accurately represent local topographical effects restrict their suitability for short-term operational applications. Statistical methods, on the other hand, are effective in capturing correlations at specific temporal scales, yet their reliance on linear assumptions constrains their ability to model the inherently nonlinear and multi-scale structure of wind dynamics.

For these reasons, data-driven machine learning and deep learning approaches have become increasingly prevalent in wind forecasting research. In particular, recurrent neural network families capable of processing sequential data, along with hybrid architectures and attention-based models, have gained prominence due to their ability to simultaneously represent short-term fluctuations and slowly evolving trends in wind-related time series. Given the layered nature of wind speed dynamics, which combines abrupt turbulent components with daily and seasonal cycles, models that are sensitive to both instantaneous variations and long-term temporal dependencies naturally exhibit superior predictive performance. Such architectures are able to internalize memory effects and temporal dependencies associated with wind resources in an explicit manner.

Rather than focusing on a single modeling framework, this study adopts a comparative evaluation of multiple deep learning architectures. LSTM- and GRU-based recurrent networks, bidirectional structures that exploit both forward and backward temporal context, hybrid architectures formed by combining sequential layers, and models enhanced with attention mechanisms are all examined using the same dataset. In this way, the extent to which different deep learning strategies can capture the complex dependencies embedded in short-term wind power generation series is assessed from a holistic perspective. The subsequent sections present the data preprocessing procedures, structural characteristics of the model architectures, training methodology, and evaluation metrics in detail.

2.1. Dataset and Study Area

The dataset used in this study consists of hourly power generation values obtained from a wind power plant located in the Selçuk district of İzmir, Türkiye. The region is characterized by a high wind energy potential due to its proximity to the Aegean Sea, the influence of land–sea thermal contrasts that drive diurnal circulation patterns, and local topographical features that channel prevailing wind flows. As a result of daily thermal processes and seasonal pressure systems, the wind regime in this area exhibits both pronounced cyclic behavior and substantial variability.

The production data were retrieved from the EPİAŞ Transparency Platform, which was established to ensure transparency and accessibility in the Turkish electricity market. A two-year observation period spanning from September 2023 to September 2025 was selected for analysis. This time window provides a sufficiently long time series to capture not only seasonal patterns but also interannual variability. The

dataset contains the actual hourly power output delivered to the grid by the wind power plant, and the total generated power is used as the primary variable in all analyses.

2.2. Data Preprocessing and Model Input Construction

An initial assessment of data integrity and quality was conducted on the raw dataset. In the records provided by EPİAŞ, missing observations and physically implausible generation values may occasionally occur due to transmission faults, maintenance activities, or synchronization issues. Within the scope of this study, missing hourly observations were imputed using appropriate techniques that preserve the local structure of the time series, while outliers deemed inconsistent with the installed capacity of the wind power plant and attributed to measurement errors were excluded from the analysis. All generation values were subsequently rescaled to a predefined range in order to enhance numerical stability during model training. This step contributed to faster convergence and improved stability of the optimization process, which is particularly important for learning time-dependent patterns.

The hourly generation series was transformed into input–output sequences using a sliding window approach. A consecutive segment of hourly power values with a fixed length was defined as the model input, while the immediately following observation was assigned as the prediction target. The window length was selected to adequately represent daily cycles while maintaining a balanced trade-off with computational cost. Preserving the temporal order of the data, the period from September 2023 to June 2025 was allocated for training and validation, whereas the interval from July 2025 to September 2025 was reserved as an independent test set. This separation enabled an objective evaluation of the models' generalization capability on a previously unseen time horizon.

2.3. Model Architecture and Experimental Setup

For short-term wind power forecasting, six different deep learning architectures were evaluated rather than relying on a single modeling approach. This strategy enables both the assessment of baseline recurrent structures and a comparative examination of the behavioral characteristics of their extended variants. The considered models include a unidirectional long short-term memory network, a unidirectional gated recurrent unit, a bidirectional long short-term memory network, a bidirectional gated recurrent unit, a hybrid architecture combining stacked long short-term memory and gated recurrent unit layers, and an attention-enhanced long short-term memory model.

The unidirectional long short-term memory model learns generation dynamics by exploiting a cell state that represents long-range temporal dependencies within the time series. The gated recurrent unit model adopts a similar memory concept while employing a more compact gating mechanism, thereby reducing the number of trainable parameters and offering a computationally lighter structure. In bidirectional architectures, the time series is processed in both forward and backward directions, which expands the contextual information available at each time step and enhances representational capacity. In the hybrid model, an initial layer designed to capture long-term dependencies is refined by subsequent gated structures, whereas in the attention-based model, the time steps that contribute most significantly to the forecast are emphasized through learnable weighting coefficients.

All models were configured with comparable capacity levels. The input layers receive generation sequences with the same window length, and the number of hidden units in intermediate layers was selected to ensure a fair comparison across architectures. The output layer produces a single hourly power generation value in all cases, allowing the models to be evaluated under an identical prediction task.

During training, the Adam optimization algorithm and the mean squared error loss function were employed. The learning rate, number of epochs, and regularization parameters were determined by monitoring validation error, and training was terminated using an early stopping mechanism when no further improvement in validation performance was observed. This procedure mitigated overfitting to the training data and promoted solutions with stronger generalization capability.

2.3.1. Fundamental Principle and Mathematical Structure of the LSTM Architecture

The LSTM architecture is based on a cell state mechanism that enables time-dependent information to be preserved over long temporal horizons. This structure operates through a set of gating mechanisms that regulate which information should be retained and which should be attenuated as the sequence progresses. The first step in this process is governed by the forget gate, which determines the extent to which information from previous time steps should be maintained. The forget gate coefficient f_t is computed using the current input vector x_t and the hidden state vector from the previous time step h_{t-1}. This linear combination is scaled by the weight matrices W_f and U_f, followed by the addition of a bias term b_f, and subsequently passed through a sigmoid activation function. As a result, the forget gate coefficient is obtained as expressed in Equation (2).

$$f_t = \sigma\left(W_f x_t + U_f h_{t-1} + b_f\right) \quad (2)$$

Following the forget mechanism, the extent to which new information is incorporated into the cell state is determined based on the current input x_t and the previous hidden state h_{t-1}. These terms are linearly transformed using the weight matrices W_i and U_i, respectively, after which a bias term b_i is added and the result is constrained through a sigmoid activation function. This process is formally expressed in Equation (3).

$$i_t = \sigma(W_i x_t + U_i h_{t-1} + b_i) \quad (3)$$

At the same time, the candidate information to be added to the cell state, denoted as $\tilde{c}_t$, is computed. This candidate cell state is obtained by applying a hyperbolic tangent activation function to the linear combination of the input vector and the previous hidden state. In this formulation, W_c and U_c represent the corresponding weight matrices, while b_c denotes the bias term. The candidate information term is modeled as given in Equation (4).

$$\tilde{c}_t = \tanh\left(W_c x_t + U_c h_{t-1} + b_c\right) \quad (4)$$

The updated cell state c_t is obtained through a controlled combination of information carried from the past and newly computed candidate information. This integration is achieved by scaling the previous cell state c_{t-1} with the forget gate coefficient f_t and adding the candidate information weighted by the input gate coefficient i_t. Accordingly, the cell state is updated as expressed in Equation (5).

$$c_t = f_t c_{t-1} + i_t \tilde{c}_t \quad (5)$$

In the final stage, the information to be propagated from the cell state to the output is determined through the output gate. The output gate coefficient o_t is computed using the current input x_t and the previous hidden state h_{t-1}, scaled by the weight matrices W_o and U_o, followed by the addition of a bias term b_o, and subsequently passed through a sigmoid activation function. This operation is expressed in Equation (6).

$o_t = \sigma(W_o x_t + U_o h_{t-1} + b_o)$	(6)

Finally, the updated cell state c_t is scaled through a hyperbolic tangent activation function and multiplied by the output gate coefficient o_t to obtain the hidden state vector h_t. This vector represents the output produced by the LSTM cell at time step *t* and is defined as given in Equation (7).

$h_t = o_t \tanh(c_t)$	(7)

Owing to this structure, the LSTM model is able to learn short-term fluctuations and long-term trends simultaneously, providing a strong representational capability for systems with pronounced temporal dependencies, such as wind power generation.

2.3.2. Fundamental Principle and Mathematical Structure of the GRU Architecture

The GRU architecture employs a simpler memory management mechanism compared to the LSTM structure, updating information directly through the hidden state rather than maintaining a separate cell state. In this architecture, the manner in which information is propagated over time and the extent to which it is updated are governed by two fundamental gating mechanisms. The first of these is the update gate, which controls the proportion of past information that is carried forward to the new time step.

The update gate coefficient $z_t$is computed using the current input vector x_t and the hidden state vector from the previous time step h_{t-1}. This linear combination is scaled by the weight matrices W_z and U_z, followed by the addition of a bias term b_z, and subsequently passed through a sigmoid activation function. As a result, the update gate coefficient is obtained as expressed in Equation (8).

$z_t = \sigma(W_z x_t + U_z h_{t-1} + b_z)$	(8)

Following the update mechanism, the reset gate is computed to determine the extent to which past information is taken into account when forming the candidate hidden representation. The reset gate coefficient r_t is calculated using the input vector x_t and the previous hidden state h_{t-1}, scaled by the weight matrices W_r and U_r, followed by the addition of a bias term b_r, and subsequently constrained through a sigmoid activation function. This operation is expressed in Equation (9).

$r_t = \sigma(W_r x_t + U_r h_{t-1} + b_r)$	(9)

The candidate hidden state $\tilde{h}_t$, constructed using the reset gate coefficient, enables a controlled reinterpretation of past information. At this stage, the previous hidden state h_{t-1} is element-wise

multiplied by the reset gate coefficient r_t to regulate its influence, and then linearly combined with the input vector x_t. This combination is scaled by the weight matrices W_h and U_h, followed by the addition of a bias term b_h, and subsequently transformed through a hyperbolic tangent activation function. The candidate hidden state is computed as given in Equation (10).

$$\tilde{h}_t = \tanh\left(W_h x_t + U_h(r_t h_{t-1}) + b_h\right) \quad (10)$$

In the final stage, the updated hidden state h_t of the GRU cell is obtained through a weighted combination of the previous hidden state h_{t-1} and the candidate hidden state $\tilde{h}_t$. In this combination, the update gate coefficient z_t determines the extent to which new information is incorporated into the model, while the term $(1 - z_t)$ represents the proportion of past information that is retained. Accordingly, the updated hidden state is defined as given in Equation (11).

$$h_t = (1 - z_t)h_{t-1} + z_t\tilde{h}_t \quad (11)$$

Due to its reduced number of parameters compared to the LSTM architecture, this model lowers computational cost and provides a faster and more stable learning process, particularly for highly volatile time series in which abrupt power variations are dominant. These characteristics make GRU-based models an effective alternative for short-term forecasting problems.

2.3.3. Fundamental Principle and Mathematical Structure of Bidirectional Architectures

BiLSTM and BiGRU models are bidirectional architectures developed to overcome the limitation of conventional unidirectional recurrent neural networks, which rely solely on past information. In these models, the time series is processed both in chronological order and in reverse, producing two distinct contextual representations for each time step. This approach enables a richer representation, particularly in scenarios where future observations can contribute to the interpretation of the current time step.

In the forward pass, the time series progresses starting from t = 1, and at each time step the forward hidden state vector $\vec{h}_t$ is computed using the current input x_t and the forward hidden state from the previous time step $\vec{h}_{t-1}$. This transformation is performed through a nonlinear function $f(.)$ that represents the internal structure of either an LSTM or a GRU cell, depending on the chosen architecture. The forward hidden state is expressed as given in Equation (12).

$$\vec{h}_t = f\left(x_t, \vec{h}_{t-1}\right) \quad (12)$$

In the backward pass, the time series is processed in reverse order, allowing contextual information derived from future observations to be incorporated at each time step. The backward hidden state vector $\overleftarrow{h}_t$ is computed using the current input x_t together with the backward hidden state from the subsequent time step $\overleftarrow{h}_{t-1}$. As in the forward direction, this process is modeled using the same cell function $f(.)$ and is defined as expressed in Equation (13).

$\overleftarrow{h}_t = f(x_t, \overleftarrow{h}_{t-1})$	(13)

For each time step, the forward and backward hidden state vectors are combined to form the final representation used by the model. This combination is typically achieved through vector concatenation, resulting in a bidirectional hidden state vector h_t, which is expressed as given in Equation (14).

$h_t = [\vec{h}_t, \overleftarrow{h}_t]$	(14)

Through this structure, BiLSTM and BiGRU models are able to consider not only past trends but also future-oriented structural information simultaneously. This capability facilitates the learning of a broader temporal context and contributes to improved forecasting performance, particularly for time series characterized by high irregularity and abrupt variations, such as hourly wind power generation.

2.3.4. Fundamental Principle and Mathematical Structure of the Hybrid LSTM–GRU Architecture

In the hybrid approach, LSTM and GRU layers are arranged sequentially in order to model the dynamics of the time series at different temporal scales simultaneously. Within this architecture, the LSTM layer is responsible for learning long-term dependencies and seasonal trends. The input time series observation x_t is processed by the LSTM cells to generate a hidden state vector h_t^{LSTM}, which represents the long-term contextual information at time step *t*. This representation is then forwarded to the GRU layer, which, owing to its more compact structure, is able to respond more rapidly to abrupt changes in the data. Consequently, the inter-layer information flow of the hybrid architecture is summarized as expressed in Equation (15).

$h_t^{LSTM} = \mathrm{LSTM}(x_t), h_t^{GRU} = \mathrm{GRU}(h_t^{LSTM})$	(15)

In this architecture, h_t^{LSTM} denotes the intermediate representation that encapsulates long-term temporal dependencies, whereas h_t^{GRU} represents a reformulated version of this information that is sensitive to short-term fluctuations. In the final stage, the hidden state vector produced by the GRU layer is subjected to a linear transformation to compute the predicted output value. This transformation utilizes the weight vector W_y and the bias term b_y, and the predicted output $\hat{y}_t$ is defined as given in Equation (16).

$\hat{y}_t = W_y h_t^{GRU} + b_y$	(16)

Through this hybrid architecture, the model is able to capture seasonal patterns and long-term trends observed in wind power generation via the LSTM layer, while simultaneously learning short-term turbulence and abrupt power variations more efficiently through the GRU layer. As a result, the multi-scale structure of the wind power generation time series is represented in a more effective and balanced manner within a single integrated model.

2.3.5. Fundamental Principle and Mathematical Structure of the Attention Mechanism

The attention mechanism is a weighting strategy that differentiates the contribution of each time step to the forecasting process through learnable weights, rather than assuming equal importance across the entire time series. This structure enables the model to focus on critical time steps, particularly in time series characterized by abrupt and influential changes. In the first stage, an importance score is computed to represent the relative contribution of the hidden state vector h_t at each time step to the final prediction.

This score is obtained by applying a linear transformation to the hidden state vector, followed by scaling through a hyperbolic tangent activation function, and then computing the inner product with a learnable attention vector *v*. In this formulation, the weight matrix W_h and the bias term b_h are employed, and the importance score is defined as given in Equation (17).

$$e_t = v^{\top} \tanh\left(W_h h_t + b_h\right)$$	(17)

The obtained importance scores are normalized to ensure comparability across different time steps. This normalization is performed using the softmax function, through which the attention coefficient α_t for each time step is computed by dividing the exponential of its score by the sum of exponentials over all time steps. Consequently, the attention coefficients form a probability distribution whose total equals one, as expressed in Equation (18).

$$\alpha_t = \frac{\exp\left(e_t\right)}{\sum_{k=1}^{T} \exp\left(e_k\right)}$$	(18)

Using the normalized attention coefficients, a weighted combination of the hidden states across the time series is constructed. The resulting context vector c represents a summarized representation utilized by the model for prediction, where the contribution of each hidden state is scaled by its corresponding attention coefficient. The context vector is computed as defined in Equation (19).

$$c = \sum_{t=1}^{T} \alpha_t h_t$$	(19)

In the final stage, the resulting context vector is subjected to a linear transformation to compute the final prediction value. This transformation employs the weight matrix W_c and the bias term b_c, and the predicted output $\hat{y}$ is defined as given in Equation (20).

$$\hat{y} = W_c c + b_c$$	(20)

Through this attention-based structure, the model is able to assign greater importance to time steps at which abrupt and influential wind variations occur during the forecasting process, thereby enabling a more effective learning of the irregular and highly volatile nature of the time series.

2.3.6. Overall Modeling Framework and Mathematical Summary

All deep learning models employed in this study were trained under the same data preprocessing pipeline and training strategy in order to ensure a fair and comparable evaluation framework. The time series

composed of hourly wind power generation data is defined as a univariate sequence of length *T*, where each observation x_T represents the generated power value at time step *t*, and is expressed as follows:

$X = \{x_1, x_2, \dots, x_T\}$	(21)

To transform the time series forecasting problem into a supervised learning framework, a sliding window approach is employed. In this approach, input sequences consisting of *L* consecutive observations with a fixed length are defined, and for each time step the input vector X_t provided to the model is constructed to include the power generation values from the previous *L* time steps. Accordingly, the input sequence is defined as given in Equation (22).

$X_t = [x_{t-L+1}, \dots, x_t]$	(22)

Under this formulation, the objective of the model is to predict the power generation value at the subsequent time step using the input sequence X_t. The predicted value $\hat{y}_{t+1}$ is obtained through a nonlinear function $F_\theta(.)$, parameterized by the set θ, and is expressed as given in Equation (23).

$\hat{y}_{t+1} = F_\theta(X_t)$	(23)

During the training process, the mean squared error is employed as the loss function in order to quantify the agreement between model predictions and the corresponding ground-truth observations. For a training dataset consisting of *N* samples, this loss function is computed as the average of the squared differences between the true value y_i and the predicted value $\hat{y}_i$ for each sample. Accordingly, the optimization objective is to minimize the loss function defined as given in Equation (24).

$\mathcal{L} = \frac{1}{N}\sum_{i=1}^{N}(y_i - \hat{y}_i)^2$	(24)

Through this unified training and data processing framework, the LSTM, GRU, BiLSTM, BiGRU, and attention-based hybrid models are evaluated under the same dataset, identical windowing strategy, and the same error metric. Consequently, the resulting outcomes reflect differences attributable solely to model architectures, enabling an objective and consistent comparison of the performance of the proposed methods.

3. Results and Discussion

The model performances obtained on the independent test set are presented in Table 1. The reported root mean square error, mean absolute error, mean squared error, coefficient of determination, and percentage-based error metrics indicate that all models exhibit comparable performance in hourly short-term wind power forecasting, while certain architectures outperform others under specific evaluation criteria.

Table 1. Comparative Performance of the Evaluated Models on the Test Dataset

Model	RMSE	MAE	MSE	R^2 Score	MAPE	sMAPE
BiGRU	2.039473	1.363367	4.159451	0.889715	43.58732	78.37485
LSTM	2.049807	1.380082	4.201708	0.888595	43.48984	78.26997
GRU	2.051937	1.376333	4.210446	0.888363	43.40159	78.58196
BiLSTM	2.052254	1.381472	4.211745	0.888328	44.24569	78.74331
LSTM_GRU	2.05233	1.378809	4.21206	0.88832	42.76192	78.16702
LSTM_Attention	2.066958	1.395498	4.272314	0.886723	43.55124	78.70001

From the perspective of RMSE, MAE, MSE, and the coefficient of determination, the bidirectional GRU model achieves the best overall performance. The fact that BiGRU attains the lowest error values and the highest R^2 score suggests that its ability to simultaneously exploit forward and backward temporal context provides an advantage in representing short-term fluctuations in wind power generation series. The unidirectional LSTM and unidirectional GRU models closely follow this performance, with only marginal differences observed among their error values. This indicates that the baseline architectures exhibit largely comparable representational capabilities.

When percentage-based error metrics are considered, the LSTM–GRU hybrid model stands out by achieving the lowest value, particularly in terms of sMAPE. This finding implies that combining the LSTM layer, which captures long-term dependencies, with the GRU layer, which is more responsive to short-term variations, can offer advantages with respect to relative error distribution. Although the attention-based LSTM model is architecturally more complex, it does not yield the best performance on this dataset, with error values remaining slightly higher than those of the other models. This outcome can be interpreted in line with existing literature, which suggests that attention mechanisms tend to provide more pronounced benefits in multivariate settings or when longer input sequences are involved.

Figure 1 presents bar chart comparisons of the models in terms of RMSE, R^2, and sMAPE. Consistent with the numerical results, the plots indicate that performance differences among the models are relatively small in absolute terms, yet systematic in nature. The BiGRU model exhibits a slight but consistent advantage along the error-based axes, while the LSTM–GRU hybrid model clearly achieves the lowest values in the percentage-based error comparison.

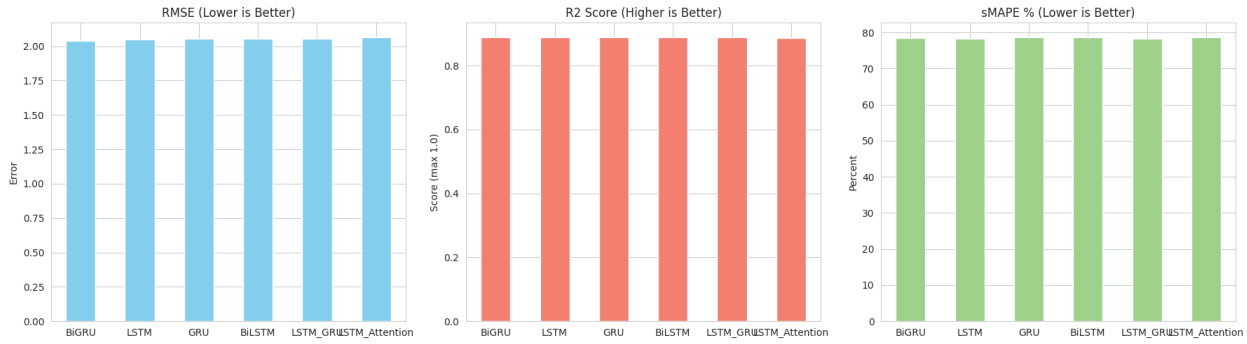

Figure 1. Comparison of Models in Terms of RMSE, R^2, and sMAPE

Figure 2 illustrates the actual power generation profile of the first 200 hours in the test set together with the predictions produced by all evaluated models. The time series plot reveals that the models track the overall trend and short-term fluctuations in a highly consistent manner. In particular, during periods of rapid increases and decreases in generation, all models accurately capture the timing of peak and trough points, while the observed discrepancies primarily manifest as slight underestimation or overestimation of peak magnitudes rather than temporal misalignment.

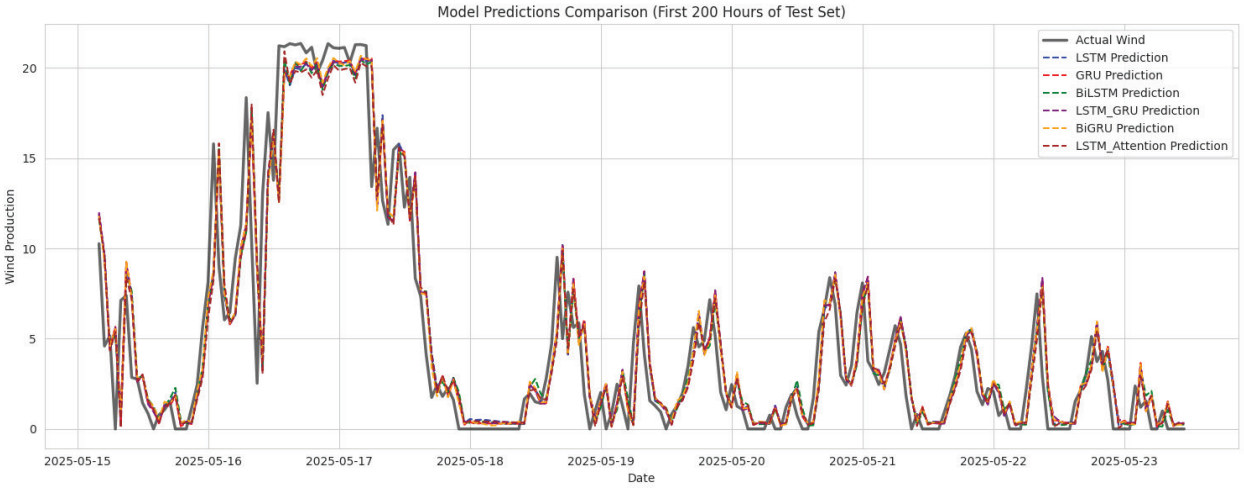

Figure 2. Actual and Predicted Wind Power Generation for the First 200 Hours of the Test Set

4. General Discussion and Recommendations

The obtained results indicate that LSTM-based and related recurrent architectures exhibit strong and closely comparable performance in hourly short-term wind power forecasting. While the BiGRU model delivers the best performance in terms of absolute error metrics, the LSTM–GRU hybrid architecture stands out with respect to percentage-based error measures. The unidirectional LSTM model, on the other hand, emerges as a well-balanced option for practical applications due to its architectural simplicity and consistently high prediction accuracy.

This study provides a comparative analysis of different deep learning architectures using data from the Turkish electricity market and offers a concrete reference framework for wind farm operators and system planners in short-term forecasting applications. For future research, the incorporation of multivariate input structures, integration of meteorological forecasts and turbine operational data, exploration of transformer-based hybrid architectures, and the adoption of probabilistic models capable of quantifying uncertainty are expected to further enhance wind power forecasting performance in terms of both accuracy and interpretability.

References

Balcı, M., Dokur, E., & Yüzgeç, U. (2025). A hybrid LSTM-single candidate optimizer model for short-term wind power prediction. *Computer Modeling in Engineering & Sciences, 144*(1), 945–968. doi:10.32604/cmes.2025.067851

Enerji Piyasaları İşletme A.Ş. (2016). *Şeffaflık platformu teknik dokümanı*.

Enerji Piyasaları İşletme A.Ş. (2023). *Transparency platform*.

Galphade, M., Nikam, V. B., Banerjee, B., Kiwelekar, A. W., & Sharma, P. (2025). Stacked LSTM for short-term wind power forecasting using multivariate time series data. *International Journal of Interactive Multimedia and Artificial Intelligence, 9*(3), 71–81. doi:10.9781/ijimai.2024.07.002

Graves, A., Mohamed, A.-R., & Hinton, G. (2013). Speech recognition with deep recurrent neural networks. In *Proceedings of the IEEE International Conference on Acoustics, Speech and Signal Processing* (pp. 6645–6649).

Harrou, F., Dairi, A., Dorbane, A., & Sun, Y. (2024). Enhancing wind power prediction with self-attentive variational autoencoders: A comparative study. *Results in Engineering, 23*, 102504. doi:10.1016/j.rineng.2024.102504

Hochreiter, S., & Schmidhuber, J. (1997). Long short-term memory. *Neural Computation, 9*(8), 1735–1780.

Ibrahim, A. B. A. (2023). LSTM deep learning techniques for wind power generation forecasting. *Journal of Soft Computing and Artificial Intelligence, 4*(2), 45–60.

Ibrahim, A. B. A., & Altun, K. (2024). LSTM deep learning techniques for wind power generation forecasting. *Journal of Soft Computing and Artificial Intelligence, 5*(1), 41–47. doi:10.55195/jscai.1471257

Kaplan Yalçın, K., & Saray, U. (2014). Examination of Turkey's renewable energy and fossil energy consumption with analytic hierarchy process (AHP). *Journal of New Results in Science*, (5), 28–36.

Karamollaoğlu, H. (2025). Hybrid deep learning framework for short-term electricity generation forecasting in Türkiye using multi-source data. *Turkish Journal of Electrical Power and Energy Systems, 5*(3), 152–160. doi:10.5152/tepes.2025.25029

Karijadi, I., Chou, S.-Y., & Dewabharata, A. (2023). Wind power forecasting based on hybrid CEEMDAN-EWT deep learning method. *Renewable Energy, 218*, 119357. doi:10.1016/j.renene.2023.119357

Liu, Z., Guo, H., Zhang, Y., & Zuo, Z. (2025). A comprehensive review of wind power prediction based on machine learning: Models, applications, and challenges. *Energies, 18*(2), 350. doi:10.3390/en18020350

Lüy, M., & Saray, U. (2012). Wind speed estimation for missing wind data with three different backpropagation algorithms. *Energy Education Science and Technology Part A: Energy Science and Research, 30*(1), 45–54.

Ma, Z., & Mei, G. (2022). A hybrid attention-based deep learning approach for wind power prediction. *Applied Energy, 323*, 119608.

Rushdi, M. A., Abdallah, A., Abdel-Aziz, M., & El-Deeb, A. (2024). Deep learning approaches for power prediction in wind turbines. *Energies, 17*(15), 3630.

Saray, U., Lüy, M., & Çam, E. (2011). Amasya ili için yapay sinir ağları ile rüzgar hızı tahmini. *EMO Elektrik Elektronik Mühendisliği Günleri, ODTÜ Kültür ve Kongre Salonu* (ss. 420–423).

Saray, U., Yücehan, T., & Önal, S. (2017). Implementing modern estimation methods for long-term wind speed estimates in the province of Şanlıurfa in the Southeastern Anatolia region. *International Refereed Journal of Engineering and Science (IRJES), 6*(9), 63–75.

Wang, Y., Zou, R., Liu, F., Zhang, L., & Liu, Q. (2021). A review of wind speed and wind power forecasting with deep neural networks. *Applied Energy, 304*, 117766.

Wu, Z., Luo, G., & Yang, Z. (2022). A comprehensive review on deep learning approaches in wind forecasting applications. *CAAI Transactions on Intelligence Technology, 7*(1), 129–143.

Yelgeç, M. A., & Bingöl, O. (2024). Wind power forecasting with LSTM and comparison with different machine learning algorithms: A case study of southwestern Turkey. *Electric Power Components and Systems*. doi:10.1080/15325008.2024.2327826

Chapter 8

COMPARATIVE ANALYSIS OF MACHINE LEARNING–BASED SURROGATE MODELS FOR FAST RESONANCE CHARACTERISTIC PREDICTION OF SQUARE-RING FREQUENCY SELECTIVE SURFACES

Mehmet YERLİKAYA [1]

1 Asst. Prof. Dr., Selcuk University, School of Civil Aviation, Department of Airframe and Powerplant Maintenance, mehmet.yerlikaya@selcuk.edu.tr, ORCID: 0000-0001-8018-840X.

1. INTRODUCTION

Frequency selective surfaces (FSSs) are periodically arranged conductive patterns placed on dielectric substrates to manipulate electromagnetic wave behavior. By appropriately designing the geometry and material properties of these patterns, FSSs can be engineered to selectively transmit, reflect, or attenuate electromagnetic (EM) waves within specific frequency bands. The electromagnetic response of an FSS is strongly influenced by factors such as element shape, periodicity, substrate characteristics, and operating frequency. When an incident plane wave impinges normally on the surface and its frequency aligns with the resonant behavior of the FSS unit cell, significant transmission or reflection occurs, depending on the surface design. (Anwar et al., 2018; Munk, 2005). Due to these properties, FSSs have been widely employed in modern microwave and millimeter-wave applications such as radomes (Costa & Monorchio, 2012), filters (Bayatpur & Sarabandi, 2010), absorbers (Costa et al., 2016), antennas (Gültekin & Yerlikaya, 2024), and electromagnetic shielding systems (Sivasamy et al., 2017). Among various geometrical configurations, square-ring FSS structures are particularly attractive owing to their compact geometry, polarization stability, and tunable resonance behavior (Yerlikaya & Duysak, 2022).

The electromagnetic response of an FSS is strongly dependent on both material characteristics and geometrical parameters, including dielectric constant, substrate thickness, and unit-cell dimensions (Costa & Monorchio, 2012). Accurate determination of resonance characteristics traditionally relies on full-wave electromagnetic solvers such as CST. Although these tools provide reliable results, repeated simulations become computationally expensive when conducting parametric sweeps or optimization studies over large design spaces. As a result, surrogate modeling techniques have emerged as an efficient alternative for accelerating the FSS design process (Wang et al., 2023).

In recent years, machine learning (ML) based surrogate models have gained increasing attention in electromagnetic analysis and design. Early studies primarily focused on artificial neural networks (ANNs) to estimate resonance frequency, bandwidth, or scattering parameters of antennas and frequency-selective structures. ANN-based models demonstrated strong nonlinear mapping capabilities; however, they often require careful architecture tuning and relatively large datasets to avoid overfitting (Fontoura et al., 2021; Mishra, 2002).

Beyond conventional ANN-based approaches, alternative machine learning techniques have been increasingly investigated to enhance prediction accuracy while reducing model complexity and training requirements. Support vector regression (SVR) has emerged as a powerful surrogate modeling technique due to its strong generalization capability and robustness when working with relatively small datasets (Vapnik, 2013). By employing kernel-based nonlinear mapping, SVR can effectively capture the complex relationships between FSS geometrical parameters and their corresponding resonance characteristics.

Ensemble learning methods, particularly tree-based models, have also demonstrated promising performance in electromagnetic modeling applications. Random forest (RF) regression constructs multiple decision trees using bootstrap sampling and feature randomness, leading to improved prediction stability and resistance to overfitting (Breiman, 2001). Similarly, Gradient boosting (GB) methods iteratively combine weak learners to minimize prediction errors, enabling accurate modeling of highly nonlinear electromagnetic responses (Friedman, 2001). These ensemble approaches often outperform single learners in complex design spaces while requiring less extensive hyperparameter tuning compared to deep neural networks. In parallel, Gaussian process regression

(GPR) has emerged as a powerful probabilistic surrogate model, particularly suited for small datasets, offering not only accurate predictions but also uncertainty quantification (Williams & Rasmussen, 2006).

Recent studies have demonstrated the effectiveness of machine learning–based surrogate models for predicting resonance frequencies and scattering parameters of frequency selective surfaces and periodic electromagnetic structures. For instance, ML-assisted frameworks have been applied to ring-type and patch-based FSS unit cells, significantly reducing the number of full-wave simulations required during optimization processes (Calik et al., 2021; Fontoura et al., 2021). However, most of these studies focus on a single learning technique or a specific FSS geometry, limiting the ability to draw generalized conclusions regarding the comparative performance of different ML models.

Despite the growing body of literature, comparative studies that systematically evaluate multiple ML-based surrogate models under identical conditions remain limited in the context of square-ring FSS resonance prediction. Most existing works focus on a single learning algorithm, making it difficult to assess the relative strengths and weaknesses of different approaches when applied to the same dataset. This study provides a comparative evaluation of four ML–based surrogate models for fast prediction of the resonance characteristics of square-ring frequency selective surfaces. Using a common simulation-generated data set and uniform evaluation metrics, the work aims to identify the most suitable surrogate modeling approach for FSS design and optimization with respect to accuracy, robustness, and practical applicability.

2. MACHINE LEARNING METHODS

Machine learning (ML) based surrogate modeling has become an effective tool for accelerating electromagnetic design processes by replacing repeated full-wave simulations with fast data-driven predictors. By learning the relationship between geometric and material parameters and the resulting electromagnetic response, these models enable rapid performance estimation while significantly reducing computational cost. In recent years, various regression-based machine learning techniques have been successfully applied to antenna, metasurface, and FSS modeling, particularly in scenarios involving limited datasets and highly nonlinear parameter interactions (Abdullah & Koziel, 2021; Belen et al., 2022; Dokmetas et al., 2024; Koziel & Pietrenko-Dabrowska, 2020).

2.1.Support Vector Regression

Support Vector Regression (SVR) is a kernel-based learning method derived from statistical learning theory. SVR seeks to find an optimal function that minimizes prediction error while maintaining model flatness, using an ε-insensitive loss function. By employing nonlinear kernel functions such as the radial basis function (RBF), SVR can accurately model complex nonlinear relationships with good generalization capability (Vapnik, 2013). SVR has been used in various electromagnetic applications, including antenna synthesis and microwave circuit modeling, where accurate prediction with limited datasets is required (Khan & Roy, 2019)

2.2.Random Forest

Random Forest (RF) is an ensemble learning algorithm that combines multiple decision trees trained on bootstrap-resampled subsets of the training data. Each tree is constructed using a random subset of input features, which reduces correlation among individual trees and improves generalization performance. RF is particularly robust against noise and overfitting, and it can efficiently handle nonlinear relationships between input parameters and target variables (Breiman,

2001). In electromagnetic modelling, Random Forest has been successfully applied for surrogate modelling of antennas and periodic structures, providing reliable performance with limited training data (Fontoura et al., 2021).

2.3.Gradient Boosting

Gradient Boosting is an ensemble method that builds a strong learner by sequentially combining multiple weak learners, typically shallow decision trees. Each new learner is trained to correct the prediction errors of the previous model using gradient descent in function space. This approach allows Gradient Boosting models to achieve high accuracy, especially in regression problems with complex nonlinear interactions among input parameters (Friedman, 2001). In electromagnetic applications, Gradient Boosting has shown strong performance in surrogate modeling and inverse design tasks (Li et al., 2022; Zhou et al., 2023).

2.4.Gaussian Process Regression

Gaussian Process Regression (GPR) is a regression method that learns the relationship between input variables and outputs directly from data without assuming a fixed model structure. It uses a kernel function to capture similarities between data points, which enables accurate modeling of complex behaviors (Williams & Rasmussen, 2006). An important advantage of GPR is that it provides both prediction values and associated uncertainty information, making it well suited for electromagnetic applications where material and fabrication variations can affect performance (Zhang et al., 2021).

2.5.Comparative Framework for Machine Learning–Based Surrogate Models

In this study, four data-driven regression models were implemented to construct surrogate models for predicting the electromagnetic behavior of square-ring FSS structures. The selected models represent different learning philosophies, including ensemble learning, kernel-based probabilistic modeling, and margin-based regression. To ensure a fair comparison, identical training and testing datasets and preprocessing steps were applied to all models.

Before model training, the input parameters were standardized using z-score normalization. Model hyperparameters were optimized using five-fold cross-validation on the training set. The fundamental characteristics, strengths, and limitations of the selected machine learning models are summarized in Table 1.

Table 1. Characteristics of the machine learning models considered in this work

Model	Learning Type	Main Strength	Typical Weakness
Support Vector Regression (SVR)	Margin-based / Kernel	Good generalization	Sensitive to kernel selection
Random Forest (RF)	Bagging Ensemble	Robust to noise, stable	Limited extrapolation
Gradient Boosting (GB)	Boosting Ensemble	High nonlinear modelling capability	Risk of overfitting
Gaussian Process Regression (GPR)	Kernel / Probabilistic	High accuracy, uncertainty estimation	High computational cost

3. SQUARE-RING FSS GEOMETRY AND SIMULATION SETUP

The FSS investigated in this study is based on a periodic square-ring unit cell printed on a dielectric substrate. The conductive square-ring element is located on one side of the substrate, while

the opposite side is assumed to be free of metallization. A three-dimensional view of the unit cell geometry is illustrated in Fig. 1.

The substrate is characterized by its relative permittivity (εr), thickness (hs), and unit-cell width (W). The square-ring conductor is defined by its outer width (Wo) and inner width (Wi), which together determine the effective electrical size of the resonant element. Hereafter, the normalized outer and inner ring dimensions are denoted as x and y, respectively. By systematically varying five parameters, a comprehensive dataset was generated to capture the influence of both material properties and geometrical dimensions on the electromagnetic response of the FSS structure. The ranges and discrete values of the input parameters considered in the simulations are summarized in Table 2.

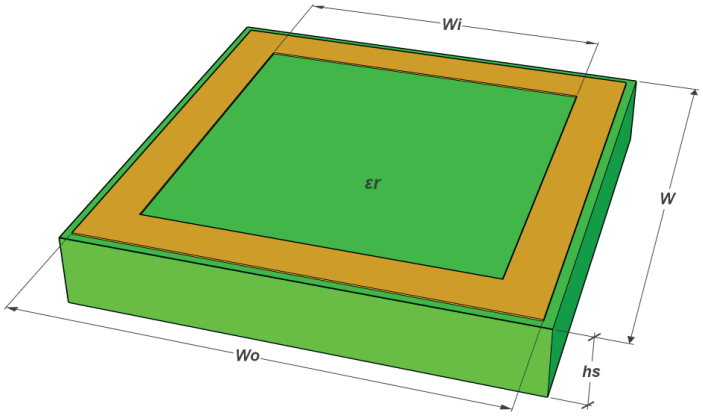

Figure 1. Three-dimensional geometry of the square-ring FSS unit cell

Fig. 1 Three-dimensional geometry of the square-ring FSS unit cell.

A total of 108 distinct square-ring FSS configurations were analyzed using a full-wave electromagnetic solver. All simulations were performed using CST, a commercially available finite element method–based electromagnetic simulation software. Periodic boundary conditions were applied to model an infinite array of unit cells, while appropriate excitation was used to investigate plane-wave incidence.

Table 2. Geometrical and material parameters used in the full-wave simulations of square-ring FSS structure

W	*x (Wo/W)*	*y (Wi/W)*	h_s	ε_r
8 mm	0.5	0.1	0.8 mm	2.33
10 mm	0.7	0.2	1.6mm	4.3
	0.9	0.4		6.15

The transmission coefficient (S_{21}) was evaluated as a function of frequency for both transverse electric (TE) and transverse magnetic (TM) polarizations under normal incidence. Resonance frequencies were identified at points where the transmission magnitude dropped below −20 dB. Across the entire dataset, the extracted resonance frequencies span a wide range, from approximately 4.9 GHz to 29.05 GHz, indicating strong sensitivity of the electromagnetic response to variations in the design parameters.

The selected dielectric constants of 2.33, 4.3, and 6.15 correspond to commonly used commercial substrate materials, namely Rogers RT/duroid 5870, FR-4, and Rogers RO3006,

respectively. Similarly, substrate thickness values of 0.8 mm and 1.6 mm were chosen as they are widely available for these materials. This selection ensures that the generated dataset remains practically relevant while covering a broad design space suitable for surrogate model development. The simulation results obtained from this parametric study form the basis of the machine learning dataset used in the subsequent surrogate modeling framework, which is described in the following section.

4. METHODOLOGY

Based on the parametric full-wave simulations described in Section II, a dataset was constructed to establish a mapping between the physical design parameters of the square-ring FSS and its resonance characteristics. Each data sample corresponds to a unique FSS configuration defined by five input parameters: relative permittivity (εr), unit-cell width (W), substrate height (hs), and two geometric parameters describing the square-ring dimensions (x and y). The target outputs of the learning problem are the resonance frequency (fr) and the corresponding bandwidth (BW), extracted from the simulated transmission coefficient responses. This formulation enables the surrogate models to learn the nonlinear relationship between the design variables and the electromagnetic behavior of the FSS structure.

4.1.Data Preprocessing and Normalization

Prior to model training, the input features were standardized using z-score normalization. This preprocessing step ensures numerical stability during training and prevents features with larger magnitudes from dominating the learning process. Normalization was applied only during the training phase; all reported predictions and comparisons were transformed back to their original physical scales (Hastie, 2009).

To evaluate model generalization performance, the dataset was randomly divided into training and test subsets, with 80% of the samples used for training and 20% reserved for testing. The same data partitioning strategy was applied consistently to all machine learning models to ensure an unbiased comparison.

4.2.Model Training and Hyperparameter Optimization

All surrogate models were trained using the same normalized training dataset to ensure consistency. Model hyperparameters were optimized through five-fold cross-validation performed exclusively on the training data. This procedure enables the selection of optimal model configurations while avoiding information leakage from the test set. The optimized models were then retrained using the complete training dataset before being evaluated on the unseen test data. This strategy ensures that the reported results reflect true generalization performance.

4.3.Performance Evaluation and Comparison Criteria

The predictive accuracy of the surrogate models was systematically evaluated using standard error metrics, namely Mean Absolute Error (MAE) and Root Mean Square Error (RMSE), while R^2 was used to indicate the level of agreement between predicted and reference results, thereby reflecting model reliability and generalization performance. These metrics provide complementary insight into absolute prediction error, variance-sensitive error behavior, and overall goodness of fit.

In addition to numerical metrics, parity plots comparing simulated and predicted values were employed to visually evaluate model accuracy across the entire design space. By applying identical

evaluation criteria to all models, the proposed framework enables a direct and fair comparison of different machine learning techniques for surrogate modeling of square-ring FSS structures.

5. RESULTS AND DISCUSSION

This section presents and discusses the predictive performance of the proposed machine learning–based surrogate models for square-ring FSSs. The results are analyzed separately for resonance frequency and bandwidth prediction to provide a clear assessment of model behavior with respect to different electromagnetic characteristics.

5.1.Resonance Frequency Prediction Performance

The test performance metrics for resonance frequency prediction are summarized in Table 3. Among the four surrogate models, GPR demonstrates the highest prediction accuracy, achieving an RMSE of 0.135 and an R^2 value of 0.999. This result indicates an excellent agreement between the predicted and simulated resonance frequencies across the entire test dataset.

Table 3. Performance metrics for resonance frequency prediction of the square-ring FSS

	MAE	**RMSE**	**R^2**
RF	1.832	2.543	0.776
GPR	0.100	0.135	0.999
SVR	2.292	3.581	0.556
GB	0.357	0.433	0.993

GB also shows strong predictive capability, with an RMSE of 0.433 and an R^2 value of 0.993. The ensemble-based learning strategy enables GB to effectively capture nonlinear interactions between the geometric and material parameters of the FSS structure. However, its performance remains slightly inferior to GPR, particularly for configurations exhibiting sharp resonance shifts.

In contrast, RF and SVR exhibit comparatively lower prediction accuracy. RF yields an RMSE of 2.543 with an R^2 of 0.776, while SVR records the highest error among the evaluated models, with an RMSE of 3.581 and an R^2 of 0.556. These results suggest that RF and SVR struggle to fully model the complex nonlinear relationship governing the resonance frequency of square-ring FSSs within the considered design space.

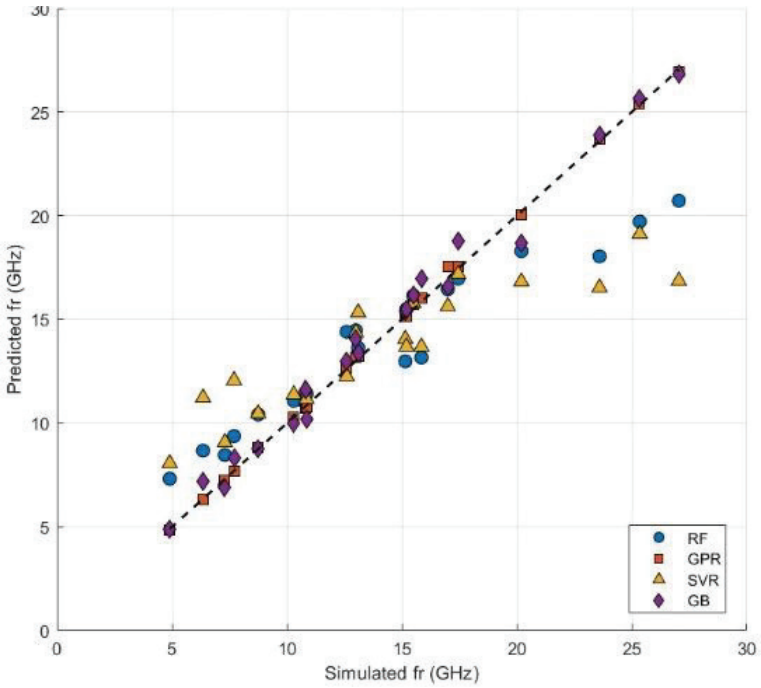

Figure 2. Comparison of the square-ring FSS resonance frequency prediction

The parity plot presented in Fig. 2 visually confirms these observations. GPR predictions closely follow the ideal y = x line, indicating minimal deviation from the simulated values. GB predictions also exhibit a strong linear correlation, whereas RF and SVR show increased scatter, particularly at higher frequency ranges.

5.2.Bandwidth Prediction Performance

The comparative bandwidth prediction performances of the examined regression models are summarized in Table 4 and further illustrated in Fig. 3. Among all approaches, GPR clearly outperforms the others, yielding the lowest MAE and RMSE values of 0.162 and 0.201, respectively, along with a very high coefficient of determination (R^2 = 0.993). These results indicate that GPR provides highly accurate and consistent bandwidth estimates, which can be attributed to its non-parametric structure and strong capability to capture complex, nonlinear relationships between the input parameters and bandwidth response.

GB demonstrates the second-best performance, achieving an RMSE of 0.672 and an R^2 value of 0.926. While its prediction accuracy is notably lower than that of GPR, GB is still able to model the overall bandwidth behavior with reasonable precision. The relatively moderate MAE suggests that GB performs adequately for most samples, although larger deviations may occur in certain operating regions.

RF exhibits a further reduction in predictive accuracy, with MAE and RMSE values of 0.805 and 1.050, respectively, and an R^2 of 0.820. These results imply that, although RF captures some of the underlying trends, it struggles to fully represent the sensitivity of bandwidth to variations in geometric and material parameters.

SVR shows the weakest performance among the evaluated models. Its high MAE (1.164) and RMSE (1.621), combined with a relatively low R^2 value of 0.570, indicate limited capability in accurately predicting bandwidth. This performance degradation suggests that SVR is less effective in handling the intricate dependencies and sharp variations inherent in bandwidth estimation problems.

Table 4. Performance metrics for bandwidth prediction of the square-ring FSS

	MAE	RMSE	R^2
RF	0.805	1.050	0.820
GPR	0.162	0.201	0.993
SVR	1.164	1.621	0.570
GB	0.445	0.672	0.926

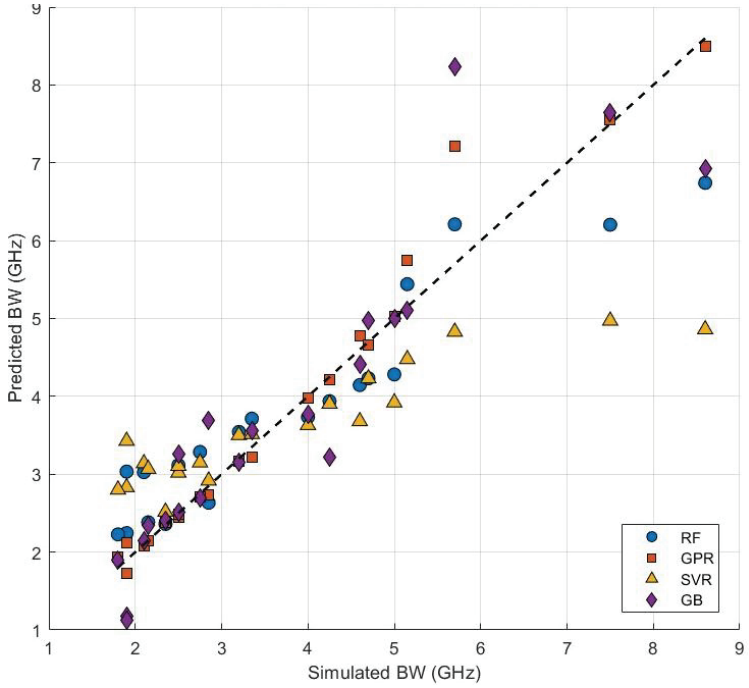

Figure 3. Comparison of the square-ring FSS bandwidth prediction

Overall, the results confirm that bandwidth prediction is a more challenging task compared to resonance frequency estimation, and highlight GPR as the most reliable and robust model for this purpose.

5.3.Combined Evaluation and Comparative Analysis

A detailed comparison between simulated and predicted values for both resonance frequency and bandwidth is provided in Table 5. This table includes the original physical input parameters alongside the corresponding predictions obtained from all surrogate models, allowing direct assessment of model accuracy on a sample-by-sample basis.

The numerical results further highlight the superior performance of GPR, which consistently produces predictions that closely match the simulated values across a wide range of FSS configurations. GB offers competitive performance, particularly for resonance frequency estimation, while RF and SVR exhibit noticeable discrepancies for several test cases.

In summary, the comparative evaluation confirms that Gaussian Process Regression provides the highest prediction accuracy for both resonance frequency and bandwidth estimation of square-ring FSSs, followed by Gradient Boosting. The systematic framework presented in this study enables fair and transparent comparison of different machine learning techniques and highlights the potential of data-driven surrogate modeling for accelerating electromagnetic design processes.

Table 5. Model prediction performance on FSS test dataset

Input Parameters					Output-1 (Resonance Frequency)					Output-2 (Bandwidth)				
ε_r	W	h_s	x	y	fr Real	fr RF	fr GPR	fr SVR	fr GB	BW Real	BW RF	BW GPR	BW SVR	BW GB
2.33	8	0.8	0.75	0.4	29,05	21,46	29,01	16,74	28,64	2,45	3,32	2,78	3,37	2,86
2.33	10	0.8	0.75	0.4	23,60	17,50	23,55	15,99	23,26	8,60	6,41	8,39	4,88	8,35
2.33	10	0.8	0.9	0.1	10,35	11,63	10,45	11,69	9,94	4,65	3,99	4,51	3,92	4,43
2.33	10	0.8	0.9	0.2	15,35	14,67	15,34	16,61	15,30	8,35	6,23	7,90	5,00	7,32
2.33	8	1.6	0.5	0.2	10,30	11,93	10,32	11,24	10,58	2,50	3,04	2,45	2,99	2,21
2.33	8	1.6	0.75	0.1	8,35	10,33	8,42	10,17	7,61	3,80	3,68	3,69	3,43	3,99
2.33	10	1.6	0.5	0.1	17,70	16,82	17,68	17,61	18,22	2,25	2,41	2,17	2,86	2,19
2.33	10	1.6	0.9	0.1	13,30	13,93	13,39	15,41	12,92	8,90	6,75	8,63	5,56	8,41
2.33	10	1.6	0.9	0.4	14,65	15,50	14,38	14,97	14,97	1,90	2,25	1,95	2,55	2,16
4.3	8	0.8	0.5	0.4	16,75	15,09	16,62	14,65	17,23	6,90	5,83	6,80	5,30	6,53
4.3	8	0.8	0.75	0.1	10,15	11,25	10,11	11,21	9,14	2,85	3,41	2,85	3,15	4,60
4.3	10	0.8	0.5	0.1	12,15	12,05	12,06	12,37	11,82	3,85	3,97	4,04	3,86	5,74
4.3	10	0.8	0.5	0.2	13,30	15,15	13,16	14,07	13,89	1,45	1,94	1,52	2,04	1,31
4.3	10	0.8	0.9	0.2	17,75	18,28	17,61	16,04	17,36	1,40	2,78	1,21	3,10	0,58
4.3	8	1.6	0.5	0.1	5,65	7,74	5,66	7,81	5,90	2,60	3,05	2,60	2,94	2,29
4.3	10	1.6	0.5	0.4	18,70	16,93	18,45	15,79	18,88	2,75	2,60	2,43	2,83	2,57
4.3	10	1.6	0.75	0.1	6,35	8,62	6,32	9,54	6,30	3,35	3,67	3,27	3,72	3,22
6.15	8	0.8	0.5	0.4	15,75	15,77	15,40	14,33	15,68	2,35	2,44	2,11	2,54	2,01
6.15	10	0.8	0.75	0.2	9,80	11,77	9,92	13,32	9,19	7,10	5,95	7,07	4,91	7,15
6.15	10	1.6	0.5	0.1	13,55	15,35	13,54	13,20	13,56	1,65	2,16	1,48	2,29	1,55
6.15	10	1.6	0.5	0.4	15,40	17,12	15,26	14,45	15,33	1,30	2,73	1,01	3,53	1,22

6. CONCLUSION

This study presented a comparative evaluation of four machine learning–based surrogate models for fast prediction of the resonance characteristics of square-ring frequency selective surfaces (FSSs). Using a common simulation-generated dataset and identical evaluation conditions, the predictive capabilities of Random Forest (RF), Support Vector Regression (SVR), Gradient Boosting (GB), and Gaussian Process Regression were systematically assessed.

The numerical results clearly indicate that Gaussian Process Regression provides the highest prediction accuracy for both resonance frequency and bandwidth estimation. For resonance frequency prediction, GPR achieved an RMSE of approximately 0.135 GHz with an R^2 value close to 0.999, demonstrating an excellent agreement with full-wave simulation results. In bandwidth prediction, GPR similarly outperformed the other models, yielding the lowest error metrics and the most stable predictions. GB showed competitive performance, particularly for resonance frequency estimation, while RF and SVR exhibited larger prediction errors, especially in bandwidth estimation.

Overall, the findings confirm that GPR-based surrogate modeling offers a powerful and computationally efficient alternative to conventional full-wave simulations for square-ring FSS analysis. The proposed framework can significantly accelerate the design, optimization, and parametric analysis of FSS structures and can be readily extended to other periodic electromagnetic surfaces and advanced optimization tasks in future studies.

REFERENCES

Abdullah, M., & Koziel, S. (2021). Surrogate-assisted design of checkerboard metasurface for broadband radar cross-section reduction. *IEEE Access*, *9*, 46744-46754.

Anwar, R. S., Mao, L., & Ning, H. (2018). Frequency selective surfaces: A review. *Applied Sciences*, *8*(9), 1689.

Bayatpur, F., & Sarabandi, K. (2010). Miniaturized FSS and patch antenna array coupling for angle-independent, high-order spatial filtering. *IEEE Microwave and Wireless Components Letters*, *20*(2), 79-81.

Belen, A., Tarı, Ö., Mahouti, P., Belen, M. A., & Caliskan, A. (2022). Surrogate-based design optimization of multi-band antenna. *Applied Computational Electromagnetics Society Journal*.

Breiman, L. (2001). Random forests. *Machine learning*, *45*(1), 5-32.

Calik, N., Belen, M. A., Mahouti, P., & Koziel, S. (2021). Accurate modeling of frequency selective surfaces using fully-connected regression model with automated architecture determination and parameter selection based on Bayesian optimization. *IEEE Access*, *9*, 38396-38410.

Costa, F., Kazemzadeh, A., Genovesi, S., & Monorchio, A. (2016). Electromagnetic absorbers based on frequency selective surfaces. Forum For Electromagnetic Research Methods And Application Technologies,

Costa, F., & Monorchio, A. (2012). A frequency selective radome with wideband absorbing properties. *IEEE Transactions on Antennas and Propagation*, *60*(6), 2740-2747.

Dokmetas, B., Shinde, S. S., & Belen, M. A. (2024). Artificial Intelligence Based Deep Learning Surrogate Model for Design Optimization of Microstrip Frequency Selective Surface. 2024 International Conference on Emerging Smart Computing and Informatics (ESCI),

Fontoura, L. C., Lins, H. W. D. C., Bertuleza, A. S., D'assunção, A. G., & Neto, A. G. (2021). Synthesis of multiband frequency selective surfaces using machine learning with the decision tree algorithm. *IEEE Access*, *9*, 85785-85794.

Friedman, J. H. (2001). Greedy function approximation: a gradient boosting machine. *Annals of statistics*, 1189-1232.

Gültekin, S. S., & Yerlikaya, M. (2024). Enhanced gain dual-port compact printed meandered log-periodic monopole array antenna design with octagonal-ring shaped FSS for broadband 28 GHz applications. *Arabian Journal for Science and Engineering*, *49*(12), 16729-16741.

Hastie, T. (2009). The elements of statistical learning: data mining, inference, and prediction. In: Springer.

Khan, T., & Roy, C. (2019). Prediction of slot-position and slot-size of a microstrip antenna using support vector regression. *International Journal of RF and Microwave Computer-Aided Engineering*, *29*(3), e21623.

Koziel, S., & Pietrenko-Dabrowska, A. (2020). *Performance-driven surrogate modeling of high-frequency structures*. Springer Nature.

Li, W. T., Tang, H. S., Cui, C., Hei, Y. Q., & Shi, X. W. (2022). Efficient online data-driven enhanced-XGBoost method for antenna optimization. *IEEE Transactions on Antennas and Propagation*, *70*(7), 4953-4964.

Mishra, R. K. (2002). An overview of neural network methods in computational electromagnetics. *International Journal of RF and Microwave Computer-Aided Engineering*, *12*(1), 98-108.

Munk, B. A. (2005). *Frequency selective surfaces: theory and design*. John Wiley & Sons.

Sivasamy, R., Moorthy, B., Kanagasabai, M., Samsingh, V. R., & Alsath, M. G. N. (2017). A wideband frequency tunable FSS for electromagnetic shielding applications. *IEEE Transactions on Electromagnetic Compatibility*, *60*(1), 280-283.

Vapnik, V. (2013). *The nature of statistical learning theory*. Springer science & business media.

Wang, N., Wan, G., Ding, Q., & Ma, X. (2023). A novel dataset sampling method for deep learning-based absorption prediction of FSS absorbers. *AEU-International Journal of Electronics and Communications*, *170*, 154813.

Williams, C. K., & Rasmussen, C. E. (2006). *Gaussian processes for machine learning* (Vol. 2). MIT press Cambridge, MA.

Yerlikaya, M., & Duysak, H. (2022). Estimating the Resonance Frequency of Square Ring Frequency Selective Surfaces by Using ANN. The International Conference on Artificial Intelligence and Applied Mathematics in Engineering,

Zhang, Z., Jiang, F., Jiao, Y., & Cheng, Q. S. (2021). Low-cost surrogate modeling of antennas using two-level Gaussian process regression method. *International Journal of Numerical Modelling: Electronic Networks, Devices and Fields*, *34*(5), e2886.

Zhou, Z., Wei, Z., Ren, J., Yin, Y., Pedersen, G. F., & Shen, M. (2023). Representation learning-driven fully automated framework for the inverse design of frequency-selective surfaces. *IEEE Transactions on Microwave Theory and Techniques*, *71*(6), 2409-2421

Chapter 9

THE IMPORTANCE OF SCIENTIFIC THINKING AND CREATIVITY IN R&D

Elifcan GÖÇMEN POLAT,[1] Andaç İMAK[2],

Ceren ÜNLÜKAL[3]

1 Doç. Dr. Munzur Üniversitesi, Mühendislik Fakültesi, Endüstri Mühendisliği, Tunceli, Türkiye, ORCID: 0000-0002-0316-281X

2 Dr. Öğr. Üyesi Munzur Üniversitesi, Mühendislik Fakültesi, Elektrik-Elektronik Mühendisliği, Tunceli, Türkiye, ORCID: 0000-0002-3654-040X

3 Arş. Gör. Dr. Munzur Üniversitesi, Mühendislik Fakültesi, Endüstri Mühendisliği, Tunceli, Türkiye, ORCID: 0000-0001-9997-7310

1. Introduction

Scientific thinking is a critical cognitive activity that shapes the way humans think about knowing and problem-solving. The nature of scientific thinking is a philosophy of hesitant enquiry including observation, analysis, hypothesizing, testing and concluding (Popper, 1959). This method is one of the best methods to stimulate creativity and evolution in scientific researches as well as in engineering applications. In the modern world the role of scientific thinking with more and more research and development (R&D) became even more vital. R&D is not only about the generation of new knowledge, but also about converting that knowledge into economic, technological and social value through innovative applications (OECD, 2015).

It is the capacity to think in a scientific and creative way that is the biggest factor in determining the success of the R&D process. While scientific thinking offers systematic exploration and verification, creativity gives rise to new insights and novel answers. When these two themes intersect, they create the seeds of innovation and long-term advancements in technology (Amabile, l996). Therefore, the fusion of creativity and scientific thinking can add value in a lot of areas-of ranging from process improvement to product innovation, particularly in practice-oriented fields.

Scientific thinking is based on questioning assumptions, analyzing experimental data, and producing verifiable knowledge. In this sense, it reduces errors and grounds decision-making processes on rational foundations within engineering R&D activities (Kuhn, 1970). Creativity complements this process by allowing movement beyond established scientific methods, fostering alternative perspectives, and enabling the emergence of innovative solutions (Runco & Jaeger, 2012). The integration of these two capabilities forms the basis of innovation and competitive advantage in modern engineering.

In the context of engineering, scientific thinking is applied not only to the development of theoretical models but also to the continuous improvement of production, logistics, and service processes. In this regard, R&D can be defined as a systematic innovation process aimed at increasing an organization's operational efficiency, quality level, and sustainability (Drucker, 2007). Within this process, creativity plays a crucial role-particularly in problem-solving, process design, and product development stages. For example, in the design of lean manufacturing systems or artificial intelligence (AI)-assisted optimization projects, innovative thinking styles are combined with scientific analysis methods (Nonaka & Takeuchi, 1995).

The scientific approach at the core of R&D not only advances technical knowledge but also fosters an organizational culture based on learning and innovation. At this point, scientific thinking promotes data-driven decision-making, while creativity enables the generation of meaningful, applicable, and original solutions from data. Indeed, in Schumpeter's (1934) theory of innovation, the concept of "creative destruction" emphasizes that the driving force of economic growth is innovative activity nourished by scientific thinking.

The value of creative thinking in R&D is not limited to the development of new products or processes. It also manifests in reinterpreting existing knowledge, integrating different disciplines, and discovering new modes of interaction within complex systems (Florida, 2014). For instance, digital transformation and Industry 4.0 applications have emerged as a result of combining creativity with

data science, automation, and artificial intelligence technologies. These developments require engineers to integrate analytical and creative thinking skills alongside technical competence (Rosenberg, 2010).

The role of scientific thinking in the R&D process is made explicit in knowledge production and validation, while creativity is revealed through the transformation of knowledge into novel products and processes. As such, the R&D process must integrate the full cognitive toolkits of analytical thinking and conceptual exploration. Here, engineering education and R&D organizations should give individuals the opportunity to learn scientific methods and thinking, while developing a creative thinking mind-set (Goffin & Mitchell, 2017).

Scientific thinking and creative thinking are two sides of a coin in the R&D process. Scientific methods enable us to be certain that the knowledge we produce is true, while creativity is what enable us to do new things with that knowledge. The synergy between these two skills in such fields as engineering facilitates not only technological advances, but also economic growth, sustainability and social well-being. Hence, the harmonious blend of scientific thinking and creativity in R&D is a requisite for long-term excellence in academic as well as in industrial arena.

2. Scientific Research Methodologies and R&D Processes

Scientific research is the fundamental tool for the systematic production of knowledge. Designed to explain, understand, or predict a phenomenon, this process encompasses the stages of observation, hypothesis formulation, data collection, analysis, and drawing conclusions (Creswell, 2014). The methodology of scientific research enables the researcher to systematically answer not only the question of "what" but also "how" and "why." This method forms the structural foundation of R&D processes as well. This is because R&D, by its very nature, represents an applied extension of the scientific method-integrating theory and practice to produce innovative solutions (Godin, 2019).

2.1. Definition and Stages of Scientific Research

Scientific research is an objective and systematic process. Its primary purpose is to expand existing knowledge or generate new knowledge. Although this process may vary across disciplines, it generally consists of the following stages (Neuman, 2014):

1. **Problem Definition:** This forms the starting point of the research. Clearly defining the problem determines the direction of the study.
2. **Literature Review:** Evaluating the existing body of knowledge reveals the level of originality and innovation of the research.
3. **Hypothesis Formation and Modeling:** The researcher builds hypotheses, which are testable assertions about relationships between phenomena.
4. **Data Collection and Analysis:** Data resulting from such application of the techniques are subjected to analysis for the purpose of accepting or rejecting the prior hypotheses.
5. **Interpretation of Results:** The process of contrasting results with prior research enhances the capacity to generate new knowledge

These stages constitute the building blocks of a scientifically grounded innovation approach within R&D processes. Particularly in engineering, the accurate design of research methodology minimizes errors in experimental design, modeling, and simulation processes (Montgomery, 2017).

2.2. Conceptual Structure of R&D Processes

R&D is the term used to describe the inventive or systematic work or endeavor which is conducted on a firm basis with the objective of gaining new knowledge or understanding, as well as applying such knowledge in developing new products (OECD, 2015). Moreover, the process of R&D includes the use and also refinement of existing procedures or products, not only the development of new ones. In this context, the R&D process can be characterized by means of three basic phases:

1. **Research:** Activity of producing new knowledge by means of theoretical or experimental work. Basic research is motivated by the desire to understand the relations among natural phenomena according to scientific principles.
2. **Discovery:** That stage which allows research results to be transformed into a product. In this stage ideas are "fought out" and prototypes are created.
3. **Development:** The structured exploitation and the conversion of knowledge into meaningful products, processes or technologies (Trott, 2021).

This triadic cycle defines the dynamic nature of R&D. The success of the process depends not only on the rigorous application of scientific methods but also on the integration of creativity and experimental flexibility into the process (Tidd & Bessant, 2018).

2.3. The Interaction Between the Scientific Method and R&D

The scientific method lies at the core of R&D. Particularly in the fields of engineering and technology development, the scientific method plays a critical role in problem definition, experimental design, and the generalization of results (Bell, 2022). The effectiveness of R&D depends on the ability to integrate the systematic approach of the scientific method with creative thinking. In this context, the scientific method supports analytical reasoning in stages such as causal analysis, hypothesis testing, and experimental validation, while the creative nature of R&D transforms this knowledge into innovative solutions.

2.4. Data Collection, Analysis, and Validation Methods

In R&D processes, data constitutes the most fundamental input for decision-making. The data collection techniques used in scientific research-such as surveys, observation, experimental measurement, and big data analytics-are also employed in R&D activities. Especially in the context of Industry 4.0, sensor data, real-time production line information, and AI-driven analytics are redefining R&D processes (Lee et al., 2015).

Scientific verification provides reproducibility as well as reliability of results. In R&D type of projects, validation is commonly performed by testing prototypes, by verification of models, and by analysis of performance. In these phases, quantitative (e.g., descriptive and inferential statistics, regression, analysis of variance) and qualitative (e.g., user's feedback, expert opinions) approaches have been considered as complementary in conducting phases (Hair et al., 2021).

2.5. The Importance of Scientific Methodology in R&D Processes

Scientific methods are essential in R&D projects to control uncertainty and to confirm orderly progression. Risk and uncertainty are part of any new product development activity (Cooper, 2011). Scientific techniques convert these uncertainties into parameters that can be measured and made manageable. Furthermore, due to the systematic approach of the scientific method, the objectivity, repeatability and validity of project results are guaranteed.

In this sense, the R&D process is successful not simply by having a wild hair creative idea at its core, but also by nurturing that idea in scientifically attended ways. Therefore, modern R&D centers aim to optimize both scientific and creative capacities by bringing together interdisciplinary research teams (Chesbrough, 2020).

2.6. The Dynamic Structure of the Research-Discovery-Development Cycle

Research R&D is not a linear process but is iterative and feedback driven. The knowledge gained in the research stage is verified in the development stage; the results of these verifications, in turn, give rise to new research problems (Rothwell, 1994). Hence, R&D follows a path of continuous learning and renewal. This dynamic arrangement has come to define contemporary innovation systems.

This cycle is largely replicated in university-industry relations. Theoretical foundations are reinforced by academic research, and the practical worth of that knowledge is proven in industrial applications. As such, the flow of knowledge within R&D networks is two ways: science informs practice, and practice informs science (Etzkowitz & Leydesdorff, 2000).

3. The Role of Creativity in R&D Processes

Creativity is the fundamental driving force behind scientific progress and technological innovation. R&D activities do not rely solely on systematic data analysis and experimental validation processes; they also require the ability to think innovatively, develop different perspectives, and combine existing knowledge in new ways. In this context, creativity serves as both the starting point and the sustaining element of R&D (Amabile, 1996).

3.1. Conceptual Foundations of Creativity

Creativity is broadly defined as “the capability to come up with ideas that are both new and appropriate” (Sternberg & Lubart, 1999). This definition includes both the creation of original ideas on an individual basis and the application of ideas. In terms of R&D processes, creativity can be found at two levels:

1. **Individual Creativity:** The extent to which the scientist or engineer can invent new ideas, think intuitively, and solve problems.
2. **Organizational Creativity:** The organizational culture and structure that encourages creative thinking, supports risk taking, and facilitates cross-disciplinary communication is (Woodman et al., 1993).

Together, these two levels are mutually supportive. The effectiveness of creative individuals depends on organizational structures that nurture and support their innovation potential. Therefore, modern R&D centers develop flexible organizational models that integrate individual creativity into systematic innovation processes (Anderson et al., 2014).

3.2. The Relationship Between Creativity and Scientific Thinking

Science is a way of thinking about and producing objective, systematic and verifiable knowledge. Creativity, on the other hand, is based on intuition, imagination and different ways of seeing things. At a glance, these two ideas may appear at odds with each other, but in practice they work together. Scientific inquiry is facilitated not simply by following accepted paradigms, but also by questioning and going beyond them (Kuhn, 1970).

Scientific creativity emerges through the ability to define a problem differently, move beyond conventional methods, and recognize unexpected relationships (Feist, 1998). For example, Henry Ford's design of the assembly line system was rooted not only in engineering efficiency but also in a creative reframing approach. Similarly, the simulation and optimization techniques used in modern engineering represent concrete examples of how creative thinking can be harmonized with the scientific method.

3.3. The Function of Creativity in R&D Processes

By its very nature, R&D involves uncertainty, complexity, and risk. In this context, creativity is defined as the ability to see new possibilities, to come up with alternative solutions and to learn from mistakes (Runco & Jaeger, 2012). The following statement best describes the impact of creativity on the different phases of the R&D process:

- **In the Research Stage:** Creativity is required to form new hypotheses and identify voids in literature.
- **In the Discovery Stage:** Creativity combinations arise as different technological solutions are tested, prototypes designed and new processes evaluated.
- **In the Development Stage:** During the optimization of products or processes, innovative solutions must be produced under technical constraints.

Thus, creativity functions not only as a driver of idea generation but also as a dynamic force throughout all stages of R&D (Dyer et al., 2011).

3.4. Applications for Creativity in Engineering

The thinking analogue of engineering is the thinking that takes place when an engineer is engaged in his or her work. Engineering creativity is more than just coming up with original ideas; it is the integration of scientific knowledge, structured problem-solving, and technical solutions to achieve a practical outcome (Cross, 2008). Nowadays, idea generation engineering has been considered as an essential ingredient in aiding engineers to devise sustainable, cost effective and user-friendly solutions for intricate problems.

Engineering branches each have their own application of creativity:

- **Mechanical and Manufacturing Engineering:** Creativity is essential when altering manufacturing procedures, automating manufacturing processes, and working on eye and hand movement. Methodologies such as Lean Manufacturing and Six Sigma promote the use of innovative practices to minimize waste and enhance quality (Liker, 2004).
- **Electrical and Electronic Engineering:** Activities such as circuit design and embedded system development, energy efficiency and security can be approached with inventive methods that produce state-of-the-art solutions both in hardware and software. A good example of engineering imagination is in the conception of combined systems in renewable energy technologies (Kalogirou, 2014).
- **Software and Computer Engineering:** Creativity in software engineering is essential with respect to algorithm design, user experience (UX) design, and the construction of artificial intelligence-based systems. "Design Thinking" and "Agile" processes make it possible to have innovative ideas systematically tested and refined through the software development cycle (Brown, 2009).
- **Civil Engineering and Architecture:** In these spheres, creativity can be understood as a compromise between beauty, usability and viability. New and innovative building materials, environmentally friendly architectural designs and energy-saving structural techniques are but a few examples that illustrate how engineering creativity is applied in (Kibert, 2016).
- **Industrial and Systems Engineering:** Creative problem-solving is also key in the process optimization, production planning, supply chain management, and analysis based on simulation. For instance, the development of alternative scenarios and the modification of model parameters in simulation-based design constitute direct applications of engineering creativity (Banks et al., 2010).

3.4.1. Creative Problem-Solving and Design Processes

In engineering, creativity lies at the heart of the design process. This process typically consists of the following stages:

1. **Problem Definition:** The engineer identifies which aspects of a system or product can be improved.
2. **Generation of Alternatives:** Various solution approaches are developed through techniques such as brainstorming, morphological analysis, or TRIZ.
3. **Modeling the Solution:** Candidate solutions are evaluated via mathematical models, simulation, or CAD tools.
4. **Prototyping and Evaluation:** The technical and business viability of the innovative solution is evaluated.
5. **Continuous Improvement:** The design cycle is repeated in subsequent design activities based on the feedback obtained.

This cycle demonstrates that creative thinking can be systematically applied in engineering (Dym et al., 2005). In particular, the *Design Thinking* approach promotes creativity in engineering education by introducing a user-centered perspective into problem-solving processes.

3.4.2. Digital Technologies and Creativity

Digital transformation, including forced cloud adoption, has also changed what it means to be creative in engineering. Artificial intelligence (AI), generative design, augmented reality (AR), and 3D printing technology allow engineers to create solutions that are faster, more complex, and more original (Bogue, 2013). For instance, generative design algorithms can consider engineering constraints and suggest thousands of different alternative design solutions, become an "artificial creative partner" that complements and augments human ingenuity.

3.4.3. The Importance of Creativity in Engineering Education

Creativity is considered a key aspect of professional practice and a core aim within engineering education. Engineering students should be taught to think analytically and creatively. Thus, a number of universities have begun to offer courses like creative problem-solving, design thinking and innovation management as part of the regular curriculum (Sheppard et al, 2009). This perspective seeks to equip future engineers to address complex issues, challenging them to think both multidimensionally and creatively.

4. Problem-Solving Approaches and Creativity Techniques

Success in R&D depends on the ability to combine the discipline of the scientific method with creative techniques. In this context, the problem-solving approaches and creativity techniques discussed below provide practical tools for the systematic application of innovative thinking in engineering.

4.1. The Scientific and Creative Nature of Problem-Solving

Solution generation is the central knowledge activity in all disciplines and is present in, for example, engineering and social sciences. Essentially, process addressing is about changing the difference between the actual state and the goal state to reach a goal (Newell & Simon, 1972). This process requires not only analytical but also creative thinking.

Creative problem-solving seeks to go beyond traditional methods by generating original, applicable, and innovative ideas (Isaksen & Treffinger, 2004). This approach is particularly effective in R&D contexts characterized by high uncertainty, where conventional methods often fall short in producing novel solutions.

4.2. The Scientific Approach to Problem-Solving

Scientific problem-solving involves systematic data collection, hypothesis formulation, and verification processes. This approach typically consists of the following stages (Polya, 1957):

1. Understanding the problem
2. Developing a solution strategy
3. Implementing the strategy
4. Evaluating the result

This method can be applied in various R&D areas such as prototype design, process optimization, or product development. The strength of the scientific approach lies in its ability to ensure that solutions are reproducible and verifiable. However, given the inherently exploratory nature of R&D, not all problems can be solved solely through measurable data-this is where creative techniques become essential.

4.3. Creativity-Based Problem-Solving Techniques

The next section reviews a number of basic creative problem-solving methods used extensively in scientific and engineering applications.

4.3.1. Brainstorming

Originating from engineering and later expanded into business and management, brainstorming is one of the most widely known group creativity techniques due to Osborn's (1953) initial work. Participants can share as many ideas as they like without being criticized; these ideas will be assessed according to their value, and the most applicable ones will be selected. In R&D projects, brainstorming is particularly used during the concept development phase. The integration of experts from different domains of knowledge allows the fusion of multiple viewpoints (Paulus & Nijstad, 2003).

4.3.2. TRIZ

TRIZ (Theory of Inventive Problem-Solving) was created by the Soviet inventor and science fiction writer Genrich Altshuller in 1946. On analysis of more than 200,000 patents, the technique offers a generalizable method to solve technical problems (Altshuller, 1984). Main goal of TRIZ is to resolve engineering contradictions and generate innovative ideas in a structured manner. The approach is built upon 40 inventive principles and 39 engineering parameters. For example, principles such as the “use of counteraction” (Principle 13) or “segmentation” (Principle 1) are applied to develop original solutions in complex systems (Mann, 2007).

4.3.3. Design Thinking

Design Thinking is portrayed as the human condition for innovation (Brown, 2009). The methodology has five phases: empathize, define, ideate, prototype, and test (d.school, Stanford, 2010). This model treats creativity not merely as an aesthetic pursuit but as a structured way of generating functional solutions. In R&D teams it is especially prevalent in product development and user-experience design. Design Thinking encourages innovation and at the same time reduces the associated risks as ideas are quickly tested and evolved through iterative feedback (Liedtka, 2015).

4.3.4. SCAMPER Technique

The SCAMPER method was created by Bob Eberle based on Alex Osborn’s process of generating ideas (Eberle, 1971). The acronym stands for the following steps:

- **S (Substitute)**
- **C (Combine)**

- **A (Adapt)**
- **M (Modify)**
- **P (Put to another use)**
- **E (Eliminate)**
- **R (Reverse)**

Substitute, Combine, Adapt, Modify, Put to other uses, Eliminate and Reverse (SCAMPER) is a great tool for reimagining the engineering design of an existing product or process. It is particularly popular in the field of industrial design and product redesign, for which the systematized variation of ideas serves as a stimulus for innovation.

4.3.5. Morphological Analysis

Developed by Fritz Zwicky, morphological analysis enables the systematic exploration of multidimensional solution spaces for complex problems (Zwicky, 1969). In this method, the parameters of a problem and their possible values are defined, and then all potential combinations are analyzed. For example, in designing a new vehicle, variables such as energy source, material type, and aerodynamic structure can be combined to generate hundreds of alternative design options. In this sense, morphological analysis supports the quantitative diversification of ideas in R&D processes.

4.4. Integration of Systematic and Creative Approaches

Success in R&D processes depends not only on the generation of creative ideas but also on their integration with scientific methods. In this context, the analytical and creative components of problem-solving approaches must be balanced (Basadur, 1994).

For example:

- Brainstorming is effective at promoting the diversity of ideas,
- TRIZ solves technical contradictions in systems,
- Design Thinking considers user needs,
- Morphological analysis ensures systematic variation.

The combined use of these instruments reinforces the cyclical process of innovation and the effectiveness of R&D (Tidd & Bessant, 2018).

5. Conclusion

Scientific thinking and creativity, being the two essential pillars of engineering and R&D processes, serve as the keystone in the formation of new conceptually innovative solutions and technological progression. These two aspects/ideas when considered integrated together lead to the creation of new knowledge can be applied that is practical in nature, sustainable over a period of time and socially positive.

By rational exploitation of the principles of systematic dissection, empirical validation, and critical examination, scientific thinking also supports engineering problem-solving. Creativity has to

do with how this can be made innovatively or originally, creating new ideas outside the traditional box. The apportionate blend of these two philosophies in R&D work acts as a catalyst to allow the diversified and ever-changing engineering disciplines within an organization to continuously evolve and the organization itself to learn at an accelerating rate.

Modern engineering practice demands not only knowledge of technology but a multi-disciplinary, innovative thinking attitude that could conform to rapidly changing situations. In this context project management, innovation strategies and problem-solving techniques are fundamental in the success of the R&D process. Particularly, open innovation, digital transformation, and sustainable engineering methodologies are defining the future scope of R&D. To conclude, the interplay of scientific thinking, creativity, and strategic R&D management turns engineering which is concerned normally with production and improvement into knowledge, innovation and value generating discipline. Institutionalizing this view at the organizational level is the most effective lever by which to effect work in sustainable performance and competitive advantage in the academic as well as the industrial setting.

References

Altshuller, G. S. (1984). *Creativity as an exact science: The theory of the solution of inventive problems*. CRC Press.

Amabile, T. M. (1996). *Creativity in context: Update to the social psychology of creativity*. Routledge.

Anderson, N., Potočnik, K., & Zhou, J. (2014). Innovation and creativity in organizations: A state-of-the-science review. *Journal of Management, 40*(5), 1297–1333.

Banks, J., Carson, J. S., Nelson, B. L., & Nicol, D. M. (2010). *Discrete-event system simulation* (5th ed.). Pearson Education, New Delhi.

Basadur, M. (1994). *Simplex: A flight to creativity*. Creative Education Foundation.

Bell, J. (2022). *Doing your research project*. McGraw-Hill Education.

Bogue, R. (2013). 3D printing: the dawn of a new era in manufacturing?. *Assembly Automation, 33*(4), 307–311.

Brown, T. (2009). *Change by design: How design thinking transforms organizations and inspires innovation*. Harper Collins.

Chesbrough, H. (2020). *Open innovation results: Going beyond the hype and getting down to business*. Oxford University Press.

Cooper, R. G. (2011). *Winning at new products: Creating value through innovation*. Basic Books.

Creswell, J. W. (2014). *Research design: Qualitative, quantitative, and mixed methods approaches*. Sage.

Cross, N. (2008). *Engineering design methods: Strategies for product design*. Wiley.

d.school, Stanford University. (2010). *An introduction to design thinking: Process guide*. Stanford University.

Drucker, P. F. (2007). *Innovation and entrepreneurship*. Routledge.

Dyer, J., Gregersen, H., & Christensen, C. M. (2011). *The innovator's DNA: Mastering the five skills of disruptive innovators*. Harvard Business Press.

Dym, C. L., Agogino, A. M., Eris, O., Frey, D. D., & Leifer, L. J. (2005). Engineering design thinking, teaching, and learning. *Journal of Engineering Education, 94*(1), 103–120.

Eberle, B. (1971). *SCAMPER: Games for imagination development*. D.O.K. Publishers.

Etzkowitz, H., & Leydesdorff, L. (2000). The dynamics of innovation: From National Systems and "Mode 2" to a Triple Helix of university–industry–government relations. *Research Policy, 29*(2), 109–123.

Feist, G. J. (1998). A meta-analysis of personality in scientific and artistic creativity. *Personality and Social Psychology Review, 2*(4), 290–309.

Florida, R. (2014). *The rise of the creative class–revisited*. Basic Books.

Goffin, K., & Mitchell, R. (2017). *Innovation management: Effective strategy and implementation*. Palgrave Macmillan.

Godin, B. (2019). *The invention of technological innovation: Languages, discourses and ideology in historical perspective*. Edward Elgar.

Hair, J. F., Black, W. C., Babin, B. J., & Anderson, R. E. (2021). *Multivariate data analysis*. Pearson.

Isaksen, S. G., & Treffinger, D. J. (2004). *Celebrating 50 years of reflective practice: Versions of creative problem solving*. *The Journal of Creative Behavior, 38*(2), 75–101.

Kalogirou, S. A. (2014). *Solar energy engineering: Processes and systems* (2nd ed.). Academic Press.

Kibert, C. J. (2016). *Sustainable construction: Green building design and delivery* (4th ed.). Wiley.

Kuhn, T. S. (1970). *The structure of scientific revolutions*. University of Chicago Press.

Lee, J., Bagheri, B., & Kao, H. A. (2015). A cyber-physical systems architecture for Industry 4.0-based manufacturing systems. *Manufacturing Letters, 3*, 18–23.

Liedtka, J. (2015). Perspective: Linking design thinking with innovation outcomes through cognitive bias reduction. *Journal of Product Innovation Management, 32*(6), 925–938.

Liker, J. K. (2004). *The Toyota way: 14 management principles from the world's greatest manufacturer*. McGraw-Hill.

Mann, D. (2007). *Hands-on systematic innovation*. CREAX Press.

Montgomery, D. C. (2017). *Design and analysis of experiments*. Wiley.

Neuman, W. L. (2014). *Social research methods: Qualitative and quantitative approaches*. Pearson.

Newell, A., & Simon, H. A. (1972). *Human problem solving*. Prentice Hall.

Nonaka, I., & Takeuchi, H. (1995). *The knowledge-creating company*. Oxford University Press.

OECD. (2015). *Frascati Manual 2015: Guidelines for collecting and reporting data on research and experimental development*. OECD Publishing.

Paulus, P. B., & Nijstad, B. A. (2003). *Group creativity: Innovation through collaboration*. Oxford University Press.

Polya, G. (1957). *How to solve it: A new aspect of mathematical method*. Princeton University Press.

Popper, K. (1959). *The logic of scientific discovery*. Hutchinson.

Rosenberg, N. (2010). *Inside the black box: Technology and economics*. Cambridge University Press.

Rothwell, R. (1994). Towards the fifth-generation innovation process. *International Marketing Review, 11*(1), 7–31.

Runco, M. A., & Jaeger, G. J. (2012). The standard definition of creativity. *Creativity Research Journal, 24*(1), 92–96.

Schumpeter, J. A. (1934). *The theory of economic development*. Harvard University Press.

Sheppard, S. D., Macatangay, K., Colby, A., & Sullivan, W. M. (2009). *Educating engineers: Designing for the future of the field*. Jossey-Bass.

Sternberg, R. J., & Lubart, T. I. (1999). The concept of creativity: Prospects and paradigms. In R. J. Sternberg (Ed.), *Handbook of creativity* (pp. 3–15). Cambridge University Press.

Tidd, J., & Bessant, J. (2018). *Managing innovation: Integrating technological, market and organizational change*. Wiley.

Trott, P. (2021). *Innovation management and new product development*. Pearson.

Woodman, R. W., Sawyer, J. E., & Griffin, R. W. (1993). Toward a theory of organizational creativity. *Academy of Management Review, 18*(2), 293–321.

Zwicky, F. (1969). *Discovery, invention, research through the morphological approach*. Macmillan.

Chapter 10

ARTIFICIAL INTELLIGENCE-BASED DIGITAL TWIN APPROACHES FOR STRUCTURAL HEALTH MONITORING AND PREDICTIVE MAINTENANCE IN WIND TURBINES

Umut Saray[1]

1 Department of Electronic Automation, Turhal Vocational School, Tokat Gaziosmanpaşa University, Tokat, Türkiye,(umutsaray@gmail.com) (ORCID: 0000-0003-3339-6876)

1. Introduction

Wind energy has established a strong position among "clean and domestic" options in the energy transition; however, the real-world operation of wind turbines is far from being as smooth as theoretical models suggest (Lüy & Saray, 2012). A wind turbine operates like a complex organism composed of interconnected subsystems, including blades, tower, gearbox/generator, bearings, power electronics, pitch–yaw systems, and control software. The primary challenge faced by this organism is continuity: unplanned downtime, production losses, high maintenance costs, and, in some cases, cascading failures triggered by a single fault.

In recent years, image processing and deep learning–based approaches for damage detection and condition monitoring of wind turbines have gained significant momentum in the literature. Particularly for the detection of blade surface damages—such as cracks, erosion, and delamination marks—a broad toolbox has emerged, ranging from classical digital image processing techniques to modern object detection networks. For instance, studies adopting digital image processing–based approaches for blade defect detection (Deng, Guo, & Chai, 2021), as well as improved YOLO-based models capable of identifying surface damage even in low-quality UAV images (Liao et al., 2024), stand out as practical, easily deployable "see-and-detect" solutions in real-world applications. These approaches are highly effective for rapid field inspection and operational decision support; however, they often fall short in fully addressing critical questions such as "why did the damage occur?", "how fast will it propagate?", and "when will it lead to system shutdown?"

At this point, the concept of the digital twin comes into play. In its simplest form, a digital twin is a virtual counterpart of a physical asset—such as a turbine, a subcomponent, or an entire wind farm—that lives in a digital environment and is continuously updated with real-world data. The key nuance here is that a digital twin is not a static simulation model; rather, it is a dynamic framework that is fed by sensor and data streams, continuously calibrated, capable of self-correction, and able to establish a bidirectional interaction with the physical system. Efforts toward standardization of the digital twin concept have also emerged in industry. For example, ISO has published the ISO 23247 series, which defines a digital twin framework for manufacturing systems (ISO, 2021). Studies analyzing this standard enable a more systematic understanding of the conceptual components of digital twins, such as physical assets, data connections, models, and service layers (Shao, Frechette, & Srinivasan, 2023). In the context of wind energy, digital twins aim to integrate rich field data—including SCADA, vibration, temperature, oil analysis, power electronics measurements, meteorological data, and even lidar—with physics-based models and artificial intelligence techniques, thereby bringing real-time monitoring, predictive maintenance, and optimization together under a unified framework (De Kooning et al., 2021).

1.1. Why an "AI-Supported" Digital Twin?

The idea of a digital twin can, in theory, be established based solely on physics-based models. However, in systems such as wind turbines that operate under variable environmental conditions, experience continuously fluctuating load spectra, and exhibit a wide variety of failure modes, a purely physics-based approach can be limited in practice. This is because:

- Models that represent each component with high accuracy result in high computational cost.

- Missing data, noise, and measurement uncertainty in field data are inevitable.
- Failure data are often imbalanced (rare failures), and labeled data are limited.

Component aging and site-specific characteristics (turbine model, site topography, wind regime) further challenge generalization.

For this reason, the current trend is to construct digital twins in a hybrid manner, where physics + data + artificial intelligence are combined within the same framework. For example, hybrid digital twin approaches that train physics-based models of wind turbine drivetrain systems using operational data and address practical issues such as synthetic data generation for fault scenarios are clearly observed in the literature (Pujana et al., 2023). Similarly, in critical problems such as main bearing fatigue, physics-informed digital twin approaches that also account for uncertainties aim to mitigate some of the weaknesses of purely "black-box" models (Yucesan & Viana, 2023).

An even more interesting example is provided by studies that aim to transfer the flow field to the digital twin at the wind farm scale rather than focusing on a single turbine. Digital twin approaches that combine lidar measurements, Navier–Stokes equations, and turbine modeling through physics-informed neural networks aim to estimate the wind field over the entire site as a "full-field" representation, opening a powerful pathway for farm-level control and load assessment (Zhang & Zhao, 2023). As the scale increases, the digital twin moves beyond being merely a "maintenance tool" and transforms into a decision-support layer that extends to planning, control, and grid integration decisions.

1.2. Data Backbone of the Wind Turbine Digital Twin

In the world of wind turbines, data is the "blood" of the digital twin. In practice, the most common data sources include:

- SCADA data: Power output, wind speed, rotor speed, temperatures, yaw/pitch angles, alarm codes, etc. SCADA data provide broad coverage but are often characterized by low sampling rates.
- Condition monitoring system (CMS) sensors: Vibration, acoustic emission, bearing/gearbox measurements, oil debris analysis, etc. These data sources typically operate at higher frequencies and can be more sensitive to fault-related signals.
- Image/UAV data: Highly effective for visual faults such as blade surface damage; image processing and deep learning solutions can produce results that are close to real field conditions (Deng et al., 2021; Liao et al., 2024).
- Remote sensing and lidar: Provide valuable information for flow field characterization, wake effects, turbine-to-turbine interactions, and wind farm optimization (Zhang & Zhao, 2023).

Each of these data sources has value on its own; however, the digital twin concept gains real meaning only to the extent that they can be interpreted together. For example, image-based damage detection can state "the damage has been observed," whereas a digital twin aims to relate the same damage to load history, wind regime, operating modes, and vibration signatures, and to infer that "this damage may be growing through a specific mechanism and the risk may increase within a certain time window." This represents a direct and practical difference that significantly affects maintenance planning in the field.

1.3. Target Outputs of the Digital Twin

The outputs most frequently targeted by AI-supported digital twins in wind energy can be grouped under three main categories:

- Monitoring: “What is happening right now?” Alarm levels, anomaly detection, and component health indicators.
- Prognostics: “Where is it heading?” Remaining useful life (RUL), failure probability, and uncertainty bounds (Yucesan & Viana, 2023).
- Optimization: “What should be done to improve performance?” Maintenance scheduling, production–load balance, control parameter tuning, and farm-level strategies (De Kooning et al., 2021; Zhang & Zhao, 2023).

These outputs are typically delivered not by a single model, but through a modular architecture. The review study by De Kooning et al. highlights an important perspective by stating that the balance between model accuracy and computational burden in a digital twin is determined by the “use case” (De Kooning et al., 2021). In other words, a digital twin does not always need to employ the “most accurate model”; in some cases, a model that is “sufficiently accurate and fast” for real-time field operation is more valuable.

The aim of this section is to address the concept of the digital twin in wind energy systems not merely at the level of definition, but as a practical framework strengthened by artificial intelligence. By bringing together standard and generic architectural perspectives (ISO, 2021; Shao et al., 2023) with recent wind turbine–focused literature (De Kooning et al., 2021; Leon-Medina, Tibaduiza, Parés, & Pozo, 2025), the topic will be concretized through hybrid models (Pujana et al., 2023), physics-informed approaches (Yucesan & Viana, 2023), and wind farm–scale digital twins (Zhang & Zhao, 2023). In addition, by linking the previously discussed image-based damage detection line to the digital twin domain, the integration of the “detection → diagnosis → prognostics” chain will be discussed (Deng et al., 2021; Liao et al., 2024).

In the remainder of the chapter, the following topics will be addressed in sequence: digital twin architecture and components, the data layer and data-related challenges encountered in the field, integration of AI/ML methods into digital twins (anomaly detection, remaining useful life estimation, physics-informed learning), example application patterns at the wind turbine and wind farm scales, and limitations and future research directions.

2. Digital Twin Concept and Architectural Framework

Although the concept of the digital twin has been widely used in many engineering fields in recent years, it represents a framework whose meaning may vary from one application to another. Therefore, when addressing the digital twin in the context of wind energy, it is more appropriate to consider the concept not as an abstract “digital copy,” but as a multi-layered and evolving structure that continuously exchanges data with the physical system. Particularly when operational objectives such as maintenance, monitoring, and prognostics are concerned, the way the digital twin is structured becomes at least as critical as the artificial intelligence model employed (De Kooning et al., 2021).

2.1. Fundamental Definition of the Digital Twin

In its most general definition, a digital twin refers to the representation of a physical asset (such as a wind turbine or a specific component of a turbine) in a virtual environment, the continuous updating of this representation with data obtained from the field, and the use of the resulting outputs to better understand or guide the physical system. The key point here is that a digital twin is not a static simulation model. Changes occurring in the physical system, measurements, and environmental effects are transferred to the digital twin, and the results obtained within the digital twin are fed back to the physical system for maintenance, control, or operational decision-making.

This bidirectional interaction distinguishes the digital twin from classical modeling approaches. The ISO 23247 standard addresses the digital twin within this context and provides a framework that encompasses data connections, model layers, and service components (ISO, 2021). The core approach of the standard is to define the digital twin not merely as a software model, but as an ecosystem in which data, models, and decision-making mechanisms operate together. This framework is particularly important for reducing conceptual ambiguity in complex industrial systems (Shao, Frechette, & Srinivasan, 2023).

2.2. Why Is a Digital Twin Challenging for Wind Turbines?

Wind turbines are systems that are as attractive as they are challenging for digital twin applications. The main reasons for this challenge can be summarized under several points. First, turbines operate in highly variable environments. Sudden changes in wind speed, turbulence, wake effects, and environmental conditions (temperature, humidity, icing) directly affect both mechanical loads and electrical behavior. Second, although turbine components are designed for long service life, failures typically develop gradually and in a hidden manner. This makes early-stage fault detection difficult.

The third and perhaps most critical issue is the nature of the data obtained from the field. Although SCADA data provide broad coverage, they are often characterized by low sampling rates; high-frequency vibration data, on the other hand, are richer but involve large data volumes and high processing costs. Image-based inspections are generally periodic and do not provide continuous monitoring (Deng et al., 2021; Liao et al., 2024). This heterogeneous data structure renders the construction of a digital twin based on a single data source impractical.

For this reason, digital twins for wind turbines are often designed with a multi-layered and modular architecture. De Kooning et al. (2021), in their review of the literature, emphasize that there is an inevitable trade-off between model accuracy and computational burden, and that this balance must be consciously established according to the intended use case of the digital twin. In other words, a digital twin does not always have to be the “most detailed model”; field operability is often the determining factor.

2.3. Digital Twin Architecture: A Layered Perspective

Wind turbine digital twins are generally addressed through three main layers: the data layer, the model layer, and the service (application) layer. This separation both facilitates understanding of the system and clarifies where and how artificial intelligence components should be integrated (ISO, 2021; Shao et al., 2023).

2.3.1. Data Layer

The data layer forms the foundation of the digital twin. This layer contains all measurements obtained from the physical system. For wind turbines, these data typically consist of SCADA data, condition monitoring sensors, image/UAV records, and environmental measurements. The primary challenge here is not only data acquisition, but also practical issues such as time synchronization, missing data management, and handling noise.

For example, associating image-based damage detected on a blade surface with wind conditions and load history from the same time interval increases the value of the digital twin. Otherwise, image data cannot go beyond providing simple "damage present/absent" information (Liao et al., 2024). For this reason, the data layer is not only the entry point of the digital twin, but also its most fragile component.

2.3.2. Model Layer

The model layer can be considered the "brain" of the digital twin. This layer includes physics-based models, data-driven models, and hybrid approaches operating together. For wind turbines, these models cover subdomains such as aerodynamics, structural dynamics, drivetrain behavior, and control logic.

In recent years, hybrid digital twins have emerged as a prominent trend in the literature. For example, a physics-based model of the drivetrain can be trained together with operational data to provide a structure that is both realistic and computationally manageable (Pujana et al., 2023). Similarly, for long-term problems such as main bearing fatigue, physics-informed artificial intelligence approaches enable more reliable predictions by explicitly accounting for uncertainties (Yucesan & Viana, 2023).

The key point to note here is that the model layer is not a singular structure. In most applications, different sub-models operate together for different purposes. Functions such as damage detection, condition monitoring, and remaining useful life estimation can be represented by different models within the same digital twin.

2.3.3. Service and Application Layer

The service layer is the part where the outputs of the digital twin are delivered to users and operational systems. This layer includes decision-support dashboards, alarm systems, maintenance planning tools, and reporting mechanisms. Whether a digital twin truly generates value in the field is often determined at this layer.

For example, a digital twin may predict an increasing failure probability for a specific component; however, if this information does not reach the maintenance team in an understandable and timely manner, its practical impact remains limited. As emphasized by De Kooning et al. (2021), the success of a digital twin should be measured not only by model accuracy, but also by its integration into decision-making processes.

2.4. Scope of the Digital Twin: Component-Level or System-Level?

In wind energy applications, digital twins can be addressed at different scales. At the narrowest scope, a digital twin can be developed for a single component (for example, a gearbox or a main bearing).

This approach is particularly common for high-cost and critical components (Yucesan & Viana, 2023). At a broader scope, system-level digital twins representing the entire turbine can be developed.

Another notable trend in recent years is the development of digital twins at the wind farm scale. In this approach, interactions between turbines, wake effects, and the overall flow structure across the site are taken into account. Studies that transfer these interactions into the digital twin using physics-based deep learning open a new window for farm optimization and load management (Zhang & Zhao, 2023). However, as the scale increases, data management and computational cost also increase significantly, further emphasizing the importance of architectural design.

In summary, the concept of a digital twin for wind turbines should be considered as a layered structure in which data, physics, and artificial intelligence operate together, rather than as a single model. If the architecture is not properly designed, even the most advanced artificial intelligence model may fail to deliver the expected contribution in real-world applications. Therefore, digital twin design should begin with the question "which problem are we trying to solve?", and data sources, model complexity, and the service layer should be shaped in line with this objective.

3. Artificial Intelligence–Based Digital Twin Systems

The ability of the digital twin approach to generate practical value in wind energy applications is largely related to how artificial intelligence methods are integrated into this structure. Although the digital twin provides a strong conceptual framework when considered on its own, transforming the complex and high-volume data obtained from the field into meaningful information often requires going beyond traditional modeling approaches. At this point, artificial intelligence emerges as the "interpretive" and "predictive" layer of the digital twin.

In the literature, the relationship between digital twins and artificial intelligence is generally defined through a hybrid structure in which data-driven learning, physics-based knowledge, and decision-support mechanisms are jointly considered (Tao et al., 2019; Tao, Qi, Liu, & Kusiak, 2018). For complex and variable systems such as wind turbines, this hybrid approach provides a decisive advantage in terms of both model accuracy and field applicability.

3.1. Role of Artificial Intelligence in the Digital Twin

Artificial intelligence can be positioned in different roles within the digital twin architecture. At the most basic level, it is used for processing large volumes of data and extracting patterns. However, in practical applications, this role is often extended further. Artificial intelligence becomes not only a component that "interprets data," but also one that predicts the future behavior of the system and provides inputs to decision-making processes.

For example, fault diagnosis and condition monitoring problems in wind turbines have long been areas where machine learning and deep learning methods are extensively applied. Numerous studies have shown that deep learning–based approaches achieve higher performance than traditional methods for mechanical problems such as gearbox or bearing failures (Wang, Chen, & Lu, 2023). In the context of a digital twin, such models continuously update the digital representation by interpreting real-time data obtained from the physical system.

A critical point here is that the artificial intelligence model should not operate as an independent black box within the digital twin. Otherwise, the digital twin may turn into a fragmented structure consisting merely of "multiple models placed side by side." Instead, artificial intelligence components should be positioned in alignment with the overall objectives of the digital twin (monitoring, prognostics, optimization).

3.2. Data-Driven Approaches: CNN, RNN, and Their Variants

In digital twins developed for wind turbines, the most common artificial intelligence approaches are data-driven models. These models offer strong performance, particularly when labeled data are available. In image-based damage detection, convolutional neural networks (CNNs) stand out, while in time-series data, recurrent neural networks (RNNs) and architectures such as LSTM and GRU are widely used.

When image data are considered, CNN-based models can be regarded as the "perception layer" of the digital twin. Blade surface data obtained from UAV images can be processed through CNN models and transferred to the digital twin in the form of damage types. This approach enables the digital twin to create a realistic representation, especially for components such as blades, where visual inspection is challenging (Deng et al., 2021; Liao et al., 2024).

For time-series data, LSTM and similar architectures are used for anomaly detection and short-term prediction by learning the historical behavior of the turbine. Such models operate on SCADA or vibration data and form the "memory" of the digital twin. However, the most important limitation of data-driven approaches is their requirement for sufficient and representative data. For rare failures and long-term fatigue processes, this can become a serious challenge.

3.3. Predictive Maintenance and Remaining Useful Life (RUL) Estimation

One of the most concrete outputs of digital twin–artificial intelligence integration is predictive maintenance applications. Classical maintenance strategies are often periodic or reactive in nature; in contrast, the digital twin approach enables maintenance decisions to be based on the actual condition of the system and its predicted future state.

In this context, Remaining Useful Life (RUL) estimation emerges as one of the core functions of digital twins. Comprehensive reviews on machine health prognostics indicate that data-driven methods are increasingly used for RUL estimation (Lei et al., 2018). Within a digital twin, RUL estimation not only answers the question "when will a failure occur?", but also directly influences operational decisions such as maintenance scheduling, spare parts planning, and minimization of production losses.

In the case of wind turbines, RUL estimation involves uncertainty due to variable load conditions and environmental effects. Therefore, digital twin–based approaches often aim to present prediction results together with uncertainty bounds. In this way, maintenance decisions can be made based not on a single predicted value, but on risk-based assessments.

3.4. Physics-Informed and Hybrid Approaches

Although data-driven artificial intelligence models are successful in many problems, using these models alone is not always sufficient for systems such as wind turbines, which are strongly constrained by physical laws. At this point, physics-informed approaches are increasingly gaining attention in the digital twin literature.

Physics-informed neural networks (PINNs) aim to reduce data requirements and improve generalization capability by incorporating physical equations as constraints into the learning process (Raissi, Perdikaris, & Karniadakis, 2019). In the context of digital twins, PINNs contribute to a more realistic representation of physical processes such as aerodynamics, structural dynamics, and fatigue. It has been shown that digital twins supported by physics-based knowledge can produce more reliable results in long-term problems such as main bearing fatigue (Yucesan & Viana, 2023).

The hybrid digital twin approach refers to a structure in which physics-based models and data-driven artificial intelligence models are used together. Hybrid digital twins developed for drivetrain systems offer significant advantages in practical problems such as synthetic fault data generation and modeling of rare failures (Pujana et al., 2023). Such approaches enhance both the explainability and field applicability of the digital twin.

Artificial intelligence is one of the fundamental components that enable digital twins to generate real value in wind energy applications. However, the role of artificial intelligence is not limited to developing “high-accuracy models.” In the context of digital twins, the key issue is which decisions artificial intelligence models support, which uncertainties they manage, and how they are integrated into field operations.

For this reason, AI-based digital twins developed for wind turbines should consider data-driven, physics-informed, and hybrid approaches together. When this balance is properly established, the digital twin becomes not only a monitoring tool, but also a decision-support system that plays an active role in maintenance, planning, and optimization processes.

4. Structural Health Monitoring (SHM) and Digital Twin Integration

Structural Health Monitoring (SHM) in wind turbines is one of the areas where the digital twin approach provides the most concrete and direct benefits. The primary objective of SHM is to monitor the condition of a structure or mechanical system over time, detect damage formation at an early stage, and interpret the progression of this damage. In long-lifespan and high-cost systems such as wind turbines, this approach is critically important not only from a safety perspective but also in terms of economic sustainability.

Traditional SHM applications are often based on a single data source or a limited group of sensors. However, such approaches may be insufficient to fully explain the origin and evolution of damage in complex systems such as wind turbines. Digital twin integration transforms SHM from a static monitoring mechanism into a time-dependent, contextual, and predictive structure (De Kooning et al., 2021).

4.1. Scope of the SHM Approach in Wind Turbines

Structural Health Monitoring (SHM) in wind turbines requires different methods for different components. Subsystems such as blades, towers, gearboxes, and main bearings differ significantly in terms of the loads they are exposed to, failure mechanisms, and measurability. For this reason, SHM applications are often addressed in a component-specific manner.

For blade structures, SHM generally focuses on surface damage and structural degradations. Image-based methods, particularly when combined with UAV-assisted inspections, are widely used in this area. Damage types such as cracks, erosion marks, and delamination can be detected using image processing and deep learning techniques (Deng et al., 2021; Liao et al., 2024). However, such detections are often instantaneous and provide limited information about the temporal evolution of the damage.

For mechanical components, sensor-based measurements such as vibration, temperature, and oil analysis become more prominent. These data are valuable for capturing internal degradations that cannot be directly observed at the early stages of damage. The digital twin approach enables a more holistic evaluation by integrating these different SHM methods under a unified framework.

4.2. Key Advantages of Digital Twin–Supported SHM

The most significant contribution of digital twin integration to SHM is its ability to analyze not only the presence of damage, but also its context. For example, damage detected on a blade surface provides limited information when evaluated in isolation. However, when this damage is considered through the digital twin together with wind conditions, load history, operating modes, and the overall condition of the turbine, it becomes far more meaningful.

In this context, the digital twin provides three main advantages for SHM:

- Temporal continuity: The initial occurrence of damage, its growth rate, and its progression toward critical thresholds can be monitored.
- Contextual analysis: Damage is evaluated not merely as a geometric defect, but as the outcome of operational and environmental conditions.
- Scenario-based assessment: The question “what happens if operation continues in this manner?” can be simulated through the digital twin.

A significant portion of digital twin approaches developed for wind energy systems in the literature aim to address SHM within these three dimensions (Leon-Medina et al., 2025; De Kooning et al., 2021).

4.3. Combined Use of Multiple Data Sources in SHM

At the point where SHM is integrated with the digital twin, data diversity plays a decisive role. Single data sources often reveal only one aspect of damage. For example, vibration data can capture mechanical degradations at an early stage; however, they provide limited information about the physical location or type of the damage. Image data, on the other hand, can clearly show the location and geometry of damage, but do not directly provide clues about load history or internal damage mechanisms.

The digital twin enhances the comprehensiveness of SHM by evaluating these data types together. Supporting image-based damage detection with sensor data contributes to the reduction of false alarms and improves the reliability of damage classification (Deng et al., 2021). This approach becomes particularly important in situations where maintenance decisions are critical.

Nevertheless, the integration of multiple data sources involves significant practical challenges. Time synchronization, data quality, missing measurements, and differing sampling rates are key issues that must be considered in the design of digital twin–based SHM systems. When these challenges cannot be addressed, the digital twin fails to deliver the expected added value for SHM applications.

4.4. Transition from SHM to Prognostics: The Role of the Digital Twin

Classical SHM applications often conclude at the "detection" stage. However, for wind turbines, the truly critical issue is understanding how the detected damage will evolve over time. The digital twin enables this transition by utilizing SHM data.

For example, an anomaly observed in a specific component can be evaluated under different load scenarios within the digital twin to analyze the damage propagation potential. This approach transforms SHM into a direct input for predictive maintenance strategies (Yucesan & Viana, 2023). Consequently, maintenance decisions can be based not only on the current condition, but also on predicted risk levels.

When considered at the wind farm scale, digital twin–supported SHM also allows turbine-to-turbine interactions to be taken into account. Wake effects and site-wide wind distribution can increase structural loads on specific turbines. Evaluating such effects together with SHM data contributes to the development of more balanced maintenance and operational strategies at the farm level (Zhang & Zhao, 2023).

Structural health monitoring is one of the strongest application areas of the digital twin approach in wind energy. Through digital twin integration, SHM moves beyond being merely a tool for damage detection and becomes a decision-support mechanism that analyzes the causes, progression, and potential consequences of damage.

The success of this transformation depends on effective management of data diversity, proper scaling of models, and meaningful transfer of the generated information into maintenance processes. When properly designed, digital twin–supported SHM directly contributes to increasing the reliability of wind turbines, reducing maintenance costs, and ensuring operational continuity.

5. Predictive Maintenance and the Digital Twin Approach

Maintenance strategies in wind turbines have a direct and decisive impact on system reliability and life-cycle costs. As discussed in previous sections, the digital twin approach enables monitoring and prognostics through a virtual representation of the physical system. Within this framework, predictive maintenance stands out as one of the application areas where the digital twin produces the most practical and measurable outputs (De Kooning et al., 2021).

Traditional maintenance approaches are often based on time-based schedules or post-failure interventions. However, in systems such as wind turbines that operate under variable loads, these

approaches may lead either to unnecessary maintenance actions or to unexpected downtime. Digital twin–supported predictive maintenance aims to shape maintenance decisions based on the current condition of the system, its historical behavior, and its predicted future state. This approach transforms maintenance activities from a reactive process into a strategic decision-making mechanism (Leon-Medina et al., 2025).

5.1. Position of Predictive Maintenance in the Context of the Digital Twin

In predictive maintenance systems, the digital twin provides more than a mere "computational engine"; it offers a reference framework that establishes the context of maintenance decisions. Sensor and operational data obtained from the physical turbine are integrated within the digital twin, allowing the system behavior to be continuously updated. In this way, maintenance decisions can be based not only on past failures, but also on risks that are likely to occur in the future.

The literature reports that digital twin–supported maintenance approaches reduce downtime by optimizing maintenance scheduling, particularly in complex energy systems (De Kooning et al., 2021). This represents a significant advantage in ensuring operational continuity in wind power plants.

5.2. Remaining Useful Life (RUL) Estimation and the Digital Twin

Remaining Useful Life (RUL) estimation, which lies at the core of predictive maintenance, refers to the prediction of the time remaining until a component falls below acceptable performance limits. In the digital twin approach, RUL estimation is not merely a statistical output, but a dynamic process associated with the physical and operational context of the system.

Especially for critical components such as gearboxes and main bearings in wind turbines, RUL estimation plays a decisive role in maintenance planning. Physics-informed (PINN) digital twin approaches can provide more reliable predictions for such components by explicitly accounting for uncertainties (Yucesan & Viana, 2023). In this way, maintenance decisions can be based not on a single predicted value, but on a risk-based assessment.

Classical studies in the field of machine health prognostics demonstrate the effectiveness of data-driven and hybrid approaches for RUL estimation (Jardine et al., 2006; Si et al., 2011). The digital twin combines these methods with the operating conditions specific to wind turbines, producing more realistic results.

5.3. Uncertainty, Risk, and Maintenance Decisions

Under real field conditions, RUL predictions always involve a certain degree of uncertainty. Variability in wind conditions, fluctuations in load spectra, and measurement noise are the main sources of this uncertainty. The digital twin approach contributes to more flexible and reliable maintenance decisions by explicitly modeling these uncertainties (Leon-Medina et al., 2025).

Risk-based maintenance approaches become particularly important at the wind farm scale. Risk profiles generated through the digital twin can guide the prioritization of maintenance actions and the efficient allocation of resources (Zhang & Zhao, 2023). This helps keep maintenance costs under control in power plants consisting of a large number of turbines.

5.4. Maintenance Optimization with the Digital Twin

The digital twin is not limited to fault prediction; it is also a powerful tool for optimizing maintenance strategies. Different maintenance scenarios can be virtually tested on the digital twin and compared in terms of production loss, cost, and risk. This approach enables the evaluation of maintenance activities not only from a technical perspective but also from an economic one (ISO, 2021).

In the industrial maintenance literature, it has long been known that predictive maintenance applications, when properly designed, increase system availability while reducing total life-cycle costs (Randall & Basciftci, 2025). The digital twin makes this classical knowledge more applicable in the context of wind energy by combining it with up-to-date data and models.

Predictive maintenance is one of the areas where the digital twin approach offers the highest added value for wind turbines. The structural health monitoring and artificial intelligence–based modeling approaches discussed in previous sections are transformed in this section into a framework that directly influences maintenance decisions. Through the digital twin, maintenance processes move away from intuition-based, retrospective approaches toward a data-, model-, and risk-driven structure.

The success of this approach depends on the accuracy of RUL predictions, proper management of uncertainties, and the effective integration of the generated information into maintenance processes. When properly designed, digital twin–supported predictive maintenance systems make significant contributions to increasing the reliability of wind turbines, reducing maintenance costs, and ensuring operational continuity.

6. Literature Comparison and Discussion

Digital twin applications in wind turbines are addressed in the literature from different perspectives and with varying priorities. While some studies position the digital twin primarily as a physics-based simulation tool, others propose more flexible approaches that place data-driven artificial intelligence models at the center. In this section, the existing literature is comparatively examined in terms of approach type, data sources used, targeted outputs, and field applicability, and the strengths and weaknesses of digital twin–based solutions are discussed.

As noted in previous sections, the concept of the digital twin in wind energy systems is often addressed with a focus on maintenance, monitoring, and prognostics. In this context, a significant portion of the studies in the literature position the digital twin directly as an operational decision-support tool (De Kooning et al., 2021; Leon-Medina et al., 2025).

6.1. Physics-Based Approaches and Their Limitations

In the early applications of digital twins, physics-based models played a dominant role. Aerodynamic behavior, structural dynamics, and mechanical component behavior were represented through mathematical models. Such approaches are strong in terms of explicitly reflecting the physical principles of the system. However, in systems such as wind turbines that operate under variable environmental conditions, achieving high accuracy with these models requires intensive computational power and detailed parameter information.

The literature emphasizes that physics-based digital twins are particularly limited in real-time applications. As model complexity increases, computational burden also increases, making online (real-time) deployment in the field more difficult (De Kooning et al., 2021). This situation may restrict the use of digital twins to offline analyses only, thereby limiting their operational contribution.

6.2. Data-Driven and Artificial Intelligence–Centered Studies

Data-driven digital twin approaches have shown a significant increase in the literature, particularly in recent years. In these studies, the digital twin is often represented through artificial intelligence models trained on sensor data and historical operational records. Image-based damage detection, vibration analysis, and prognostics based on SCADA data are typical examples of this approach (Deng et al., 2021; Liao et al., 2024).

The most important advantage of data-driven approaches is their ability to capture complex system behaviors without requiring an explicit physical model definition. However, this also brings two major challenges: data dependency and generalizability. Rare failures, incomplete labeling, and site-specific conditions can limit the performance of data-driven models. Therefore, the literature frequently emphasizes that such approaches alone are not sufficient and that a more holistic structure, consistent with the spirit of the digital twin concept, is required.

6.3. The Rise of Hybrid Digital Twin Approaches

Recent studies of particular interest focus on hybrid digital twin approaches that combine physics-based models with data-driven artificial intelligence methods. These approaches aim to bridge the gap between physical knowledge and data. Especially in problems such as fatigue, bearing wear, and long-term performance degradation in wind turbines, hybrid models have been observed to produce more balanced results (Yucesan & Viana, 2023).

Hybrid approaches are often described in the literature as “more complex but more reliable.” This once again highlights that the intended use case is a determining factor in digital twin design. While simpler models may be sufficient for real-time monitoring, hybrid structures are preferred for long-term maintenance and risk analysis (Leon-Medina et al., 2025).

6.4. The Issue of Scale: Turbine or Wind Farm?

Another important point of differentiation among studies in the literature is the scale at which the digital twin is addressed. Digital twins developed at the turbine scale generally focus on the health or maintenance needs of a specific component. This approach is more controlled in terms of modeling and data management.

In contrast, digital twins developed at the wind farm scale take into account turbine-to-turbine interactions and wake effects. These studies offer significant potential, particularly for production optimization and farm-level maintenance planning (Zhang & Zhao, 2023). However, as the scale increases, data volume, model complexity, and computational requirements also increase, which in turn makes field applicability more challenging.

6.5. General Evaluation and Discussion

When the literature is evaluated as a whole, it is observed that digital twin studies in the field of wind energy have not yet reached a uniform level of maturity. While some studies remain limited to providing conceptual frameworks, others propose in-depth applications for specific components. This diversity reveals both the strengths and weaknesses of the digital twin concept.

In light of the studies discussed in this section, the following points stand out:

- When the digital twin is limited to either physics or artificial intelligence alone, it struggles to deliver the expected benefits.
- Hybrid approaches provide more balanced results, particularly for predictive maintenance and long-term performance analysis.
- There is a significant difference in methods and priorities between turbine-scale and wind farm–scale applications.

The number of studies with field validation in the literature is still limited, which slows down the industrial adoption of digital twins. These discussions indicate that the digital twin remains an evolving research area in wind energy and that methodological diversity is expected to increase in the coming years.

7. Future Perspectives and Open Research Problems

Although the digital twin approach in wind energy systems has gained significant momentum in recent years, an overall assessment of the literature indicates that this field has not yet reached a mature stage. The studies discussed in previous sections demonstrate that digital twins offer substantial potential in terms of monitoring, predictive maintenance, and decision support. Nevertheless, a wide range of methodological and practical problems remain unresolved in both academic research and industrial applications.

In this section, future perspectives on digital twin–based approaches for wind turbines are addressed, and open research problems that have not yet been clearly defined or have been examined in a limited number of studies in the literature are discussed.

7.1. Real-Time and Autonomous Digital Twins

A significant portion of existing digital twin applications relies on offline analyses or near-real-time systems. However, for systems such as wind turbines that are exposed to rapidly changing environmental conditions, there is a growing need for digital twins that can be updated in real time and make autonomous decisions. Such a structure would enable the digital twin to become not merely an analysis tool, but an active operational component.

In the literature, the concept of autonomous digital twins is being discussed with increasing frequency, and it is anticipated that such systems could minimize human intervention by automating maintenance and operational decisions (Fuller et al., 2020). However, the requirement for real-time operation also introduces fundamental challenges, including data processing capacity and computational cost.

7.2. Edge AI and Computational Architectures

Another prominent research direction in the future of digital twins is the shift of computational workload from centralized systems to the field level. Edge AI–based approaches aim to reduce latency and improve system response time by deploying artificial intelligence models closer to sensors or turbine control units.

In the context of wind turbines, edge-based digital twins can provide advantages particularly in early anomaly detection and situations that require rapid decision-making. However, edge architectures also face constraints such as limited hardware resources and energy consumption. Therefore, future studies are expected to address the balance between model complexity and field applicability in a more systematic manner (Jones et al., 2020).

7.3. Digital Twins at Multi-Turbine and Wind Farm Scale

To date, the majority of existing studies have focused on single turbines or individual components. However, in wind power plants, maintenance and operational decisions are often made at the farm scale. This makes the scalability of the digital twin approach a critical research topic.

Digital twins at the wind farm scale require consideration of turbine-to-turbine interactions, wake effects, and site-wide wind distribution. Developing such models involves significant challenges in terms of data volume and computational requirements. The number of studies in this area remains limited in the literature and is generally simulation-oriented. In the future, an increase in field-validated, farm-scale digital twins is expected (Grieves & Vickers, 2017).

7.4. Standardization, Data Sharing, and Interoperability

One of the most significant barriers to the widespread adoption of digital twin applications is the lack of standardization and data incompatibility. Sensors, data formats, and control systems used in turbines from different manufacturers exhibit substantial diversity. This situation limits the generalizability and portability of digital twin solutions.

Standardization efforts are critically important for establishing a common language and architectural framework for digital twins. In particular, steps taken in the areas of data sharing and interoperability will enable wider industrial acceptance of digital twin–based solutions (Boschert & Rosen, 2016). However, data security and commercial sensitivities are important factors that complicate this process.

7.5. Explainable Artificial Intelligence and the Issue of Trust

As the complexity of artificial intelligence models used in digital twin systems increases, the issue of explainability becomes increasingly important. Especially in situations where critical decisions related to maintenance and safety are made, it is necessary to understand why the system generates a particular warning or recommends a specific maintenance action.

In the literature, the integration of explainable artificial intelligence (XAI) approaches with digital twins remains limited. This situation can negatively affect the level of trust that industrial users place

in digital twin–based systems. Future studies are expected to focus on digital twin architectures that strike a balance between high accuracy and explainability (Cerrone et al., 2014).

When evaluated in light of future perspectives, it is clear that the digital twin approach in wind energy systems has significant transformational potential. However, realizing this potential depends not only on the development of more advanced artificial intelligence models, but also on a holistic consideration of system architecture, standardization, data management, and user trust.

In this context, the digital twin is regarded not merely as a technical innovation in the field of wind energy, but as a paradigm that reshapes operation, maintenance, and decision-making processes. In the coming years, research in this area is expected to evolve from conceptual discussions toward field-validated and scalable solutions.

8. Conclusion

In this section, the artificial intelligence–assisted digital twin approach for wind energy systems has been examined together with its conceptual framework, architectural components, and application areas. The complex structure of wind turbines, their operation under variable environmental conditions, and high maintenance costs clearly reveal the limitations of conventional monitoring and maintenance approaches. The digital twin approach offers a holistic solution framework to overcome these limitations.

Throughout the study, it has been emphasized that a digital twin is not merely a numerical replica of a physical system, but a dynamic structure in which data, models, and decision-making mechanisms continuously interact. The contributions provided by digital twins in key application areas such as structural health monitoring, predictive maintenance, and maintenance optimization explain why this approach has attracted increasing attention in the wind energy sector. In particular, the integration of artificial intelligence methods into digital twin architectures enables more accurate interpretation of system behavior and strengthens future-oriented predictions.

The literature and discussions addressed in this section indicate that digital twin solutions developed for wind turbines do not yet represent a single, mature, and uniform structure, but rather flexible approaches shaped according to different needs. Physics-based models, data-driven artificial intelligence methods, and hybrid approaches offer different advantages and limitations depending on the intended use, scale, and field conditions. This situation demonstrates that, instead of a “one-size-fits-all” solution, balanced and problem-specific architectures should be preferred in digital twin design.

In conclusion, the artificial intelligence–assisted digital twin approach can be considered not only a technical innovation in wind energy systems, but also a strategic tool that transforms maintenance, operation, and decision-making processes. The wider adoption of this approach in the future will depend on progress achieved in areas such as real-time capability, scalability, explainability, and standardization. In this direction, field-validated and industrial-scale digital twin solutions are expected to make significant contributions to the reliability and sustainability of wind energy systems.

References

Ahmad, R., & Kamaruddin, S. (2012). An overview of time-based and condition-based maintenance in industrial application. Computers & Industrial Engineering, 63(1), 135–149. https://doi.org/10.1016/j.cie.2012.02.002

Boschert, S., & Rosen, R. (2016). Digital twin—The simulation aspect. In Mechatronic futures (pp. 59–74). Springer. https://doi.org/10.1007/978-3-319-32156-1_5

Cerrone, A., Hochhalter, J., Heber, G., & Ingraffea, A. (2014). On the effects of modeling as-manufactured geometry: Toward digital twin. International Journal of Aerospace Engineering, 2014, 439278. https://doi.org/10.1155/2014/439278

De Kooning, J. D. M., Stockman, K., De Maeyer, J., Jarquin-Laguna, A., & Vandevelde, L. (2021). Digital twins for wind energy conversion systems: A literature review of potential modelling techniques focused on model fidelity and computational load. *Processes, 9*(12), 2224. https://doi.org/10.3390/pr9122224

Deng, L., Guo, Y., & Chai, B. (2021). Defect detection on a wind turbine blade based on digital image processing. *Processes, 9*(8), 1452. https://doi.org/10.3390/pr9081452

Fırat, H., & Hanbay, D. (2021). 4CF-Net: Hiperspektral uzaktan algılama görüntülerinin spektral uzamsal sınıflandırılması için yeni 3B evrişimli sinir ağı. *Gazi Üniversitesi Mühendislik Mimarlık Fakültesi Dergisi, 37*(1), 439–454. https://doi.org/10.17341/gazimmfd.901291

Fuller, A., Fan, Z., Day, C., & Barlow, C. (2020).Digital twin: Enabling technologies, challenges and open research. IEEE Access, 8, 108952–108971. https://doi.org/10.1109/ACCESS.2020.2998358

Grieves, M., & Vickers, J. (2017). Digital twin: Mitigating unpredictable, undesirable emergent behavior in complex systems. In Transdisciplinary perspectives on complex systems (pp. 85–113). Springer.

ISO. (2021). *ISO 23247-1:2021 Automation systems and integration — Digital twin framework for manufacturing — Part 1: Overview and general principles*. International Organization for Standardization.

Jardine, A. K. S., Lin, D., & Banjevic, D. (2006). A review on machinery diagnostics and prognostics implementing condition-based maintenance. Mechanical Systems and Signal Processing, 20(7), 1483–1510. https://doi.org/10.1016/j.ymssp.2005.09.012

Jones, D., Snider, C., Nassehi, A., Yon, J., & Hicks, B. (2020). Characterising the digital twin: A systematic literature review. CIRP Journal of Manufacturing Science and Technology, 29, 36–52. https://doi.org/10.1016/j.cirpj.2020.02.002

Lei, Y., Li, N., Guo, L., Li, N., Yan, T., & Lin, J. (2018). Machinery health prognostics: A systematic review. Mechanical Systems and Signal Processing, 104, 799–834. https://doi.org/10.1016/j.ymssp.2017.11.016

Leon-Medina, J. X., Tibaduiza, D. A., Parés, N., & Pozo, F. (2025). Digital twin technology in wind turbine components: A review. *Intelligent Systems with Applications, 26*, 200535. https://doi.org/10.1016/j.iswa.2025.200535

Liao, Y., Lv, M., Huang, M., Qu, M., Zou, K., Chen, L., & Feng, L. (2024). An improved YOLOv7 model for surface damage detection on wind turbine blades based on low-quality UAV images. *Drones, 8*(9), 436. https://doi.org/10.3390/drones8090436

Lüy, M., & Saray, U. (2012). Wind speed estimation for missing wind data with three different backpropagation algorithms. Energy Education Science and Technology Part A: Energy Science and Research, 30(1), 45–54.

Pujana, A., Esteras, M., Perea, E., Maqueda, E., & Calvez, P. (2023). Hybrid-model-based digital twin of the drivetrain of a wind turbine and its application for failure synthetic data generation. *Energies, 16*(2), 861. https://doi.org/10.3390/en16020861

Raissi, M., Perdikaris, P., & Karniadakis, G. E. (2019). Physics-informed neural networks: A deep learning framework for solving forward and inverse problems. Journal of Computational Physics, 378, 686–707. https://doi.org/10.1016/j.jcp.2018.10.045

Randall, N., & Basciftci, B. (2025). Risk-averse contextual predictive maintenance and operations scheduling with flexible generation under wind energy uncertainty. European Journal of Operational Research, 327(1), 174–190. https://doi.org/10.1016/j.ejor.2025.06.005

Shao, G., Frechette, S. P., & Srinivasan, V. (2023). An analysis of the new ISO 23247 series of standards on digital twin framework for manufacturing. In *2023 MSEC Manufacturing Science & Engineering Conference*. https://doi.org/10.1115/MSEC2023-101127

Si, X. S., Wang, W., Hu, C. H., & Zhou, D. H. (2011). Remaining useful life estimation: A review on the statistical data-driven approaches. European Journal of Operational Research, 213(1), 1–14. https://doi.org/10.1016/j.ejor.2010.11.018

Tao, F., Qi, Q., Liu, A., & Kusiak, A. (2018). Data-driven smart manufacturing. Journal of Manufacturing Systems, 48(Part C), 157–169. https://doi.org/10.1016/j.jmsy.2018.01.006

Tao, F., Zhang, H., Liu, A., & Nee, A. Y. C. (2019). Digital twin in industry: State-of-the-art. IEEE Transactions on Industrial Informatics, 15(4), 2405–2415. https://doi.org/10.1109/TII.2018.2873186

Wang, M.-H., Chen, F.-H., & Lu, S.-D. (2023). Research on Fault Diagnosis of Wind Turbine Gearbox with Snowflake Graph and Deep Learning Algorithm. *Applied Sciences*, *13*(3), 1416. https://doi.org/10.3390/app13031416

Yucesan, Y. A., & Viana, F. A. C. (2023). Physics-informed digital twin for wind turbine main bearing fatigue: Quantifying uncertainty in grease degradation. *Applied Soft Computing*, 110921. https://doi.org/10.1016/j.asoc.2023.110921

Zhang, J., & Zhao, X. (2023). Digital twin of wind farms via physics-informed deep learning. *Energy Conversion and Management, 293*, 117507. https://doi.org/10.1016/j.enconman.2023.117507

Chapter 11

ON CHIP LIDAR

İremnur DURU[1], Timuçin Emre TABARU[2]

1 Research Assistant, Department of Electrical and Electronics Engineering, Sivas University of Science and Technology, Sivas, Türkiye, ORCID: 0000-0001-5492-803X
2 Associate Professor, Department of Electrical and Electronics Engineering, Sivas University of Science and Technology, Sivas, Türkiye, ORCID: 0000-0002-1373-3620

1. Introduction

Traditional LiDAR systems typically consist of mechanical scanning mechanisms, large optical components, and independent optoelectronic modules. This structure increases the system's complexity and cost while also acting as a limiting factor in terms of reliability and long-term stability (Geophysics & 1969, n.d.). Demands from various fields, such as high reliability in autonomous driving, lightness in aviation and drone applications, and low cost in consumer electronics, have made integration and miniaturization processes in LiDAR technologies inevitable (ME Warren-2019 Symposium on VLSI Circuits & 2019, n.d.; geography & 2008, 2008; Risbøl et al., 2018). This requirement is one of the strongest motivators for redesigning systems used in different industries with a more compact, functional, and economical approach (Nanxi Li et al., 2022a). In this regard, integration-focused photonic platforms—such as silicon photonics (Doylend et al., n.d.-a; Risbøl et al., 2018), silicon nitride due to low propogation loss and higher integration capabilites (Buzaverov et al., 2024; Doylend et al., n.d.-b), and heterogeneous III–V integration technologies—enable the combination of fundamental functions such as light generation, steering, phase control, and detection on a single microchip. Heterogeneous integration enables the low-loss waveguide infrastructure of the silicon photonic platform to be combined with the high-efficiency laser, modulator, and detector properties of III-V semiconductors, thereby consolidating performance on a single platform (Xiang et al., n.d.). These platforms not only reduce the size of existing LiDAR systems but also add value to the technology by offering critical advantages such as increased optical performance, improved energy efficiency, and suitability for mass production (J. Bowers-2015 Optical Fiber Communications Conference & 2015, n.d.; Liang et al., 2021). Photonic integration offers a revolutionary approach to both reducing hardware complexity and improving performance stability in LiDAR systems (Xu et al., 2025). Integrated photonic circuits combine various components such as light sources, modulators, phase shifters, detectors, and control electronics on a single silicon substrate, providing effective solutions to problems such as optical alignment, packaging, and signal loss. This enables LiDAR systems to achieve higher bandwidth, lower energy consumption, and a compact structure. Furthermore, CMOS-compatible manufacturing processes replace costly assembly stages in traditional optical systems with wafer-level production and high repeatability (Hu et al., 2023). These advantages are emerging as one of the most important factors accelerating the commercialization of LiDAR technology, particularly in areas such as autonomous vehicles and portable sensor applications (Behroozpour et al., n.d.). Traditional mechanical LiDAR systems are limited in scalable applications due to high cost, large size, and reliability issues caused by moving parts. In this context, on-chip photonic LiDAR systems are attracting attention with their low power consumption, compact size, and integration advantages with electronics. The on-chip LiDAR concept aims to perform the basic functions of LiDAR systems—light generation, modulation, steering, scanning, and detection—on a single integrated photonic chip (Raj et al., n.d.; Zhou et al., 2023). This approach enables the development of systems that are faster, more durable, and more stable against environmental factors compared to traditional mechanical scanning units. Furthermore, integrated systems enable multi-channel architectures and parallel data acquisition capabilities, offering high scanning speeds and three-dimensional (3D) imaging capabilities (Nevlacsil et al., 2020). Soon,

with the development of high-efficiency chip-on-laser sources and low-noise detectors, these systems are expected to offer widespread and scalable solutions in various fields such as autonomous vehicles, robotic sensing, augmented reality (AR), and mobile device sensors (Zhou et al., 2023). Recently, FMCW (Frequency Modulated Continuous Wave) LiDAR architectures have been gaining attention, offering high distance resolution thanks to their ability to measure speed directly through Doppler shift (Sayyah et al., n.d.). The study investigates on-chip LiDAR sensors within a Cyber-Physical System (CPS) framework, demonstrating how real-time obstacle recognition can be achieved using machine learning algorithms. The authors implement and compare multiple approaches—including multilayer perceptrons, self-organizing maps, and support vector machines—on LiDAR-generated point cloud data. Their results highlight the potential of on-chip LiDAR for scalable sensor networks and embedded systems in dynamic environments (Castaño et al., n.d.; Nanxi Li et al., 2022b). These systems deliver stable performance even in challenging environments with intense ambient light or bright surface reflections (Nanxi Li et al., 2022b). These qualities are driving increased interest in FMCW LiDAR(Zhang et al., n.d.) , particularly in automotive and industrial sensor systems where reliability is critical. In parallel, beam steering technology based on optical phased array (OPA) offers a fast and long-lasting solution without moving parts as an alternative to mechanical scanning systems (Nanophotonics & 2017, 2017a). OPA architectures have the potential to perform beam steering operations with high accuracy and repeatability. However, the transition of this technology to practical application is still limited by certain technical barriers. These challenges include engineering problems such as maintaining phase accuracy, suppressing sidelobes, balancing optimization between wide field of view and beam width control, and sustaining phase stability on the chip (He et al., n.d.). Resolving these issues is crucial for OPA-based LiDAR systems to realize their full performance potential. These technical limitations are largely directly related to the performance of on-chip lasers and the requirements of integration-based amplifiers (Yi et al., n.d.). Parameters such as output power, narrow spectral linewidth, scanning accuracy, and linear frequency modulation capabilities are key factors determining the success of integrated LiDAR systems. The current literature comprehensively addresses both theoretical and experimental approaches to meeting these requirements. In particular, studies on chip-scale laser integration and OPA-based beam steering solutions provide an important foundation for the design of next-generation LiDAR systems by facilitating a better understanding of current technological developments. The aim of this study is to comprehensively and systematically evaluate the current state of integrated photonic-based LiDAR systems and to analyze the fundamental components and challenges encountered in the field. In this context, LiDAR architectures will be examined comparatively, the technical capabilities and limitations of on-chip components will be evaluated, and the advantages and disadvantages of different integration platforms will be detailed. Furthermore, focusing on the engineering challenges encountered in system-level integration processes, recommendations for future research directions and improvement strategies will be presented.

2. Fundamentals of Photonic Integrated LiDAR

Photonic integrated LiDAR systems leverage advanced photonic integration technologies to implement the core functionalities of LiDAR—including optical signal generation, modulation, beam steering, and detection—within compact, chip-scale platforms (She & Friedman, 2022a). Using photonic integrated circuits (PICs), these systems replace bulky free-space optical components and mechanically actuated scanning mechanisms with fully integrated photonic elements (H. Hashemi-2022 IEEE Custom Integrated Circuits Conference & 2022, n.d.). This paradigm shift results in enhanced mechanical robustness, improved long-term stability, and significant reductions in system size, weight, and power consumption, while enabling scalable and cost-effective manufacturing (Doylend et al., n.d.-c).

In addition, photonic integration enables precise and repeatable control over key optical parameters such as phase, amplitude, and frequency, which is essential for the realization of solid-state beam steering and coherent detection techniques (Lukashchuk et al., n.d.-a). These capabilities allow photonic integrated LiDAR systems to achieve high angular resolution, fast scanning rates, and improved resilience to environmental variations compared to conventional LiDAR implementations (Y. Yi-From 2D to 3D Photonic Integrated Circuits & 2025, 2026; Falconi et al., n.d.; Lukashchuk et al., n.d.-b). By consolidating optical and, in many cases, electronic functionalities on a common platform, photonic integrated LiDAR architectures provide a promising pathway toward high-performance, three-dimensional sensing systems suitable for a wide range of emerging applications(Kutila et al., n.d.; Vierhub-Lorenz et al., n.d.).

2.1 Fundamental Operating Principles and Platform Architecture

The operating principles of photonic integrated LiDAR systems are fundamentally based on the generation of optical signals, their propagation toward remote targets, and the subsequent detection of the light reflected or scattered back from the scene (Wang et al., n.d.). Depending on the LiDAR modality, this detection process may be realized through either coherent or incoherent techniques, each imposing different requirements on system design and signal processing(She & Friedman, 2022b). The underlying platform architecture typically consists of integrated laser sources, high-speed modulators, low-loss waveguides, beam steering elements, and photodetectors, which are often co-integrated with electronic control and signal processing circuitry to enable precise system operation(Lukashchuk et al., n.d.-b).

The selection of the material platform and overall system architecture plays a decisive role in determining key performance metrics, including optical output power, wavelength tuning range, phase noise and stability, and overall system robustness (Hammer et al., n.d.). Trade-offs among these parameters must be carefully considered during the design process, as they directly influence sensing range, resolution, and reliability. Consequently, the co-design of photonic components, electronic control, and system architecture is essential for achieving high-performance and scalable photonic integrated LiDAR systems (Geophysics & 1969, n.d.).

2.2 Time-of-Flight and Continuous-Wave LiDAR Architectures

LiDAR systems can be broadly categorized into time-of-flight (ToF) (Incoronato et al., n.d.) and continuous-wave (CW) architectures (C. Li et al., n.d.; Mei et al., 2015), each offering distinct advantages and trade-offs in terms of range, resolution, and system complexity. ToF-based systems determine target distance by measuring the propagation delay of optical pulses (Chen et al., n.d.), while CW-based systems extract distance information from modulated or frequency-swept continuous optical signals. Amplitude-modulated continuous-wave (AMCW) LiDAR encodes distance information in the phase delay of an amplitude-modulated optical carrier (Godbaz et al., 2013). This approach enables relatively simple system implementation and is well suited for short- to mid-range applications, although its performance is limited by modulation frequency, ambiguity range, and sensitivity to ambient light. Frequency-modulated continuous-wave (FMCW) LiDAR employs a linearly chirped laser source to simultaneously measure range and velocity through coherent detection of the beat frequency between transmitted and reflected signals (Isaac et al., n.d.; Martin et al., 2018; Sayyah et al., n.d.). FMCW LiDAR offers superior range resolution, improved signal-to-noise ratio, and inherent immunity to interference, making it particularly attractive for long-range and high-precision sensing applications(Kim et al., n.d.).

2.3 Performance Metrics

The performance of photonic integrated LiDAR systems is commonly evaluated using key metrics such as detection range, spatial and range resolution, measurement accuracy, and signal-to-noise ratio (SNR). These metrics are influenced by factors including optical output power, modulation bandwidth, laser linewidth, receiver sensitivity, and system noise. Understanding the trade-offs among these parameters is essential for optimizing LiDAR architectures for specific application requirements (Kutila et al., n.d.; Mattson et al., n.d.).

3. Photonic Integration Technologies for LiDAR

Photonic integration technologies form the technological foundation for the realization of compact, robust, and scalable LiDAR systems by enabling the integration of multiple optical functions onto a single chip-scale platform. Widely used photonic integrated circuit (PIC) platforms include silicon (Hu et al., 2023), silicon nitride(Buzaverov et al., 2024), and III–V semiconductor technologies (Liang et al., 2021; Luo et al., n.d.), each offering distinct advantages with respect to optical confinement, propagation loss, and the availability of active photonic functionalities. The selection of a suitable platform is therefore closely linked to the targeted LiDAR architecture and performance requirements.

Advances in photonic integration have enabled the realization of key on-chip components, including integrated light sources (Sayyah et al., n.d.), high-speed optical modulators, and highly sensitive photodetectors, thereby significantly reducing system complexity and footprint. In addition, optical phased arrays (OPAs) implemented on photonic integrated platforms enable precise electronic beam steering without the need for mechanical motion (McManamon et al.,

n.d.). This capability is central to the development of solid-state LiDAR systems, offering improved reliability, faster scanning speeds, and enhanced integration potential for next-generation sensing applications (Son et al., n.d.; Zhao et al., n.d.).

4. Integrated LiDAR Architectures

Integrated LiDAR architectures seek to co-integrate transmitter and receiver functionalities within a unified photonic platform in order to reduce system complexity, improve alignment stability, and enhance overall performance (Nanophotonics & 2017, 2017b). By consolidating optical emission, beam steering (Cao et al., n.d.), and detection on a single photonic integrated circuit, these architectures minimize the need for discrete optical components and enable compact, robust system implementations. Such co-integration also facilitates improved synchronization between transmission and reception paths, which is particularly critical for coherent LiDAR techniques (Martin et al., 2018).

Solid-state scanning approaches, most notably those based on optical phased arrays (OPAs), enable rapid and precise beam steering through electronic control of the optical phase without relying on mechanically moving parts (Son et al., n.d.; Zhao et al., n.d.). This capability significantly improves system reliability, scanning speed, and lifetime compared to traditional mechanically scanned LiDAR systems. Recent LiDAR-on-chip demonstrations have validated the practicality of these integrated approaches, showcasing fully integrated photonic systems capable of high-resolution, high-speed three-dimensional imaging, and underscoring their strong potential for scalable and cost-effective LiDAR solutions (Kavitha et al., 2025a, 2025b).

5. Conclusion

Despite the significant progress achieved to date, photonic integrated LiDAR systems continue to face a number of technical and practical challenges, particularly in the areas of heterogeneous integration, thermal management, advanced packaging, and large-scale manufacturability. The co-integration of dissimilar material platforms, such as III–V gain media on silicon, introduces complexity in fabrication, yield, and long-term reliability. In addition, thermal effects can adversely impact laser stability, phase control, and overall system performance, underscoring the need for effective thermal design and control strategies. Addressing these challenges is essential for translating laboratory-scale demonstrations into robust, commercially viable LiDAR products. Nevertheless, photonic integrated LiDAR exhibits strong potential across a broad range of application domains, including autonomous vehicles, robotics, industrial automation, and remote sensing, where compactness, reliability, and high performance are critical requirements. Continued advances in material platforms, photonic–electronic integration strategies, and system-level architectures are expected to drive future research toward improved performance, reduced cost, and increased levels of integration. As these technologies mature, photonic integrated LiDAR is poised to play a central role in the widespread adoption of solid-state three-dimensional sensing systems.

REFERENCES

Behroozpour, B., … PAM Sandborn-IEEE, & 2017, undefined. (n.d.). Lidar system architectures and circuits. *Ieeexplore.Ieee.Org*. Retrieved 14 November 2025, from https://ieeexplore.ieee.org/abstract/document/8067701/

Buzaverov, Kirill A., Baburin, Aleksandr S., Sergeev, Evgeny V., Avdeev, Sergey S., Lotkov, Evgeniy S., Bukatin, Sergey V., Stepanov, Ilya A., Kramarenko, Aleksey B., Amiraslanov, Ali Sh, Kushnev, Danil V., Ryzhikov, Ilya A., & Rodionov, Ilya A. (2024). Silicon nitride integrated photonics from visible to mid-infrared spectra. *Wiley Online Library*, *18*(12). https://doi.org/10.1002/LPOR.202400508

Cao, X., Qiu, G., Wu, K., Li, C., Letters, J. Chen-Optics, & 2020, undefined. (n.d.). Lidar system based on lens assisted integrated beam steering. *Opg.Optica.Org*. Retrieved 20 December 2025, from https://opg.optica.org/abstract.cfm?uri=ol-45-20-5816

Castaño, F., Beruvides, G., Haber, RE, Sensors, A. Artuñedo-, & 2017, undefined. (n.d.). Obstacle recognition based on machine learning for on-chip LiDAR sensors in a cyber-physical system. *Mdpi.Com*. Retrieved 14 November 2025, from https://www.mdpi.com/1424-8220/17/9/2109

Chen, G., Wiede, C., Journal, R. Kokozinski-IEEE Sensors, & 2020, undefined. (n.d.). Data processing approaches on SPAD-based d-TOF LiDAR systems: A review. *Ieeexplore.Ieee.Org*. Retrieved 19 December 2025, from https://ieeexplore.ieee.org/abstract/document/9261382/

Circuits, ME Warren-2019 Symposium on VLSI, & 2019, undefined. (n.d.). Automotive LIDAR technology. *Ieeexplore.Ieee.Org*. Retrieved 14 November 2025, from https://ieeexplore.ieee.org/abstract/document/8777993/

Circuits, Y. Yi-From 2D to 3D Photonic Integrated, & 2025, undefined. (2026). Fundamentals of Photonic Integrated Circuits. *Springer*, 17–31. https://doi.org/10.1007/978-3-031-91508-6_2

Conference, H. Hashemi-2022 IEEE Custom Integrated Circuits, & 2022, undefined. (n.d.). A review of silicon photonics LiDAR. *Ieeexplore.Ieee.Org*. Retrieved 24 December 2025, from https://ieeexplore.ieee.org/abstract/document/9772845/?casa_token=WWnl7vvwR48AAAAA:PpHnvmwaltIavKiD1rzj73KCT-eRLXQ2_6o5Jm2qR82oI6qousl4fL7G_pc0jasiaJ3nRKM_rQ

Conference, J. Bowers-2015 Optical Fiber Communications, & 2015, undefined. (n.d.). Heterogeneous silicon III–V Photonic Integrated Circuits. *Ieeexplore.Ieee.Org*. Retrieved 14 November 2025, from https://ieeexplore.ieee.org/abstract/document/7121893/

Doylend, JK, XV, S. Gupta-Silicon Photonics, & 2020, undefined. (n.d.-a). An overview of silicon photonics for LIDAR. *Spiedigitallibrary.Org*. https://doi.org/10.1117/12.2544962.SHORT

Doylend, JK, XV, S. Gupta-Silicon Photonics, & 2020, undefined. (n.d.-b). An overview of silicon photonics for LIDAR. *Spiedigitallibrary.Org*. https://doi.org/10.1117/12.2544962.SHORT

Doylend, JK, XV, S. Gupta-Silicon Photonics, & 2020, undefined. (n.d.-c). An overview of silicon photonics for LIDAR. *Spiedigitallibrary.Org*. https://doi.org/10.1117/12.2544962.SHORT

Falconi, F., Melo, S., Scotti, F., … MN Malik-Journal of Lightwave, & 2020, undefined. (n.d.). A combined radar & lidar system based on integrated photonics in silicon-on-insulator. *Ieeexplore.Ieee.Org*. Retrieved 24 December 2025, from https://ieeexplore.ieee.org/abstract/document/9195117/?casa_token=5aKYWInAnHsAAAAA:COydVK7uruYM_s-wArDrI2kEf8p9_3YCCoOxbXol_P2OcjfOrYFwmCgnRWiGckg5C6yWX2zc0Q

geography, X. Liu-Progress in physical, & 2008, undefined. (2008). Airborne LiDAR for DEM generation: some critical issues. *Journals.Sagepub.Com*, *32*(1), 31–49. https://doi.org/10.1177/0309133308089496

Geophysics, RTH Collis-Advances in, & 1969, undefined. (n.d.). Lidar. *Elsevier*. Retrieved 14 November 2025, from https://www.sciencedirect.com/science/article/pii/S0065268708605099

Godbaz, John P., Dorrington, Adrian A., & Cree, Michael J. (2013). Understanding and ameliorating mixed pixels and multipath interference in amcw lidar. *Springer*, *9783642275234*, 91–116. https://doi.org/10.1007/978-3-642-27523-4_5

Hammer, M., Hebel, M., … M. Laurenzis-Emerging Imaging and, & 2018, undefined. (n.d.). Lidar-based detection and tracking of small UAVs. *Spiedigitallibrary.Org*. https://doi.org/10.1117/12.2325702.SHORT

He, J., Dong, T., Access, Y. Xu-IEEE, & 2020, undefined. (n.d.). Review of photonic integrated optical phased arrays for space optical communication. *Ieeexplore.Ieee.Org*. Retrieved 14 November 2025, from https://ieeexplore.ieee.org/abstract/document/9222022/

Hu, Mingxuan, Pang, Yajun, & Gao, Long. (2023). Advances in Silicon-Based Integrated Lidar. *Sensors 2023, Vol. 23, Page 5920*, *23*(13), 5920. https://doi.org/10.3390/S23135920

Incoronato, A., Locatelli, M., Sensors, F. Zappa-, & 2021, undefined. (n.d.). Statistical modelling of SPADs for time-of-flight LiDAR. *Mdpi.Com*. Retrieved 19 December 2025, from https://www.mdpi.com/1424-8220/21/13/4481

Isaac, BJ, Song, B., Pinna, S., … LA Coldren-IEEE Journal of, & 2019, undefined. (n.d.). Indium phosphide photonic integrated circuit transceiver for FMCW LiDAR. *Ieeexplore.Ieee.Org*. Retrieved 14 November 2025, from https://ieeexplore.ieee.org/abstract/document/8693564/

Kavitha, S., Processing, M. Baskaran-Analog Integrated Circuits and Signal, & 2025, undefined. (2025a). A review of optical beam steering technologies in LiDAR photonic chips. *Springer*, *124*(1). https://doi.org/10.1007/S10470-025-02404-1

Kavitha, S., Processing, M. Baskaran-Analog Integrated Circuits and Signal, & 2025, undefined. (2025b). A review of optical beam steering technologies in LiDAR photonic chips. *Springer*, *124*(1). https://doi.org/10.1007/S10470-025-02404-1

Kim, C., Jung, Y., Sensors, S. Lee-, & 2020, undefined. (n.d.). FMCW LiDAR system to reduce hardware complexity and post-processing techniques to improve distance resolution. *Mdpi.Com*. Retrieved 20 December 2025, from https://www.mdpi.com/1424-8220/20/22/6676

Kutila, M., Pyykönen, P., … H. Holzhüter-2018 21st, & 2018, undefined. (n.d.). Automotive LiDAR performance verification in fog and rain. *Ieeexplore.Ieee.Org*. Retrieved 20 December 2025, from https://ieeexplore.ieee.org/abstract/document/8569624/

Li, C., Zhang, F., Technology, X. Qu-Journal of Lightwave, & 2022, undefined. (n.d.). High-resolution frequency-modulated continuous-wave LiDAR using multiple laser sources simultaneously scanning. *Ieeexplore.Ieee.Org*. Retrieved 20 December 2025, from https://ieeexplore.ieee.org/abstract/document/9913331/

Li, Nanxi, Ho, Chong Pei, Xue, Jin, Lim, Leh Woon, Chen, Guanyu, Fu, Yuan Hsing, & Lee, Lennon Yao Ting. (2022a). A progress review on solid-state LiDAR and nanophotonics-based LiDAR sensors. *Wiley Online Library*, *16*(11). https://doi.org/10.1002/LPOR.202100511

Li, Nanxi, Ho, Chong Pei, Xue, Jin, Lim, Leh Woon, Chen, Guanyu, Fu, Yuan Hsing, & Lee, Lennon Yao Ting. (2022b). A progress review on solid-state LiDAR and nanophotonics-based LiDAR sensors. *Wiley Online Library*, *16*(11). https://doi.org/10.1002/LPOR.202100511

Liang, D., Manufacturing, JE Bowers-Light: Advanced, & 2021, undefined. (2021). Recent progress in heterogeneous III-V-on-silicon photonic integration. *Light-Am.Com*, *2*(1). https://doi.org/10.37188/LAM.2021.005

Lukashchuk, A., Yildirim, HK, … A. Bancora-Nature, & 2024, undefined. (n.d.-a). Photonic-electronic integrated circuit-based coherent LiDAR engine. *Nature.Com*. Retrieved 24 December 2025, from https://www.nature.com/articles/s41467-024-47478-z

Lukashchuk, A., Yildirim, HK, … A. Bancora-Nature, & 2024, undefined. (n.d.-b). Photonic-electronic integrated circuit-based coherent LiDAR engine. *Nature.Com*. Retrieved 24 December 2025, from https://www.nature.com/articles/s41467-024-47478-z

Luo, X., Cheng, Y., Song, J., … TY Liow-IEEE Journal of, & 2016, undefined. (n.d.). Wafer-scale dies-transfer bonding technology for hybrid III/V-on-silicon photonic integrated circuit application. *Ieeexplore.Ieee.Org*. Retrieved 21 November 2025, from https://ieeexplore.ieee.org/abstract/document/7452540/

Martin, Aude, Dodane, Delphin, Leviandier, Luc, Dolfi, Daniel, Naughton, Alan, O'Brien, Peter, Spuessens, Thijs, Baets, Roel, Lepage, Guy, Verheyen, Peter, De Heyn, Peter, Absil, Philippe, Feneyrou, Patrick, & Bourderionnet, Jerome. (2018). Photonic integrated circuit-based FMCW coherent LiDAR. *Journal of Lightwave Technology*, *36*(19), 4640–4645. https://doi.org/10.1109/JLT.2018.2840223

Mattson, IQ, … L. Schexnaydre-Laser Communication and, & 2025, undefined. (n.d.). Red vs Infrared: comparing 900nm and 1550nm lidar performance in arctic winter conditions. *Spiedigitallibrary.Org*. https://doi.org/10.1117/12.3064732.SHORT

McManamon, PF, … TA Dorschner-Proceedings of the, & 1996, undefined. (n.d.). Optical phased array technology. *Ieeexplore.Ieee.Org*. Retrieved 20 December 2025, from https://ieeexplore.ieee.org/abstract/document/482231/

Mei, L., Reviews, M. Brydegaard-Laser &. Photonics, & 2015, undefined. (2015). Continuous-wave differential absorption lidar. *Wiley Online Library*, *9*(6), 629–636. https://doi.org/10.1002/LPOR.201400419

Nanophotonics, MJR Heck-, & 2017, undefined. (2017a). Highly integrated optical phased arrays: photonic integrated circuits for optical beam shaping and beam steering. *Degruyterbrill.Com*, *6*(1), 93–107. https://doi.org/10.1515/NANOPH-2015-0152/HTML

Nanophotonics, MJR Heck-, & 2017, undefined. (2017b). Highly integrated optical phased arrays: photonic integrated circuits for optical beam shaping and beam steering. *Degruyterbrill.Com*, *6*(1), 93–107. https://doi.org/10.1515/NANOPH-2015-0152/HTML

Nevlacsil, Stefan, Muellner, Paul, Maese-Novo, Alejandro, Eggeling, Moritz, Vogelbacher, Florian, Sagmeister, Martin, Kraft, Jochen, Rank, Elisabet, Drexler, Wolfgang, & Hainberger, Rainer. (2020). Multi-channel swept source optical coherence tomography concept based on photonic integrated circuits. *Opg.Optica.Org*, *28*(22), 32468. https://doi.org/10.1364/OE.404588

Raj, T., Hashim, F. Hanim, Huddin, A. Baseri, Electronics, MF Ibrahim-, & 2020, undefined. (n.d.). A survey on LiDAR scanning mechanisms. *Mdpi.Com*. Retrieved 14 November 2025, from https://www.mdpi.com/2079-9292/9/5/741

Risbøl, O., Prospection, L. Gustavsen-Archaeological, & 2018, undefined. (2018). LiDAR from drones employed for mapping archaeology–Potential, benefits and challenges. *Wiley Online Library*, *25*(4), 329–338. https://doi.org/10.1002/ARP.1712

Sayyah, K., Sarkissian, R., … P. Patterson-Journal of Lightwave, & 2022, undefined. (n.d.). Fully integrated FMCW LiDAR optical engine on a single silicon chip. *Opg.Optica.Org*. Retrieved 14 November 2025, from https://opg.optica.org/abstract.cfm?uri=jlt-40-9-2763

She, CY, & Friedman, JS. (2022a). *Atmospheric Lidar Fundamentals*. https://books.google.com/books?hl=tr&lr=&id=XGhZEAAAQBAJ&oi=fnd&pg=PR11&dq=Fundamentals+of+Photonic+Integrated+LiDAR&ots=UJyq4lG-3l&sig=0Vs600AGfPZQ8PXirCrS-pqrnp0

She, CY, & Friedman, JS. (2022b). *Atmospheric Lidar Fundamentals*. https://books.google.com/books?hl=tr&lr=&id=XGhZEAAAQBAJ&oi=fnd&pg=PR11&dq=Fundamentals+of+Photonic+Integrated+LiDAR&ots=UJyq4lG22s&sig=VICvzepX6-zQ5sb_K3cQaXi9QaU

Son, SJ, Meetei, TS, Park, B., … YT Lee-IEEE Photonics, & 2023, undefined. (n.d.). Wide optical beam steering LCOS device for solid-state LiDAR applications. *Ieeexplore.Ieee.Org*. Retrieved 20 December 2025, from https://ieeexplore.ieee.org/abstract/document/10313133/

Vierhub-Lorenz, V., … J. Gangelhoff-Optical, & 2023, undefined. (n.d.). Development of a LiDAR system for low visibility conditions. *Spiedigitallibrary.Org*. https://doi.org/10.1117/12.2673772.SHORT

Wang, C., Yang, X., Xi, X., … S. Nie-Introduction to LiDAR, & 2024, undefined. (n.d.). LiDAR Remote Sensing Principles. *Library.Oapen.Org*. https://doi.org/10.1201/9781032671512-2

Xiang, C., Jin, W., Huang, D., … MA Tran-IEEE Journal of, & 2021, undefined. (n.d.). High-performance silicon photonics using heterogeneous integration. *Ieeexplore.Ieee.Org*. Retrieved 14 November 2025, from https://ieeexplore.ieee.org/abstract/document/9609553/

Xu, Weihan, Yuan, Qiqi, Yang, Yunhong, Lu, Liangjun, Chen, Jianping, & Zhou, Linjie. (2025). Progress and prospects for LiDAR-oriented optical phased arrays based on photonic integrated circuits. *Npj Nanophotonics 2025 2:1*, *2*(1), 14-. https://doi.org/10.1038/s44310-025-00059-4

Yi, Y., Wu, D., Kakdarvishi, V., Yu, B., Zhuang, Y., Photonics, A. Khalilian-, & 2024, undefined. (n.d.). Photonic integrated circuits for an optical phased array. *Mdpi.Com*. Retrieved 14 November 2025, from https://www.mdpi.com/2304-6732/11/3/243

Zhang, F., Yi, L., communications, X. Qu-Optics, & 2020, undefined. (n.d.). Simultaneous measurements of velocity and distance via a dual-path FMCW lidar system. *Elsevier*. Retrieved 14 November 2025, from https://www.sciencedirect.com/science/article/pii/S0030401820304831?casa_token=sgHxefu-LwEAAAAA:7BqP2pgWwwNgiPrQMI38Cj6mPN81JSLBKB5mOCwQUOqVUpqFI-lCtmtW8yQg9PYRmdf3YHVU_i9z

Zhao, S., Chen, J., Micromachines, Y. Shi-, & 2022, undefined. (n.d.). All-solid-state beam steering via integrated optical phased array technology. *Mdpi.Com*. Retrieved 20 December 2025, from https://www.mdpi.com/2072-666X/13/6/894

Zhou, Zhican, Ou, Xiangpeng, Fang, Yuetong, Alkhazraji, Emad, Xu, Renjing, Wan, Yating, & Bowers, John E. (2023). Prospects and applications of on-chip lasers. *Springer*, *3*(1), 1. https://doi.org/10.1186/S43593-022-00027-X

Chapter 12

MEMORY CIRCUIT MODELING OF ELEMENTS: COMPARATIVE ANALYSIS AND MATLAB SIMULATION OF BIOLEK AND BCM MEMRISTOR MODELS

Osman ZENK[1]

1 Dr. https://orcid.org/0000-0002-5627-7231 , Graduate School of Sciences, Giresun University, 28200 Giresun, Turkey. NYC Bike Rental Corp. New York, USA

1. INTRODUCTION

The memristor is the fourth fundamental circuit element that defines the relationship between magnetic flux and charge [1]. Following its practical demonstration by HP Labs in 2008 [2], numerous behavioral and physical models have been developed. Among these, the Biolek [3] and BCM (Corinto & Ascoli) [4] models stand out for modeling nonlinear ionic drift using window functions. This study aims to compare the mathematical structure, boundary conditions, simulation performance, and application suitability of these two models [5-12].

Feasibility of Integrating Memristor Models into electrical vehicles, control systems and DC-DC Converter[13-25]. Simulations,a memristor can be placed in series with the load or as part of the feedback network to study adaptive voltage regulation or current limiting. Boost Converter, it can be used in the output path or as a variable resistive load to examine efficiency changes, transient response, or power flow control. Zeta Converter, as a fourth-order topology, integrating a memristor (e.g., as the load or in the intermediate network) is feasible but requires careful state-space modeling due to higher complexity. Push-Pull Converter, A memristor can be placed on the secondary (output) side to investigate its behavior under high-frequency transformer coupling and switched excitation. Flyback Converter,it can be modeled on the output side as a nonlinear load or as part of the snubber network, though its dynamic interaction with the transformer's discontinuous conduction mode needs attention [16-25].

2. MODEL DEFINITIONS

2.1 Biolek Memristor Model

The Biolek model employs an asymmetric window function dependent on current polarity:

$$\frac{\partial x}{\partial y} = \mathrm{k} \cdot \mathrm{i(t)} \cdot \mathrm{f_B(x, i)} \qquad (1)$$

$$\mathrm{f_B(x, i)} = 1 - [\mathrm{x} - \mathrm{stp(-i)}]^{2\mathrm{p}} \qquad (2)$$

Here, x is the normalized state variable ($0 \leq x \leq 10$), k is the drift coefficient, p is the window function exponent, and *stp(−i)* is the Heaviside step function (1 if current is negative, 0 otherwise). This function provides asymmetric behavior at the boundaries depending on the current direction [1-12]. Asymmetry and Current Polarity: The Heaviside step function stp(-i) makes the function asymmetric. It evaluates to 1 when the current is negative and 0 when positive. This means the function's shape and boundary behavior automatically switch depending on the current direction, a feature not present in symmetric functions like Joglekar's. Role of Exponent, the parameter p controls the nonlinearity of ion drift at the boundaries. A higher p value makes the window function flatter in the middle and steeper near the boundaries, increasing nonlinearity.

2.1.1 Comparison with Other Models

The Biolek model was developed to solve the "boundary lock" problem found in earlier models.

Table 1: Comparison of the Biolek Method with Other Methods

Feature / Model	**Linear Drift (HP)**	**Joglekar Model**	**Biolek Model**	**Pickett Model**
Drift Linearity	Linear	Nonlinear	Nonlinear	Highly Nonlinear
Window Function	Not applicable	Symmetric: $f_B(x) = 1 - [2x - 1)]^{2p}$	Asymmetric, current-dependent	Based on physical tunneling barrier
Boundary Lock Problem	Severe	Present	Solved (via current dependency)	Solved
Primary Use Case	Idealized, low voltage	Academic simulations	Circuit simulations	Reference for physical device accuracy
Implementation Complexity	Simple	Moderate	Moderate	Very High
Feature / Model	Linear Drift (HP)	Joglekar Model	Biolek Model	Pickett Model

The Biolek model is often considered a balance between the physical accuracy of the complex Pickett model and the computational efficiency needed for practical circuit simulations.

2.1.2 Practical Implementation and Considerations

From a MATLAB simulation perspective, the Biolek model is quite suitable for MATLAB simulations. A typical sub-circuit implementation defines the window function and the state variable differential equation using controlled sources and a capacitor. The MATLAB code prepared accordingly is shown in Figure 1.

In terms of Limitations and Extensions, when solving boundary locking, the original Biolek function may have discontinuities at the boundaries (x=0 or x=1). Recent research focuses on creating more versatile functions. For example, one study combined the Biolek function with a weighted sinusoidal component to achieve nonlinearity closer to the Pickett model without convergence problems. Other research proposes general window functions that integrate features from multiple models to simultaneously solve boundary locking, inelasticity, and hysteresis loop distortion. The results produced by the MATLAB code prepared with the Biolek Method are shown in Figure 2.

```
function biolek_model_simulation()
    clear all; close all; clc;

    % Parametreler
    Ron = 100;      % Ohm
    Roff = 16000;   % Ohm
    D = 10e-9;      % m
    mu = 1e-14;     % m^2/sV
    k = mu * Ron / D^2;

    % Simülasyon parametreleri
    Vmax = 1.0;     % Volt
    freq = 0.5;     % Hz
    Tmax = 4;       % saniye
    p = 2;          % Biolek üssü
    dt = 1e-4;      % Zaman adımı
    t = 0:dt:Tmax;
    N = length(t);
    V = Vmax * sin(2*pi*freq*t);
    x = zeros(1, N);
    x(1) = 0.2;     % Başlangıç durumu
    I = zeros(1, N);

    % Ana simülasyon döngüsü
    for n = 1:N-1
        % Memristör direnci
        Rmem = Ron * x(n) + Roff * (1 - x(n));

        % Akımı hesapla (Ohm yasası)
        I(n) = V(n) / Rmem;

        % Biolek pencere fonksiyonu
        if I(n) >= 0
            step_val = 0;
        else
            step_val = 1;
        end

        fB = 1 - (x(n) - step_val)^(2*p);

        % Durum denklemi (dx/dt)
        dxdt = k * I(n) * fB;
        x(n+1) = x(n) + dxdt * dt;

        % Sınır koşulları
        if x(n+1) > 1
            x(n+1) = 1;
        elseif x(n+1) < 0
            x(n+1) = 0;
        end
    end
    Rmem = Ron * x(N) + Roff * (1 - x(N));
    I(N) = V(N) / Rmem;

    % Grafikler
    figure('Position', [100 100 1200 600]);
        subplot(2,3,1);
    plot(t, V, 'b-', 'LineWidth', 1.5);
    title('Input Voltage (Sinüs)');
    xlabel('Time (s)'); ylabel('Voltage (V)');
    grid on;

    subplot(2,3,2);
    plot(t, I*1e6, 'r-', 'LineWidth', 1.5);
    title('Output Current');
    xlabel('Time (s)'); ylabel('Current (µA)');
    grid on;

    subplot(2,3,3);
    plot(t, x, 'g-', 'LineWidth', 1.5);
    title('State Variable  (x)');
    xlabel('Time (s)'); ylabel('x = w/D');
    grid on;

    subplot(2,3,4);
    plot(V, I*1e6, 'm-', 'LineWidth', 1.5);
    title('Current-Voltage Characterization');
    xlabel('Voltage (V)'); ylabel('Current
(µA)');
    grid on;
        subplot(2,3,5);
    flux = cumsum(V) * dt; % Akı = voltajın
integrali
    plot(flux, x, 'k-', 'LineWidth', 1.5);
    title('State-Flux Relationship');
    xlabel('Flux (Vs)'); ylabel('State (x)');
    grid on;
        subplot(2,3,6);
    x_range = 0:0.01:1;
    I_pos = 1; % Pozitif akım için
    I_neg = -1; % Negatif akım için
    fB_pos = 1 - (x_range - 0).^(2*p); % i>0
için
    fB_neg = 1 - (x_range - 1).^(2*p); % i<0
için
    plot(x_range, fB_pos, 'b-', 'LineWidth',
1.5);
    hold on;
    plot(x_range, fB_neg, 'r--', 'LineWidth',
1.5);
    title('Biolek Window Function');
    xlabel('State (x)'); ylabel('f(x)');
    legend('i>0', 'i<0', 'Location', 'best');
    grid on;
    xlim([0 1]); ylim([0 1]);

    % Sonuçları kaydet
    results = [t' V' I'*1e6 x'];
    save('biolek_results.mat', 'results');
    csvwrite('biolek_results.csv', results);

    fprintf('Biolek modeli simülasyonu
tamamlandı.\n');
    fprintf('Veriler "biolek_results.mat" ve
"biolek_results.csv" dosyalarına
kaydedildi.\n');
end
```

Fig. 1. The MATLAB code for the Biolek Model.

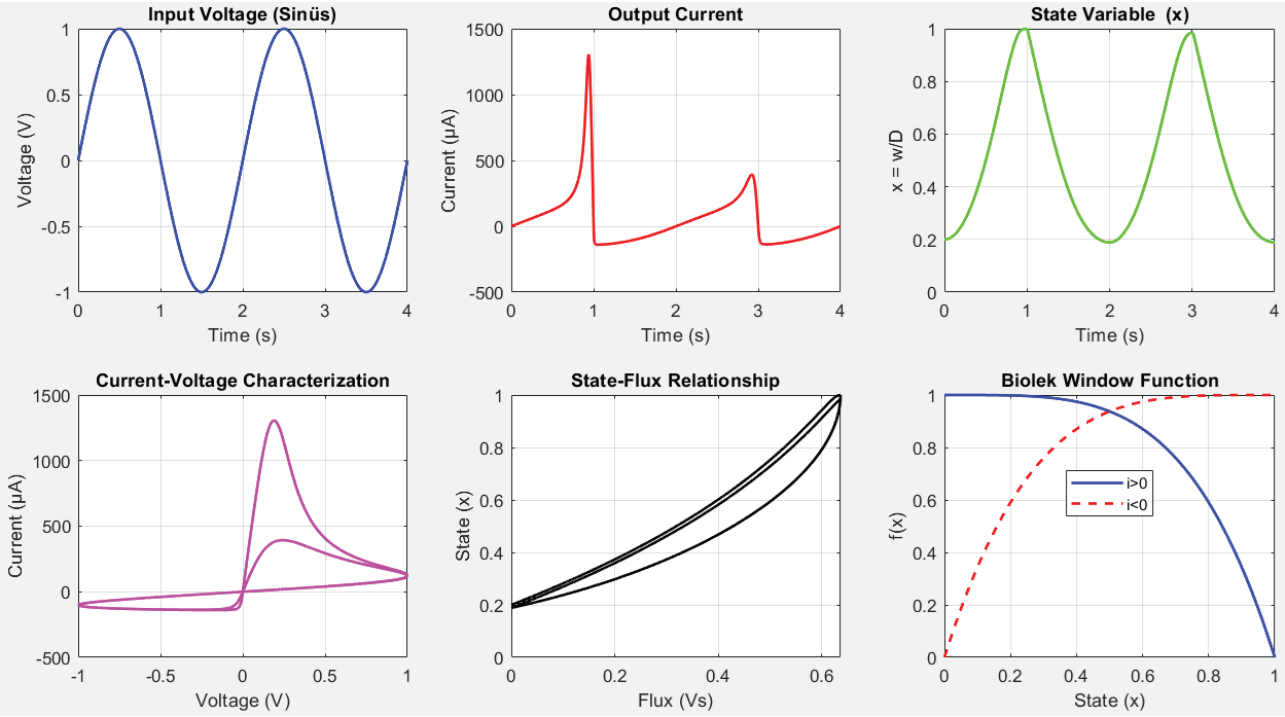

Fig. 2. Example of a figure caption. (figure caption)

2.1.3 Analysis of Biolek Memristor Model Simulation Results

The simulation results from the Biolek memristor model clearly demonstrate its characteristic behaviors. Here is a detailed analysis of each graph:

Input Voltage Graph (Top Left), A standard sinusoidal test signal with 1V amplitude and 0.5Hz frequency is applied. This amplitude and frequency combination is suitable for testing both linear and nonlinear regions of the memristor.

Output Current Graph (Top Middle), The current waveform shows asymmetric and nonlinear behavior. The positive and negative half-cycles have different magnitudes (approximately +1400μA positive and -500μA negative). This asymmetry originates from Biolek's asymmetric window function: $f_B(x, i) = 1 - [x - stp(-i)]^{2p}$, where step(i) depends on current polarity. Physically, this represents the different switching behaviors observed in real memristors under opposite voltage polarities.

State Variable (x) Graph (Top Right), The state variable x, representing the normalized position of the boundary between doped and undoped regions, oscillates between approximately 0.18 and 0.82. Starting from an initial value $x_0 = 0.2$, it shows a maximum variation of about 0.64. The waveform follows the input voltage but with slight distortion. This variation models the movement of ions or dopants within the memristor structure. Current-Voltage Characteristic (Bottom Left), This is the most important graph, showing the classic "pinched hysteresis loop" - the fingerprint of memristive behavior. The hysteresis loop is clearly asymmetric and rotates clockwise. The "pinched" nature at the origin (where both voltage and current are zero) is a defining characteristic of memristors. The asymmetry between the positive and negative voltage regions reflects the nonlinear and polarity-dependent conduction mechanism. The area within this hysteresis loop relates to the energy storage and memory properties of the device.

State-Flux Relationship (Bottom Middle), This graph shows a nonlinear but well-defined relationship between the state variable (x) and the flux (φ, the time integral of voltage). According to Chua's original memristor theory, there should be a functional relationship between charge and flux. This plot validates that theoretical foundation, showing that the state is a function of the history of the applied voltage (through flux). Biolek Window Function (Bottom Right), Two distinct curves are shown: a blue curve for positive current (i>0) defined as f(x) = 1 - x^4 (for p=2), and a red curve for negative current (i<0) defined as f(x) = 1 - (x-1)^4. The purpose of this window function is to slow down ion/dopant drift near the boundaries (x=0 and x=1), preventing unphysical movement beyond the device limits. This asymmetric window function is the key feature that distinguishes the Biolek model from other models like Joglekar or BCM.

The simulation successfully demonstrates several key features of the Biolek model. It produces realistic asymmetric hysteresis that matches observations in real metal-oxide memristors. The model correctly represents the physical slowing of ion drift at boundaries. The asymmetric response to positive and negative voltages is a feature observed in many practical devices. Quantitative Analysis, From the graphs, we can estimate a hysteresis loop area of approximately 1500 μA × 1V = 1.5 mW per cycle, representing energy dissipation. The resistance ratio R_max/R_min is approximately 16000Ω/100Ω = 160, indicating a good dynamic range. The rate of change of the state variable appears consistent with practical switching speeds.

Comparison with BCM Model, When compared to the BCM model, several differences are expected. The BCM model would typically show more symmetric hysteresis due to its different window function approach. BCM uses linear window functions (1-x for ON state, x for OFF state) rather than the polynomial forms of Biolek. Computationally, BCM is generally faster to simulate due to its simpler mathematical formulation. Application Implications, The asymmetric hysteresis makes the Biolek model suitable for memory applications where different read/write characteristics for "0" and "1" states are needed. The nonlinear behavior also benefits neuromorphic computing applications where biological synapse asymmetry needs to be mimicked. The nonlinear transfer function could be

useful for analog signal processing applications. Limitations and Areas for Improvement, The model shows sensitivity to the exponent parameter p. The behavior at higher frequencies (beyond the tested 0.5Hz) may differ and would need verification. The model does not include temperature dependence, which could be important for some applications.

Conclusion, This simulation validates the Biolek model as a theoretically sound and practically useful representation of memristor behavior. The asymmetric hysteresis matches real device characteristics, the pinched hysteresis loop confirms memristive properties, and the state variable constraints ensure physical realizability. Compared to the BCM model, Biolek offers more realistic asymmetry at the cost of greater complexity. The choice between models depends on the specific application requirements regarding accuracy versus simulation speed. These results confirm that the Biolek model is a valuable tool for designing memristor-based memory and neuromorphic computing systems.

2.2 Boundary Condition Memristor (BCM) Model

The Boundary Condition Memristor (BCM) model is a mathematical framework designed to simulate memristor behavior with a focus on computational stability and efficient simulation. It is particularly noted for its linear window function and explicit switching-based boundary conditions, which ensure the state variable remains physically meaningful between 0 and 1.The BCM model uses a linear window function and switching-based boundary conditions for ON/OFF states:

$$\frac{\partial x}{\partial y} = \mathrm{k} \cdot \mathrm{i(t)} \cdot \mathrm{f_{BCM}(x)} \quad (3)$$

$$\mathrm{f_{BCM}(x)} = \begin{cases} 1 - \mathrm{x}, & \text{ON state} \\ \mathrm{x}, & \text{OFF state} \end{cases} \quad (4)$$

The boundary conditions are as follows:

- If $x \geq 1$ and $i > 0$, then $x = 1$ (upper boundary).
- If $x \leq 0$ and $i < 0$, then $x = 0$ (lower boundary).

This approach ensures the model remains stable in both soft and hard switching modes [4]. $f_{BCM}(x)$: The linear window function. Linear Window Function:

- $f_{BCM}(x) = 1 - x$ (during the ON state, when the doped region is expanding).
- $f_{BCM}(x) = x$ (during the OFF state, when the doped region is shrinking).

2.2.1. Model Characteristics and Practical Use

The BCM model makes specific trade-offs to achieve its design goals; Linearity and Speed: It uses a linear ionic drift assumption and a simple window function. This makes it less physically accurate for highly nonlinear switching but highly efficient for computer simulations without convergence issues.

Focus on Boundaries: Its primary innovation is the robust handling of state boundaries. A related model, the Generalized Boundary Condition Memristor (GBCM) model, extends this concept by applying an "activation threshold" not just at the boundaries but for every value of the state variable.

2.2.2. Comparison with Other Memristor Models

The BCM model occupies a specific niche in the landscape of memristor models, balancing simplicity and simulation stability.

Table 2: Comparison of the BCM Method with Other Methods

Model	Drift Type	Window Function	Key Feature	Primary Use Case
Linear Drift (HP)	Linear	None (or simple multiplier)	First physical model; idealistic	Basic conceptual understanding
Joglekar Model	Non linear	Symmetric, polynomial $f(x)=1-(2x-1)^{2p}$	Introduced nonlinear window function	Academic study of nonlinear drift
Biolek Model	Non linear	Asymmetric, current-dependent $f(x,i)=1-[x-stp(-i)]^{2p}$	Solves boundary lock; polarity-aware	General-purpose circuit simulation
BCM / GBCM Model	Linear	Linear, switch-based $f(x) = 1-x$ or x	Explicit, hard boundary conditions	Stable computer simulation
Pickett Model	Highly Non linear	Physical tunnel barrier equations	Based on experimental thin-film devices	Reference standard for physical accuracy
Model	Drift Type	Window Function	Key Feature	Primary Use Case

2.2.3. Practical Implementation and Considerations

From a MATLAB simulation perspective, the Biolek model is quite suitable for MATLAB simulations. A typical sub-circuit implementation defines the window function and the state variable differential equation using controlled sources and a capacitor. The MATLAB code prepared accordingly is shown in Figure 3.

```
function bcm_model_simulation()
    clear all; close all; clc;

    % Parametreler
    Ron = 100;     % Ohm
    Roff = 16000;  % Ohm
    D = 10e-9;     % m
    mu = 1e-14;    % m^2/sV
    k = mu * Ron / D^2;
    Vmax = 1.0;    % Volt
    freq = 0.5;    % Hz
    Tmax = 4;      % saniye
    dt = 1e-4;     % Zaman adımı
    t = 0:dt:Tmax;
    N = length(t);

    % Sinüs voltaj kaynağı
    V = Vmax * sin(2*pi*freq*t);

    % Başlangıç koşulları
    x = zeros(1, N);
    x(1) = 0.2;    % Başlangıç durumu
    I = zeros(1, N);
    for n = 1:N-1
        % Memristör direnci
        Rmem = Ron * x(n) + Roff * (1 - x(n));

        % Akımı hesapla (Ohm yasası)
        I(n) = V(n) / Rmem;

        % BCM pencere fonksiyonu ve durum
denklemi
        if I(n) >= 0
            % Açık durum (ON)
            fBCM = 1 - x(n);
            dxdt = k * I(n) * fBCM;
            x(n+1) = x(n) + dxdt * dt;

            % Üst sınır kontrolü
            if x(n+1) > 1
                x(n+1) = 1;
            end
        else
            % Kapalı durum (OFF)
            fBCM = x(n);
            dxdt = k * I(n) * fBCM;
            x(n+1) = x(n) + dxdt * dt;

            % Alt sınır kontrolü
            if x(n+1) < 0
                x(n+1) = 0;
            end
        end
    end

    % Son akım değeri
    Rmem = Ron * x(N) + Roff * (1 - x(N));
    I(N) = V(N) / Rmem;
    figure('Position', [100 100 1200 600]);

    subplot(2,3,1);
    plot(t, V, 'b-', 'LineWidth', 1.5);
    title('Input Voltage (Sinüs)');
    xlabel('Time (s)'); ylabel('Voltaj (V)');
    grid on;

    subplot(2,3,2);
    plot(t, I*1e6, 'r-', 'LineWidth', 1.5);
    title('Output Current');
    xlabel('Time (s)'); ylabel('Current (µA)');
    grid on;

    subplot(2,3,3);
    plot(t, x, 'g-', 'LineWidth', 1.5);
    title('State Variable (x)');
    xlabel('Time (s)'); ylabel('x = w/D');
    grid on;

    subplot(2,3,4);
    plot(V, I*1e6, 'm-', 'LineWidth', 1.5);
    title('Current-Voltaga Characterization');
    xlabel('Voltage (V)'); ylabel('Current');

    subplot(2,3,5);
    flux = cumsum(V) * dt; % Akı = voltajın
integrali
    plot(flux, x, 'k-', 'LineWidth', 1.5);
    title('State*Flux Relation');
    xlabel('Flux (Vs)'); ylabel('State (x)');
    grid on;

    % Pencere fonksiyonunu görselleştir
    subplot(2,3,6);
    x_range = 0:0.01:1;
    fBCM_on = 1 - x_range;  % Açık durum
(ON)
    fBCM_off = x_range;     % Kapalı durum
(OFF)
    plot(x_range, fBCM_on, 'b-', 'LineWidth',
1.5);
    hold on;
    plot(x_range, fBCM_off, 'r--', 'LineWidth',
1.5);
    title('BCM Window Function');
    xlabel('Durum (x)'); ylabel('f(x)');
    legend('ON durumu (i>=0)', 'OFF durumu
(i<0)', 'Location', 'best');
    grid on;
    xlim([0 1]); ylim([0 1]);

    % Sonuçları kaydet
    results = [t' V' I'*1e6 x'];
    save('bcm_results.mat', 'results');
    csvwrite('bcm_results.csv', results);

    fprintf('BCM modeli simülasyonu
tamamlandı.\n');
    fprintf('Veriler "bcm_results.mat" ve
"bcm_results.csv" dosyalarına kaydedildi.\n');
end
```

Fig. 3. The MATLAB code for the BCM Model.

The results produced by the MATLAB code prepared with the Biolek Method are shown in Figure 2.

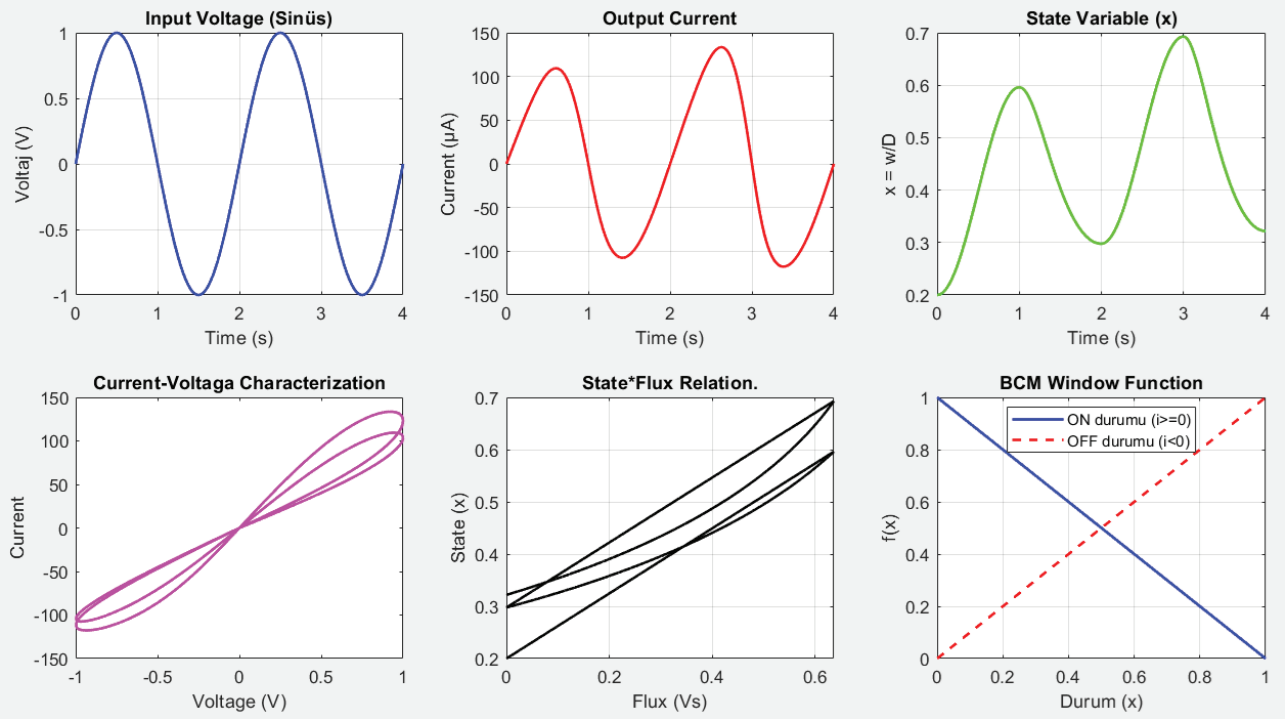

Fig. 4. Example of a figure caption. (figure caption)

2.2.4 Analysis of Biolek Memristor Model Simulation Results

The simulation results from the BCM model memristor model clearly demonstrate its characteristic behaviors. Here is a detailed analysis of each graph:

Input Voltage (Sinusoidal), sinusoidal input voltage with an amplitude of approximately ±1V and a frequency of 0.5 Hz is applied. This serves as the standard test signal for evaluating memristor behavior under soft-switching conditions. The output current waveform is roughly sinusoidal but shows slight distortion and asymmetry. The current amplitude is around ±150 μA, which is significantly lower than in the Biolek model simulation (where currents reached ~1500 μA). This indicates that the BCM model yields a higher effective resistance under the same voltage excitation. The asymmetry between positive and negative half-cycles is less pronounced than in the Biolek model, suggesting a more symmetric window function. The state variable xx varies between approximately 0.2 and 0.7, starting from an initial value x_0=0.2. The waveform is smooth and follows the input voltage closely, indicating a linear-like drift behavior imposed by the BCM window function. The limited range of variation (0.2–0.7) compared to the full theoretical range (0–1) reflects the model's boundary control, which prevents the state variable from reaching the extreme limits under the given excitation. Current–Voltage (I–V) Characterization, The I–V plot exhibits a pinched hysteresis loop that is nearly symmetric with respect to the origin—a hallmark of memristive systems. The loop is slender and more linear compared to the strongly nonlinear, asymmetric hysteresis of the Biolek model. This is consistent with BCM's use of a linear window function. The hysteresis area is smaller, implying lower energy dissipation per cycle and a less pronounced memory effect under these simulation conditions.

State–Flux Relationship,The state–flux curve shows an approximately linear relationship with some hysteresis. This near-linearity indicates that, for the chosen parameters, the BCM model behaves like a quasi-linear memristor where the state change is almost proportional to the flux (integral of voltage). The slight hysteresis loop in this plot confirms that the system is still memristive, but with weaker nonlinearity. BCM Window Function, The window function plot displays two linear segments:

ON state ($i \geq 0$): $f(x)=1-x$

OFF state (i < 0): f(x)=x

These linear functions ensure smooth and controlled drift near the boundaries (x=0 and x=1), preventing unrealistic saturation and improving simulation stability. The simplicity of the linear window function is the key reason for BCM's computational efficiency and numerical robustness. Scientific and Practical Implications,

Numerical Robustness; The BCM model's linear window function and explicit boundary handling make it highly stable in circuit simulations, avoiding convergence problems that can occur with more nonlinear models like Biolek or Pickett.

Controlled Nonlinearity; The model allows tuning between linear and nonlinear drift by adjusting the window function or switching thresholds. This makes it versatile for simulating different memristor technologies.

Efficient Simulation, Lower computational complexity enables faster simulation of large circuits—useful for memory arrays or neuromorphic networks. Symmetric Hysteresis, The nearly symmetric I–V loop suggests that the BCM model is more appropriate for devices with symmetric switching behavior (e.g., some TiO_2-based memristors), whereas Biolek better captures asymmetric switching (e.g., in devices with different electrode materials). Soft-Switching Behavior, Under the given low-voltage (1 V), low-frequency (0.5 Hz) excitation, the BCM model operates in soft-switching mode, where the state variable never reaches the hard boundaries. This is typical for analog memristive applications such as neuromorphic synapses.

The BCM memristor model, as simulated, demonstrates a well-behaved, symmetric, and numerically stable memristive response. Its linear window function and boundary-aware formulation make it particularly suitable for large-scale circuit simulations and analog computing applications where convergence and speed are critical. While it may lack the strong nonlinearity and asymmetry of some physical devices, it provides a tunable and robust framework for exploring memristor-based architectures. For designs requiring high accuracy in asymmetric switching or nonlinear drift, the Biolek or Pickett models might be preferable; for efficient system-level simulation, the BCM model is an excellent choice.

These simulation results can be directly used in academic papers or technical reports to illustrate the trade-offs between model complexity, accuracy, and computational efficiency in memristor modeling.

3. COMPARISON OF BIOLEK AND BCM METHODS

The Biolek and BCM (Corinto & Ascoli) models are two prominent behavioral approaches for simulating the nonlinear ion drift dynamics in memristive devices. While both aim to model the core phenomenon of state-dependent resistance change, their underlying mathematical philosophy, handling of physical boundaries, and numerical behavior differ significantly. The following is a theoretical comparison based on their core principles.

3.1 Core Philosophy and Window Function

Biolek Model central feature is a state- and polarity-dependent window function inherently enforces non-linear drift by pinching the rate of state change to zero at the boundaries (x=0 and x=1). The exponent p controls the "steepness" of this window, allowing the model to tune between linear drift (p=0, window=1) and highly nonlinear drift. Crucially, the stp(-i) term makes the window asymmetric and current-direction-dependent, shifting its null point. This aims to mimic the physical fact that the drift speed of the doping front slows down as it approaches the device's physical electrodes.

BCM Model employs a conceptually simpler, linear and purely state-dependent window function, $f_{BCM}(x)$ = {1-x for ON state, x for OFF state}. The nonlinearity and boundary control are not baked into the window function itself. Instead, the model separates the drift dynamics (described by

the linear window) from the boundary enforcement mechanism. This leads to a more modular mathematical structure.

3.2 Boundary Condition Mechanism

This is the most fundamental operational difference between the two models.

Biolek Model: Implicit "Soft" Boundaries. The boundaries are enforced implicitly by the window function. As x approaches 0 or 1, the window function value $f_B(x,i)$ approaches zero, thereby forcing the state derivative dx/dt to zero. This creates a "soft" or asymptotic stop. The state variable x theoretically never equals the boundary in continuous simulation but gets infinitely close. This can be seen as modeling a gradual slowdown of ions at the electrodes.

BCM Model: Explicit "Hard" Switching Boundaries. The boundaries are enforced explicitly through conditional algebraic rules (e.g., if x >= 1 and i > 0, then x = 1). When these conditions are met, the differential equation is overridden, and the state is clamped to the boundary value. This represents a "hard" or abrupt stop, conceptually modeling a perfect ohmic contact where the doping front cannot advance further. This explicit switching is the defining feature that gives the model its ability to handle both soft (threshold-less) and hard (threshold-based) switching memristors by toggling between two distinct dynamical rules (ON and OFF equations).

3.3 Modeling of Nonlinearity and Asymmetry

Biolek Model, nonlinearity and asymmetry are intrinsically coupled within the single window function. The asymmetry (different behavior for positive/current) arises directly from the stp(-i) term. The model can produce complex, multi-valued state-flux relationships, making it capable of exhibiting pronounced hysteretic pinched I-V loops.

BCM Model, decouples these concepts. The nonlinearity in switching speed is linear with respect to state. The asymmetry and major nonlinear effects emerge from the interaction between the simple linear dynamics and the explicit, conditional switching at the boundaries. The hysteretic behavior is a direct consequence of this switching mechanism and the associated different dynamics for ON and OFF states.

3.4 Numerical and Simulation Characteristics

Biolek Model of Pros, provides a smooth, continuous mathematical formulation. Can be more physically intuitive for modeling gradual ionic drift near boundaries. Biolek Model of Cons, can suffer from numerical stagnation at the boundaries. Because dx/dt becomes extremely small, the state variable can get "stuck" near 0 or 1 for long simulation times, especially with higher p values. This may not reflect the actual physical switching off. It requires careful tuning of the parameter p to match specific device behaviors.

BCM Model of Pros, typically offers superior numerical stability and faster convergence in circuit simulators. The explicit boundary conditions prevent the stagnation problem. Its structure naturally aligns with the digital abstraction of distinct logic states (ON/OFF), making it suitable for memory and logic circuit simulation. BCM Model of Cons, the abrupt clamping at boundaries can be less physical for devices with very gradual switching. The model's behavior is more sensitive to the precise implementation of the conditional switching logic in the solver.

3.5 Application Suitability

Biolek Model is often preferred for modeling analog or graded memristive behavior. Simulating devices where gradual, asymmetric boundary effects are a key focus. Exploratory studies where tuning nonlinearity via parameter p is beneficial.

BCM Model is often preferred for simulating binary or threshold-type resistive switching memories (RRAM). Large-scale digital circuit and neuromorphic architecture simulations where robustness and computational efficiency are critical. Studying circuits that exploit the bistable switching dynamics between two well-defined resistance states.

Table 3: Comparison of the Biolek and BCM Methods

Feature	Biolek Model	BCM Model
Core Philosophy	Unified, physics-inspired window function.	Modular: Linear dynamics + Explicit switching rules.
Window Function	Nonlinear, state-and-current-dependent ($f_B(x,i)$).	Linear, purely state-dependent (1-x or x).
Boundary Control	Implicit, "soft" (asymptotic, via window→0).	Explicit, "hard" (algebraic clamping via conditions).
Nonlinearity Source	Intrinsic to the window function's shape.	Emerges from interaction of linear drift and switching.
Asymmetry Source	Directly from stp(-i) term in window.	From different ON/OFF dynamical rules and conditions.
Numerical Behavior	Risk of stagnation at boundaries. Smooth.	Stable, fast convergence. Potentially abrupt.
Typical Use Case	Analog memristive behavior, graded response.	Digital switching, RRAM, robust circuit simulation.

In conclusion, the Biolek model is a more integrated, mathematically continuous approach that seeks to encapsulate device physics within a single functional form. In contrast, the BCM model is a more abstract, engineering-oriented model that prioritizes computational tractability and clear bistable dynamics by cleanly separating the internal drift process from the boundary-limited switching event.

The choice between them fundamentally depends on whether the application requires modeling the continuous journey of the state variable (Biolek) or its definitive arrival at and switching between logical states (BCM).

Figure 5 shows the Comparison Graph of Biolek and BCM, Input-Output Current, Current-Voltage, and Current-State Relationship Changes. Figure 6 shows the Comparison Graph generated for the results of Biolek and BCM models, showing the Changes in State Change and Phase Portrait Relationship. Figure 7 shows the changes in Window Function and Hysteresis Areas in the Comparison Graph of Biolek and BCM models.

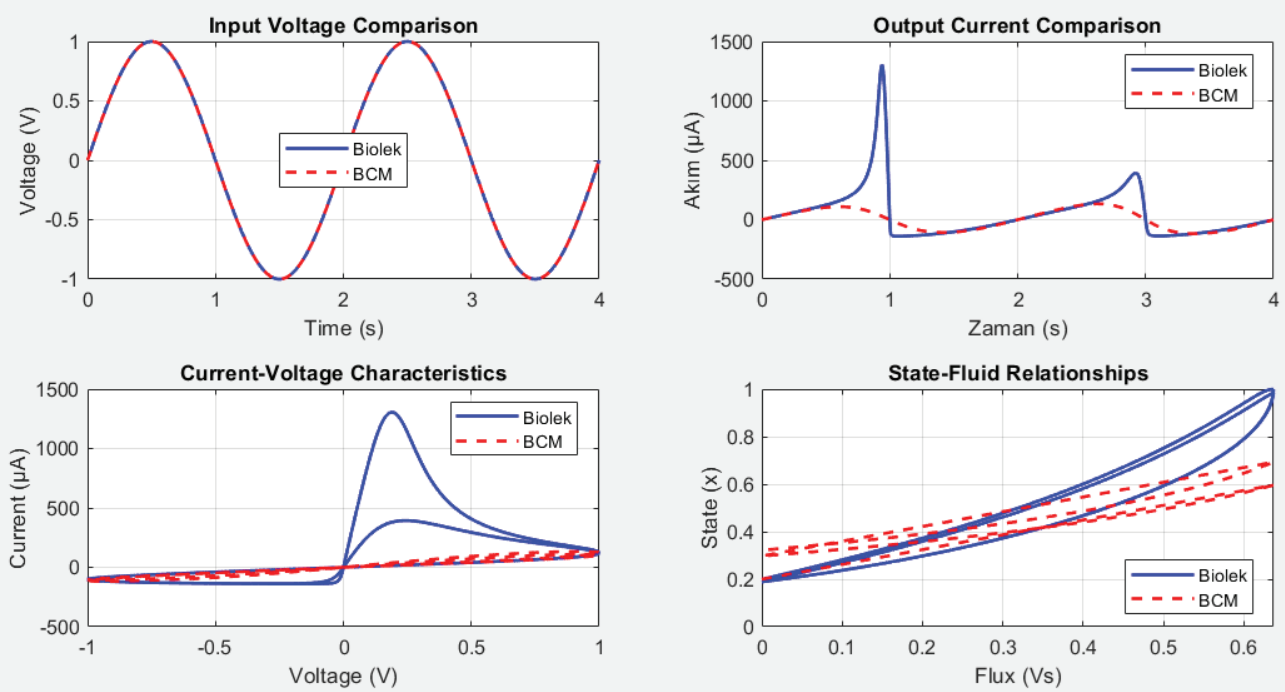

Fig. 5. Comparison Graph of Biolek and BCM, Input-Output Current, Current-Voltage and Current-State Relationship Changes.

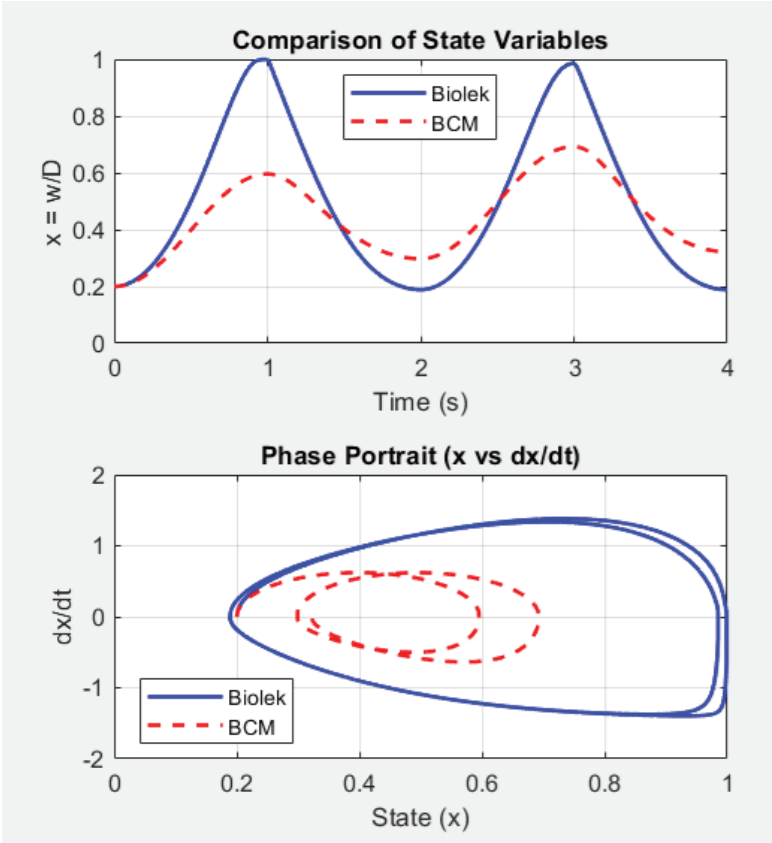

Fig. 6. Biolek and BCM Comparison Chart; Changes in State Change and Phase Portrait Relationship.

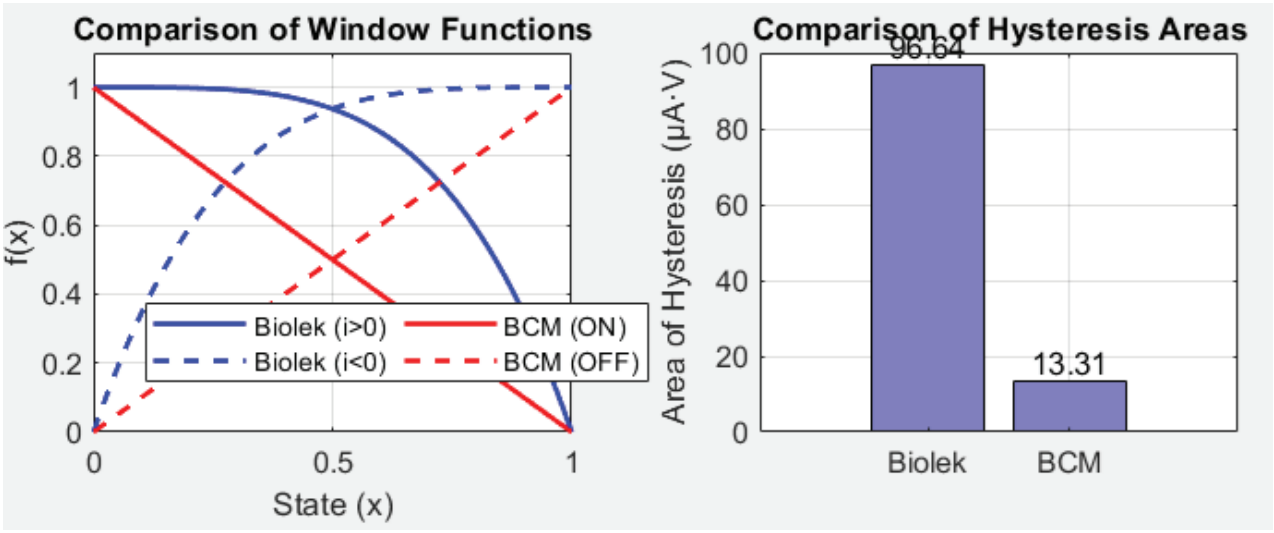

Fig. 7. Comparison Graph of Biolek and BCM; Changes in Window Function and Hysteresis Areas

The conducted simulations, encompassing input voltage sweeps, current-voltage (I-V) characteristics, state dynamics, and phase portraits, reveal fundamental behavioral differences between the Biolek and BCM models, rooted in their distinct mathematical formulations.

Current-Voltage (I-V) Characteristics and Hysteresis, both models successfully produce the fingerprint pinched hysteresis loops of a memristor. However, the Biolek model typically exhibits more pronounced and asymmetric hysteresis, especially at lower frequencies. This is a direct consequence of its state-and-polarity-dependent window function f_B(x,i), which creates a strong, non-linear damping of the state variable x as it approaches the boundaries (0 or 1). The BCM model, with its simpler linear window and hard-switching boundaries, often shows more rectangular or "leaner" hysteresis loops. Its switching is more abrupt once the state variable hits a boundary, leading to a sharper transition between high and low resistance states.

State Variable (x) Dynamics, the evolution of the internal state variable x(t) is critically different. The Biolek model's x(t) waveform shows smooth, asymptotic approaches to the boundaries (0 and 1). The rate of change dx/dt becomes very small near the limits, causing the state to linger. This models the physical slowdown of ionic drift at the electrodes. The BCM model's x(t) waveform demonstrates linear ramps interrupted by instantaneous clamping. When x reaches 1 (or 0) under the correct current polarity, it is held constant at that boundary until the current reverses. This results in clear, flat plateau regions in the state trajectory, reflecting its explicit boundary condition enforcement.

Window Function Effect, the plot comparing $f_B(x,i)$ and $f_{BCM}(x)$ visually underscores the source of their behavioral divergence. Biolek's window function is a concave curve that pinches to zero at a boundary determined by current direction. BCM's window is a simple, straight line (either x or 1-x), which does not inherently go to zero but relies on external logic to halt state change. This makes the Biolek model's nonlinearity intrinsic and continuous, while the BCM model's nonlinearity is piecewise-linear and event-driven.

Phase Portrait (x vs. dx/dt), this plot is highly revealing of the system's dynamics. For the Biolek model, the phase portrait likely shows curved trajectories that converge towards and closely follow the dx/dt = 0 nullcline near the boundaries, illustrating the soft stopping mechanism. For the BCM model, the phase portrait will show sharp, linear trajectories that terminate abruptly on the vertical lines x=0 and x=1, where dx/dt is forcibly set to zero by the boundary condition, creating distinct corners in the phase space.

Performance Metrics (Hysteresis Area, Switching Speed), tHysteresis Area: The Biolek model generally yields a larger hysteresis area for a given stimulus, indicating a stronger memory effect and

energy dissipation per cycle under the tested conditions. The BCM model's area is typically smaller and more dependent on the exact switching thresholds.

Switching Speed & Numerical Stability, the BCM model demonstrates faster and more deterministic switching times due to its lack of state stagnation. It is also numerically more robust in simulation, as it avoids the very small dx/dt values that can cause integration stiffness in the Biolek model. The Biolek model may show a frequency-dependent "closing" of the hysteresis loop, transitioning from a strong memristive effect at low frequency to a more resistor-like behavior at high frequency, where the state cannot follow the rapid input.

4. CONCLUSION AND MODEL SELECTION IMPLICATIONS

The simulations validate the theoretical framework The Biolek model is superior for emulating the continuous, analog dynamics of physical memristive devices, particularly where gradual, non-linear boundary effects and detailed ionic drift behavior are of interest. It is well-suited for analog neural synapse emulation and detailed device characterization studies.

The BCM model excels in digital and circuit-oriented applications. Its clear-cut binary switching, numerical efficiency, and inherent stability make it ideal for simulating resistive random-access memory (RRAM) cells, logic circuits, and large-scale neuromorphic arrays where reliable on/off operation is paramount.

In summary, the choice is not one of absolute superiority but of application fit: Biolek for physical accuracy and analog behavior, BCM for engineering robustness and digital switching. These results provide a clear empirical basis for selecting the appropriate model based on the target system's requirements.

REFERENCES

1. Chua, L. O. (1971). Memristor-The missing circuit element. IEEE Transactions on Circuit Theory, 18(5), 507-519.
2. Strukov, D. B., et al. (2008). The missing memristor found. Nature, 453(7191), 80-83.
3. Biolek, Z., et al. (2009). SPICE model of memristor with nonlinear dopant drift. Radioengineering, 18(2), 210-214.
4. Corinto, F., & Ascoli, A. (2012). A boundary condition-based approach to the modeling of memristor nanostructures. IEEE Transactions on Circuits and Systems I: Regular Papers, 59(11), 2713-2726.
5. Abdala, H., & Pickett, M. (2011, May). SPICE modeling of memristors. 2011 IEEE International Symposium on Circuits and Systems (ISCAS), 1832–1835. https://doi.org/10.1109/ISCAS.2011.5937942
6. Biolek, Z., Biolek, D., & Biolkova, V. (2009, June). SPICE model of memristor with nonlinear dopant drift. Radioengineering, 18(2), 210–214.
7. Chua, L., & Kang, S. (1976, February). Memristive devices and systems. Proceedings of the IEEE, 64(2), 209–223.
8. Joglekar, Y. N., & Wolf, S. J. (2009). The elusive memristor: Properties of basic electrical circuits. European Journal of Physics, 30(4), 661–675. https://doi.org/10.1088/0143-0807/30/4/001
9. Majetta, K., Clauss, C., & Schmidt, T. (2012, September). Towards a memristor model library in Modelica. 9th International Modelica Conference, 507–512. https://doi.org/10.3384/ecp12076507
10. Prodromakis, T., Peh, B. P., Papavassiliou, C., & Toumazou, C. (2011, September). A versatile memristor model with nonlinear dopant kinetics. IEEE Transactions on Electron Devices, 58(9), 3099–3105.
11. Simmons, J. G. (1963, June). Generalized formula for the electric tunnel effect between similar electrodes separated by a thin insulating film. Journal of Applied Physics, 34(6), 1793–1803.
12. Zaplatilek, K. (2011). Memristor modeling in MATLAB and SIMULINK. Proceedings of the European Computing Conference (WSEAS), 62–67.
13. Zenk, O., & Ertuğral, B. (2021). Electric Vehicle Battery Charging System Design with Dual Flyback Type Converter. International Journal of Engineering and Information Systems (IJEAIS), 5(12), pp. 12-20.
14. Zenk, O., & Ertuğral, B. (2018). An Investigation of Increasing the Performance of Electric Rickshaw-Pedicab Batteries. International Journal of Engineering and Information Systems (IJEAIS), 2(12), pp. 44-51.

15. Zenk, H. (2021). Simulink Based Modeling of Fuel Cell and Rechargeable Battery Powered Electric Vehicle.International Journal of Engineering and Information Systems (IJEAIS), 5(12), pp. 31-31.
16. Zenk, H. (2018). Comparison of Electrical Performances of Power Electronics Switches and an Effective Switch Selection Algorithm. Acta Physica Polonica A, 133(4), 897-901.
17. Zenk, H. (2018). DC-DC Converters and Simulink Applications.Innovative Approaches in Engineering, 167-194.
18. Zenk, H. (2019). Effective Control of the Developmental Current of a Serial DC Motor with a Fuzzy Tuned-PI Controller Zeta Converter. Karadeniz Fen Bilimleri Dergisi, 9(1), 196-211.
19. Zenk, H., & Akpinar, A. S. (2014). Dynamic Performance Comparison of Cúk Converter with DC Motor Driving and Using PI, PID, Fuzzy Logic Types Controllers. Universal Journal of Electrical and Electronic Engineering, 2(2), 90-96.
20. Zenk, H. (2016). In push-pull converter output voltage stability comparison with using fuzzy logic, PI and PID controllers. International Journal of Engineering Research and Management (IJERM), 3(12), 1-6.
21. Zenk, H. (2018). An Effective Flyback Converter Design for PMDC Motor Control. Karadeniz Fen Bil. Dergisi,8(2), 207-215.
22. Zenk, H., & Altinkok, A. (2017). Output Voltage Control of PI And Fuzzy Logic Based Zeta Converter. IOSR Journal of Electrical and Electronics Engineering (IOSR-JEEE), 12(6), 63-70.
23. Zenk, H. (2016). A Comparative Application of Performance of the SEPIC Converter Using PI, PID and Fuzzy Logic Controllers for PMDC Motor Speed Analysis. Journal of Multidisciplinary Engineering Science Studies (JMESS), 2(12), 1226-1231.
24. Zenk, H. (2019). Comparison of the performance of photovoltaic power generation-consumption system with push-pull converter under the effect of five different types of controllers. International Journal of Photoenergy, 2019.
25. Zenk, H. (2020). Comparison of Voltage Stability of Photovoltaic Power Source Dual Structure Flyback Converter with Fuzzy-Tuned PI and Fractional PID Type Controllers. Karadeniz Fen Bilimleri Dergisi, 10(2), 443-465.